RESEARCH ON BOUNDARY CONTROL WITH SECOND-ORDER SWITCHING SURFACE FOR POWER ELECTRONIC SYSTEMS

LEUNG KA SING

DOCTOR OF PHILOSOPHY

CITY UNIVERSITY OF HONG KONG

AUGUST 2005

LEUNG KA SING

RESEARCH ON BOUNDARY CONTROL WITH SECOND-ORDER SWITCHING SURFACE FOR POWER ELECTRONIC SYSTEMS

PhD
2005

CityU

CITY UNIVERSITY OF HONG KONG
香港城市大學

Research on Boundary Control with Second-Order Switching Surface for Power Electronic Systems
電力電子系統基於二階開關面的邊界控制之研究

Submitted to
Department of Electronic Engineering
電子工程學系
in Partial Fulfillment of the Requirements
for the Degree of Doctor of Philosophy
哲學博士學位

by

Leung Ka Sing
梁家昇

August 2005
二零零五年八月

ABSTRACT

This thesis presents research results on boundary control with second-order switching surface for power electronics systems. The proposed switching surface can achieve near-optimum large-signal responses in power electronic systems with simple circuit implementation and does not require sensing extra state variables, as compared with the first-order switching surface. Converters can exhibit good steady-state and transient behaviors in both continuous and discontinuous conduction modes with the same control law. The proposed switching surface is not only capable of controlling buck converters, but also can be extended to various types of power electronics converters, such as dc/dc converters and dc/ac converters.

The contents of this thesis are as follows.

In *Chapter 1*, control methods of power electronic converters will be discussed. Then, some control issues, such the control performance versus control complexity and dynamic performances, will be discussed. Moreover, review and discussion on the boundary control and its practical issues will be given.

In *Chapter 2*, the concept of second-order switching surface in boundary control for buck converters will be introduced. It is based on estimating the state trajectory movement after a switching action, resulting in a high state-trajectory velocity along the switching surface. This phenomenon accelerates the trajectory moving toward the target operating point. An implementation of the controller and experimental performance with a 120-W buck converter will be studied.

In *Chapter 3*, a comparative study on the performance characteristics of buck converters with boundary control using the first-order switching surface in continuous conduction mode will be presented. Performance attributes include the average output voltage, output ripple voltage, switching frequency, and large-signal characteristics. Special emphases will be given to investigate the effects of the equivalent series

resistance of the output capacitor on the above attributes, and the sensitivity of the output voltage against the variations of input voltage and circuit component values. Theoretical predictions will be verified with experimental results.

In *Chapter 4*, the scope of *Chapter 3* is extended. Major emphasis is given to converters operating in discontinuous conduction mode.

In *Chapter 5*, a detailed examination of inverters using the proposed switching surface will be carried out. Dynamic responses of an inverter supplying to different kinds of loads, including resistive load, inductive load, and diode-capacitor rectifying circuit, will be studied.

In *Chapter 6*, an overall conclusion of the research topics and some suggestions for further research will be given.

CITY UNIVERSITY OF HONG KONG

DOCTOR OF PHILOSOPHY

THESIS ACCEPTANCE

NAME OF STUDENT:	LEUNG Ka Sing
THESIS TITLE (English):	Research on Boundary Control with Second-Order Switching Surface for Power Electronic Systems
(Chinese):	電力電子系統基於二階開關面的邊界控制之研究

This is to certify that the student's thesis (as presented above) has been examined by the following examiners and has received full approval for acceptance in partial fulfillment of the requirements for the Degree of Doctor of Philosophy:

Prof. BHAT Ashoka K S	Department of Electrical & Computer Engineering University of Victoria, Canada
Prof. CHEN Guanrong	Department of Electronic Engineering City University of Hong Kong
Prof. CHUNG Shu Hung Henry	Department of Electronic Engineering City University of Hong Kong
Prof. KAZIMIERCZUK Marian K	Department of Electrical Engineering Wright State University, USA
Prof. LEE Yim Shu	Department of Electronic & Information Engineering The Hong Kong Polytechnic University

Dr. SHEK Chan Hung
Chair
Panel of Examiners
City University of Hong Kong

ACKNOWLEDGEMENT

I would like to express my sincere appreciation to my supervisor Prof. Henry S. H. Chung, for his guidance, advice and support during my study in the City University of Hong Kong. This thesis cannot be completed without his professional directions. I also deeply appreciate Prof. S. Y. R. Hui for his valuable suggestions.

I am also grateful to Julian Y. C. Chiu, research student of the City University of Hong Kong, for his great help in the past.

Finally, I would like to thank my family members for their encouragement and thank Dr. Joseph S. K. Leung, Dr. Billy M. T. Ho and Dr. Samuel S. H. Chan for their helpful discussions, recommendations and support of my research.

TABLE OF CONTENTS

CHAPTER 1

OVERVIEW AND BACKGROUND OF RESEARCH

1.1 Introduction

Control of switching converters is one of the major areas in power electronics. Since 1970, application of classical linear control techniques has been widely used to design the controller for switching mode power supplies (SMPS). Nowadays, these techniques can be found in almost all power electronics introductory textbooks [Wu 1997; Mohan *et al* 1995; Erickson and Maksimovic 2000; Silva J. F. 2001] and is well-established for engineers and mathematicians [Chetty 1982; Middlebrook 1989; Vorperian 1990]. SMPS are piecewise-linear and time-varying systems. Because of their nonlinear switching characteristics, their system differential equations cannot be generally solved in an explicitly analytical form because the switching moments and switching conditions are implicitly related. For the sake of simplicity, many existing control schemes for power electronic circuits are confined to developing a small-signal model defining around the nominal operating point. This method is a simple way for the circuit designer to determine the dynamic behavior of a regulator using classical linear system theories. For small magnitude of injected perturbations, the regulator behaves as predicted by the small-signal model, and the transients converge to the quiescent operating point. However, under large magnitude of perturbations, the nonlinear effects become significant. The steady-state response may diverge from the desired quiescent point. Although some other transients may converge, the trajectories will behave as distorted waveforms, which are different from that predicted by the small-signal model. It can also be found that the control performances including the robustness against parameter variation, stability and disturbance rejection, etc, are non-optimal. Hence, small-signal modeling is insufficient for the complete analysis of regulators.

The scope of this thesis is to propose a newly derived second-order switching surface (σ^2) which can achieve near-optimal response for load disturbance but maintain the simplicity of circuit implementation. The proposed switching surface can be applied to various power converter applications.

1.2 Control Performance versus Control Complexity

The control performance of power converters includes the steady-state accuracy, stability, robustness and dynamic performance etc. Although basic switching converter topologies like buck, boost, and buck-boost converters consist of one inductor, one capacitor and two semi-conductor switches only, their piecewise linear structures make them be categorized into non-linear systems and complicate the controller design for power electronics circuits designers. In addition, it is equally important to study the performance variation and sensitivities against parametric variations, such as the tolerance and drift of the component values and the fluctuation of the input [Garcera *et al* 1999]. Thus, in the last three decades, many publications and much research are devoted to studying those areas, in order to improve the control performance of power converters.

Apart from the control performance, circuit designers will take the implementation complexity and operation perspective into consideration. Although some methods such as the boundary control can improve the converter behaviors, circuit designers sometimes might have reservation and reluctance to apply them practically, due to the unknown controller behaviors if the converter operates outside the design boundary [Nguyen and Lee 1996; Tan *el al* 2005].

1.3 Dynamic Performance

Due to the advancements in high-speed microprocessor and digital signal processor technologies, the need of having SMPS with excellent large-signal dynamic response is drastically increased. Circuit designers generally focus on researching either the power circuit or the controller to achieve fast transient response. A general approach of improving transient response is to reduce the output filter inductor value and increase the output filter capacitance and decoupling capacitance. However, this will cause large inductor current ripple, resulting in high conduction, switching losses, and core loss in the inductor. In addition, due to the space constraint, increasing the capacitance is an impractical approach [Zhou *et al* 2000]. Much research effort has been paid on developing new converter configurations or transient compensation techniques such as synchronous topology [Miftakhutdinov 2001], multiphase interleaved topology [Huang 2000; Zhou *et al* 2000] and its enhancement with coupling inductors [Wong *et al* 2000], active voltage-positioning approach [Erisman and Redl 1999], transient cancellation control [Abu-Qahouq *et al* 2002], active transient current compensator [Luo *et al* 2002], auxiliary switching source [Barrado *et al* 2002] and stepping inductor topology [Poon *et al* 2001]. However, most of these techniques are only capable of applying to the buck converter. Moreover, additional energy storage elements and switches are required.

Parasitic component of the output capacitor is an important factor that could affect both transient and steady-state performances. The output transient voltage spike is mainly combined with the capacitor charge variation, equivalent series resistance (ESR) voltage drop and equivalent series inductor (ESL) effect [Vicor Corporation 2002]. In practice, the effect of ESL is not considered since it can be eliminated by connecting a high-frequency ceramic capacitor in parallel with the output capacitor [Yao *et al* 2004]. Because the converter performance is highly dependent on the filtering component and its value will vary with aging, ambient temperature, output current and input voltage of the converter [Lahyani *et al* 1998], the effects of parameter variation must be considered for the study of any newly proposed converter control method. Although ESR lead to various control problems and degrade the dynamic performance, some control techniques, based on the existence of ESR, such as V^2 control [Goder and Pelletier 1996; Wang 1999; On Semiconductor 2001] and hysteresis control are developed, and they are well-known by engineers due to their fast response and simple compensation [Qu 2001]. However, both of these techniques are based on neglecting the capacitive ripple and it may not always be applicable in power electronic converters since high ESR will also promote noise [On Semiconductor 1999]. Predictive control can also provide faster dynamic response [Sprock and Hsu 1997; Gow and Manning 2001; Bibian and Jin 2002], however, most of them can only be implemented by digital signal processors.

Although many control techniques focus on improving the transient response, it is interesting to note that faster loop response over a critical value cannot further attenuates the peak value of transient voltage change, but only improves the settling time [Nabeshima and Harada 1981, O'Connor 1996, Yao *et al* 2004]. In other words, if a certain control method does not include modifying the converter structure or knowing the transient action before its occurrence, there is no way to further reduce the transient voltage spike and settling time over its optimal value.

1.4 Boundary Control Overview

In the control of power electronics converters, it is suggested that most control methodologies can be classified into average-based or geometric based [Krein 1999]. Boundary control is a geometric based control technique [Greuel *et al* 1997] or a type of variable structure control [DeCarlo *et al* 1988; Hung 1993] for switching power converters and was firstly introduced in the use of power electronics in [Burns and Wilson 1976]. In boundary control, it addresses complete operation of a converter does not differentiate startup, transient, and steady-state modes [Krein 1998]. A switching surface (σ) is used to split the state plane into two regions, such that the converter switching back and forth between on-state and off-state circuit topologies.

Derivation of switching boundary is based on the system behavior shown in state-plane analysis. In the following, a brief introduction of basic concept of boundary control including state-plane, switching boundary, stability analysis, switching surface behavior and practical issues will be given.

1.4.1 State Plane

The design of the switching boundary and the system performance are based on the trajectories evolution. The state equation is used to formulate a family of system trajectories. The dimension of state plane is equal to the number of state variable in the systems and the number of switching combination determines the number of trajectory families [Oppenheimer *et al* 1996; Malesani *et al* 1995]. For any dc-dc converter, trajectories are either spirals or hyperbolae and only intersect at the equilibrium points for each set of trajectory family [Munzert 1996]. Two methods can be employed to construct the system trajectories. The most straight forward approach is to solve the system state equation by varying the initial condition in time-domain. Another approach is to solve the eigenvalue of the system state equation to obtain the motion of the dynamic system [Kundur 1994; Filho and Perin 1997; Umez-Eronini 1999]. The damping factor of the state equation is used to indicate the shape of the trajectory families.

As well as the trajectory families, an *asymptotic curve* or a *loadline* can also be determined on the state-plane. If the switching frequency tends to infinity, for a particular duty ratio, the converter state will convert to a single operating point, which lies within the state-plane. By varying the duty ratio from 0 to 1, a set of these operating points form a curve on the state-plane and is known as asymptotic curve or loadline. The loadline combined with the switching surface determines the steady-state operating point of the power converters [Bass and Krein 1991]. A typical example of state-trajectory families of buck converter is shown in Fig. 1.1.

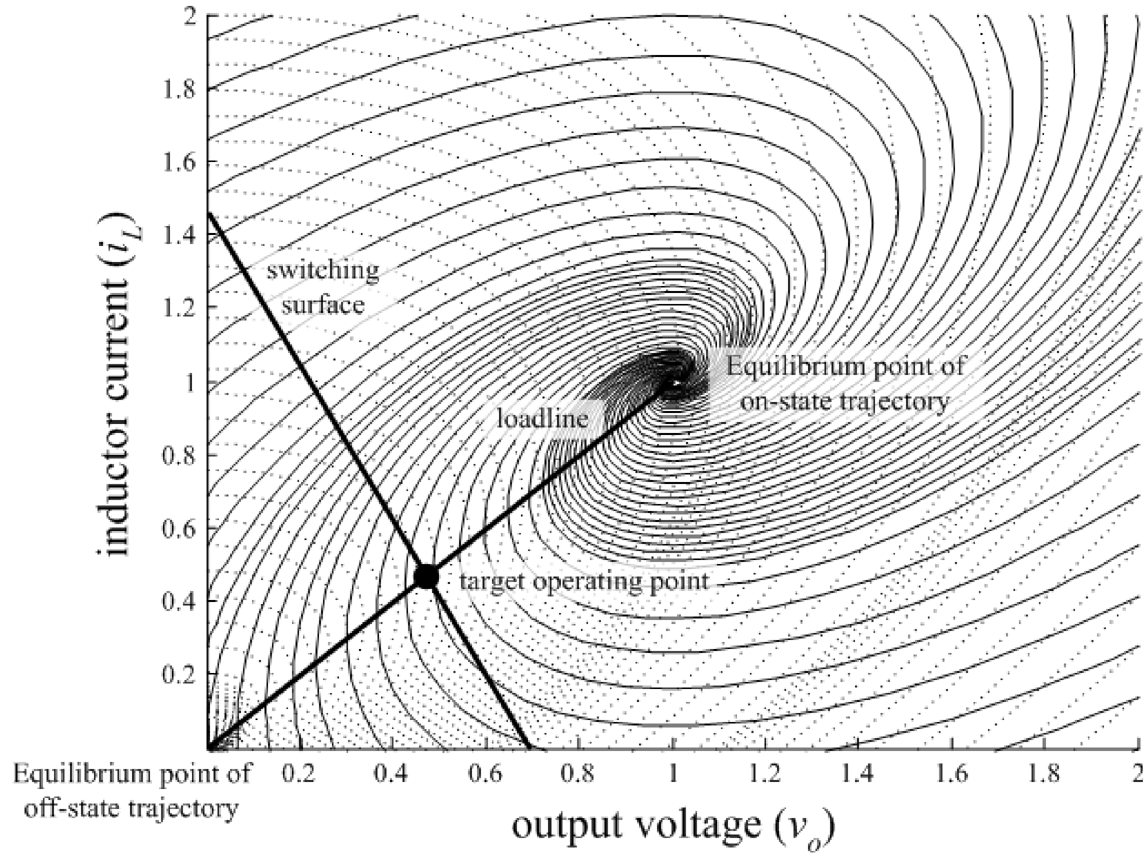

Fig. 1.1 State-trajectory families of buck converter for v_i = 1 V, L = 1 H, C = 1 F, and R = 1 Ω.

1.4.2 Switching Surface

The basic function of switching surface is used to determine the switching action of the power converters and can be classified into four types [Bass and Krein 1990]:

Bidirectional stationary (BS): a stationary boundary independent of time, switching action occurs regardless of the direction of the state came from. A sliding surface is one of the examples of BS.

Bidirectional moving (BM): a time varying moving boundary, switching action occurs similar with BS. This switching surface can be used to represent PWM switching action in state-plane.

Unidirectional stationary (US): a stationary boundary independent of time, switching action occurs only in a single direction of the state came from. A practical sliding surface with hysteresis band is an example of US.

Unidirectional moving (UM): a time varying moving boundary, switching action occurs similar with US. This kind of switching surface can be found in a single diode half-wave rectifier.

In this thesis, the use of bidirectional and unidirectional stationary switching surfaces will be focused.

Use of the bidirectional stationary switching surface in boundary control will be firstly reviewed. The *first-order switching surface* (σ^1) or *linear switching surface* is the most commonly used switching surface. By rotating the angle of the switching surface, the whole system will exhibit different dynamic and steady-state behaviors. Sliding properties is one of the behaviors along the switching surface and gives robustness performance. However, during sliding mode operation, operating the converter apart from its nominal condition will vary the dynamic performance, therefore, adaptive hysteresis [Nguyen and Lee 1995] or adaptive controller [Tan *et al* 2004] are proposed to maintain the dynamic performance.

In order to obtain optimum dynamics, a nonlinear switching boundary is required instead of the linear one. Switching surface which can achieve global stability and optimum dynamic is called *ideal switching surface* (σ^i) and should be along the only on- and off-state trajectory passes the target operating point. The first proposed switching surface in achieving optimum dynamic performance can be found in [Burn and Wilson 1977; Huffman *et al* 1977], and later near-optimum controlling method using feedforward of output current and input voltage with current-mode control is proposed in order to reduce its complexity [Redl and Sokal 1986]. By solving the eigenvalues of system state equation, an exact ideal switching surface with optimum dynamic can be obtained [Biel *et al* 1996; Biel *et al* 1998]. However, those proposed switching surface requires sophisticated computation and is load-dependent, which make it difficult to be implemented by analog circuitry. Therefore, approximation techniques are adopted in calculating the ideal switching surface. However, the procedures of generating the switching surface or the selecting the parameters for the switching surface may not be easily carried out by engineers.

1.4.3 Stability and Switching Surface Behavior

Point along switching surface can be classified into refractive, reflective, and rejective, these three possibilities are shown in Fig. 1.2 [Krein 2001].

Refractive points: state trajectory directed toward the switching surface on one side and away from the other. A typical example is to use a vertical voltage switching surface (voltage hysteresis control) to control a buck converter. Stability along this region is determined by comparing the distance of any pair of two successor points; successor point is defined as every subsequent point of switch action along the switching surface [Munzert 1996].

Reflective points: state trajectory directed toward the switching surface on both sides. Converter operating in this property is known as *sliding regime* and a lot of researches are focused on operating the converter in this property or with modification [Venkataramanan *et al* 1985; Carpita and Marchesoni 1996; Morel *et al* 2002; Ahmed *et al* 2003; Perry *et al* 2004]. If the entire switching surface exhibits this property, it is said to be *global*, otherwise, it will be termed as *local* [Sira-Ramirez and Ilic 1988]. For a first-order switching surface, once the converter operates in sliding region, it will stay in this mode except the converter is forced to change its target operating point such as reference change or load-disturbance occurs. The converter is said to be stable in sliding region because the state must move along the switching surface.

Rejective points: state trajectory directed away from the switching surface on both sides. Switching action cannot force the state move toward the boundary and the trajectory motion not under control. For a stable converter, it must prevent the converter operating in this region.

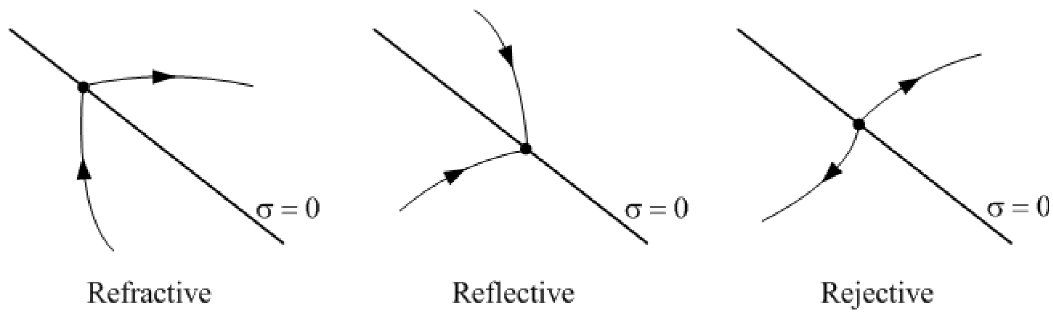

Fig. 1.2 Trajectory Behaviors along the switching surface.

In practice, although it is well-known that boundary control is stable and robust, system performance under line and load variation, components and parasitic elements variation are seldom be discussed. Recent study based on simulation and experimental observation can be found in [Ahmed *et al* 2003]; this study shows the converter operating mode is depended on the value of output load, the switching frequency is inversely proportional to the inductance value and no sufficient effect on variation of capacitor. However, there were no detail mathematical proofs or explanation provided so far in the literature.

1.4.4 Practical Issues

Although stability and robustness are the advantages of the boundary control, switching frequency variation, steady-state output voltage errors and sensing of all state variables are drawbacks of this technique [Mattavelli *et al* 1993].

In practice, the bidirectional stationary switching surface cannot be directly applied to the control circuit. For a theoretical stable switching surface, the switch turn on and off infinitely fast when the converter operates within the sliding region or near the target operating point in refractive region, this phenomenon is called *chattering* [Edwards and Spurgeon 1998]. Fig. 1.3 shows practical results when chattering occurs in buck converter, in which the system is self-oscillating at a high and uncontrollable switching frequency, resulting in high switching loss and severe electromagnetic interference problem.

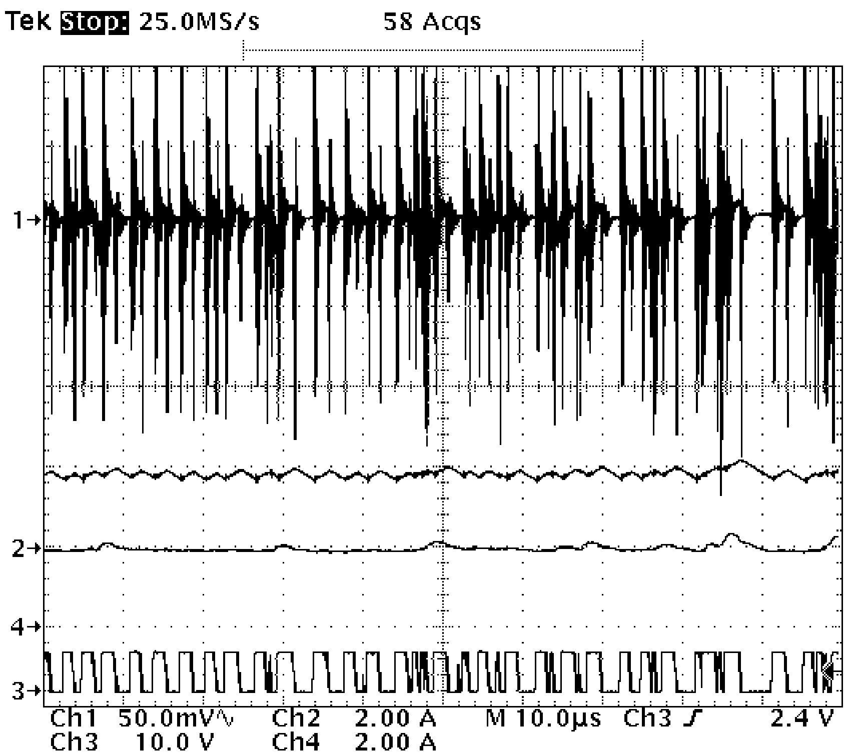

Fig. 1.3 Chattering in buck converter. [Ch1: v_o (50 mV/div), Ch3: v_{gate} (10 V/div)]

Several methods can be used to limit the switching frequency such as hysteresis, constant sampling frequency, constant on-time, constant off-time, constant switching frequency and limited maximum switching frequency. Among these schemes, hysteresis leads to the best results, in term of the steady-state and dynamic performance [Cardoso *et al* 1992]. In addition, this is a method commonly employed to alleviate the chattering effect of boundary control [Slotine and Li 1991; Tan *et al* 2005], however, the switching frequency cannot be kept constant [Szepesi 1987].

Hysteresis method divides a single switching surface into two unidirectional stationary switching surfaces, where no switching action occurs between them. Distance between the two separated switching surfaces depends on the size of hysteresis band which also decides the switching frequency at a particular input voltage and output load. Several approaches based on hysteresis method are used to limit the variation of switching frequency in analog circuit implementation, such as varying the width of hysteresis band [Malesani *et al* 1996; Kang and Liaw 2001] or the delay time in hysteresis comparator [Tso and Wu 2003]. Instead of modifying the hysteresis band, modifying the switching control law [Perry *et al* 2004], injecting a constant ramp function [Nguyen and Lee 1996; Nicolas *et al* 1996; Malesani *et al* 1997] and quasi-sliding control algorithm [Ramos *et al* 2003] are other possible solutions to keep the switching frequency constant.

Another practical issue in the boundary control is to sense the current information. A simple way is to use hall-effect current sensor, but this will increase the cost of the controller [Kelley and Titus 1991]. Although adding a series resistor can measure the current accurately, this will cause high power dissipation and increase the value of the resistance in the considered current path. An alternative solution is to connect an RC network in parallel with the output capacitance [Redl and Sokal 1986; Soto *et al* 2004]. Various current-sensing techniques can be found in [Fairchild Semiconductor 1998;

Forghani-zadeh and Rincon-Mora 2002].

In order to prevent over-current of semi-conductor switches, instead of using a single switching surface, an additional current limitation surface may be employed to limit the maximum current in the converter [Spiazzi *et al* 1997].

1.5 DC-AC Inverters

Nowadays, switch-mode inverters are widely used in power conditioning systems and ac motor drives. Their main function is to produce a sinusoidal ac output that its magnitude and frequency can be controlled. Among various types of inverters, pulsewidth-modulated (PWM) inverter is the most popular one [Kazmierkowski *et al* 2002; Batarseh 2004]. Apart from high conversion efficiency, high-performance inverter requires high input stability and reliability, fast transient response, and low output impedance, total harmonic distortion (THD), and electromagnetic interference.

A typical PWM inverter system consists of a dc source, dc-ac inverter, and LC filter. In order to minimize the THD of the output voltage, many PWM modulation methods [Taniguchi *et al* 1988; Kolar *et al* 1991; Holtz 1994] have been used to regulate the fundamental component and eliminate the low-order harmonics. Moreover, many closed-loop control schemes have been proposed, in order to attain good dynamic response [Holtz and Beyer 1993; Liao and Yeh 2000; Hur and Nam 2001]. However, design of the feedback controller for those inverter systems is generally based on the small-signal linearized model. The inverter performance will deviate much from the expected profile if the inverter is subject to a large-signal disturbance.

Boundary control can also be applied in the control of dc-ac inverter. Instead of obtaining a single asymptotic surface in dc-dc converter, inverter will obtain a family of elliptic asymptotic surfaces on the state plane [Bass and Krein 1990]; and its shape will vary by the amplitude and frequency of the sinusoidal reference [Bass and Krein 1989]. Based on this property, by selecting a suitable switching surface, the inverter can automatically generate a desired sinusoidal output without using a reference signal [Biel *et al* 2001; Biel *et al* 2004]. The boundary control technique such as hysteresis control [Kato and Miyao 1988; Jung *et al* 2002] and sliding-mode control [Silva 1992; Malesani *et al* 1996] are commonly employed in controlling power inverters to give an accurate voltage waveform for different loading condition.

1.6 Organization of the Thesis

The thesis contains six chapters. *Chapter 2* presents the concept of second-order switching surface in the boundary control in buck converter. The concept of modifying hysteresis band with state-trajectory prediction to achieve near-optimum transient response for buck converter is firstly introduced. Then, the switching criteria will be concluded from state-trajectory prediction technique, which will also be combined into a single switching surface, namely *second-order switching surface*. Theoretical predictions and experimental results, both steady-state and large-signal disturbance are given.

Chapter 3 presents a comparative study on the performance characteristics of the buck converters with boundary control using the first-order switching surface in the continuous conduction mode. Performance attributes under investigation include the average output voltage, output ripple voltage, switching frequency, and large-signal characteristics. Special emphases are given to investigate the effects of the equivalent series resistance of the output capacitor on the above attributes, and the sensitivity of the output voltage against the variations of the input voltage and circuit component values. The theoretical predictions will be verified with the experimental results.

Chapter 4 extends the scope of *Chapter 3*. Major emphasis is given to converters operating in discontinuous conduction mode (DCM).

Chapter 5 gives a detailed examination of inverters using the proposed switching surface. Dynamic responses of the inverter supplying to different kinds of loads, including resistive load, inductive load, and diode-capacitor rectifying circuit are studied.

Chapter 6 concludes the thesis, together with concise discussions on further research.

CHAPTER 2

STATE TRAJECTORY PREDICTION AND SECOND-ORDER SWITCHING SURFACE

2.1 Introduction

In this chapter, concept of modifying the hysteresis band in the state-trajectory prediction for achieving high slew-rate response to large-signal input and output disturbances will be firstly introduced. The hysteresis band is derived from the output capacitor current, which is used to predict the value of the output voltage after a hypothesized switching action. Four switching criteria are formulated to dictate the state of the main switch. The output voltage can revert to the steady state in two switching actions after a disturbance. The technique is verified with the experimental results of a 50 W buck converter.

For simplicity, the four switching criteria are combined to form a second-order switching surface. This simplification enables the use of boundary control theory to analyze the steady-state, as well as the transient responses. The formulated switching surface can make the overall converter exhibit better steady-state and transient behaviors than the one with the first-order switching surface.

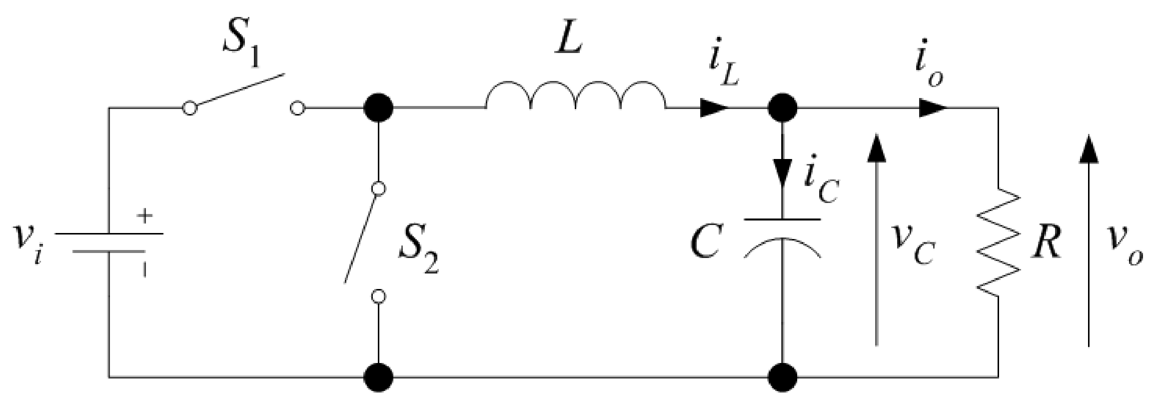

Fig. 2.1 Buck converter.

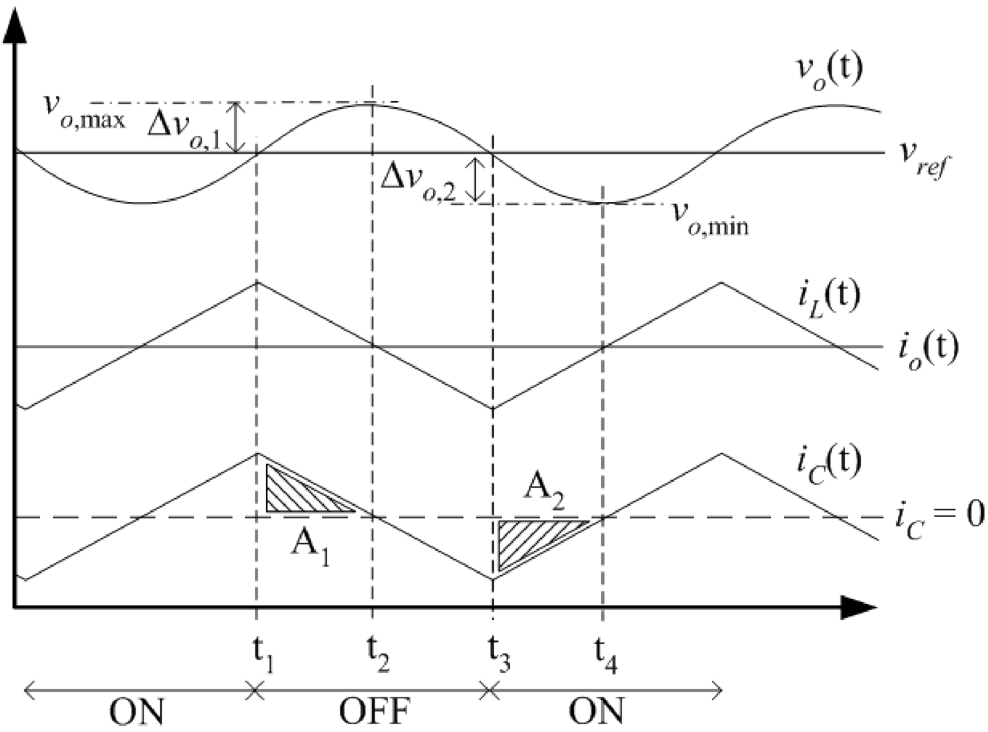

Fig. 2.2 Typical waveforms of v_o, i_L, i_C and i_o of buck converter.

2.2 Principles of Operation

Fig. 2.1 shows the circuit schematic of the buck converter. When the switch S_1 is on and S_2 is off,

$$\frac{d\,i_L}{d\,t} = \frac{1}{L}(v_i - v_o) \text{ and } \frac{d\,v_o}{d\,t} = \frac{d\,v_C}{d\,t} = \frac{1}{C}i_C \tag{2.1}$$

When S_1 is off and S_2 is on,

$$\frac{d\,i_L}{d\,t} = -\frac{1}{L}v_o \text{ and } \frac{d\,v_o}{d\,t} = \frac{d\,v_C}{d\,t} = \frac{1}{C}i_C \tag{2.2}$$

When S_1 and S_2 are off,

$$\frac{d\,i_L}{d\,t} = 0 \text{ and } \frac{d\,v_o}{d\,t} = \frac{d\,v_C}{d\,t} = \frac{1}{C}i_C \tag{2.3}$$

If the output ripple voltage is much smaller than the average output voltage at the steady state, the output current i_o is relatively constant. Since $i_L = i_C + i_o$, the change of i_L, Δi_L, equals the change of i_C, Δi_C. Fig. 2.2 shows the typical waveforms of v_o, i_L, i_C and i_o. v_o varies between a maximum value of $v_{o,\max}$ and a minimum value of $v_{o,\min}$. The state of S is determined by predicting the area under i_C with a hypothesized switching action till i_C = 0 and comparing the area with a fixed ratio of the output error at that instant.

2.2.1 Criteria for Switching off S_1

As shown in Fig. 2.2, S_1 is originally in the on state and is switched off at the hypothesized time instant t_1. The objective is to determine t_1, so that v_o will be equal to $v_{o,\max}$ at t_2 (at which $i_C = 0$). The shaded area A_1 under i_C is integrated from t_1 to t_2. Thus,

$$\Delta v_{o,1} = v_{o,\max} - v_o(t_1) = \frac{1}{C}\int_{t_1}^{t_2} i_C \, dt \tag{2.4}$$

If the area A_1 is approximated by a triangle, it can be shown that

$$\int_{t_1}^{t_2} i_C \, dt \cong \frac{1}{2}\frac{L\, i_C^{\,2}(t_1)}{v_{ref}} \tag{2.5}$$

where v_{ref} is the desired output voltage. [see derivations of (2.4) and (2.5) in the *Appendix B*.]

In order to ensure that v_o will not go above $v_{o,\max}$, S_1 should be switched off when

$$v_o(t_1) \geq v_{o,\max} - \frac{L}{2\,C\,v_{ref}}\, i_C^{\,2}(t_1) = v_{o,\max} - k_1(v_{ref})\; i_C^{\,2}(t_1) \tag{2.6}$$

and

$$i_C(t_1) > 0 \tag{2.7}$$

2.2.2 Criteria for Switching on S_1

As shown in Fig. 2.2, S_1 is originally in the off state and is switched on at the hypothesized time instant t_3. The objective is to determine t_3, so that v_o will be equal to $v_{o,\min}$ at t_4 (at which i_C = 0). The shaded area A$_2$ under i_C is integrated from t_3 to t_4. Thus,

$$\Delta v_{o,3} = v_o(t_3) - v_{o,\min} = -\frac{1}{C}\int_{t_3}^{t_4} i_C \, dt \tag{2.8}$$

Again, the area A$_2$ is approximated by a triangle, it can be shown that

$$\int_{t_3}^{t_4} i_C \, d\,t \cong -\frac{1}{2}\frac{L\, i_C^{\,2}\,(t_3)}{v_i - v_{ref}} \tag{2.9}$$

[Derivations of (2.8) and (2.9) are given in the *Appendix B*.] In order to ensure that v_o will not go below $v_{o,\min}$, S_1 should be switched on when

$$v_o(t_3) \le v_{o,\min} + \frac{L}{2\,C\left(v_i - v_{ref}\right)}\, i_C^{\,2}(t_3) = v_{o,\min} + k_2(v_i, v_{ref})\, i_C^{\,2}(t_3) \tag{2.10}$$

and
$$i_C(t_3) < 0 \tag{2.11}$$

If k_1 and k_2 are zero, the control becomes an ordinary hysteresis control. The time-varying error terms in (2.6) and (2.10) (i.e., the second term) affect the output ripple and improve the transient responses, as compared with the ordinary hysteresis control. For the sake of simplicity, v_i and v_{ref} in (2.6) and (2.10) are taken to be their nominal values. Thus k_1 and k_2 are constants. The criteria of (2.6), (2.7), (2.10), and (2.11) are applied for both steady-state operation and large-signal disturbances. Fig. 2.3 shows the block diagram of the control.

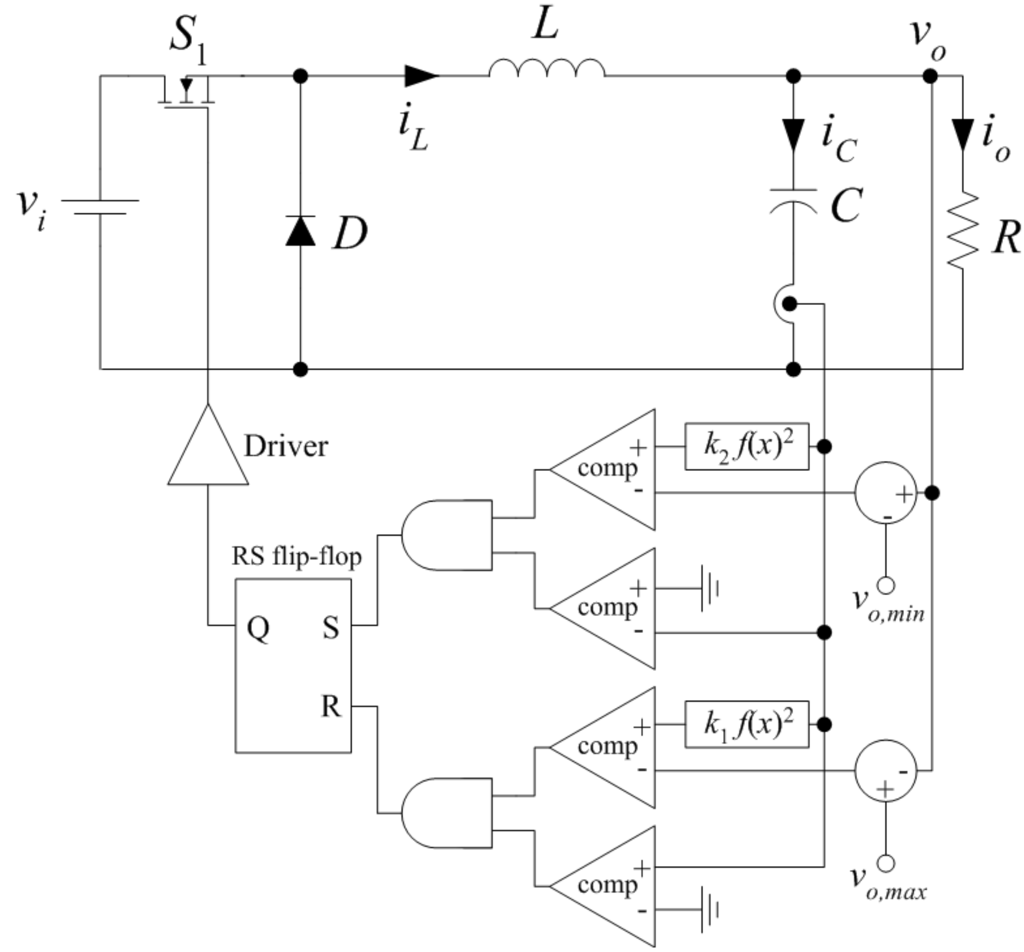

Fig. 2.3 Block diagram of STP control technique.

2.3 Experimental Verifications on STP

A 50 W 24 V/5 V prototype has been built. The component values are: L = 100 μH, C = 470 μF, r_L = 250 mΩ, r_C = 20 mΩ, $v_{o,\min}$ = 4.975 V, and $v_{o,\max}$ = 5.025 V. v_o is regulated at 5V. The converter is subject to five different load disturbances. The theoretical state-plane trajectories of the converter without and with the STP are shown in Figs. 2.4(a) and 2.4(b), respectively. They show the changes of i_L (i.e., $\hat{i}_L$) and v_o (i.e., $\hat{v}_o$) during the transient period. The origin (0, 0) represents the steady-state operating point of v_o = 5 V and i_L = 10 A. The initial deviations from the steady state operating point (i.e., the testing conditions) are labeled from '1' to '5' in the figures. The initial inductor currents prior load changes [i.e., $i_L(0^-)$], the settling time, the percentage output overshoots are tabulated in Table 2.1. The settling time is defined as the time taken that v_o falls into ±1% tolerance bands - the dash lines shown in the figures. It can be seen that the transient performances are improved with the STP, particularly when the output load is increased.

Fig. 2.5 shows the startup transients of v_o, the input current i_i, i_o, and the gate drive signal v_g without and with the STP. The settling time of the output transient without STP is 650μs, while the one with STP is 350μs. As expected, the ordinary hysteresis control turns off the main switch when v_o is higher than the hysteresis band. The stored energy in the inductor will further boost the output after the main switch is off. The output overshoot and settling time are thus increased. The output profile is much improved with the STP. However, as i_o is not in the steady state during the startup, Δi_L is different from Δi_C. There are discrepancies in predicting the output. As circled in Fig. 2.5(b), two extra switching actions are introduced, but it does not affect the overall performance. Fig. 2.6 shows the waveforms when i_o is increased suddenly from 1 A (5 W) to 10 A (50 W). The settling time of the transients without STP is 240μs and the one with STP is about 100μs. The main switch with STP is switched off earlier than the one without STP, since v_o is predicted *a priori* before switching off the main switch. The output can revert to the steady state in two switching actions. Fig. 2.7 shows the transient response when the output power is changed from 25 W to 2 W. The converter is originally in continuous conduction mode at 25 W output and is changed into discontinuous conduction mode at 2 W output. The converter can revert to steady state in 600μs and two switching actions. Thus, the STP can effectively enhance the transient response of the buck converter using hysteresis control without significant modification in the control circuit. It can operate in both continuous and discontinuous conduction modes.

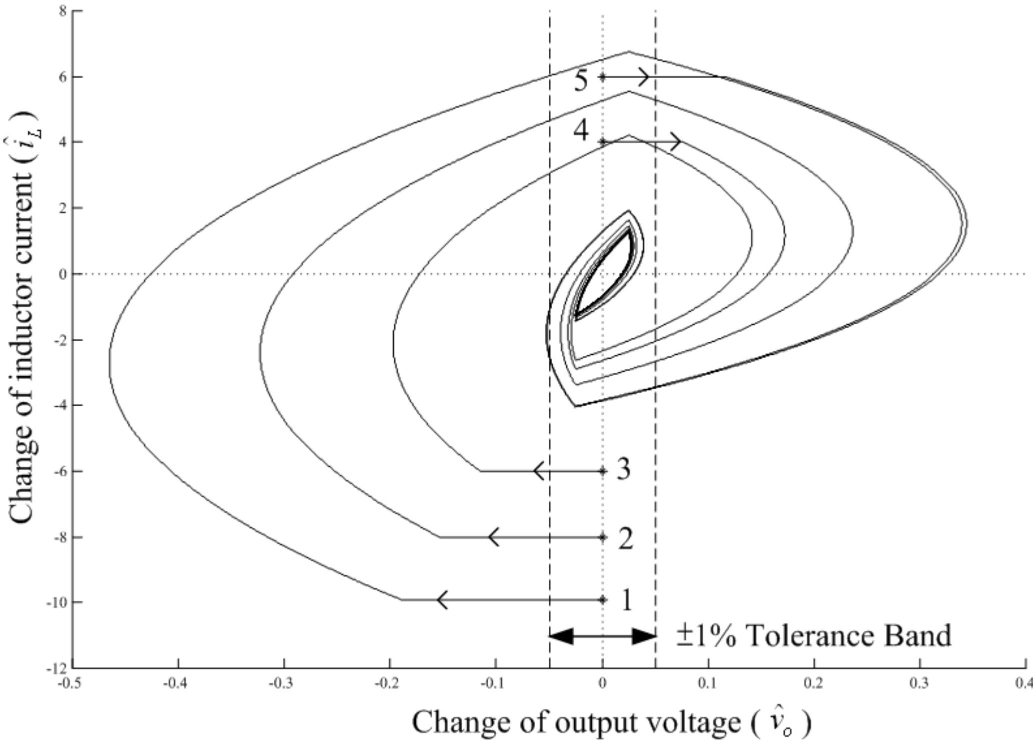

(a)

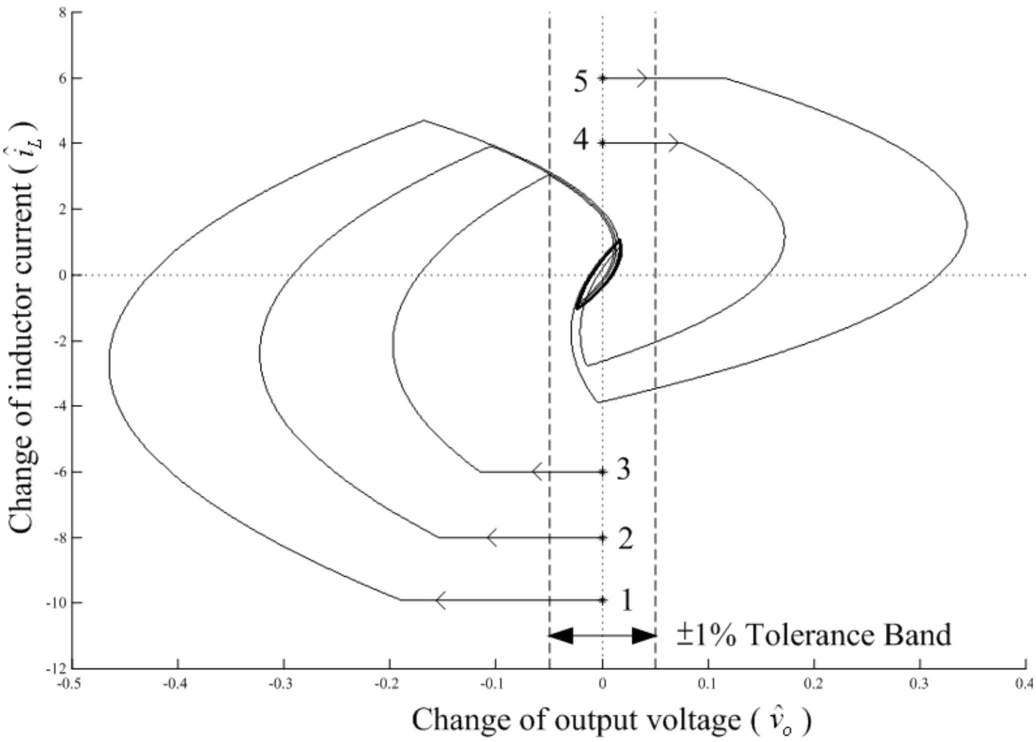

(b)

Fig. 2.4 Theoretical state-plane trajectories of the buck converter operating at the rated power from different initial conditions. (a) Without STP. (b) With STP.

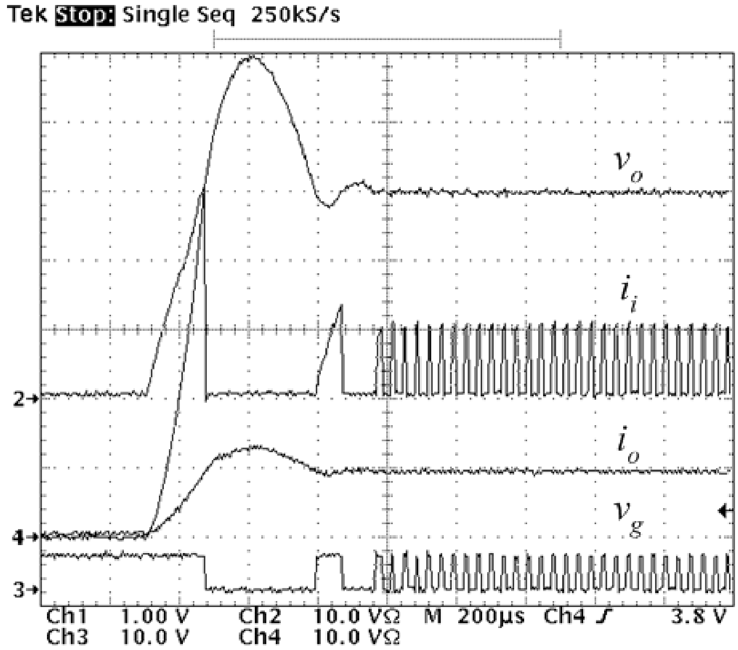

(a)

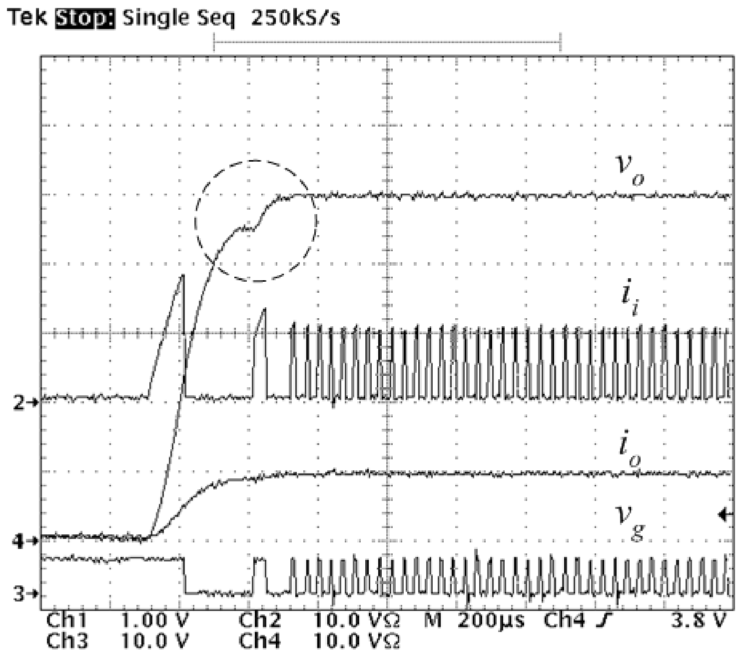

(b)

Fig. 2.5 Startup transients. [v_o: output voltage (1 V/div), i_i: input current(10 A/div), i_o: load current (10 A/div), v_g: gate drive signal(10 V/div)]. (a) Without STP. (b) With STP.

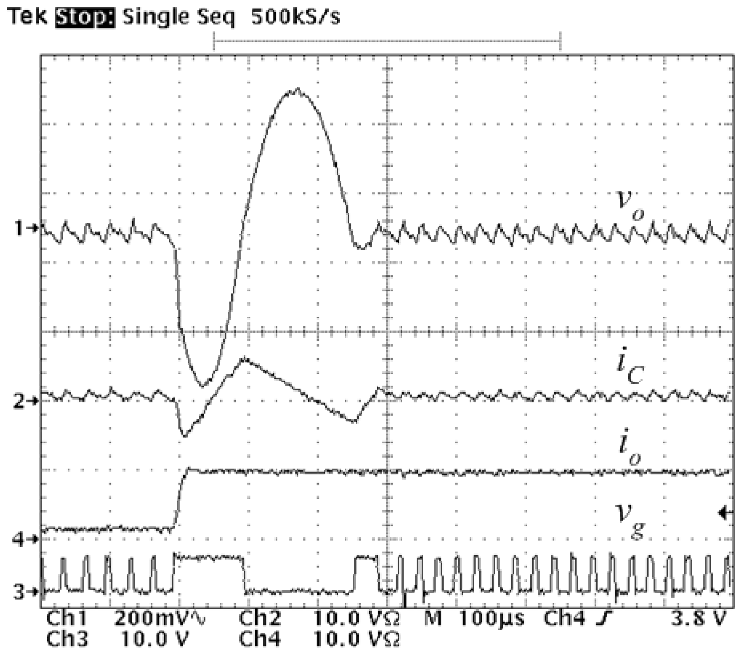

(a)

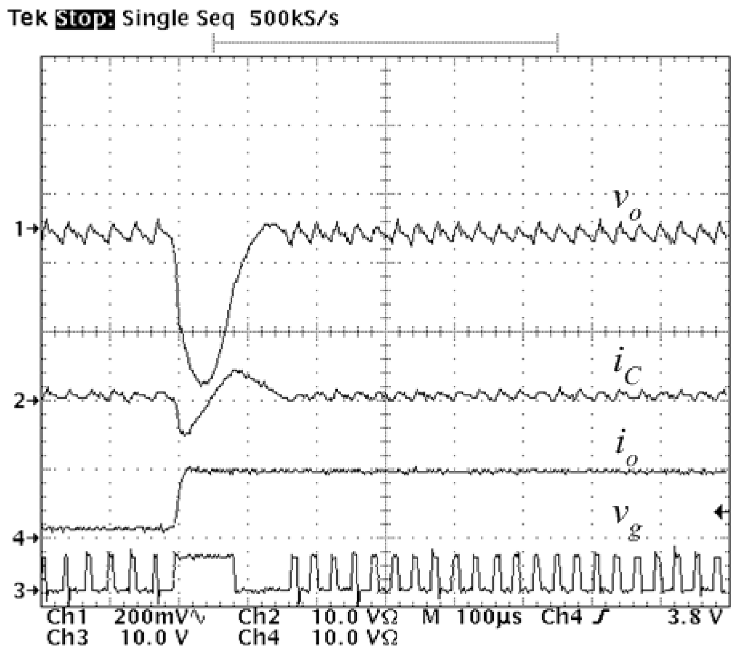

(b)

Fig. 2.6 Transient responses when i_o is changed from 1 A (5 W) to 10 A (50 W). [v_o : output voltage (200 mV/div), i_C : capacitor current(20 A/div), i_o : load current (10 A/div), v_g : gate drive signal(10 V/div)] (a) Without STP. (b) With STP.

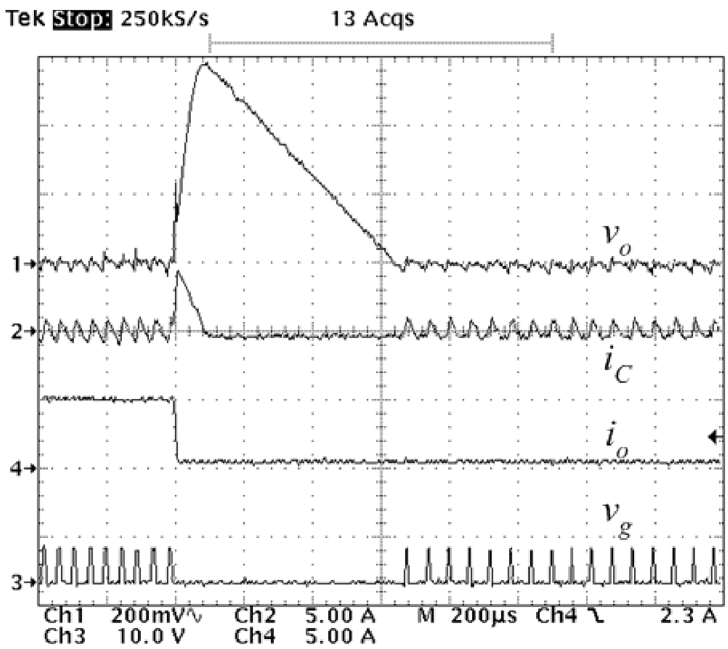

Fig. 2.7 Transient responses when i_o is changed from 5 A (25 W) to 0.4 A (2 W). [v_o: output voltage (200 mV/div), i_C: capacitor current(5 A/div), i_o: load current (5 A/div), v_g: gate drive signal(10 V/div)].

Table 2.1 Comparisons of the converter transient responses with and without the STP

Testing condition	$i_L(0^-)$ (A)		Settling time (μs)	% output overshoot	Max. inductor current (A)
1	0.1	Without STP	248.7	5.7	16.8
		With STP	102.4	0.0	14.7
2	2	Without STP	182.7	3.7	15.5
		With STP	79.3	0.0	13.9
3	4	Without STP	135.4	1.8	14.2
		With STP	53.3	0.0	13.0
4	14	Without STP	77.0	2.4	14.0
		With STP	77.0	2.4	14.0
5	16	Without STP	114.1	5.8	16.0
		With STP	118.1	5.8	16.0

The ESR of the output capacitor is neglected in the above theoretical derivations. Several simulations had been carried out to study the effects of the ESR on the transient responses. Fig. 2.8 shows the state-plane trajectories when the ESR varies from 0 Ω to 100 mΩ in step of 20 mΩ. Fig. 2.9 shows the time-domain simulation results. The initial condition of the simulations is that i_L = 0.1 A and v_o = 5 V. The output power is suddenly changed into the full load condition (50 W) (i.e., i_L = 10 A). Table 2.2 tabulates the transient performance indexes at different values of ESR. It can be observed that the percentage output undershoot increases and the settling time decreases, as the ESR increases. It is mainly because the ESR becomes a dissipative component in the circuit and damps the transient response. Thus, the transient period is shortened. Moreover, as shown in Fig. 2.9, due to the presence of the ESR, the output voltage will decrease abruptly during the transient.

Other simulations studying the change of the output power from full load (50 W) to half load (25 W) had also been carried out. The state-plane trajectories are shown in Fig. 2.10 and the time-domain simulation results are shown in Fig. 2.11. Table 2.3 tabulates the transient performance indexes. Again, the settling time is reduced, as the ESR is increased.

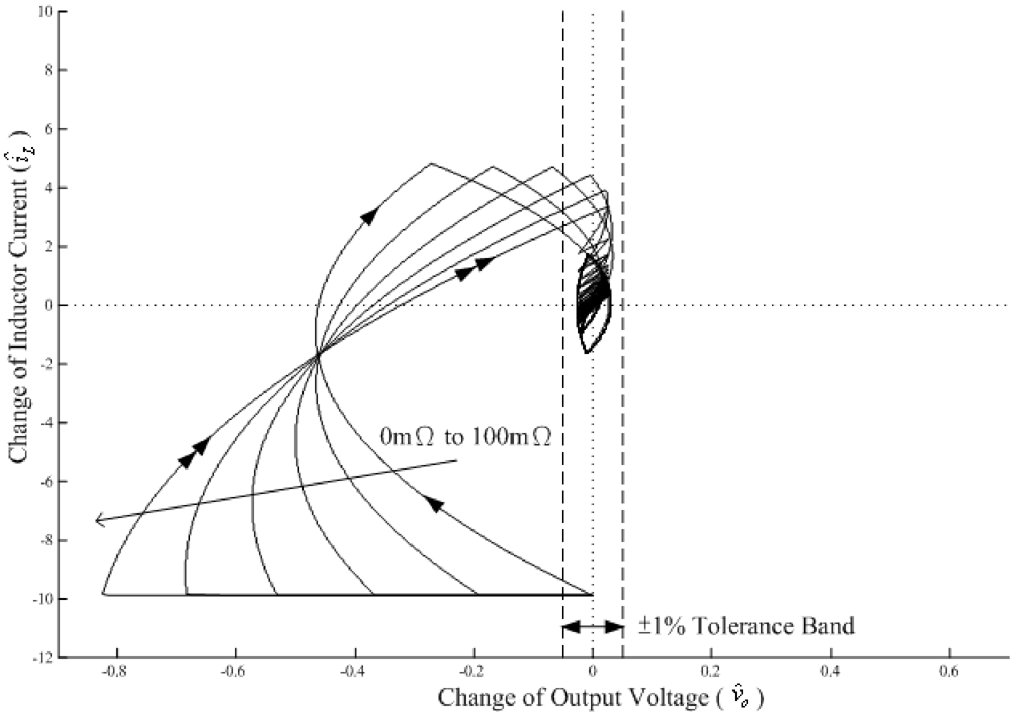

Fig. 2.8 State-plane trajectories of the converters when i_L is changed from 0.1 A to 10 A with the ESR of the output capacitor varying from 0 Ω to 100 mΩ.

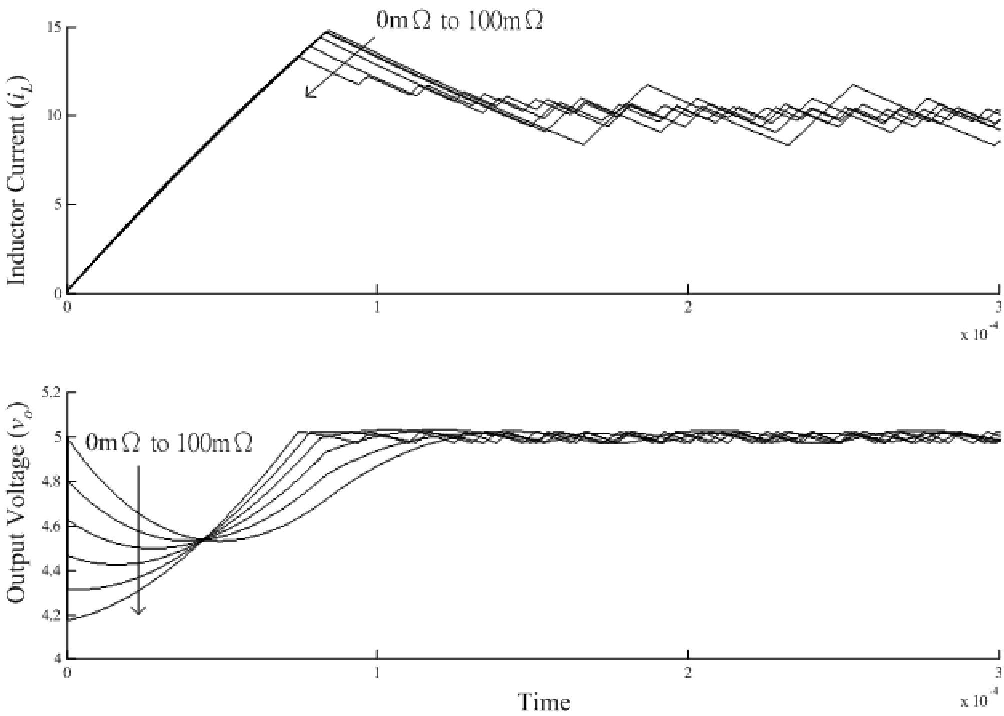

Fig. 2.9 Time-domain simulation results of the condition in Fig. 2.8.

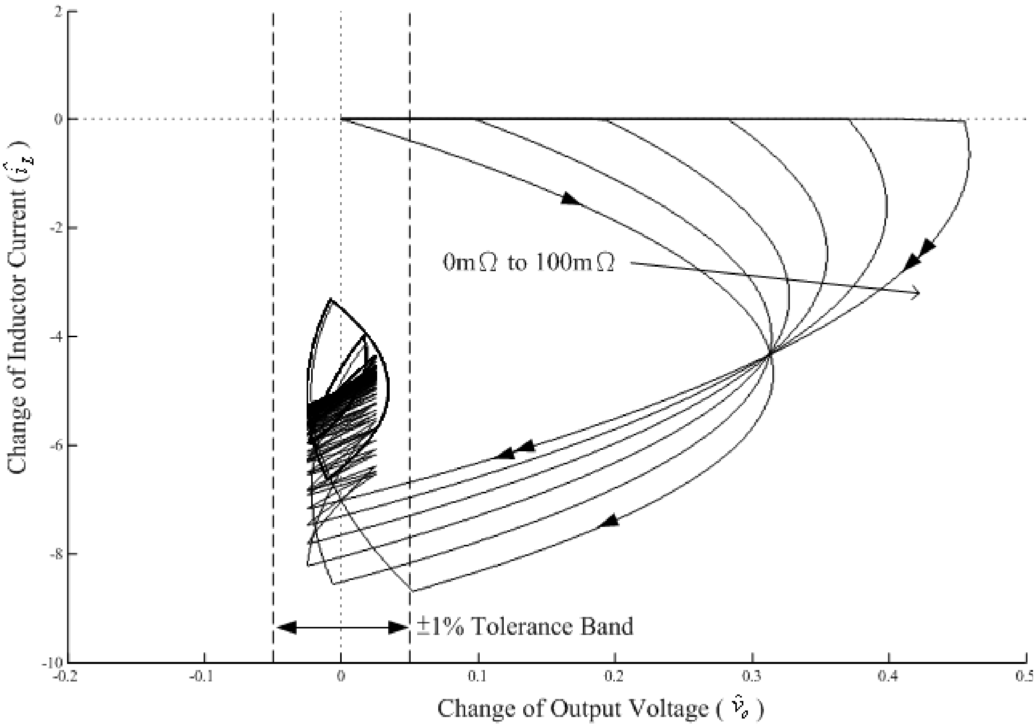

Fig. 2.10 State-plane trajectories of the converters when the converter is changed from full load to half load with the ESR of the output capacitor varying from 0 Ω to 100 mΩ.

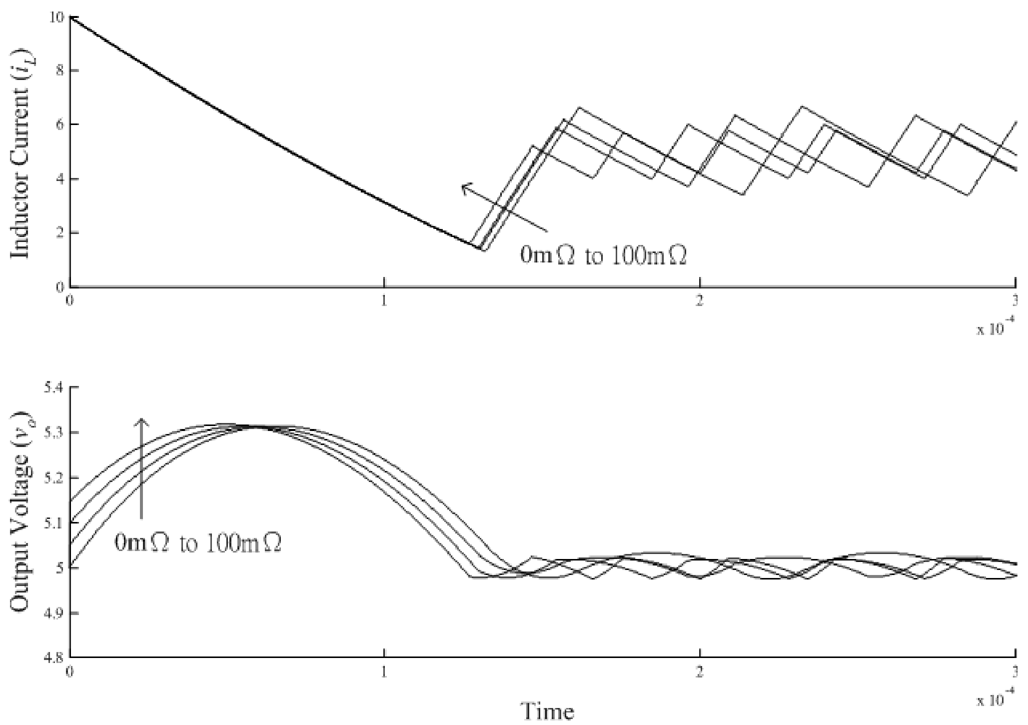

Fig. 2.11 Time-domain simulation results of the condition in Fig. 2.10.

Table 2.2 Comparisons of the transient performance indexes shown in Figs. 2.8 and 2.9

ESR	Settling time(μs)	% output undershoot	% output overshoot	Max. inductor current (A)
0 mΩ	112.7	8.41	0	14.80
20 mΩ	102.4	8.39	0	14.70
40 mΩ	86.8	9.11	0	14.68
60 mΩ	78.8	10.57	0	14.40
80 mΩ	74.1	12.83	0	13.90
100 mΩ	70.5	15.66	0	13.33

Table 2.3 Comparisons of the transient performance indexes shown in Figs. 2.10 and 2.11

ESR	Settling time(μs)	% output undershoot	% output overshoot	Max. inductor current (A)
0 mΩ	132.3	0	5.25	10
20 mΩ	122.6	0	5.23	10
40 mΩ	114.1	0	5.49	10
60 mΩ	106.9	0	6.04	10
80 mΩ	101.0	0	6.90	10
100 mΩ	96.1	0	8.09	10

2.4 First- and Second-Order Switching Surfaces

The buck converter shown in Fig. 2.1 can also be expressed by the state-space equation of

$$\dot{x} = A_0\, x + B_0\, u + (A_1\, x + B_1\, u)\, q_1 + (A_2\, x + B_2\, u)\, q_2 \tag{2.12}$$

where A_i and B_i are constant matrices and q_i represents the state of the switch S_i. S_i is on if $q_i = 1$, and is off if $q_i = 0$.

A family of the on- and off-state trajectories, as well as the load line, is shown in Fig. 2.12. They are obtained by solving (2.12) with different initial conditions. The component values used in the analysis are tabulated in Table 2.4. The on-state trajectory is obtained by setting $\{q_1, q_2\}$ = {1, 0}, while the off-state trajectory is obtained by setting $\{q_1, q_2\}$ = {0, 1}. As discussed in [Krein 2001], the tangential component of the state-trajectory velocity on the switching surface determines the rate at which successor points approach or recede from the target operating point. An ideal switching surface σ^i that gives fast dynamics should be on the only trajectory passing through the target operating point. Once the converter state reaches the surface, it will theoretically attract to the target operating point in one successive switching cycle. As shown in Fig. 2.12, the surface of σ^i above the load line should be along the only off-state trajectory that passes the target operating point and the surface of σ^i below the load line should be along the only on-state trajectory that passes the target operating point. The converter will follow the off-state trajectory, when its state is at the right hand side of σ^i. The converter will follow the on-state trajectory, when its state is at the left hand side of σ^i.

A typical first-order switching surface σ^1 is shown in Fig. 2.12 and can be written in the following single-reference form,

$$\begin{aligned}\sigma^1(i_L, v_o) &= c_1\, i_C + (v_o - v_{ref}) \\ &= c_1\,(i_L - \frac{v_o}{R}) + (v_o - v_{ref})\end{aligned} \qquad (2.13)$$

where i_C and v_o are the capacitor current and output voltage, respectively, i_L is the inductor current, c_1 is the gain, R is the load resistance, and v_{ref} is the desired output voltage.

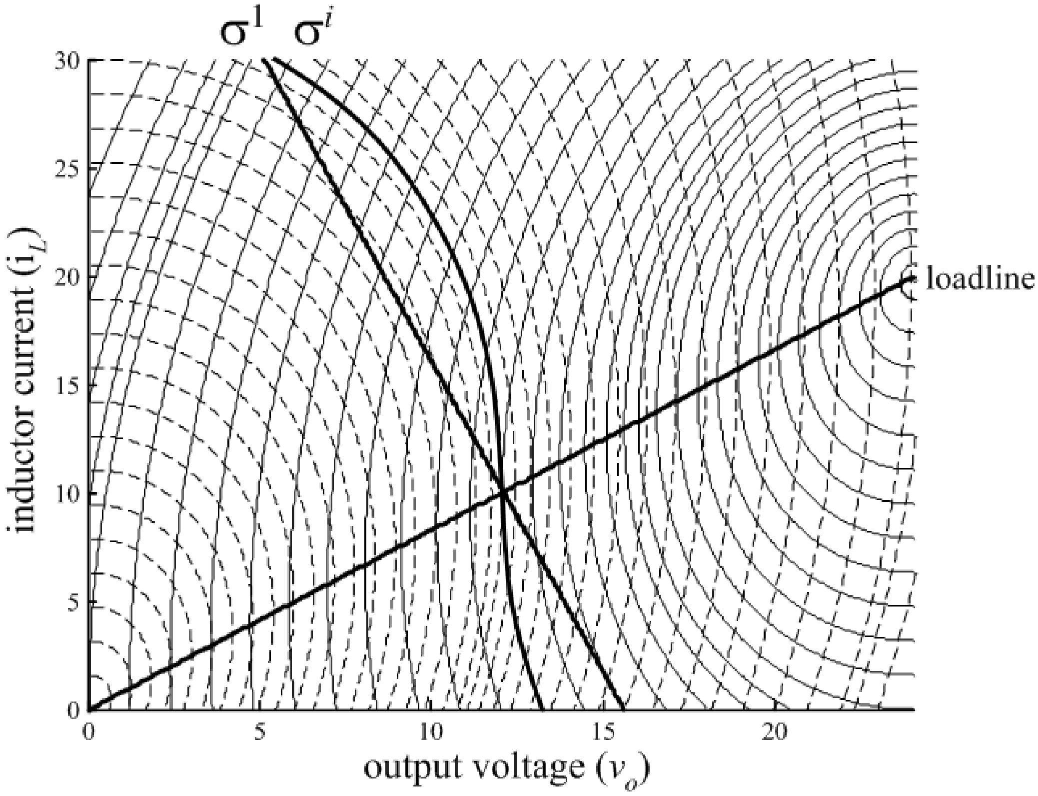

Fig. 2.12 State trajectory families of buck converter with σ^1 and σ^i. [Solid line: on-trajectories, Dotted line: off-trajectories]

Thus, the tangential state-trajectory velocity on σ^1 is non-optimal that the transient dynamics may take several switching cycles. A second-order surface σ^2, which is near to the ideal surface around the operating point, is derived in the following.

For simplicity, k_1 and k_2 in (2.6) and (2.10) are obtained by using the nominal values of v_i and v_{ref}. Based on (2.6), (2.7), (2.10), (2.11), and $v_{o,\min} = v_{o,\max} = v_{ref}$, the following σ^2 can be concluded,

$$\sigma^2(i_L, v_o) = \begin{cases} k_1 \, (i_L - \frac{v_o}{R})^2 + (v_o - v_{ref}), & (i_L - \frac{v_o}{R}) > 0 \\ -k_2 \, (i_L - \frac{v_o}{R})^2 + (v_o - v_{ref}), & (i_L - \frac{v_o}{R}) < 0 \end{cases} \tag{2.14}$$

The equation can further be written into a single expression of

$$\sigma^2(i_L, v_o) = c_2 \, (i_L - \frac{v_o}{R})^2 + (v_o - v_{ref}) \tag{2.15}$$

where $c_2 = \frac{1}{2}k_1\left(1+\mathrm{sgn}(i_L - \frac{v_o}{R})\right) - \frac{1}{2}k_2\left(1-\mathrm{sgn}(i_L - \frac{v_o}{R})\right)$.

Compared (2.15) with σ^1 in (2.13), σ^2 consists of a second-order term. σ^2 is close to σ^i near the operating point. However, discrepancies occur, when the state is far from the operating point because of the approximations in (2.5) and (2.9). Implementation of the controller is shown in Fig. 2.13. Practical Implementation of first- and second-order switching surface is shown in *Appendix A*.

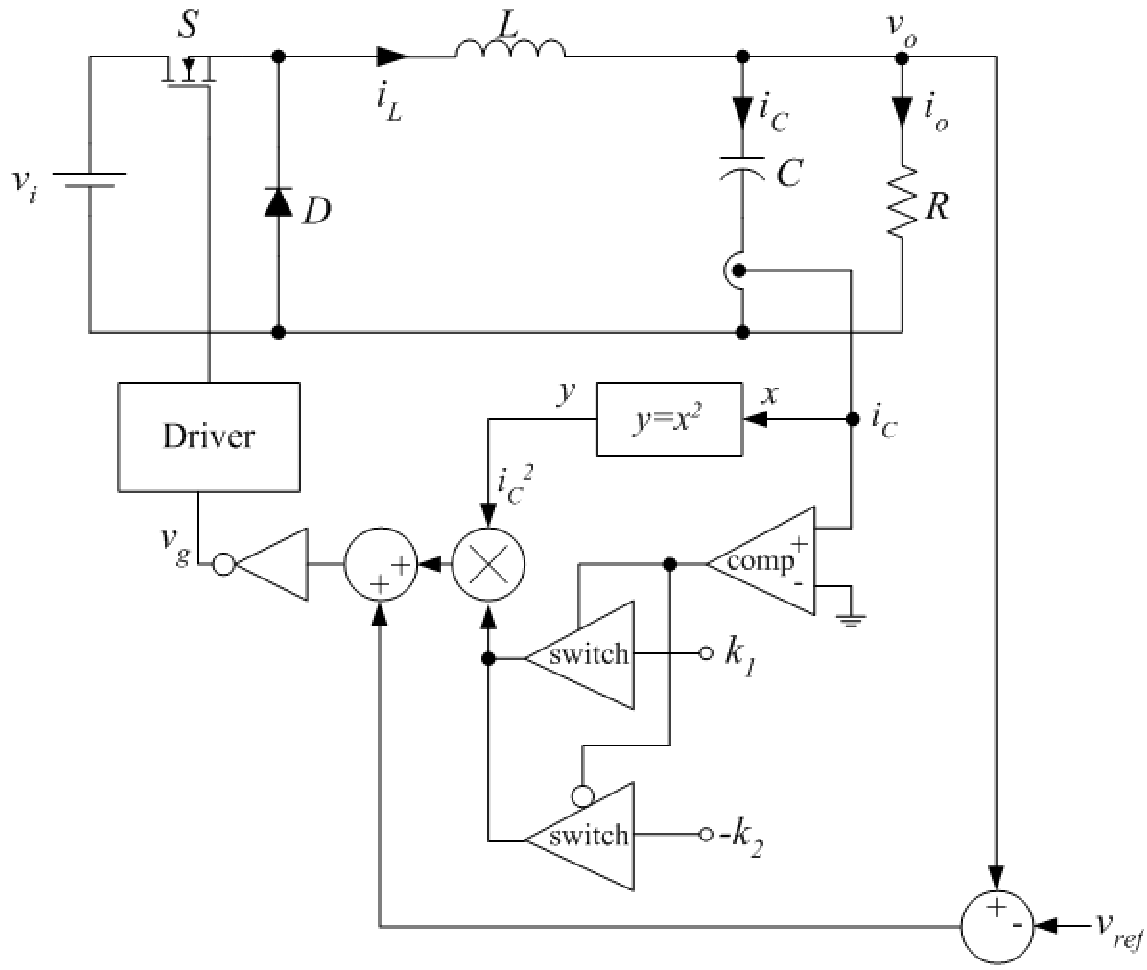

Fig. 2.13 Implementation of the controller of σ^2.

2.5 Experimental Verifications on σ^2

A buck converter with the tabulated component values in Table 2.4 is studied. Fig. 2.14 shows the start-up trajectory, together with σ^1 and σ^2. σ^1 is formulated by having the same startup transients with σ^2 (i.e., σ^1 and σ^2 intercept at the points 'A' and 'B' in Fig. 2.14). The hysteresis band in σ^1 is adjusted to give the same output ripple at the rated power as with σ^2. Fig. 2.15 shows a comparison of the simulated transient responses when R is changed from 2.4 Ω (60 W) to 1.2 Ω (120 W), and vice versa, with σ^1 and σ^2, respectively. The converter with σ^2 achieves faster transient response than that with σ^1. Fig. 2.16 shows the transient responses when R is changed from 2.4 Ω (60 W) to 24 Ω (6 W), in which the converter is operated in discontinuous conduction mode with R = 24 Ω. Results show that steady state error exists with σ^1 and is zero with σ^2. The additional boundary due to the zero inductor current causes a shift of the effective output voltage reference. Figs. 2.17 and 2.18 show the experimental results corresponding to the above testing conditions and are in close agreement with the theoretical predictions. It can be observed that the converter can go to the steady state in two switching actions.

Table 2.4 Component values of the buck converter

Parameter	Value
v_i	24 V
v_{ref}	12 V
L	100 μH
C	400 μF
R	1.2 Ω
c_1	0.2702
$\{k_1, k_2\}$	{0.0104, 0.0104}

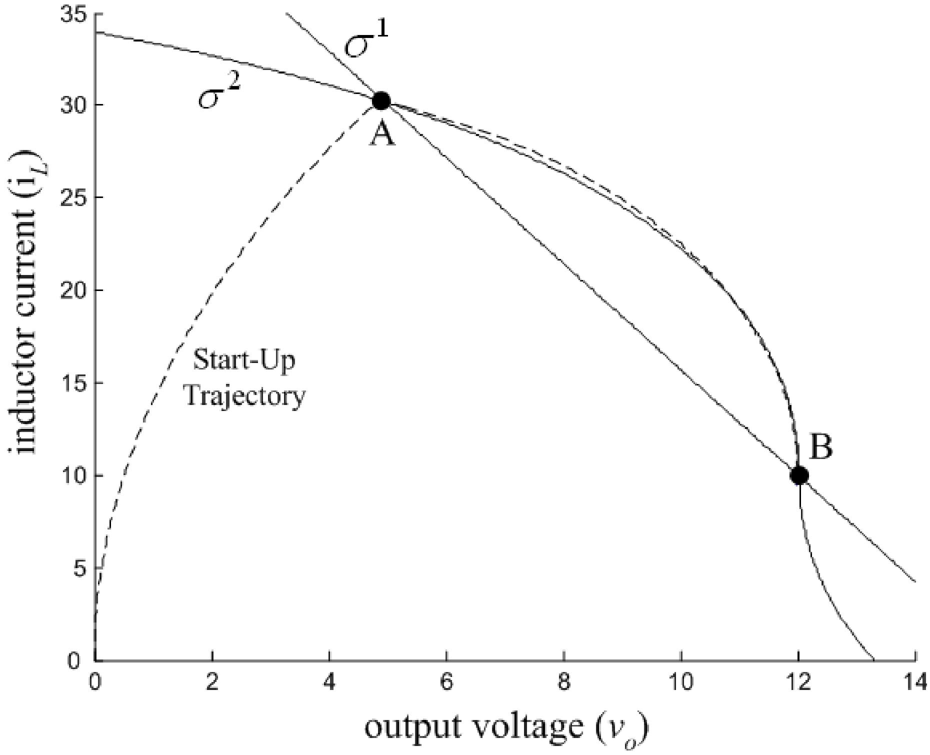

Fig. 2.14 Start-up transient response and the first and second-order switching surface. [Dotted line: start-up trajectory of buck converter]

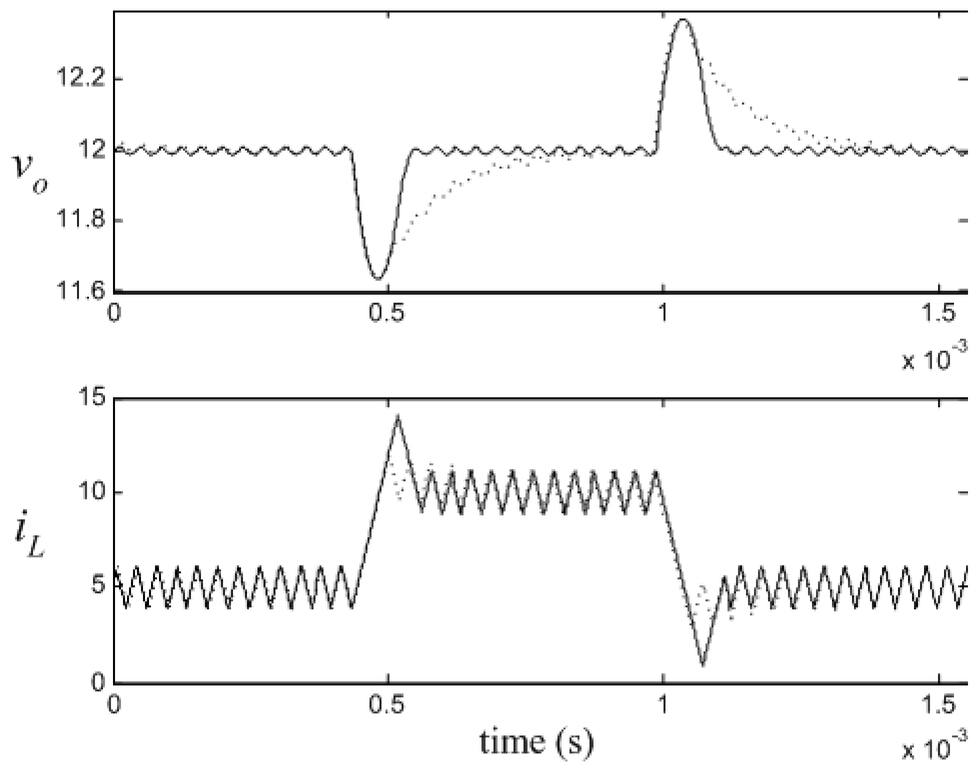

Fig. 2.15 Transient response of *R* from 2.4 Ω to 1.2 Ω and vice versus. [Solid line: σ^2, Dotted line: σ^1]

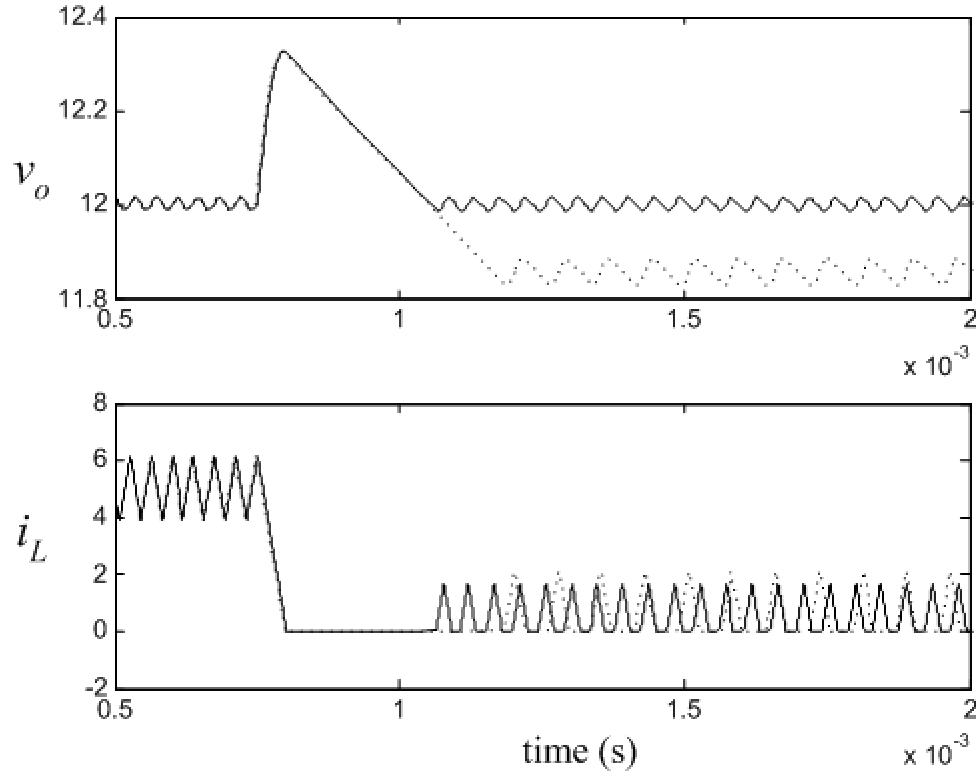

Fig. 2.16 Transient response of *R* from 2.4Ω to 24Ω. [Solid line: σ^2, Dotted line: σ^1]

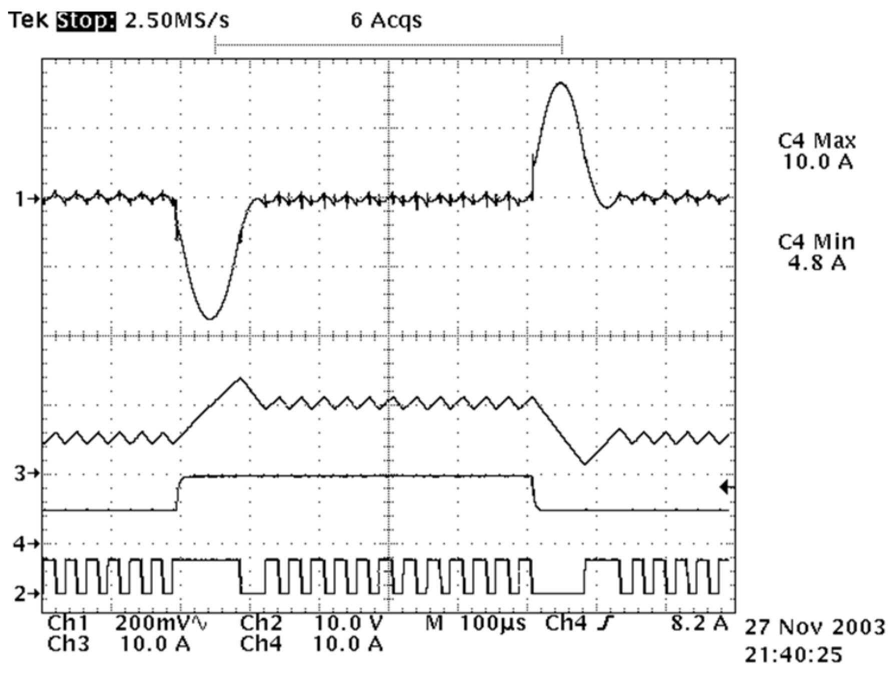

Fig. 2.17 Transient response of buck converter using second-order switching surface control. Load change from 5 A(2.4 Ω) to 10 A(1.2 Ω) and vice versus. [Ch1: v_o (200 mV/div), Ch2: v_g (10 V/div), Ch3: i_L (10 A/div), Ch4: i_o (10 A/div)] (Timebase: 100μs/div)

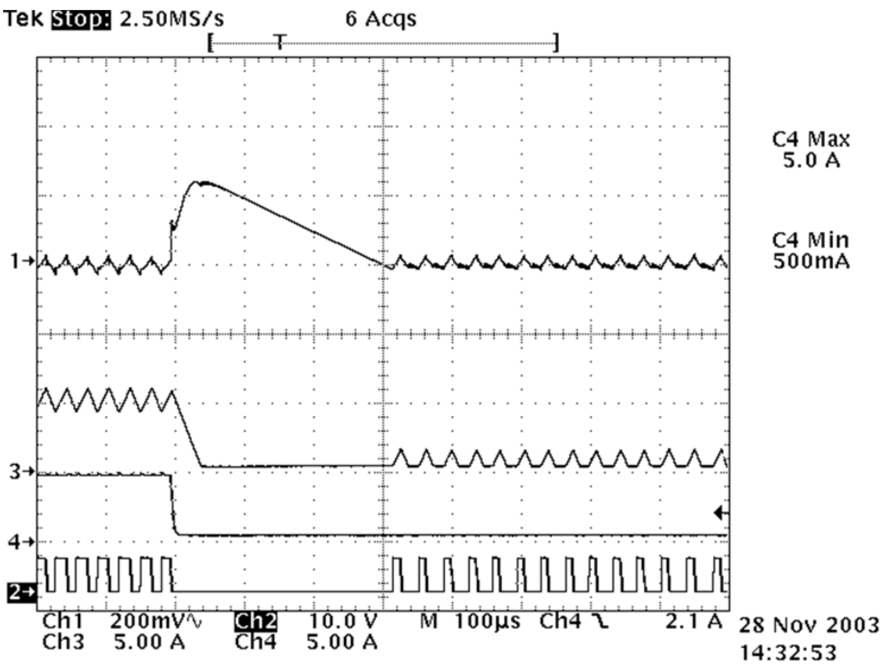

Fig. 2.18 Transient response of buck converter using second-order switching surface control. Load change from 5 A(2.4 Ω) to 0.5 A(24 Ω). [Ch1: v_o (200 mV/div), Ch2: v_g (10 V/div), Ch3: i_L (5 A/div), Ch4: i_o (5 A/div)] (Timebase: 100μs/div)

2.6 Chapter Summary

An STP technique that is applied to the hysteresis control has been proposed. It can enhance the transient response of the buck converter. The output voltage can revert to steady state within two switching actions when it is subject to large-signal disturbances. Then, a boundary control using the second order switching surfaces in buck converter has been derived. Results show that second-order switching surface can achieve near-optimum large-signal responses. The performances have been verified with experimental measurements.

CHAPTER 3

A COMPARATIVE STUDY: CONTINUOUS CONDUCTION MODE

3.1 Introduction

In this chapter, a comparative study on the performance characteristics of the buck converters with boundary control using the first-order switching surface (σ^1) and a second-order switching surface (σ^2) is presented. Performance attributes under investigation include the average output voltage, output ripple voltage, switching frequency, and large-signal characteristics. Special emphases will be given to investigate the effects of the equivalent series resistance of the output capacitor on the above attributes, and the sensitivity of the output voltage against the variations of the input voltage and circuit component values. Generally, converters with σ^2 are found to exhibit better dynamic responses than the ones with σ^1. The theoretical predictions are favorably verified with the experimental results of a 120W buck converter.

3.2 Definitions and Formulas

Fig. 3.1(a) shows the buck converter supplying from the source v_i to the load R. The output voltage is v_o. The converter can be described by the state-space equation of

$$\begin{aligned} \dot{x} &= A_0\, x + B_0\, u + (A_1\, x + B_1\, u)\, q_1 + (A_2\, x + B_2\, u)\, q_2 \\ y &= C\, x \end{aligned} \tag{3.1}$$

where $x = \begin{bmatrix} i_L & v_C \end{bmatrix}$, $y = v_o$, A_i, B_i, and C are constant matrices, and q_i represents the state of the switch S_i. If S_i is on, q_i = 1, and vice versa. S_1 is the main switch and S_2 is the diode in a buck converter. Matrices A_0, B_0, A_1, B_1, A_2, and B_2 are defined as

$$A_0 = \begin{bmatrix} 0 & 0 \\ 0 & -\dfrac{1}{C(R+r_C)} \end{bmatrix},\ B_0 = \begin{bmatrix} 0 \\ 0 \end{bmatrix},\ A_1 = A_2 = \begin{bmatrix} -\dfrac{R\,r_C}{L(R+r_C)} & -\dfrac{R}{L(R+r_C)} \\ \dfrac{R}{C(R+r_C)} & 0 \end{bmatrix},\ B_1 = \begin{bmatrix} \dfrac{1}{L} \\ 0 \end{bmatrix},$$

$$B_2 = \begin{bmatrix} 0 \\ 0 \end{bmatrix} \text{ and } C = \begin{bmatrix} \dfrac{R\,r_C}{R+r_C} & \dfrac{R}{R+r_C} \end{bmatrix}.$$

Practical output capacitors have nonzero ESRs. Thus, instead of sensing the capacitor voltage v_C, the actual load voltage v_o is sensed and is used in the practical boundary control. Thus, the phase space will study the trajectory of v_o and i_L (instead of v_C and i_L) in the following. Fig. 3.1(b) is the phase space $\{v_o, i_L\}$ showing the on-state trajectories with solid lines (i.e., when S_1 is on) and off-state trajectories with dotted lines (i.e., when S_1 is off).

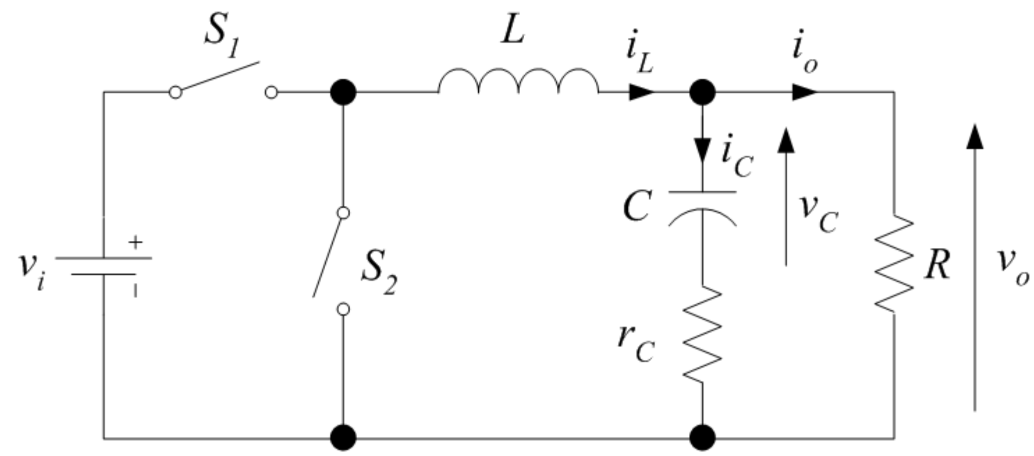

(a)

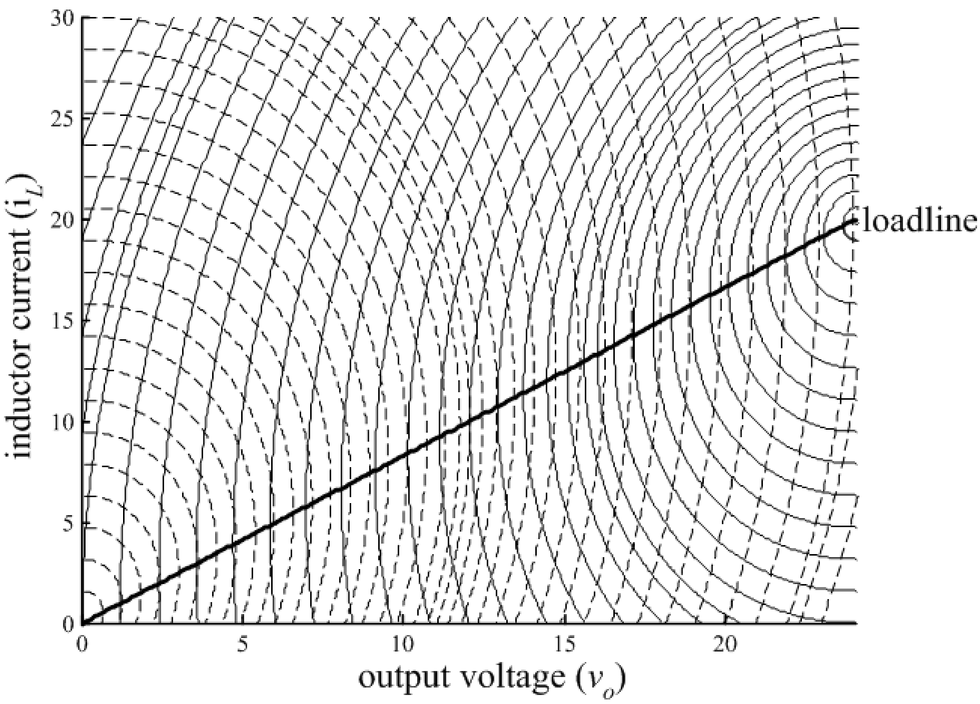

(b)

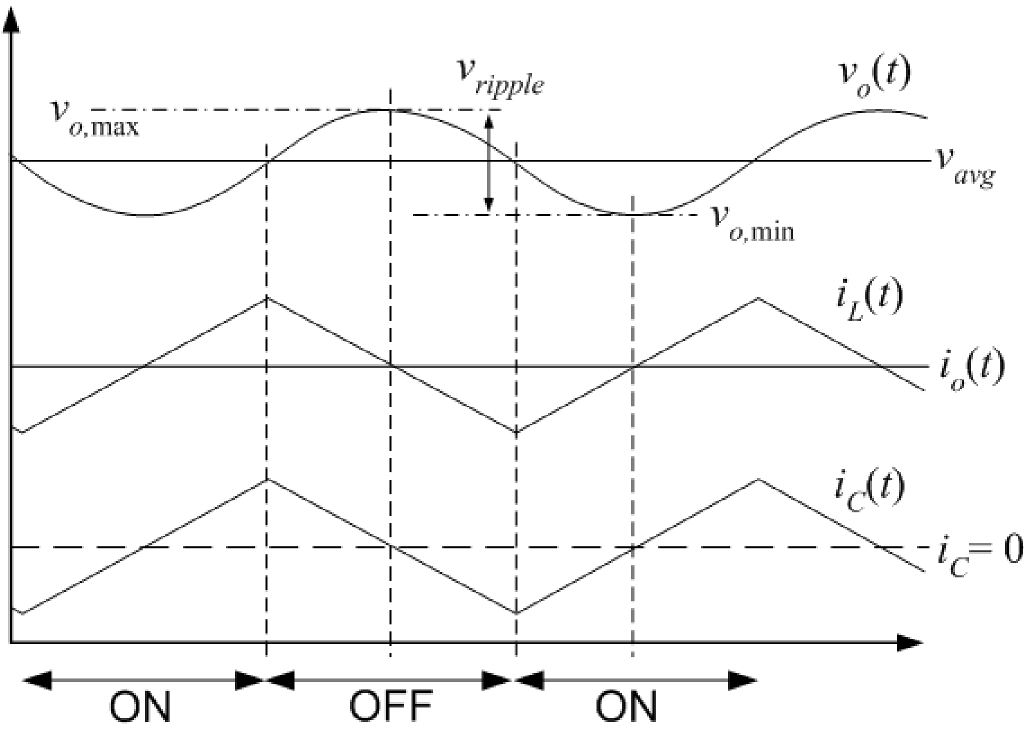

(c)

Fig. 3.1 Buck converter. (a) Circuit schematic. (b) State-plane portrait. (c) Key waveforms of the converter.

3.2.1 On- and Off-State Trajectories

When S_1 is on and S_2 is off, the on-state trajectory $\{v_{o,on}, i_{L,on}\}$ near the target operating point is

$$v_{o,on} = \frac{L}{2C(v_i - v_{ref})}\left(\left(i_{L,on} - \frac{v_{o,on}}{R}\right)^2 - \left(i_{L,0} - \frac{v_{o,0}}{R}\right)^2\right) + v_{o,0} + r_C\left(\left(i_{L,on} - \frac{v_{o,on}}{R}\right) - \left(i_{L,0} - \frac{v_{o,0}}{R}\right)\right) \quad (3.2)$$

where $i_{L,0}$ and $v_{o,0}$ are the initial values of i_L and v_o, respectively, in this stage.

When S_1 is off and S_2 is on, the off-state trajectory $\{v_{o,off}, i_{L,off}\}$ near the target operating point is

$$v_{o,off} = -\frac{L}{2Cv_{ref}}\left(\left(i_{L,off} - \frac{v_{o,off}}{R}\right)^2 - \left(i_{L,1} - \frac{v_{o,1}}{R}\right)^2\right) + v_{o,1} + r_C\left(\left(i_{L,off} - \frac{v_{o,off}}{R}\right) - \left(i_{L,1} - \frac{v_{o,1}}{R}\right)\right) \tag{3.3}$$

where $i_{L,1}$ and $v_{o,1}$ are the initial values of i_L and v_o, respectively, in this stage. Detailed proofs of (3.2)-(3.3) are given in the *Appendix C*.

3.2.2 Modeling of σ^1 and σ^2

Fig. 3.2 depicts σ^1 in [Krein 2001] and σ^2 in *Chapter 2*. The surfaces [i.e., $\sigma^1 = 0$ or $\sigma^2 = 0$] govern the switching actions. Both of them intersect the load line at the operating point 'O' and have the hysteresis bands of Δ_1 and Δ_2, respectively. Introduction of hysteresis bands is a method commonly employed to alleviate the chattering effect in boundary control [Slotine and Li 1991; Tan *et al* 2005] and obtain good results in term of the steady-state and dynamics performance, as compared with various frequency limitation technique [Cardoso *et al* 1992].

As discussed in [Nguyen and Lee 1995], a general form of σ^1 can be written as

$$\sigma^1{}_{\Delta+} = c_1\left(i_L - \frac{v_o}{R}\right) + \left(v_o - \left(v_{ref} + \Delta_1\right)\right) = 0 \tag{3.4}$$

$$\sigma^1{}_{\Delta-} = c_1\left(i_L - \frac{v_o}{R}\right) + \left(v_o - \left(v_{ref} - \Delta_1\right)\right) = 0 \tag{3.5}$$

where c_1 is a constant and v_{ref} is the reference output. i_L and v_o are in linear relationship. When $\sigma^1{}_{\Delta-} < 0$ (i.e. $\sigma^1 < -\Delta_1$), switch S_1 will be turned on. Conversely, it will be turned off, when $\sigma^1{}_{\Delta+} > 0$ (i.e. $\sigma^1 > \Delta_1$). In the region between $\sigma^1{}_{\Delta+}$ and $\sigma^1{}_{\Delta-}$, the state of the switches remains unchanged.

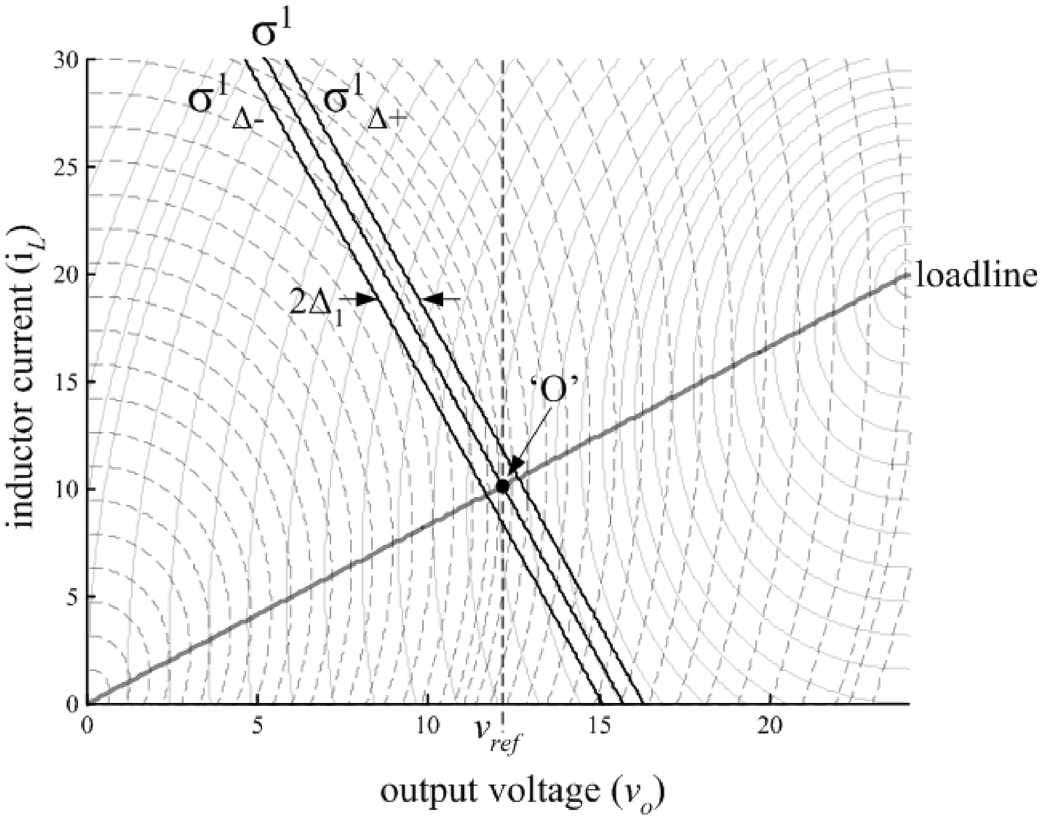

(a)

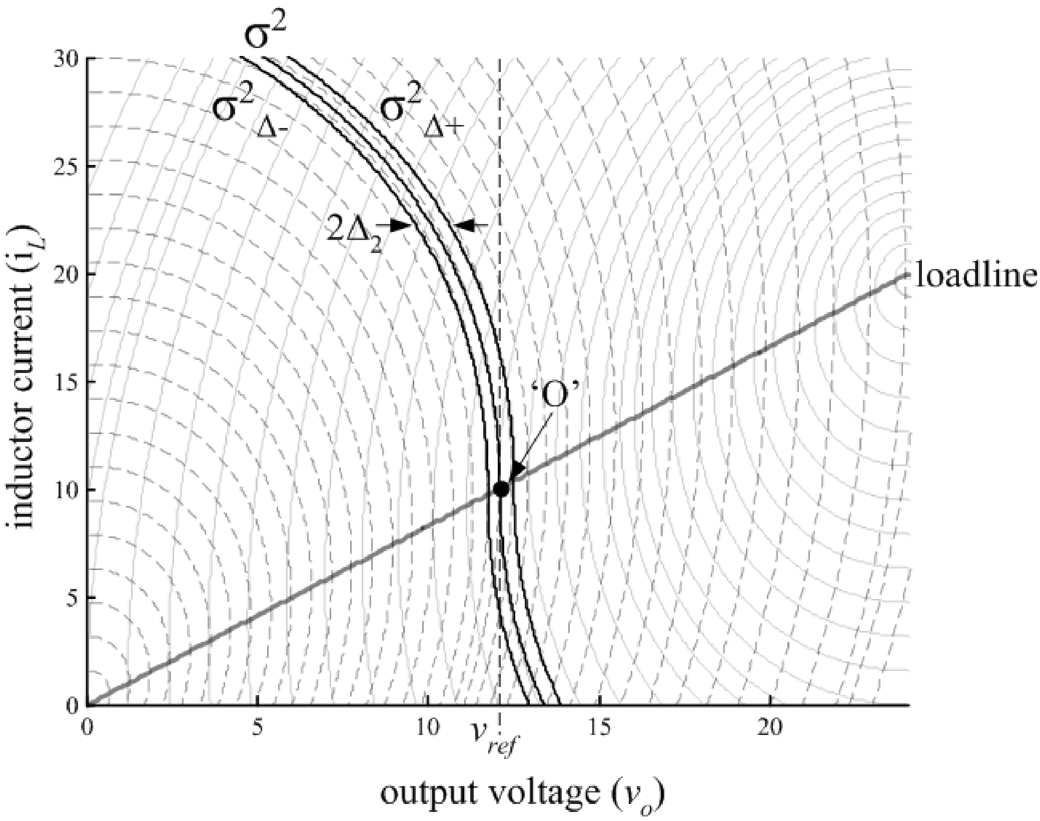

(b)

Fig. 3.2 Switching surfaces. (a) σ^1. (b) σ^2.

If c_1 is zero, σ^1 is a typical voltage hysteresis control. Dictation of S_1 is simply based on a comparison between v_o and a pair of reference values $v_{ref} + \Delta_1$ and $v_{ref} - \Delta_1$.

If c_1 is non-zero, a straight line will be formed and is popularly used in the sliding mode control. The value of c_1 defines the slope of the switching surface. A switching action takes place, when the trajectory touches $\sigma^1{}_{\Delta-}$ or $\sigma^1{}_{\Delta+}$. c_1 is chosen to attract the trajectories and to meet the sliding conditions. It is optimized by considering a particular operating point of interest, such as the steady-state behaviors and the startup profile. Detailed discussions can be found in [Greuel *et al* 1997] and [Nguyen and Lee 1995].

σ^2 is derived by estimating the trajectory movement after a switching action, resulting in a high state trajectory velocity along the surface, and thus accelerating the trajectory moving towards the operating point. It is defined as

$$\sigma^2{}_{\Delta+} = k_1 \left(i_L - \frac{v_o}{R} \right)^2 + \left(v_o - \left(v_{ref} + \Delta_2 \right) \right), \quad \left(i_L - \frac{v_o}{R} \right) > 0 \tag{3.6}$$

$$\sigma^2{}_{\Delta-} = -k_2 \left(i_L - \frac{v_o}{R} \right)^2 + \left(v_o - \left(v_{ref} - \Delta_2 \right) \right), \quad \left(i_L - \frac{v_o}{R} \right) < 0 \tag{3.7}$$

where k_1 and k_2 are constants.

As derived in *Chapter 2*, if r_C = 0, the ideal values of k_1 and k_2 are

$$\{k_1, k_2\} = \left\{ \frac{L}{2\,C\,v_{ref}}, \frac{L}{2\,C\,(v_i - v_{ref})} \right\} \tag{3.8}$$

3.2.3 Average Output Voltage and Output Ripple Voltage

As illustrated in Fig. 3.1(c), the average output voltage v_{avg} is defined as the mean of the minimum output voltage $v_{o,\min}$ and the maximum output voltage $v_{o,\max}$. That is,

$$v_{avg} = \frac{v_{o,\min} + v_{o,\max}}{2} \tag{3.9}$$

The output ripple voltage v_{ripple} is defined as

$$v_{ripple} = v_{o,\max} - v_{o,\min} \tag{3.10}$$

3.3 Steady-State Characteristics

At the steady state, the average capacitor current is zero. Thus, the average value of v_o, V_o, equals the average value of v_C, V_C, which is independent on the value of r_C. Thus, the value of V_o with $r_C \neq 0$ is the same as the value with $r_C = 0$. Fig. 3.3(a) and (b) show the steady-state trajectory with σ^1 and σ^2, respectively, with $r_C = 0$. The switch S_1 is on from t_0 to t_1 and is off from t_1 to t_2. Mathematically,

$$v_{o,2} = v_{o,0} \tag{3.11}$$

and

$$i_{L,2} = i_{L,0} \tag{3.12}$$

where $v_o(t_2) = v_{o,2}$, $v_o(t_0) = v_{o,0}$, $i_{L,2} = i_L(t_2)$, and $i_{L,0} = i_L(t_0)$.

By putting (3.11) and (3.12) into (3.2),

$$\left(i_{L,1} - \frac{v_{o,1}}{R}\right)^2 - \left(i_{L,0} - \frac{v_{o,0}}{R}\right)^2 = \frac{2\,C\,(v_i - v_{ref})}{L}\left(v_{o,1} - v_{o,0}\right) \tag{3.13}$$

where $i_{L,1} = i_L(t_1)$ and $v_o(t_1) = v_{o,1}$.

Similarly, by putting (3.11) and (3.12) into (3.3),

$$\left(i_{L,1} - \frac{v_{o,1}}{R}\right)^2 - \left(i_{L,0} - \frac{v_{o,0}}{R}\right)^2 = -\frac{2\,C\,v_{ref}}{L}\left(v_{o,1} - v_{o,0}\right) \tag{3.14}$$

It can be concluded from (3.13) and (3.14) that

$$v_{o,2} = v_{o,1} = v_{o,0} = v_o' \tag{3.15}$$

By substituting (3.15) into (3.2) and (3.3), it can be shown that

$$v_o' = \frac{L}{2\,C\,(v_i - v_{ref})}\left(\left(i_{L,1} - \frac{v_o'}{R}\right)^2 - \left(i_{L,0} - \frac{v_o'}{R}\right)^2\right) + v_o' \tag{3.16}$$

and
$$v_o' = -\frac{L}{2\,C\,v_{ref}}\left(\left(i_{L,0} - \frac{v_o'}{R}\right)^2 - \left(i_{L,1} - \frac{v_o'}{R}\right)^2\right) + v_o' \tag{3.17}$$

Thus,

$$\left(i_{L,0} - \frac{v_o'}{R}\right)^2 = \left(i_{L,1} - \frac{v_o'}{R}\right)^2 \tag{3.18}$$

Equations (3.11)-(3.18) are valid for both σ^1 and σ^2.

3.3.1 Average Output Voltage and Output Ripple Voltage

3.3.1.1 With σ^1

By putting (3.15) into (3.4) and (3.5), they give

$$\sigma^1{}_{\Delta+} = c_1\left(i_{L,1} - \frac{v_o'}{R}\right) + \left(v_o' - \left(v_{ref} + \Delta_1\right)\right) = 0 \tag{3.19}$$

$$\sigma^1{}_{\Delta-} = c_1\left(i_{L,0} - \frac{v_o'}{R}\right) + \left(v_o' - \left(v_{ref} - \Delta_1\right)\right) = 0 \tag{3.20}$$

By substituting (3.19) and (3.20) into (3.18), it gives

$$\left(\frac{v_o' - \left(v_{ref} - \Delta_1\right)}{c_1}\right)^2 = \left(\frac{v_o' - \left(v_{ref} + \Delta_1\right)}{c_1}\right)^2 \tag{3.21}$$

and thus,

$$v_o' = v_{ref} \tag{3.22}$$

By solving (3.19), (3.20), and (3.22) for $i_{L,0}$ and $i_{L,1}$, they give

$$i_{L,0} = \frac{v_{ref}}{R} - \frac{\Delta_1}{c_1} \tag{3.23}$$

$$i_{L,1} = \frac{v_{ref}}{R} + \frac{\Delta_1}{c_1} \tag{3.24}$$

$v_{o,\max}$ occurs on the off-state trajectory at t^* in Fig. 3.3(a) that $\dot{v}_o = i_C = 0$. Based on (3.3),

$$v_{o,\max} = v_{o,1} + \frac{L}{2\,C\,v_{ref}}\left(i_{L,1} - \frac{v_{o,1}}{R}\right)^2 \tag{3.25}$$

By using (3.15), (3.22) and (3.24), equation (3.25) can be expressed as

$$v_{o,\max} = v_{ref} + \frac{L}{2\,C\,v_{ref}}\left(\frac{\Delta_1}{c_1}\right)^2 \tag{3.26}$$

$v_{o,\min}$ occurs on the on-state trajectory at t^{**} in Fig. 3.3(a) that $\dot{v}_o = i_C = 0$. Based on (3.2),

$$v_{o,\min} = v_{o,0} - \frac{L}{2C\left(v_i - v_{ref}\right)}\left(i_{L,0} - \frac{v_{o,0}}{R}\right)^2 \tag{3.27}$$

By using (3.15), (3.22) and (3.23), equation (3.27) can be expressed as

$$v_{o,\min} = v_{ref} - \frac{L}{2\,C\left(v_i - v_{ref}\right)}\left(\frac{\Delta_1}{c_1}\right)^2 \tag{3.28}$$

By substituting (3.26) and (3.28) into (3.9), it can be shown that

$$v_{avg} = v_{ref} + \frac{L\,\Delta_1^{\,2}}{4\,C\,c_1^{\,2}}\,\frac{v_i - 2v_{ref}}{v_{ref}(v_i - v_{ref})} \tag{3.29}$$

Thus, the value of v_{avg} with σ^1 is dependent on Δ_1.

By putting (3.26) and (3.28) into (3.10), v_{ripple} is equal to

$$v_{ripple} = \frac{L\,\Delta_1^{\,2}}{2\,C\,c_1^{\,2}}\,\frac{v_i}{v_{ref}\;(v_i - v_{ref})} \tag{3.30}$$

The above analysis is valid for $i_L(t_0) = i_L(t_2) \geq 0$. Thus, by using (3.23), the converter is at the verge of CCM and DCM, when

$$R = R_{crit}^{<1>} = \frac{v_{ref}\;c_1}{\Delta_1} \tag{3.31}$$

where $R_{crit}^{<1>}$ is the critical load resistance. If $R < R_{crit}^{<1>}$, the converter is in CCM.

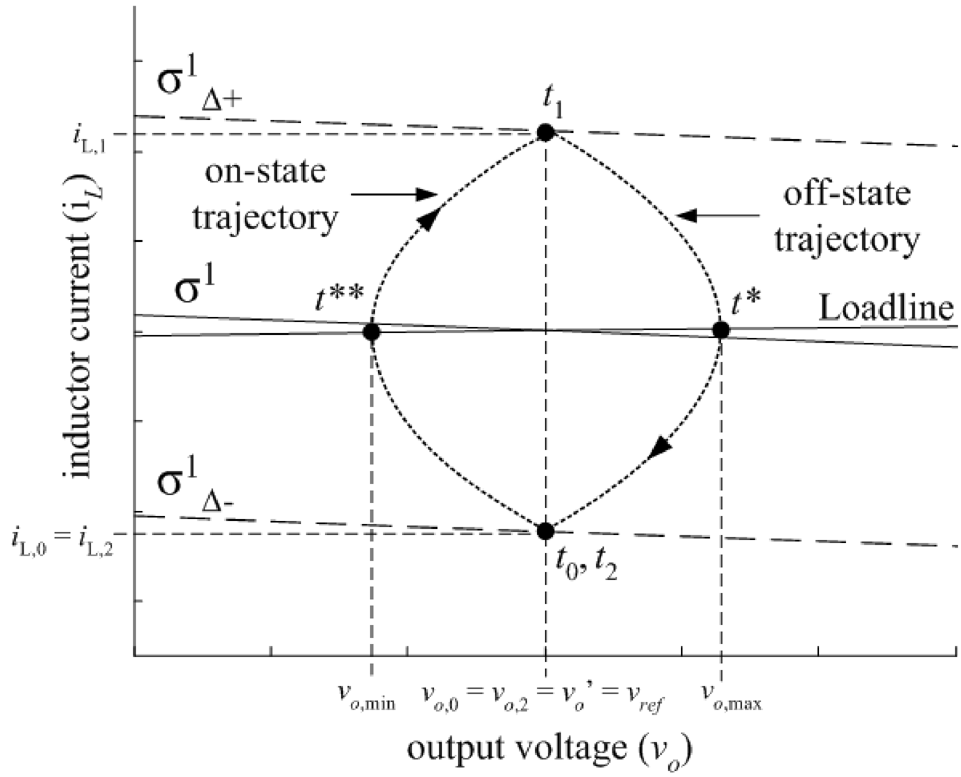

(a)

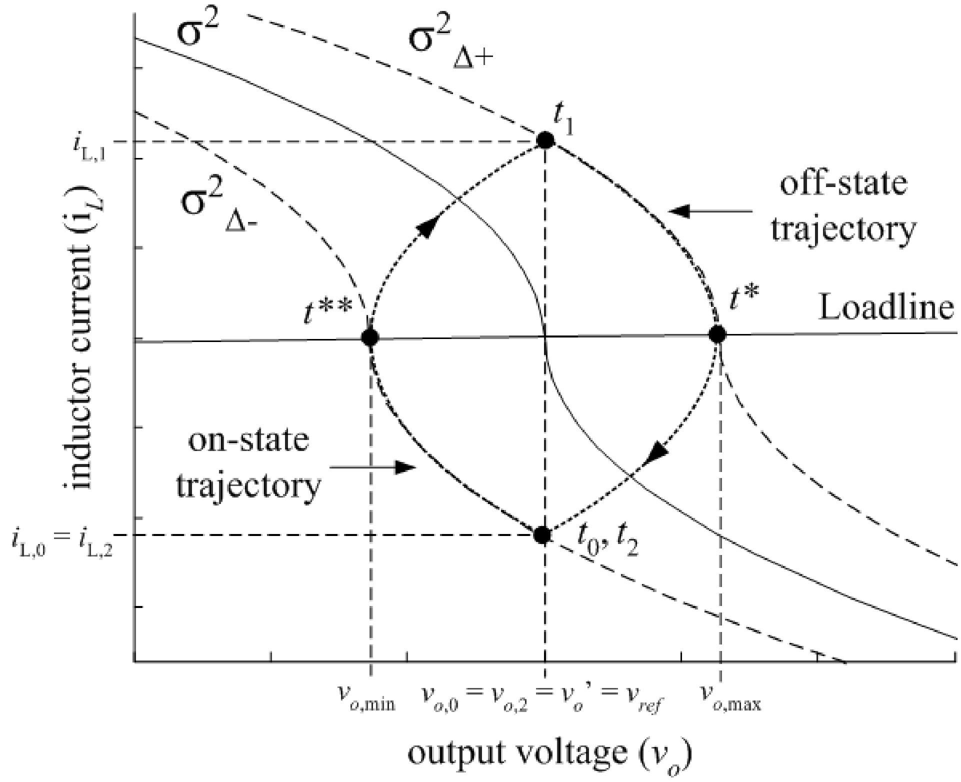

(b)

Fig. 3.3 State trajectory of the converter operating in CCM. (a) With σ^1. (b) With σ^2.

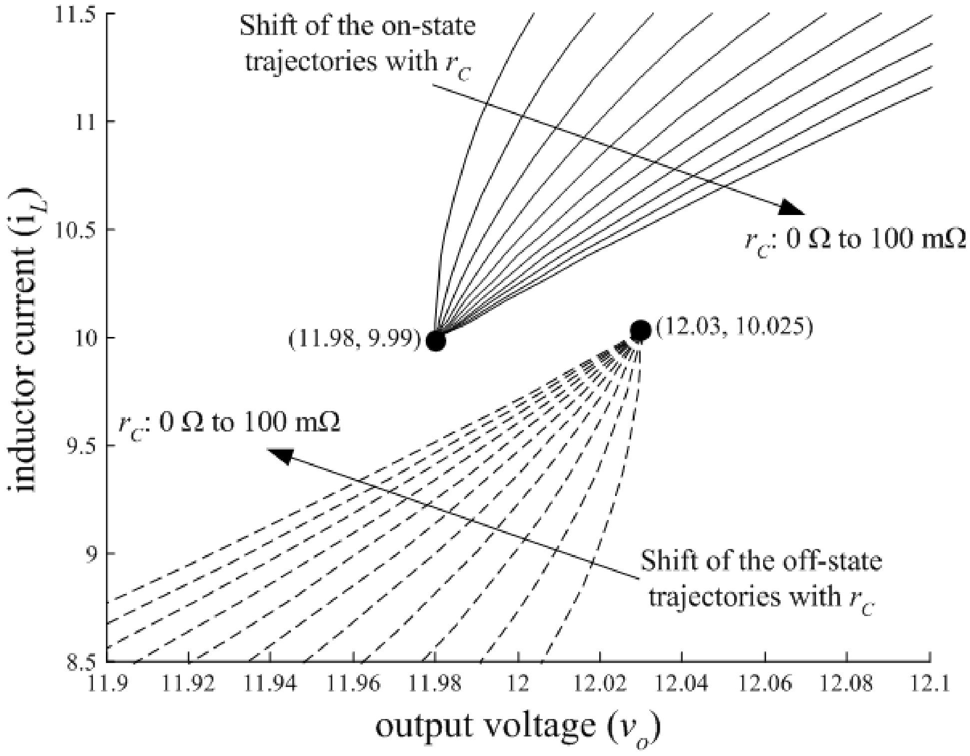

Shift of the on-state trajectories with r_C
r_C: 0 Ω to 100 mΩ
(11.98, 9.99)
(12.03, 10.025)
r_C: 0 Ω to 100 mΩ
Shift of the off-state trajectories with r_C
inductor current (i_L)
output voltage (v_o)

(a)

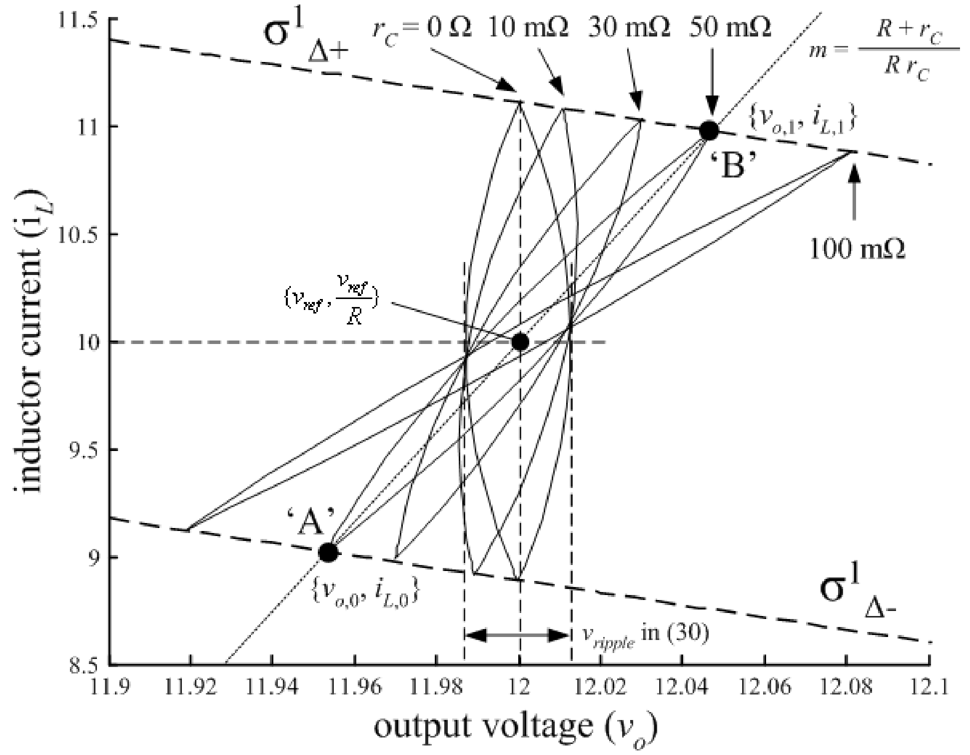

$\sigma^1_{\Delta+}$
r_C = 0 Ω 10 mΩ 30 mΩ 50 mΩ
$m = \frac{R + r_C}{R\, r_C}$
$\{v_{o,1}, i_{L,1}\}$
'B'
100 mΩ
$\{v_{ref}, \frac{v_{ref}}{R}\}$
'A'
$\{v_{o,0}, i_{L,0}\}$
$\sigma^1_{\Delta-}$
v_{ripple} in (30)
inductor current (i_L)
output voltage (v_o)

(b)

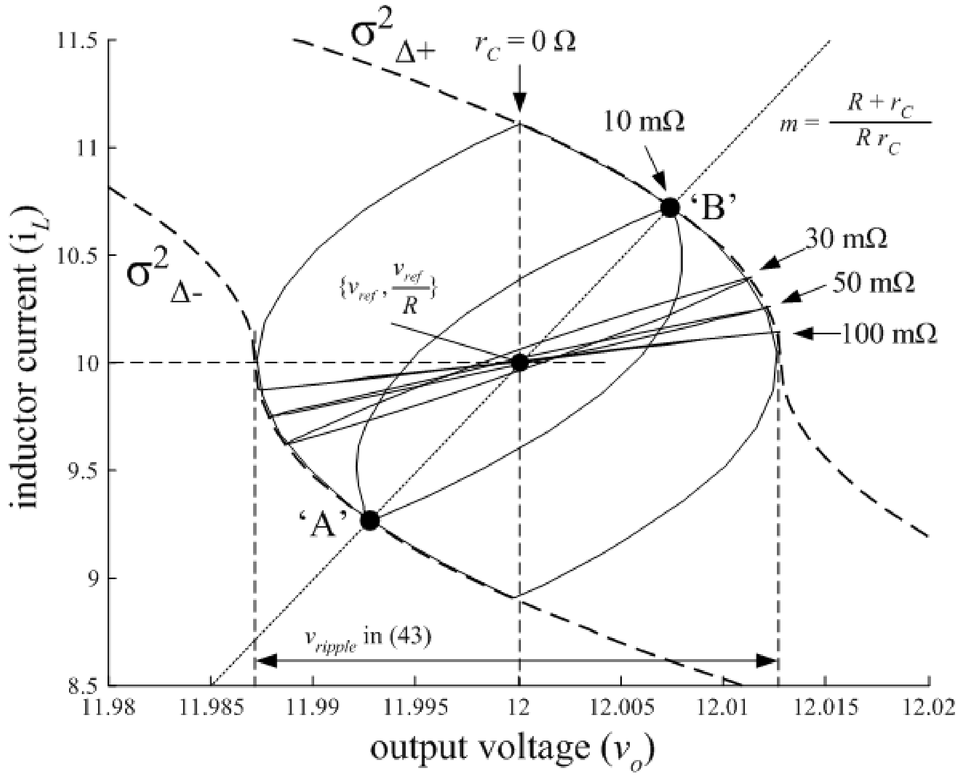

(c)

Fig. 3.4 Shift of steady-state trajectories against r_C. (a) on-state and off-state trajectories. (b) Converter trajectories with σ^1. (c) Converter trajectories with σ^2.

Table 3.1 Component values of the buck converter

Parameter	Value
v_i	24 V
v_{ref}	12 V
L	100 μH
C	400 μF
R	1.2 Ω
c_1	0.2702
$\{k_1, k_2\}$	{0.0104, 0.0104}

If r_C is nonzero, the on- and off-state trajectories vary with r_C. Fig. 3.4(a) shows the shifts of the on-state and off-state trajectories with different values of r_C. The component values are based on the ones tabulated in Table 3.1. Fig. 3.4(b) shows the steady-state trajectories with different values of r_C. By using (3.2) and (3.3), a straight line of slope *m* connecting the two switching points at t_0 (point 'A') and t_1 (point 'B') on σ^1 can be drawn. It can be shown that

$$\frac{i_{L,1} - i_{L,0}}{v_{o,1} - v_{o,0}} = \frac{R + r_C}{R\, r_C} = m \tag{3.32}$$

As $r_C \to \infty$, $m = 1/R$. The following straight equation can be derived

$$i_L = \frac{v_o}{R} \tag{3.33}$$

By solving (3.33) with (3.4) and (3.5) for the intersection points, the maximum value of v_{ripple} is

$$v_{ripple} = 2\,\Delta_1 \tag{3.34}$$

3.3.1.2 With σ^2

Fig. 3.4(c) shows the steady-state trajectories with different values of r_C. Similar to the methodology used above, by putting (3.15) into (3.6) and (3.7) with r_C = 0, they give

$$\sigma^2{}_{\Delta+} = k_1\left(i_{L,1} - \frac{v_o'}{R}\right)^2 + \left(v_o' - \left(v_{ref} + \Delta_2\right)\right) = 0 \tag{3.35}$$

$$\sigma^2{}_{\Delta-} = -k_2\left(i_{L,0} - \frac{v_o'}{R}\right)^2 + \left(v_o' - \left(v_{ref} - \Delta_2\right)\right) = 0 \tag{3.36}$$

Thus, by substituting (3.35) and (3.36) into (3.18), it gives

$$v_o' = v_{ref} - \frac{k_1 - k_2}{k_1 + k_2}\,\Delta_2 \tag{3.37}$$

By solving (3.35), (3.36), and (3.37) for $i_{L,0}$ and $i_{L,1}$, they give

$$i_{L,0} = \left(v_{ref} - \frac{k_1 - k_2}{k_1 + k_2} \Delta_2 \right) \frac{1}{R} - \sqrt{\frac{2\Delta_2}{k_1 + k_2}} \tag{3.38}$$

$$i_{L,1} = \left(v_{ref} - \frac{k_1 - k_2}{k_1 + k_2} \Delta_2 \right) \frac{1}{R} + \sqrt{\frac{2\Delta_2}{k_1 + k_2}} \tag{3.39}$$

By putting (3.15), (3.37), and (3.39) into (3.25), $v_{o,\max}$ occurs at t^* in Fig. 3.3(b) and is expressed as

$$v_{o,\max} = v_{ref} - \left(\frac{k_1 - k_2}{k_1 + k_2} - \frac{L}{C v_{ref}} \frac{1}{k_1 + k_2} \right) \Delta_2 \tag{3.40}$$

By putting (3.15), (3.37) and (3.38) into (3.27), $v_{o,\min}$ occurs at t^{**} in Fig. 3.3(b) and is expressed as

$$v_{o,\min} = v_{ref} - \left(\frac{k_1 - k_2}{k_1 + k_2} + \frac{L}{C\left(v_i - v_{ref}\right)} \frac{1}{k_1 + k_2} \right) \Delta_2 \tag{3.41}$$

Again, by substituting (3.40) and (3.41) into (3.9), v_{avg} can be expressed as

$$v_{avg} = v_{ref} + \frac{\dfrac{L}{2C v_{ref}} - \dfrac{L}{2C\left(v_i - v_{ref}\right)} - \left(k_1 - k_2\right)}{k_1 + k_2} \Delta_2 \tag{3.42}$$

By substituting (3.40) and (3.41) into (3.10),

$$v_{ripple} = \frac{L\,\Delta_2}{C\left(k_1 + k_2\right)} \frac{v_i}{v_{ref}\left(v_i - v_{ref}\right)} \tag{3.43}$$

With the ideal values of k_1 and k_2 in (3.8),

$$v_{avg} = v_{ref} \tag{3.44}$$

$$v_{ripple} = 2\Delta_2 \tag{3.45}$$

The above analysis is valid for $i_L(t_0) \geq 0$. Thus, by using (3.38), the converter is at the verge of CCM when

$$R \le R_{crit}^{<2>} = \frac{v_{ref} - \frac{k_1 - k_2}{k_1 + k_2}\Delta_2}{\sqrt{\frac{2\Delta_2}{k_1 + k_2}}} \tag{3.46}$$

where $R_{crit}^{<2>}$ is the critical load resistance. Again, if $R <$ $R_{crit}^{<2>}$, the converter is in CCM.

For $r_C \neq 0$, equation (3.32) is still valid. By solving (3.6), (3.7), and (3.33) for the intersection points, the maximum ripple with σ^2 is

$$v_{ripple} = 2\,\Delta_2, \quad \text{for } r_C \to \infty \tag{3.47}$$

3.3.2 Switching Frequency

As discussed in [Mohan *et al* 2003], the switching period T_S and the switching frequency f_S are

$$T_S = \frac{L}{v_{ref}(1-d)}\Delta I_L = \frac{L\,v_i}{v_{ref}(v_i - v_{ref})}\Delta I_L \tag{3.48}$$

$$f_S = \frac{1}{T_S} = \frac{v_{ref}(v_i - v_{ref})}{L\,v_i}\frac{1}{i_{L,1} - i_{L,0}} \tag{3.49}$$

where d (= v_{ref} / v_i) is the duty cycle of S_1 and ΔI_L is the inductor ripple current.

3.3.2.1 With σ^1

By using (3.2), (3.3), (3.4), (3.5) and (3.32), it can be shown that

$$\Delta I_L = i_{L,1} - i_{L,0} = \frac{2\,\Delta_1 (R + r_C)}{R(c_1 + r_C)} \tag{3.50}$$

By substituting (3.50) into (3.49), it can be shown that

$$f_S = \frac{v_{ref}(v_i - v_{ref})}{L\,v_i\left(1 + \frac{r_C}{R}\right)}\frac{c_1 + r_C}{2\Delta_1} \tag{3.51}$$

3.3.2.2 With σ^2

By using (3.2), (3.3), (3.6), (3.7), (3.32) and assuming that the straight line connecting points 'A' and 'B' is passing through the point $\left\{ v_{ref}, \frac{v_{ref}}{R} \right\}$ in Fig. 3.4(c), it can be shown that

$$\Delta I_L = i_{L,1} - i_{L,0} = \frac{R + r_C}{2R} \left(\frac{\sqrt{4k_1\Delta_2 + r_C^{\;2}} - r_C}{k_1} + \frac{\sqrt{4k_2\Delta_2 + r_C^{\;2}} - r_C}{k_2} \right) \tag{3.52}$$

By substituting (3.52) into (3.48), it can be shown that

$$f_S = \frac{v_{ref}\left(v_i - v_{ref}\right)}{L v_i \left(1 + \frac{r_C}{R}\right)} \frac{2}{\left(\frac{\sqrt{4k_1\Delta_2 + r_C^{\;2}} - r_C}{k_1} + \frac{\sqrt{4k_2\Delta_2 + r_C^{\;2}} - r_C}{k_2} \right)} \tag{3.53}$$

3.4 Output Voltage Drift with Variations of Component Values

As shown in (3.29) and (3.42), v_{avg} is dependent on v_i, v_{ref}, L, C, and c_1 in σ^1, and k_1 and k_2 in σ^2. v_{avg} will be drifted, if the above parameters are subject to variations. Assume that

$$v_i = v_{i,N}\ (1 + \delta_1) \tag{3.54}$$

$$L = L_N\ (1 + \delta_2) \tag{3.55}$$

$$C = C_N\ (1 + \delta_3) \tag{3.56}$$

where $v_{i,N}$, L_N, and C_N are the nominal values of v_i, L, and C, respectively, δ_1, δ_2, and δ_3 are the fractional variations of v_i, L, and C, respectively.

3.4.1 With σ^1

By substituting (3.54)-(3.56) into (3.29), the drift of v_{avg}, Δv_{avg}, from its nominal value is

$$\Delta v_{avg} = v_{avg}(v_i\,, L\,, C) - v_{avg}(v_{i,N}\,, L_N\,, C_N)$$
$$= \left(\frac{1+\delta_2}{1+\delta_3} \cdot \left(1 - \frac{D_N}{1 - D_N + \delta_1} \right) \cdot (1 - D_N) + 2\,D_N - 1 \right) \frac{L_N\,\Delta_1^{\;2}}{4\,C_N\,c_1^{\;2}\,v_{ref}\,(1 - D_N)} \quad (3.57)$$

where $D_N = \dfrac{v_{ref}}{v_{i,N}}$ is nominal duty cycle.

If $|\delta_1|$, $|\delta_2|$, and $|\delta_3|$ are less than unity, the following expressions are used to simplify (3.57),

$$\frac{1}{1+\delta} = 1 - \delta + \delta^2 - \ldots \quad (3.58)$$

$$\frac{1}{1 - D_N + \delta} = \frac{1}{1 - D_N} + \frac{1}{(1 - D_N)(D_N - 1)}\,\delta + \frac{1}{(1 - D_N)(D_N - 1)^2}\,\delta^2 + \ldots \quad (3.59)$$

Equation (3.57) becomes

$$\Delta v_{avg} = \left(\left(\frac{D_N}{1 - D_N} \right) \delta_1 + (1 - 2\,D_N)\,\delta_2 + (2\,D_N - 1)\delta_3 + \ldots \right) \frac{L_N\,\Delta_1^{\;2}}{4\,C_N\,c_1^{\;2}\,v_{ref}\,(1 - D_N)} \quad (3.60)$$

3.4.2 *With* σ^2

By substituting (3.54)-(3.56) into (3.42), the drift of v_{avg}, Δv_{avg}, from its nominal value is

$$\Delta v_{avg} = \left(\left(\frac{D_N}{1 - D_N} \right) \delta_1 + (1 - 2\,D_N)\,\delta_2 + (2\,D_N - 1)\delta_3 + \ldots \right) \Delta_2 \quad (3.61)$$

3.5 Large-Signal Characteristics

Points along $\sigma = 0$ can be classified into refractive, reflective, and rejective modes. The dynamics of the system will exhibit differently in these regions [Krein 1998]. For the sake of simplicity in the analysis, characteristics with $r_C = 0$ is firstly investigated. For nonzero r_C, the characteristics will be studied qualitatively thereafter.

3.5.1 With σ^1

The transition boundaries are obtained by differentiating (3.4) with $\Delta_1 = 0$ that

$$\left.\frac{d i_L}{d v_o}\right|_{on,off} = \frac{1}{R} + \frac{i_L - \frac{v_o}{R}}{v_o - v_{ref}} \tag{3.62}$$

Detailed derivation of (3.62) is given in the *Appendix C*.

The expression at the left-hand-side can be derived by using the state equations in (3.1). Based on (3.62), the transition boundary with S_1 off is

$$\begin{aligned}&\frac{L}{C}\left(i_L - \frac{v_o}{R}\right)\left(\frac{r_C C}{L}(-r_C i_L - v_o) + i_L - \frac{v_o}{R}\right) - (-r_C i_L - v_o)(v_o - v_{ref})\\ &+\frac{L}{RC}\left(\frac{r_C C}{L}(-r_C i_L - v_o) + i_L - \frac{v_o}{R}\right)(v_o - v_{ref}) = 0\end{aligned} \tag{3.63}$$

and the transition boundary with S_1 on is

$$\begin{aligned}&\frac{L}{C}\left(i_L - \frac{v_o}{R}\right)\left(\frac{r_C C}{L}(-r_C i_L + v_i - v_o) + i_L - \frac{v_o}{R}\right) - (-r_C i_L + v_i - v_o)(v_o - v_{ref})\\ &+\frac{L}{RC}\left(\frac{r_C C}{L}(-r_C i_L + v_i - v_o) + i_L - \frac{v_o}{R}\right)(v_o - v_{ref}) = 0\end{aligned} \tag{3.64}$$

Detailed proofs of (3.63) and (3.64) are given in the *Appendix C*.

3.5.1.1 Off-state transition boundary

The intersection points of the switching boundary σ^1 and the transition boundary with S_1 off are determined by solving (3.4) with $\Delta_1 = 0$ and (3.63) with $r_C = 0$. Two possible solutions of $[i_{L,off}, v_{o,off}]$ are

$$[i^1_{L,off}, v^1_{o,off}] = \left[\frac{v_{ref}}{R}, v_{ref}\right] \tag{3.65}$$

$$[i^2_{L,off}, v^2_{o,off}] = \left[\frac{L v_{ref}(R - c_1) + C R^2 v_{ref} c_1}{\left(L(R - c_1) + C R c_1^{\,2}\right)R}, \frac{L v_{ref}(R - c_1)}{L(R - c_1) + C R c_1^{\,2}}\right] \tag{3.66}$$

$[i^1_{L,off}, v^1_{o,off}]$ always occurs. $[i^2_{L,off}, v^2_{o,off}]$ will have real solution for

$$R > c_1 > 0 \tag{3.67}$$

Derivation of (3.67) is given in the *Appendix C*.

3.5.1.2 On-state transition boundary

The intersection points of σ^1 and the transition boundary with S_1 on are determined by solving (3.4) with $\Delta_1 = 0$ and (3.63) with $r_C = 0$. Two possible solutions of $[i_{L,on}, v_{o,on}]$ are

$$[i_{L,on}^1, v_{o,on}^1] = \left[\frac{v_{ref}}{R}, v_{ref}\right] \tag{3.68}$$

$$[i_{L,on}^2, v_{o,on}^2] = \left[\frac{Lv_{ref}(R-c_1) + CR^2 v_{ref} c_1 + CRv_i c_1 (c_1 - R)}{\left(L(R-c_1) + CRc_1^{\ 2}\right)R}, \frac{Lv_{ref}(R-c_1) + CRv_i c_1^{\ 2}}{L(R-c_1) + CRc_1^{\ 2}}\right] \tag{3.69}$$

$[i_{L,on}^1, v_{o,on}^1]$ always occurs. $[i_{L,on}^2, v_{o,on}^2]$ will have real solution for

$$R > c_1 > 0 \tag{3.70}$$

Derivation of (3.70) is given in the *Appendix C*.

Fig. 3.5(a) combines the transition boundaries of (3.63) and (3.64) with σ^1 when $r_C = 0$. When the trajectory is in the reflective region, the converter is in the sliding condition. As illustrated in Fig. 3.5(b), the transition boundaries (3.63) and (3.64) will shift with nonzero r_C. The implication is that the region of sliding will be lengthened, as r_C increases. The value of c_1 that makes the converter go through the possible operating modes are tabulated in Table 3.2.1.

3.5.2 With σ^2

The transition boundaries are obtained by differentiating (3.6) with $\Delta_2 = 0$ that

$$\left.\frac{d\,i_L}{d\,v_o}\right|_{on,off} = \frac{1}{R} + \frac{1}{2}\,\frac{i_L - \frac{v_C}{R}}{v_C - v_{ref}} \tag{3.71}$$

Derivation of (3.71) is given in the *Appendix C*.

The expression at the left-hand-side can be derived by using the state equations in (3.1). Based on (3.71), (B.12), and (B.13) in the *Appendix C*, the transition boundary with S_1 off is

$$\begin{aligned}&\frac{L}{2C}\left(i_L-\frac{v_o}{R}\right)\left(\frac{r_C C}{L}\left(-r_C i_L-v_o\right)+i_L-\frac{v_o}{R}\right)-\left(-r_C i_L-v_o\right)\left(v_o-v_{ref}\right)\\&+\frac{L}{RC}\left(\frac{r_C C}{L}\left(-r_C i_L-v_o\right)+i_L-\frac{v_o}{R}\right)\left(v_o-v_{ref}\right)=0\end{aligned} \tag{3.72}$$

and the transition boundary with S_1 on is

$$\begin{aligned}&\frac{L}{2C}\left(i_L-\frac{v_o}{R}\right)\left(\frac{r_C C}{L}\left(-r_C i_L+v_i-v_o\right)+i_L-\frac{v_o}{R}\right)-\left(-r_C i_L+v_i-v_o\right)\left(v_o-v_{ref}\right)\\&+\frac{L}{RC}\left(\frac{r_C C}{L}\left(-r_C i_L+v_i-v_o\right)+i_L-\frac{v_o}{R}\right)\left(v_o-v_{ref}\right)=0\end{aligned} \tag{3.73}$$

Fig. 3.6(a) combines the transition boundaries of (3.72) and (3.73) when r_C = 0. Ideal σ^2 is close to σ^i and should be along the boundaries between the reflective and refractive regions. However, k_1 and k_2 in (3.8) should depend on the circuit variables. They are taken to be the values with nominal v_i, *L*, and *C*. These make the converter possibly go through different operating regions before settling at the operating point. This phenomenon can be observed by considering the number of intersection points between σ^2 of (3.6) and (3.7) with $\Delta_2 = 0$ and the transition boundaries of (3.72) and (3.73).

3.5.2.1 Off-state transition boundary

The intersection points of the switching boundary σ^2 and the transition boundary with S_1 off are determined by solving (3.6) with $\Delta_2 = 0$ and (3.71) with r_C = 0. Three possible solutions of $[i_{L,off}, v_{o,off}]$ are

$$[i_{L,off}^{1}, v_{o,off}^{1}] = \left[\frac{v_{ref}}{R}, v_{ref} \right] \tag{3.74}$$

$$[i_{L,off}^{2}, v_{o,off}^{2}] = \left[\frac{\alpha_1 L}{8C^2 R^3 k_1} - \frac{\alpha_1}{8CRk_1} + \frac{R}{2k_1}, \frac{\alpha_1 L}{8C^2 R^2 k_1} \right] \tag{3.75}$$

$$[i_{L,off}^{3}, v_{o,off}^{3}] = \left[\frac{\beta_1 L}{8C^2 R^3 k_1} - \frac{\beta_1}{8CRk_1} + \frac{R}{2k_1}, \frac{\beta_1 L}{8C^2 R^2 k_1} \right] \tag{3.76}$$

where $\alpha_1 = \Phi_1 + 4\sqrt{\xi_1}$, $\beta_1 = \Phi_1 - 4\sqrt{\xi_1}$, $\Phi_1 = -4(L - CR^2)$, and

$\xi_1 = L^2 - 2CLR^2 + 4C^2 R^2 k_1 v_{ref}$.

$[i_{L,off}^{1}, v_{o,off}^{1}]$ always occurs. $[i_{L,off}^{2}, v_{o,off}^{2}]$ will have real solutions for

$$\frac{L}{2Cv_{ref}} > k_1 \geq \frac{R^2}{4v_{ref}} \quad \text{, if } L - CR^2 \geq 0 \tag{3.77}$$

and

$$\frac{L}{2Cv_{ref}} > k_1 \geq \frac{2CLR^2 - L^2}{4C^2 R^2 v_{ref}} \quad \text{, if } L - CR^2 < 0 \tag{3.78}$$

$[i_{L,off}^{3}, v_{o,off}^{3}]$ has

$$\text{no real solution} \quad \text{, if } L - CR^2 \geq 0 \tag{3.79}$$

and a real solution for

$$\frac{R^2}{4v_{ref}} \geq k_1 > \frac{2CLR^2 - L^2}{4C^2 R^2 v_{ref}} \quad \text{, if } L - CR^2 < 0 \tag{3.80}$$

Proofs of (3.77)-(3.80) are given in the *Appendix C*. By using (3.77)-(3.80), the values of k_1 that make the converter go through the possible operating modes are tabulated in Table 3.2.2.

3.5.2.2 On-state transition boundary

The intersection points of the switching boundary σ^2 and the transition boundary with S_1 on are determined by solving (3.7) with $\Delta_2 = 0$ and (3.72) with $r_C = 0$.

Three possible solutions of $[i_{L,on}, v_{o,on}]$ are

$$[i_{L,on}^1, v_{o,on}^1] = \left[\frac{v_{ref}}{R}, v_{ref}\right] \tag{3.81}$$

$$[i_{L,on}^2, v_{o,on}^2] = \left[\frac{\alpha_2 L}{8C^2R^3k_2} - \frac{\alpha_2}{8CRk_2} + \frac{CRv_i}{L} - \frac{R}{2k_2}, \frac{\alpha_2 L}{8C^2R^2k_2}\right] \tag{3.82}$$

$$[i_{L,on}^3, v_{o,on}^3] = \left[\frac{\beta_2 L}{8C^2R^3k_2} - \frac{\beta_2}{8CRk_2} + \frac{CRv_i}{L} - \frac{R}{2k_2}, \frac{\beta_2 L}{8C^2R^2k_2}\right] \tag{3.83}$$

where $\alpha_2 = \Phi_2 - 4\sqrt{\xi_2}$, $\beta_2 = \Phi_2 + 4\sqrt{\xi_2}$, $\Phi_2 = \dfrac{8C^2R^2v_ik_2}{L} + 4\left(L - CR^2\right)$, and $\xi_2 = L^2 - 2CLR^2 + 4C^2R^2k_2\left(v_i - v_{ref}\right)$.

$[i_{L,on}^1, v_{o,on}^1]$ always occurs. $[i_{L,on}^2, v_{o,on}^2]$ will have real solutions for

$$\frac{L}{2C\left(v_i - v_{ref}\right)} > k_2 \geq \frac{R^2}{4\left(v_i - v_{ref}\right)} \quad \text{, if } L - CR^2 \geq 0 \tag{3.84}$$

and

$$\frac{L}{2C\left(v_i - v_{ref}\right)} > k_2 \geq \frac{2CLR^2 - L^2}{4C^2R^2\left(v_i - v_{ref}\right)} \quad \text{, if } L - CR^2 < 0 \tag{3.85}$$

$[i_{L,on}^3, v_{o,on}^3]$ has

$$\text{no real solution,} \quad \text{if } L - CR^2 \geq 0 \tag{3.86}$$

and a real solution for

$$\frac{R^2}{4(v_i - v_{ref})} \geq k_2 > \frac{2CLR^2 - L^2}{4C^2R^2(v_i - v_{ref})}, \quad \text{if } L - CR^2 < 0 \tag{3.87}$$

Derivations of (3.84)-(3.87) are given in the *Appendix C*. By using (3.84)-(3.87), the value of k_2 that makes the converter go through the possible operating modes are tabulated in Table 3.2.2.

Fig. 3.7 illustrates the four possible cases shown in Table 3.2.2 on the phase plane. Fig. 3.8 shows the simulated time-domain waveforms of v_o, i_L, and the gate signal to S, v_g, corresponding to the four cases. In order to illustrate clearly the occurrences of different intersection points between the transition boundary and the switching surface, another set of component values tabulated in Table 3.3 is used. Generally, when the trajectory moves along the switching surface in the reflective region, the behavior is similar to the sliding-mode control that the switching frequency will be very high. When the switching surface is in the refractive region, the state will move around the operating point.

In Fig. 3.7(a), the switching surface and the transition boundaries have one intersection point (i.e., the operating point) that the switching surface is in the refractive region only. As shown in Fig. 3.8(a), the converter takes several switching cycles before settling at the operating point.

In Fig. 3.7(b), the switching surface and the transition boundaries have one intersection point (i.e., the operating point) again that the switching surface is in the reflective region only. As shown in Fig. 3.8(b), once the trajectory touches the switching surface at t_1, the switching frequency is very high, until the converter is sufficiently close to the operating point.

In Fig. 3.7(c), the switching surface and the transition boundaries have two intersection points that the switching surface can be in the reflective or refractive regions. As depicted in Fig. 3.8(c), once the trajectory touches the switching surface at t_1, the switching frequency is very high. Until t_n, the switching surface is in the refractive region. The trajectory moves around the operating point.

In Fig. 3.7(d), the switching surface and the transition boundaries have three intersection points. An initial condition of $i_L = 0.84$ A and $v_o = 0$ V is taken. As shown in Fig. 3.8(d), the switching surface is in the refractive region from t_1 to t_2. From t_2 to t_n, the switching surface is in the reflective region, in which the switching frequency is very high. From t_n to t_{n+1}, the switching surface is in the refractive region that the trajectory moves around the operating point.

As illustrated in Fig. 3.6(b), the operating characteristics vary, as r_C increases. The converter will operate more in the reflective region – sliding region.

Table 3.2.1 Intersections between switching surface and transition boundaries of σ^1

Case	No. of inter-section	Operation Mode	c_1 and off-state transition boundary	c_1 and on-state transition boundary
I	1	Refractive Region only	$c_1 = 0$	$c_1 = 0$
II	1	Reflective Region only	$c_1 > R$	$c_1 > R$
III	2	Pass Two Regions	$R > c_1 > 0$	$R > c_1 > 0$
IV	3	Pass Three Regions	No solution	No solution

Table 3.2.2(a) Intersections between switching surface and transition boundaries of σ^2

			k_1 and off-state transition boundary	
Case	No. of intersections	Operation Mode	If $L - CR^2 < 0$	If $L - CR^2 \geq 0$
I	1	Refractive region	$k_1 < \dfrac{2CR^2L - L^2}{4C^2R^2v_{ref}}$	$k_1 < \dfrac{R^2}{4v_{ref}}$
II	1	Reflective region	$k_1 \geq \max\left\{\dfrac{L}{2Cv_{ref}}, \dfrac{R^2}{4v_{ref}}\right\}$	$k_1 \geq \dfrac{L}{2Cv_{ref}}$
III	2	Pass two regions	$\max\left\{\dfrac{L}{2Cv_{ref}}, \dfrac{R^2}{4v_{ref}}\right\} > k_1 \geq \min\left\{\dfrac{L}{2Cv_{ref}}, \dfrac{R^2}{4v_{ref}}\right\}$	$\dfrac{L}{2Cv_{ref}} > k_1 \geq \dfrac{R^2}{4v_{ref}}$
IV	3	Pass three regions	$\min\left\{\dfrac{L}{2Cv_{ref}}, \dfrac{R^2}{4v_{ref}}\right\} > k_1 \geq \dfrac{2CR^2L - L^2}{4C^2R^2v_{ref}}$	No solution

Table 3.2.2(b) Intersections between switching surface and transition boundaries of σ^2

			k_2 and on-state transition boundary	
Case	No. of intersections	Operation Mode	If $L - CR^2 < 0$	If $L - CR^2 \geq 0$
I	1	Refractive region	$k_2 < \dfrac{2CR^2L - L^2}{4C^2R^2(v_i - v_{ref})}$	$k_1 < \dfrac{R^2}{4(v_i - v_{ref})}$
II	1	Reflective region	$k_1 \geq \max\left\{\dfrac{L}{2C(v_i - v_{ref})}, \dfrac{R^2}{4(v_i - v_{ref})}\right\}$	$k_1 \geq \dfrac{L}{2C(v_i - v_{ref})}$
III	2	Pass two regions	$\max\left\{\dfrac{L}{2C(v_i - v_{ref})}, \dfrac{R^2}{4(v_i - v_{ref})}\right\} > k_1 \geq \min\left\{\dfrac{L}{2C(v_i - v_{ref})}, \dfrac{R^2}{4(v_i - v_{ref})}\right\}$	$\dfrac{L}{2C(v_i - v_{ref})} > k_1 \geq \dfrac{R^2}{4(v_i - v_{ref})}$
IV	3	Pass three regions	$\min\left\{\dfrac{L}{2C(v_i - v_{ref})}, \dfrac{R^2}{4(v_i - v_{ref})}\right\} > k_1 \geq \dfrac{2CR^2L - L^2}{4C^2R^2(v_i - v_{ref})}$	No solution

Table 3.3 Component values of the buck converters

Parameter	Value
v_i	1 V
v_{ref}	0.5 V
L	1 H
C	1 F
R	1.2 Ω

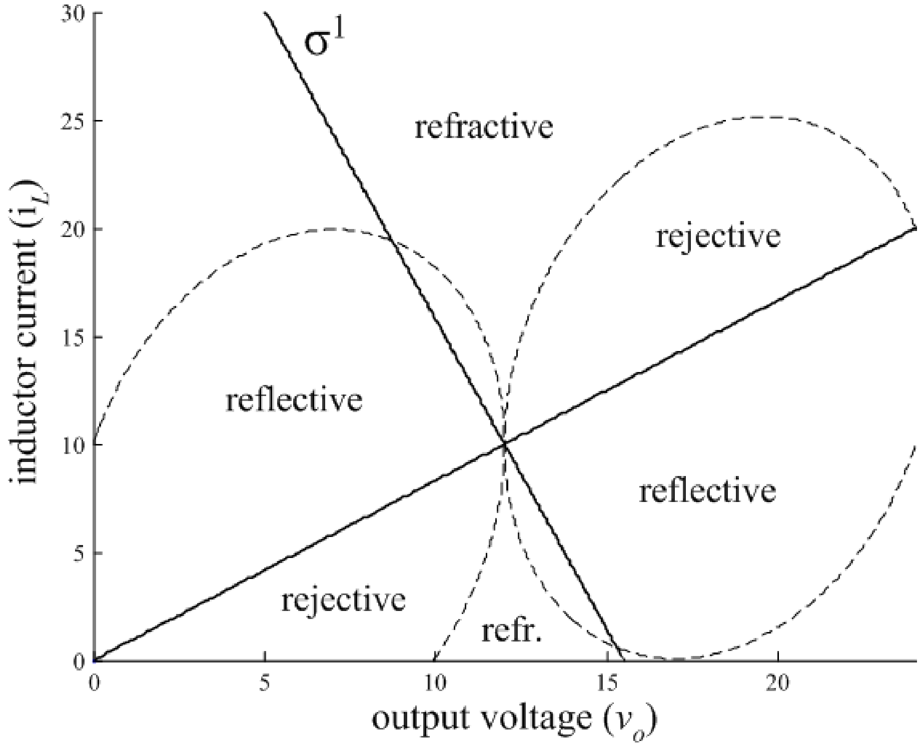

(a)

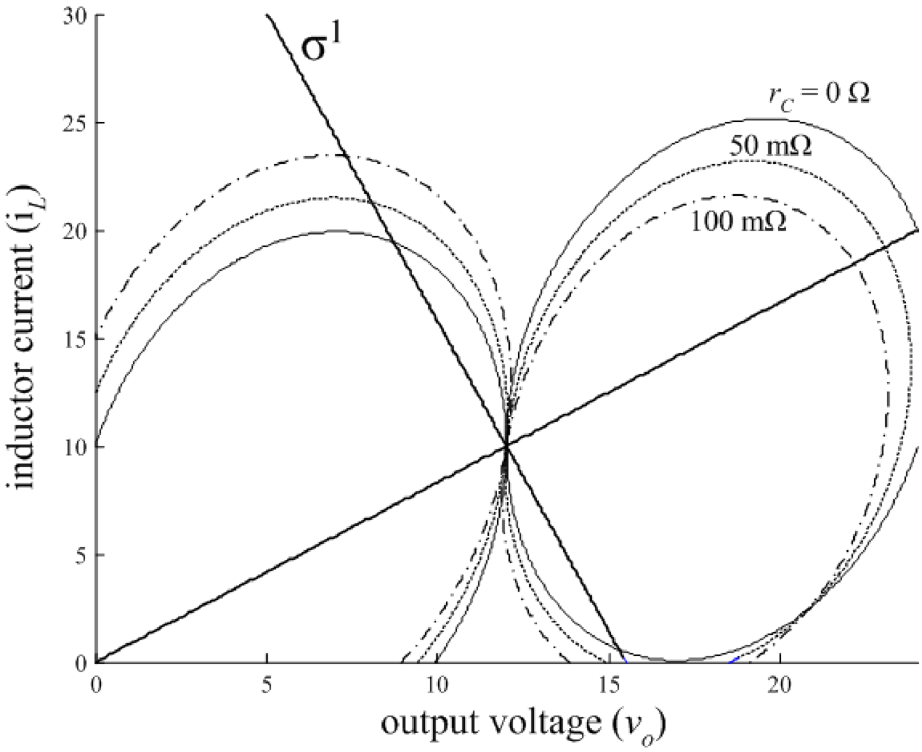

(b)

Fig. 3.5 Transition boundaries with σ^1. (a) $r_C = 0$. (b) $r_C \neq 0$.

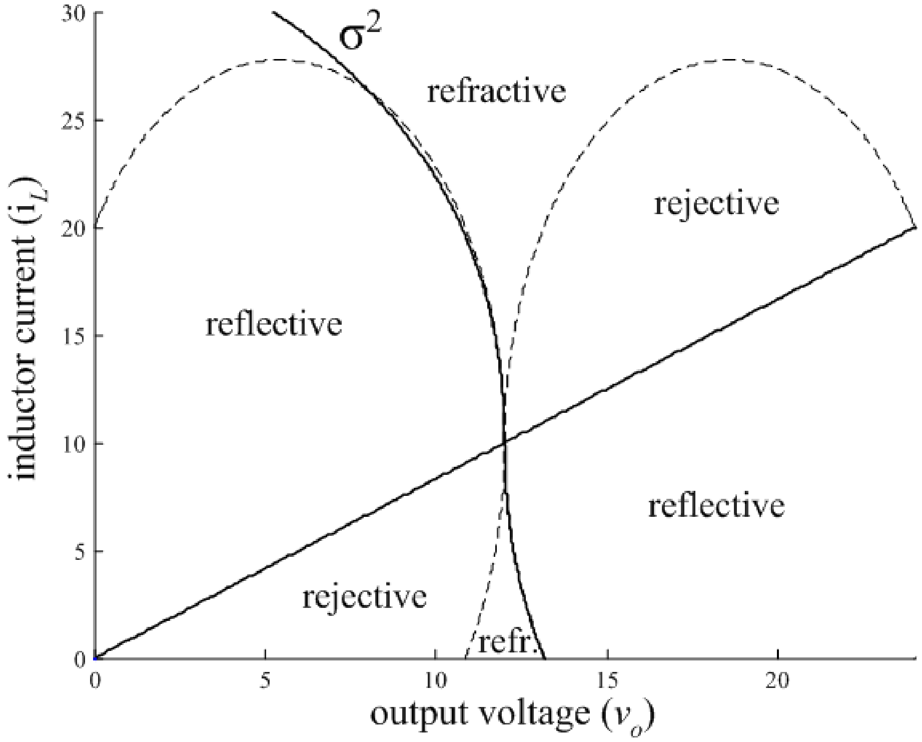

(a)

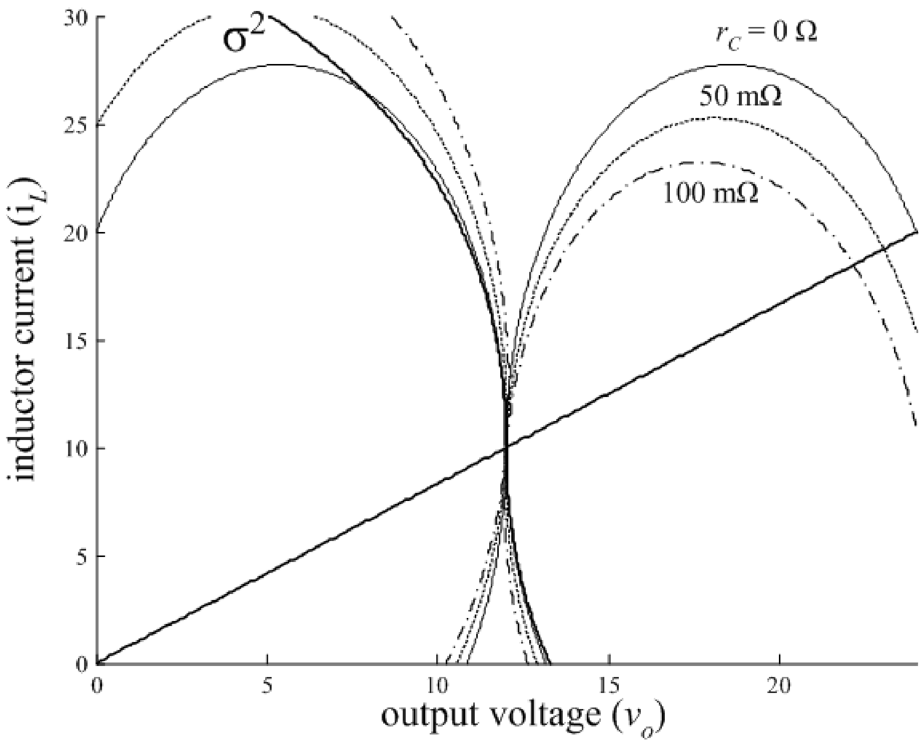

(b)

Fig. 3.6 Transition boundaries with σ^2. (a) $r_C = 0$. (b) $r_C \neq 0$.

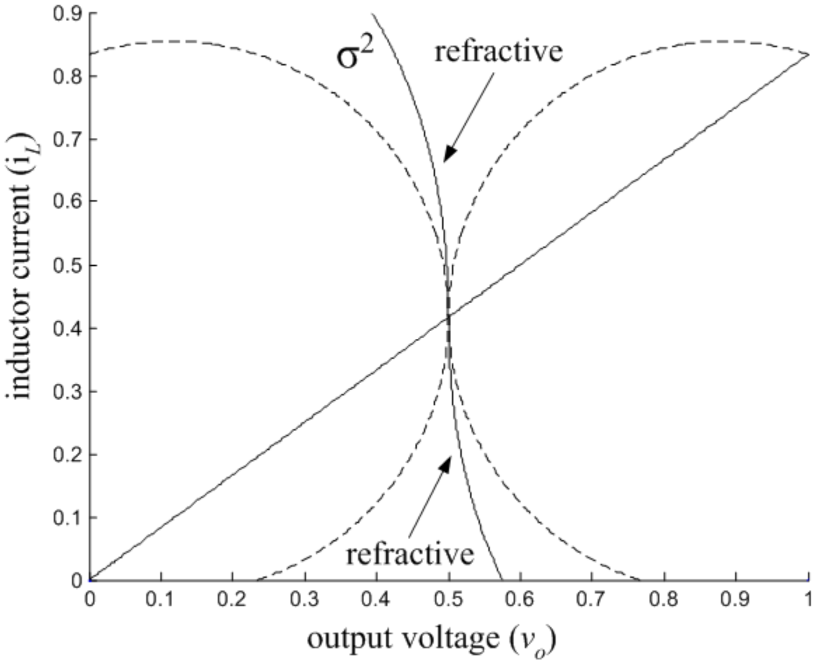
σ²
refractive
refractive
inductor current (i_L)
output voltage (v_o)
0
0.1
0.2
0.3
0.4
0.5
0.6
0.7
0.8
0.9
1

(a)

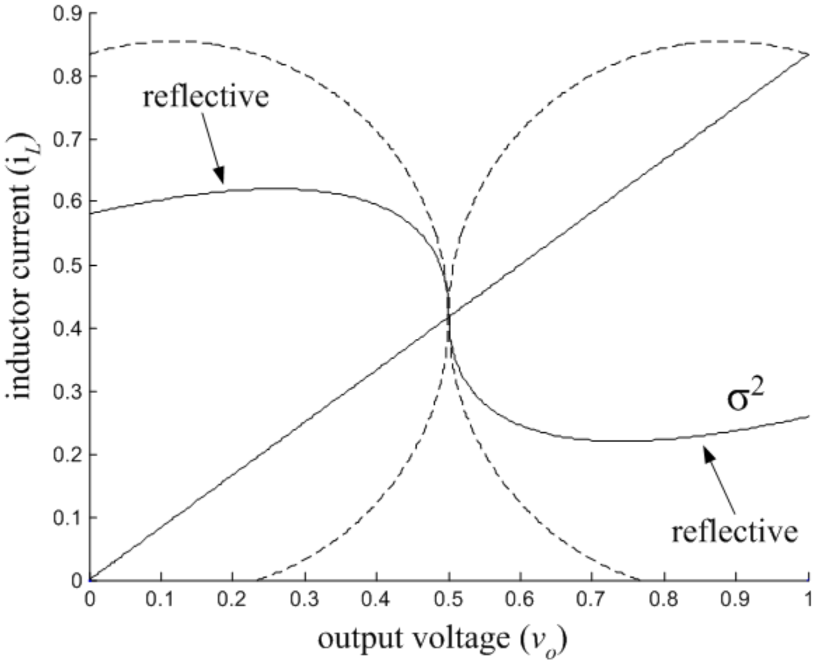
reflective
σ²
reflective
inductor current (i_L)
output voltage (v_o)
0
0.1
0.2
0.3
0.4
0.5
0.6
0.7
0.8
0.9
1

(b)

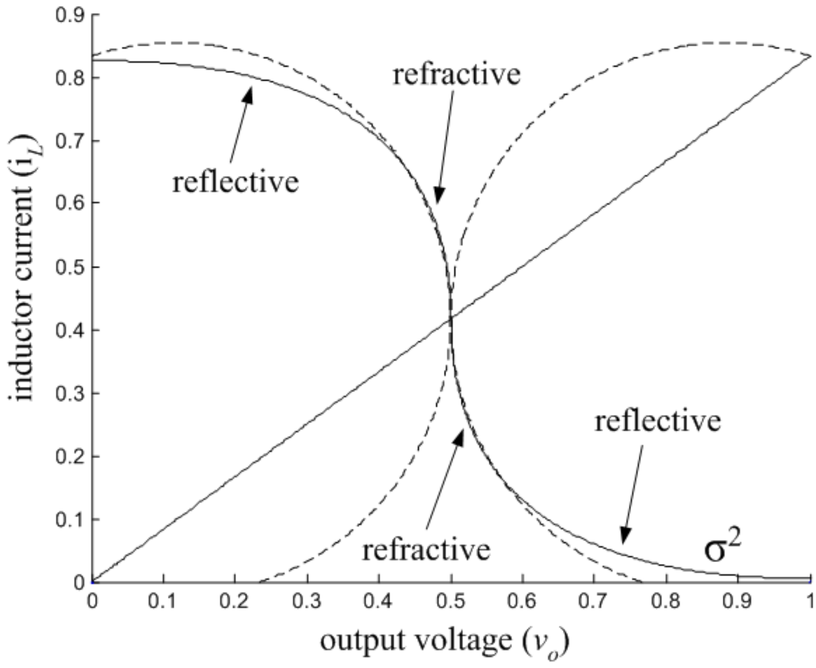

(c)

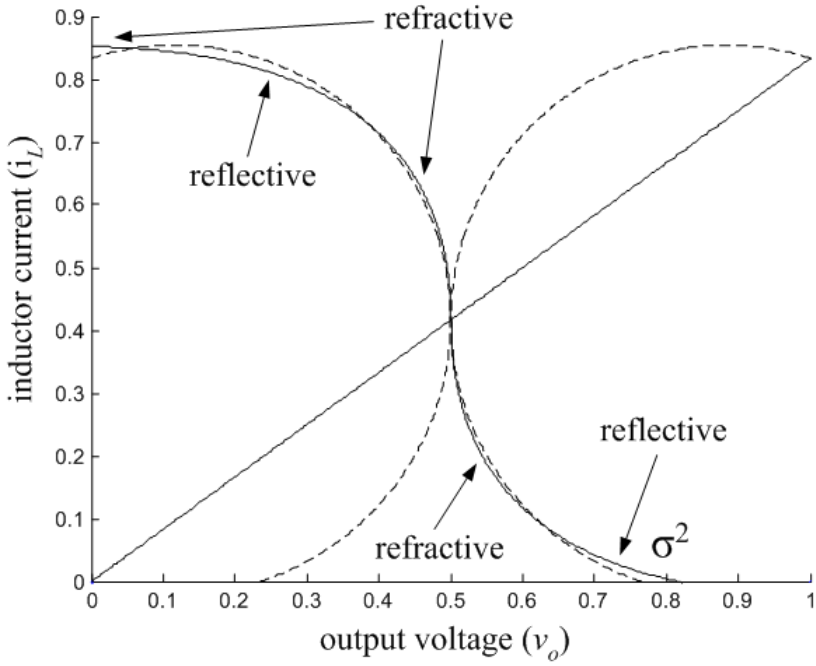

(d)

Fig. 3.7 Illustrations of possible cases in the intersections between the switching surface and transition boundaries. (a) Case I: Refractive region only with $\{k_1, k_2\} = \{0.326, 0.326\}$. (b) Case II: Reflective region only with $\{k_1, k_2\} = \{1.5, 1.5\}$. (c) Case III: Possibly in two regions with $\{k_1, k_2\} = \{0.731, 0.731\}$. (d) Case IV: Possibly in three regions with $\{k_1, k_2\} = \{0.686, 0.686\}$.

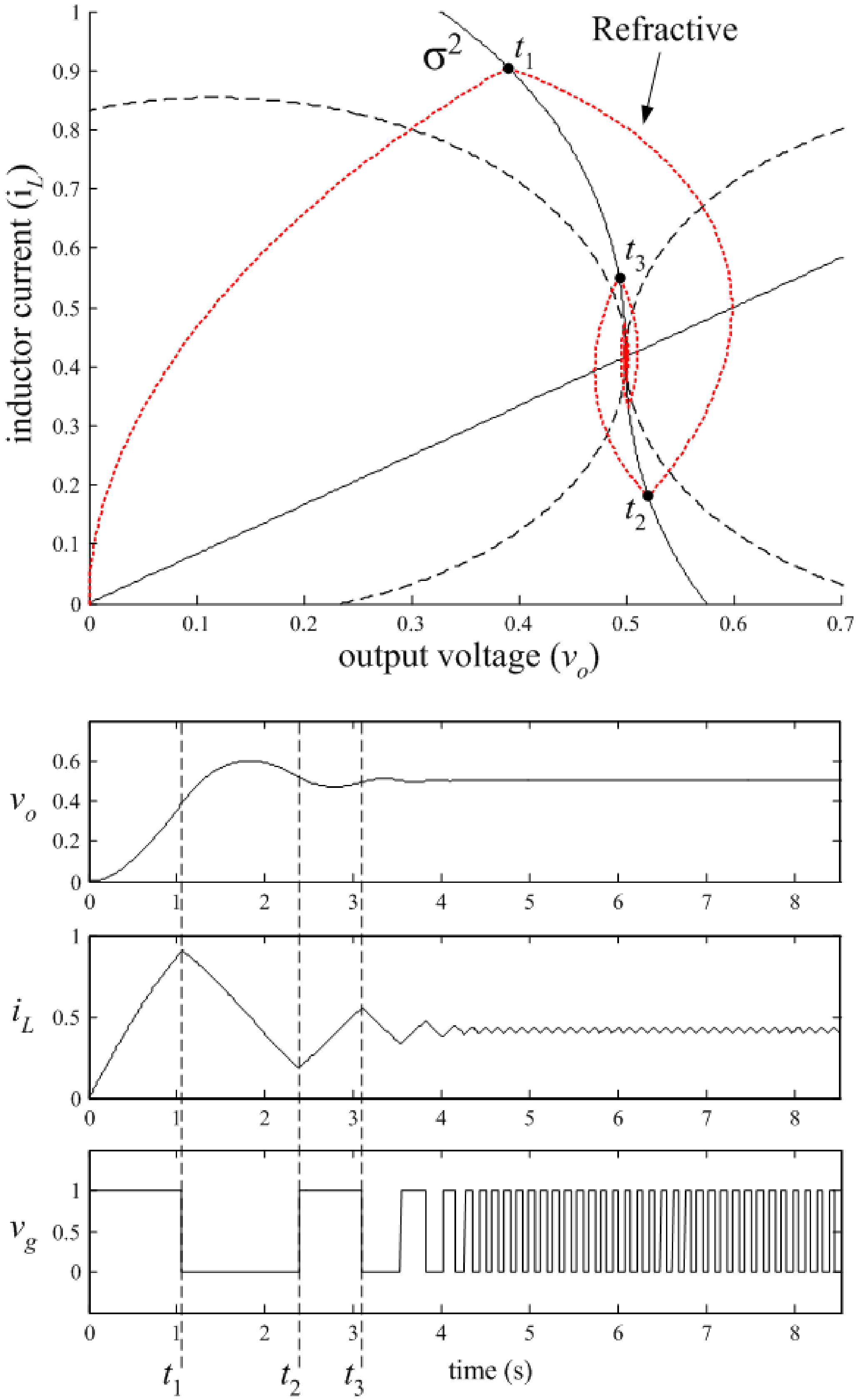

Refractive
σ^2
t_1
t_3
t_2
inductor current (i_L)
output voltage (v_o)
v_o
i_L
v_g
time (s)

(a)

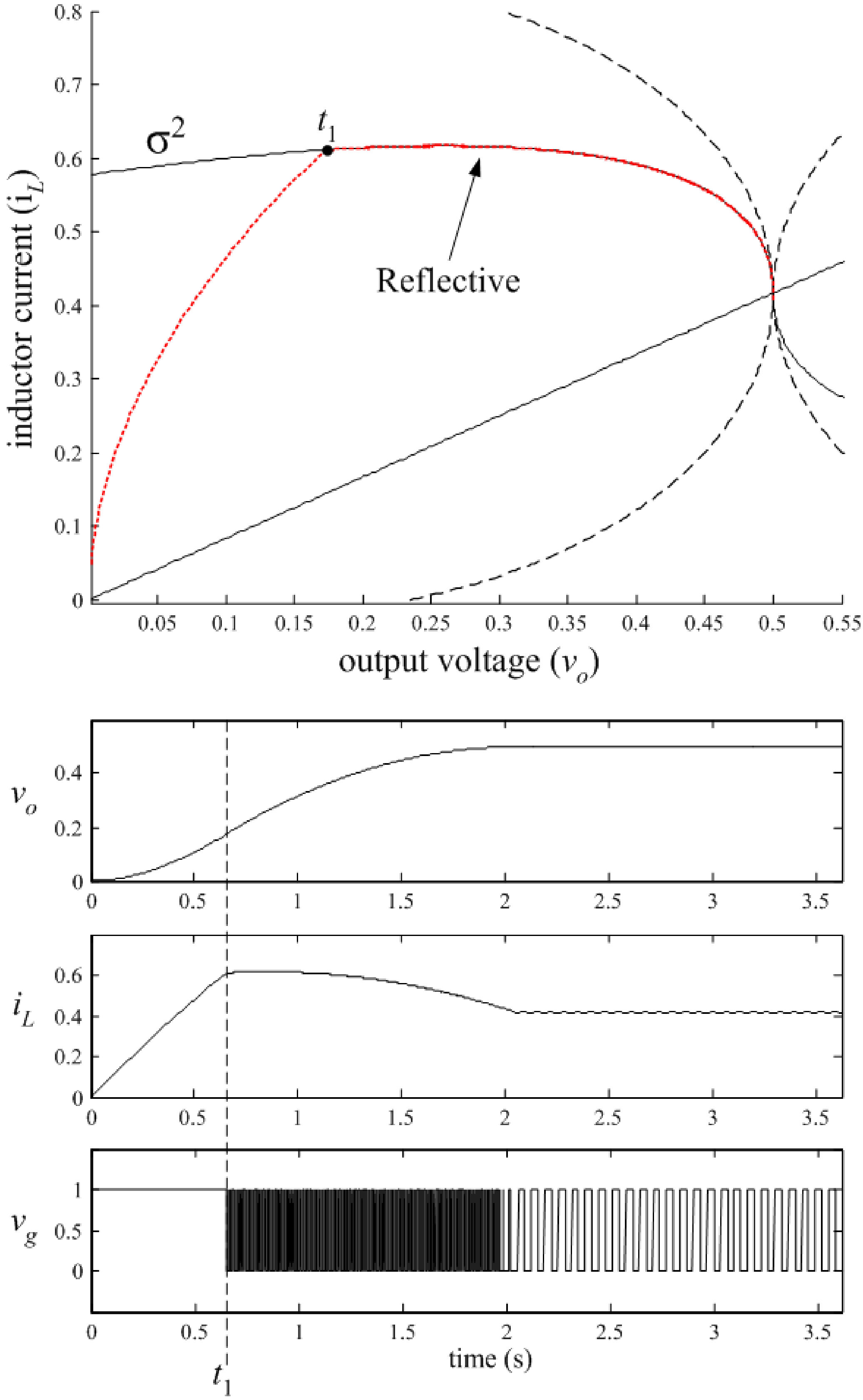

0.8
0.7
0.6
0.5
0.4
0.3
0.2
0.1
0
inductor current (i_L)
σ^2
t_1
Reflective
0.05
0.1
0.15
0.2
0.25
0.3
0.35
0.4
0.45
0.5
0.55
output voltage (v_o)
v_o
i_L
v_g
time (s)
t_1

(b)

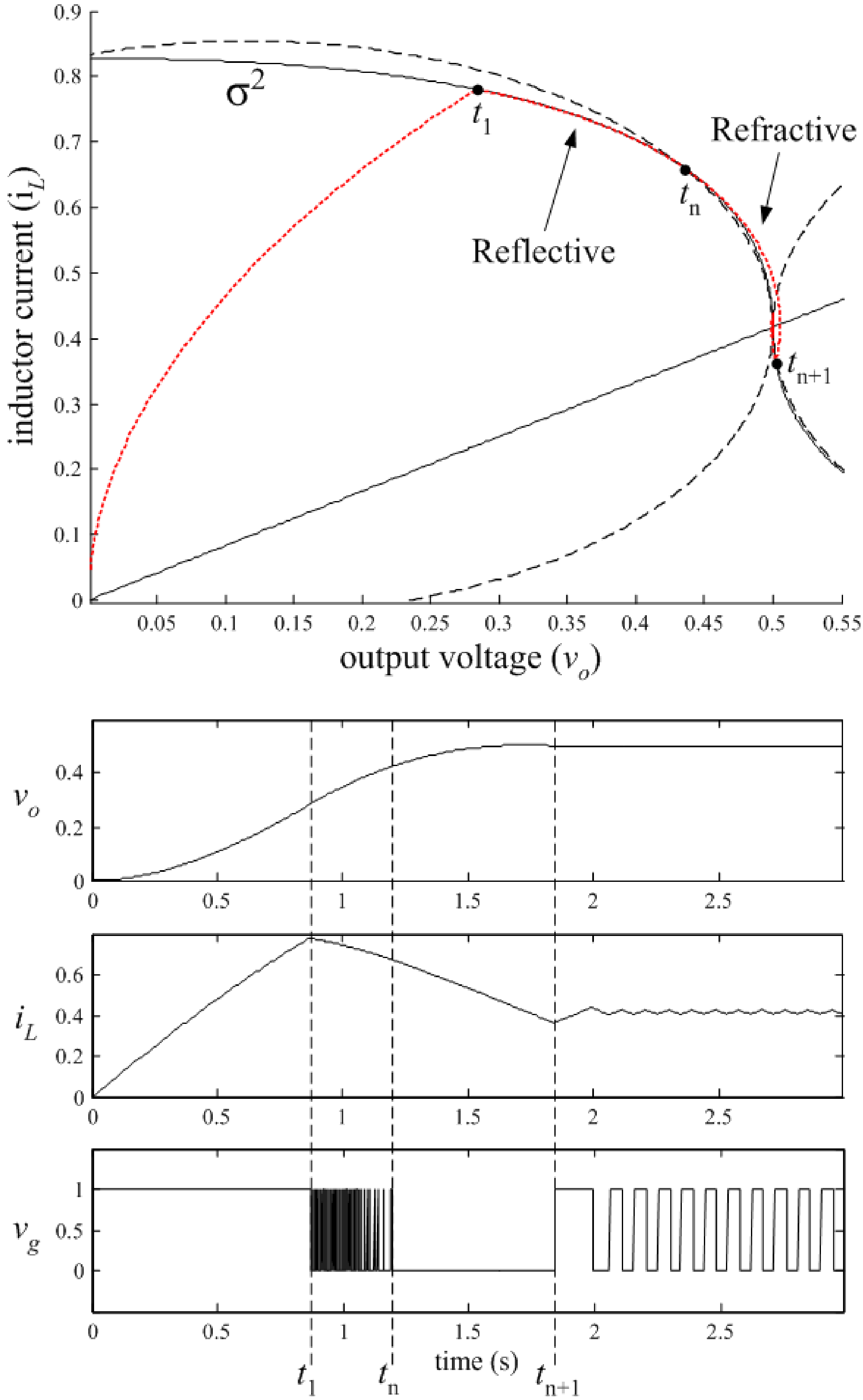

σ²
Refractive
Reflective
inductor current (i_L)
output voltage (v_o)
t_1
t_n
t_{n+1}
v_o
i_L
v_g
time (s)

(c)

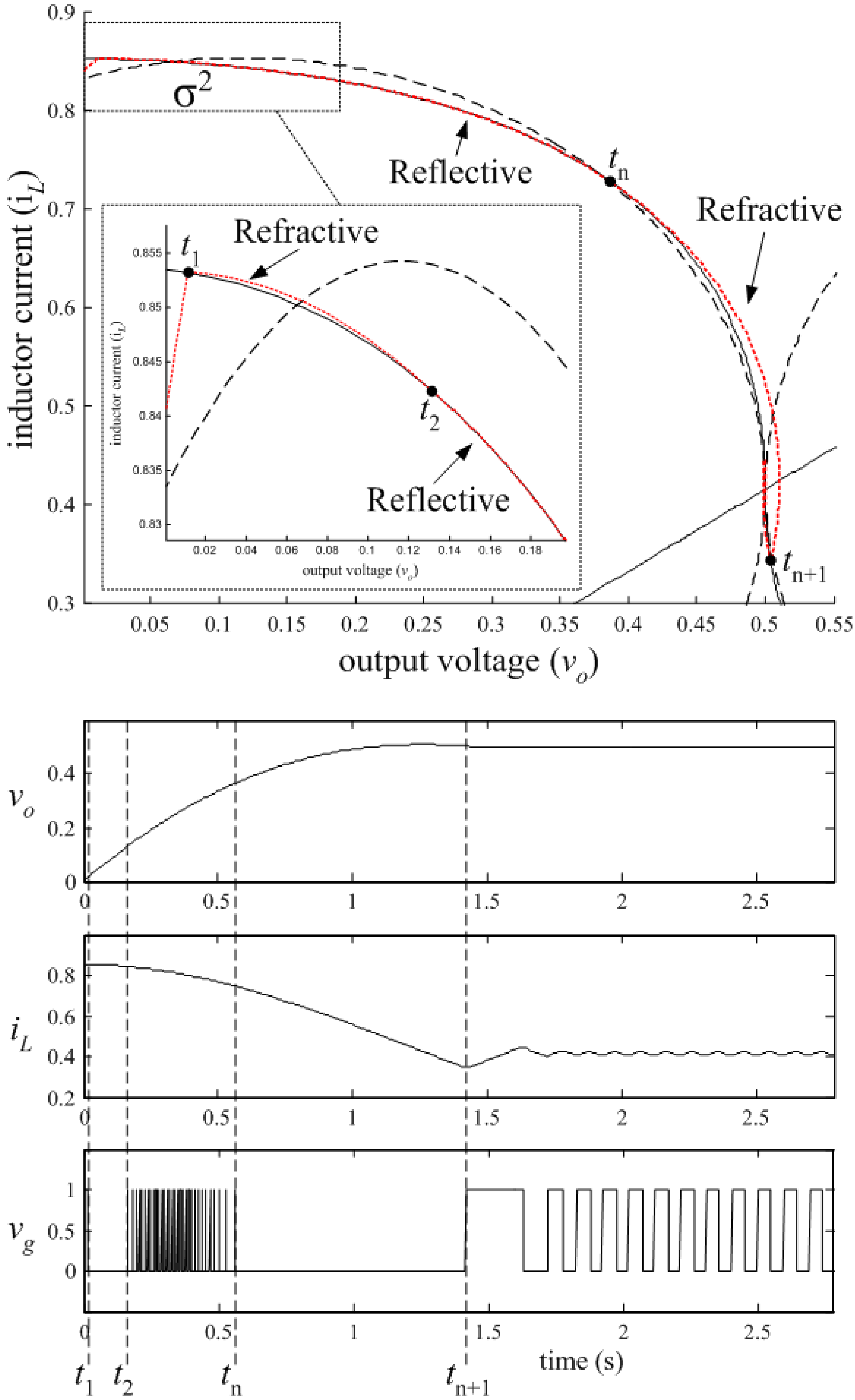

(d)

Fig. 3.8 Simulated waveforms in the cases listed in Fig. 3.7. (a) Case I. (b) Case II. (c) Case III. (d) Case IV.

3.6 Comparisons between σ^1 and σ^2

σ^1 and σ^2 are compared at two different situations. Firstly, c_1 is chosen, so that σ^1 and σ^2 give similar steady state behaviors. Secondly, c_1 is optimized at the startup transient. Both of them are discussed separately.

3.6.1 Same Steady State Behaviors

Converter performances with σ^1 and σ^2 are compared under the same steady-state conditions that v_{ripple} and f_S are the same when r_C = 0 and $r_C \to \infty$. Ideal values of k_1 and k_2 in (3.8) are used. All parameters are in nominal values. Thus, by equating (3.34) and (3.45),

$$\Delta_1 = \Delta_2 = \Delta \tag{3.88}$$

Also, by using (3.30) and (3.43), and (3.88), it can be shown that

$$\begin{aligned} \left(\frac{\Delta_1}{c_1}\right)^2 &= \frac{2\,\Delta_2}{k_1 + k_2} \\ \Rightarrow \quad c_1 &= \sqrt{\frac{k_1 + k_2}{2}\,\Delta} \end{aligned} \tag{3.89}$$

Thus, the relationship of (3.89) is used in the following discussions. It should be noted that the value of c_1 in (3.89) is not optimized for transient response with σ^1.

By putting (3.8), (3.88) and (3.89) into (3.46), it can be shown that

$$R_{crit}^{<2>} = \frac{v_{ref}\,c_1}{\Delta} - (1 - 2d)\cdot c_1 \tag{3.90}$$

By comparing $R_{crit}^{<1>}$ in (3.31) and $R_{crit}^{<2>}$ in (3.90), they are not equal if $d \neq 0.5$.

By putting (3.8) and (3.89) into (3.29), it can be shown that v_{avg} with σ^1 is equal to

$$v_{avg} = v_{ref} + (1 - 2d)\Delta_1 \tag{3.91}$$

Compared (3.91) with (3.44), v_{avg} with σ^2 is independent on Δ_2, while v_{avg} with σ^1 is dependent on Δ_1.

Based on (3.88) and (3.89), the values of f_S with σ^1 and σ^2 will be the same for $r_C = 0$ and $r_C \to \infty$. Fig. 3.9 shows the variations of f_S for $r_C \in [0, \infty]$. They give similar profile in both switching surfaces.

By substituting (3.8) and (3.89) into (3.60), (3.60) can be expressed as

$$\Delta v_{avg} = \left(\left(\frac{D_N}{1 - D_N} \right) \delta_1 + (1 - 2\, D_N)\, \delta_2 + (2\, D_N - 1) \delta_3 + \ldots \right) \Delta_2 \tag{3.92}$$

The expression is the same as (3.61). Thus, the parametric sensitivity is the same in both switching surfaces.

As illustrated in Figs. 3.5 – 3.8, σ^2 has the advantage over σ^1 that the settling time is comparatively shorter. In the ideal situation, σ^2 is on the boundary of the reflective and refractive regions. Transients can be settled in two switching actions with σ^2, while the trajectory is in sliding mode with σ^1. However, if the converter with σ^2 is subject to parametric variations, it might enter into the sliding condition (Fig. 3.6).

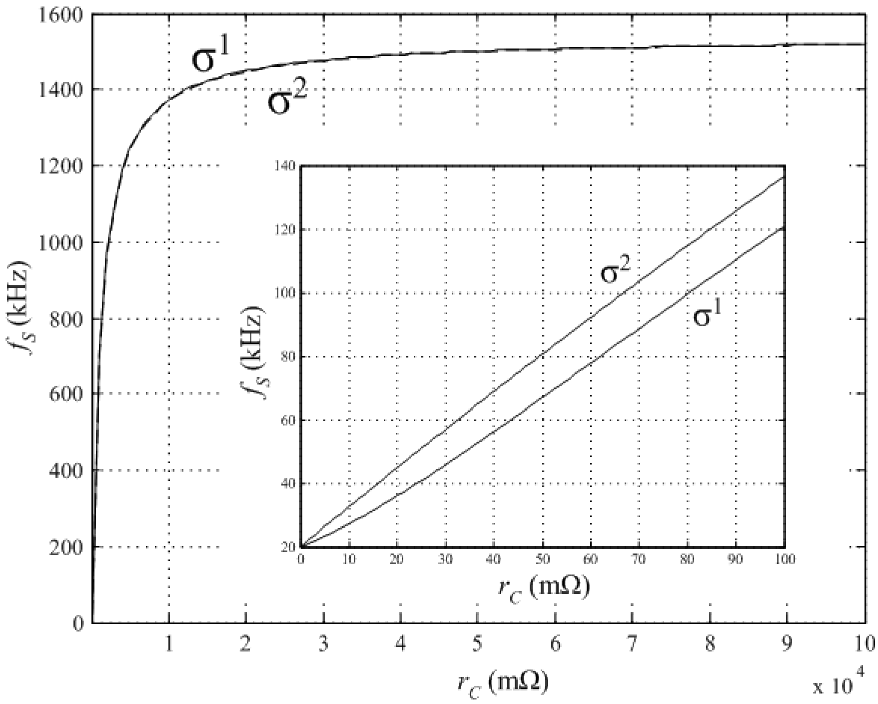

Fig. 3.9 Variations of f_S for $r_C \in [0, \infty]$.

3.6.2 Optimized c_1 at Startup

Fig. 3.10 shows the start-up trajectory, together with σ^1 and σ^2. σ^1 is formulated by having the same startup transients with σ^2 (i.e., σ^1 and σ^2 intercept at the points 'A' and 'B' in Fig. 3.10). The values of c_1 and k_1 can be shown to be equal to

$$c_1 = -\frac{v_{o,A} - v_{ref}}{i_{L,A} - \frac{v_{o,A}}{R}} \tag{3.93}$$

$$k_1 = -\frac{v_{o,A} - v_{ref}}{\left(i_{L,A} - \frac{v_{o,A}}{R}\right)^2} \tag{3.94}$$

where $v_{o,A}$ and $i_{L,A}$ are the values of v_o and i_L at point 'A', respectively.

Derivations of (3.93) and (3.94) are given in the *Appendix C*.

k_2 is obtained by considering an arbitrary point (point 'C' in Fig. 3.10) on the state plane that

$$k_2 = \frac{v_{o,C} - v_{ref}}{\left(i_{L,C} - \frac{v_{o,C}}{R}\right)^2} \tag{3.95}$$

where $v_{o,C}$ and $i_{L,C}$ are the values of v_C and i_L at point 'C', respectively.

Derivation of (3.95) is given in the *Appendix C*. Δ_1 is adjusted to give the same v_{ripple} at the rated power as with σ^2. Determinations of Δ_1 and Δ_2 are obtained by (3.51) and (3.53) with the measured values of r_C and the chosen switching frequency.

As discussed in Sec. 3.4.1, v_{avg} varies with Δ_1 in σ^1.

Since $\Delta_1 \neq \Delta_2$, changes of the switching frequencies against r_C are different with σ^1 and σ^2. Fig. 3.11 illustrates the theoretical comparison, in which the switching frequency is the same at r_C = 10 mΩ. The switching frequency increases more significantly with σ^2.

Although this method gives an optimized c_1, the performance is only optimized at the startup and is not optimized for large-signal responses.

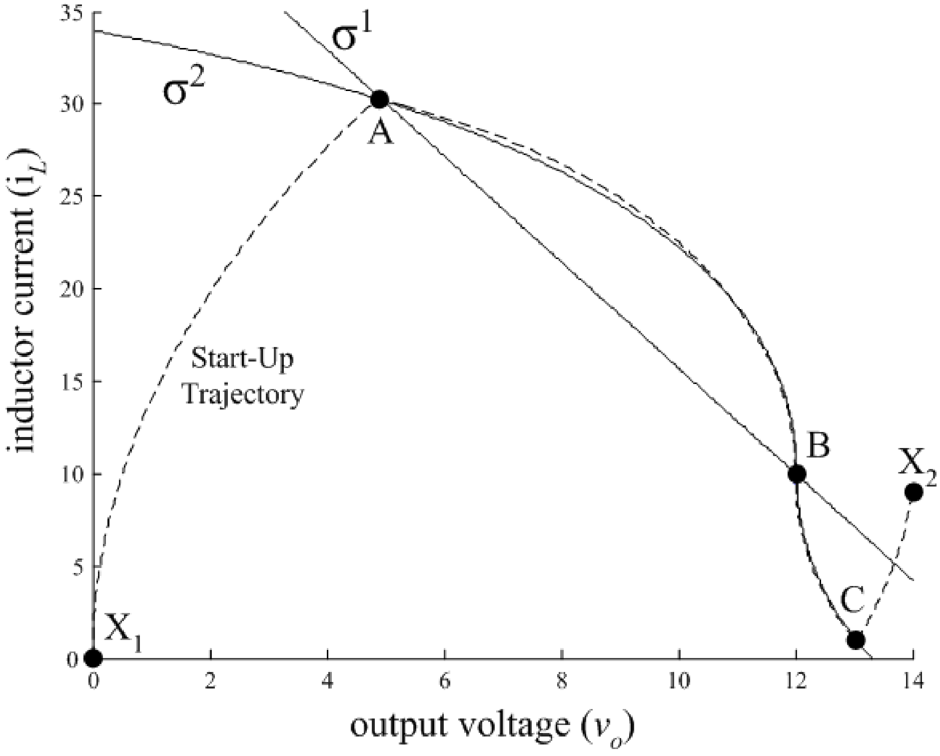

Fig. 3.10 Start-up transient response and the first and second-order switching surface. [Dotted line: start-up trajectory of buck converter]

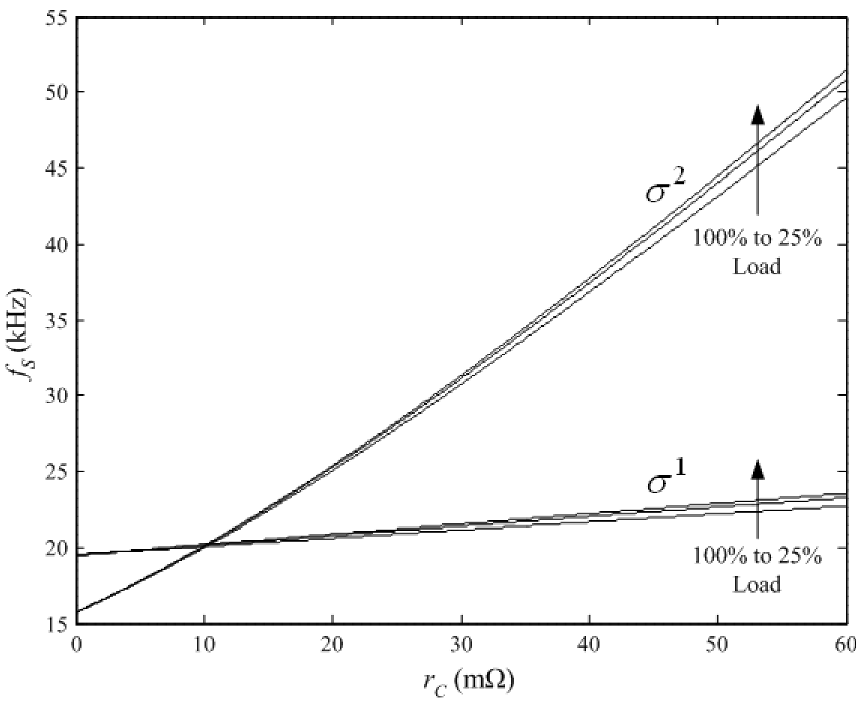

Fig. 3.11 Comparison of the switching frequency with σ^1 and σ^2.

3.7 Experimental Verifications

A buck converter with the component values tabulated in Table 3.1 is studied. c_1 is optimized with the method discussed in Sec. 3.4.2. Fig. 3.12 shows a comparison of the experimental transient responses when R is changed from 2.4 Ω (60 W) to 1.2 Ω (120 W), and vice versa, with σ^1 and σ^2, respectively. The converter with σ^2 have the same overshoot and undershoot as σ^1, and achieves faster transient response than of σ^1. The converter can go to the steady state in two switching actions under a large-signal variation. Fig. 3.13 shows different values of r_C on the transient responses with σ^1 and σ^2. With σ^1, the output ripple increases with the increase in r_C. With σ^2, the output ripple does not increase with the increase in r_C. However, the switching frequency in σ^2 increases.

Fig. 3.14 shows the time domain simulated waveforms of large signal transient with different value of k_1 and k_2. Fig. 3.14(a) shows the waveforms with ideal k_1 and k_2. The experimental results are shown in Fig. 3.12(b). Fig. 3.14(b) shows the waveforms with k_1 and k_2 are both greater than the ideal values. This will force the converter to operate in sliding mode condition during large-signal transient. High-frequency operation occurs before the converter goes into steady state operation. Fig. 3.15(a) shows the corresponding experimental results. Due to the circuit limitation, the frequency cannot go as high as the simulated waveforms during sliding mode operation region. Fig. 3.14(c) shows the waveforms with k_1 and k_2 are both smaller than the ideal values. The converter is operated in reflective region during large-signal transient. One more switching action is required before the system goes into steady state. Fig. 3.15(b) shows the corresponding experimental results.

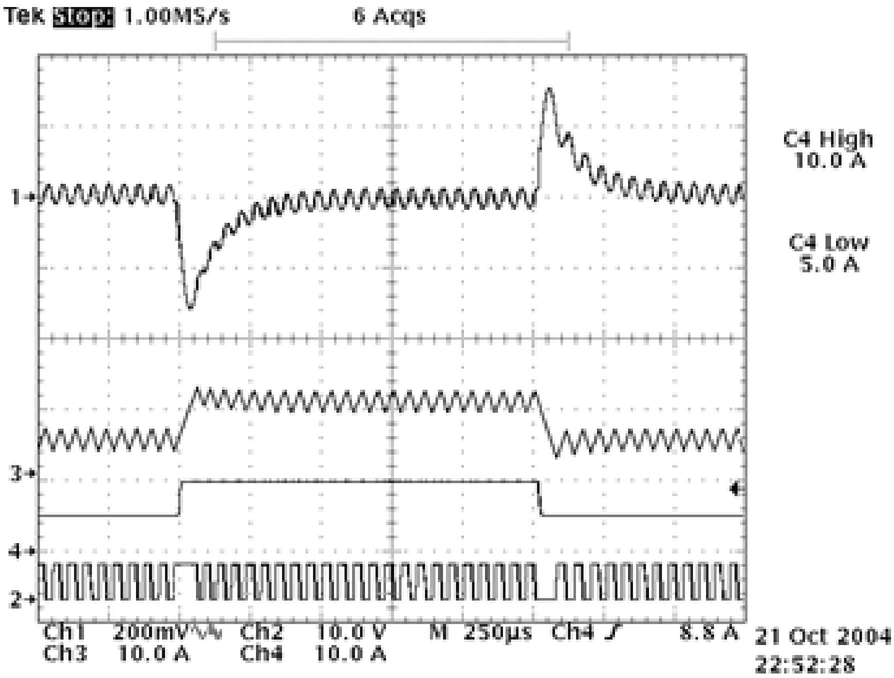

(a)

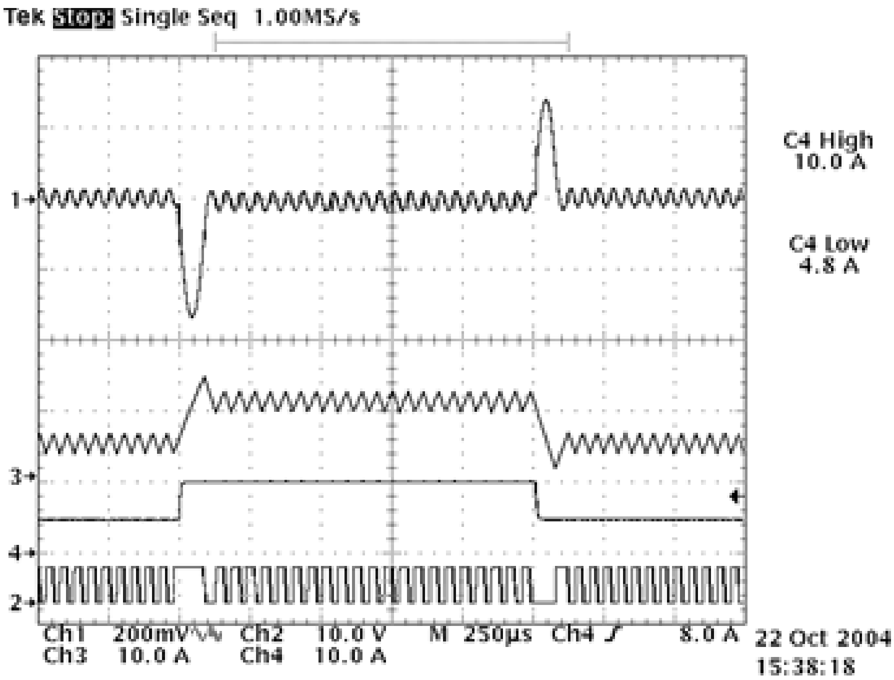

(b)

Fig. 3.12 Transient response of buck converter when load change from 5 A (60 W) to 10 A (120 W), and vice versa. [Ch1: v_o (200 mV/div), Ch2: v_g (10 V/div), Ch3: i_L (10 A/div), Ch4: i_o (10 A/div)] (Timebase: 250μs/div) (a) with σ^1. (b) with σ^2.

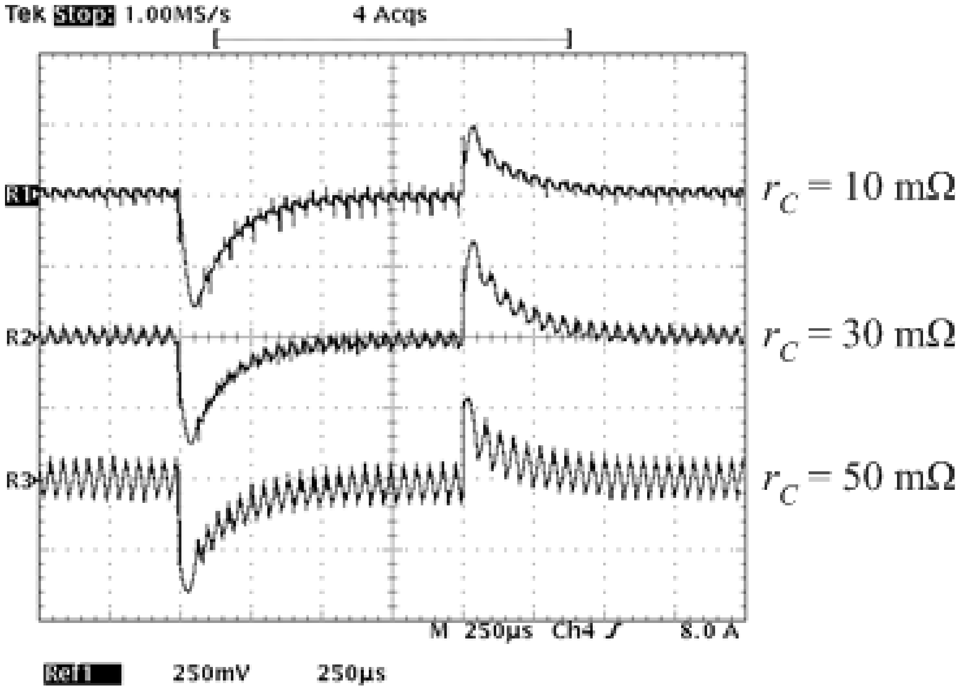

(a)

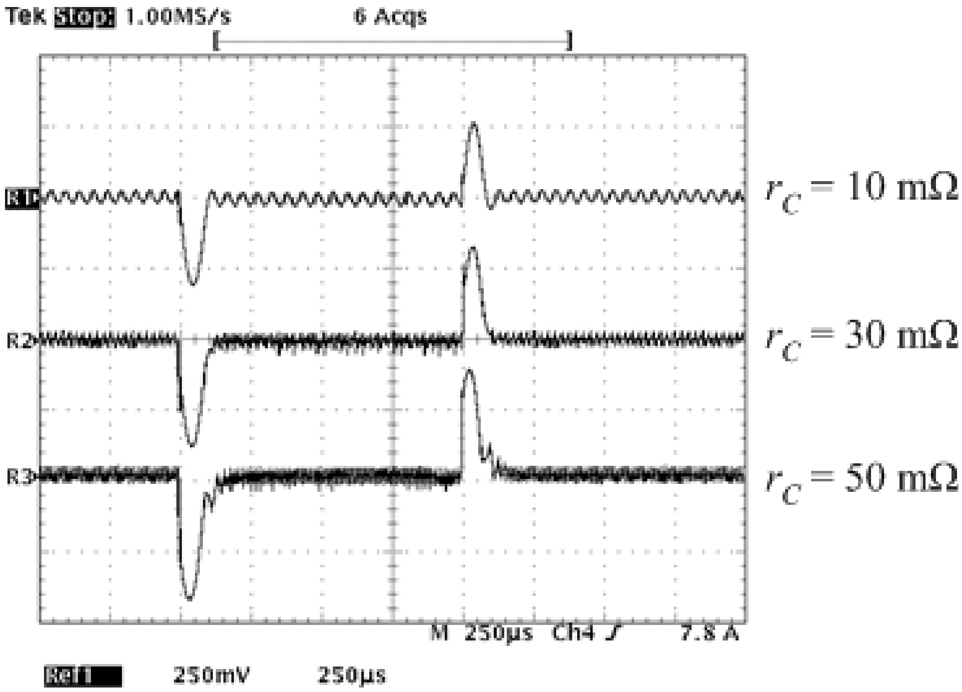

(b)

Fig. 3.13 Effects of r_C on the transient responses when load change from 5 A to 10 A and vice versa. (a) with σ^1. (b) with σ^2.

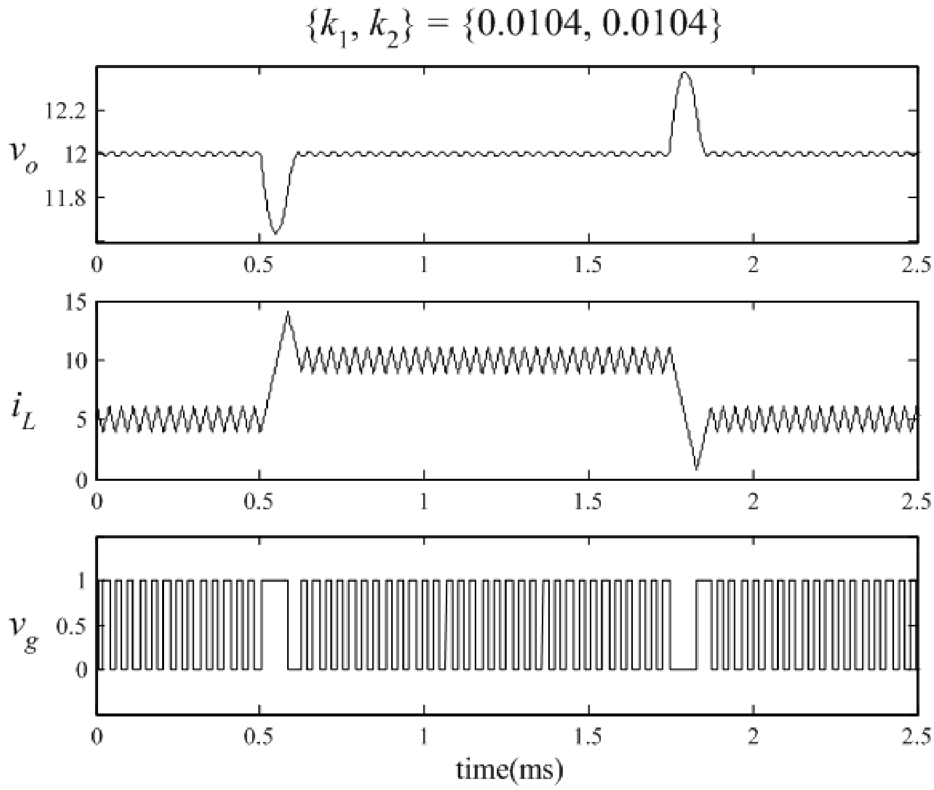

{k1, k2} = {0.0104, 0.0104}
12.2
vo
12
11.8
0
0.5
1
1.5
2
2.5
15
10
iL
5
0
1
vg
0.5
0
time(ms)

(a)

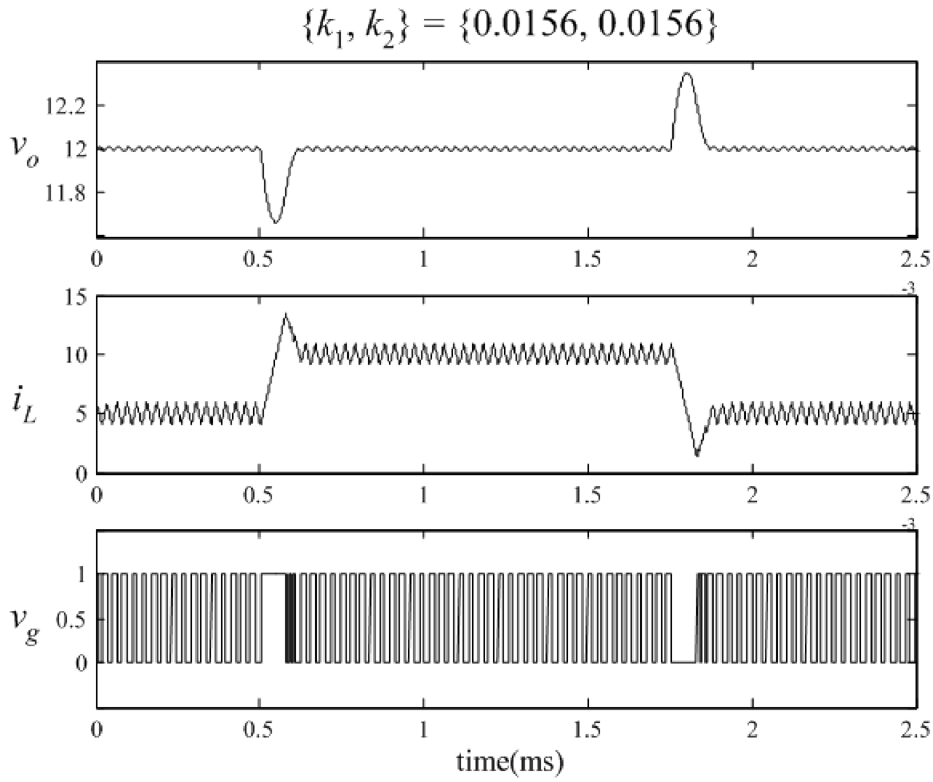

{k1, k2} = {0.0156, 0.0156}
12.2
vo
12
11.8
0
0.5
1
1.5
2
2.5
15
10
iL
5
0
1
vg
0.5
0
time(ms)

(b)

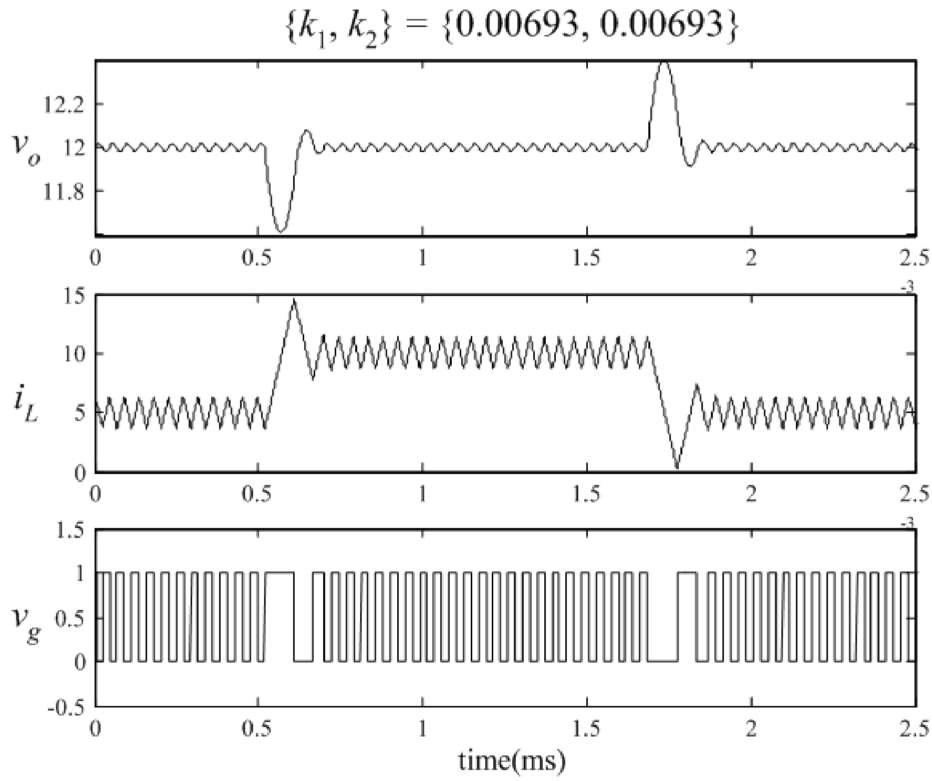

(c)

Fig. 3.14 Simulated waveforms of buck converter when load change from 5 A to 10 A and vice versa for different value of k_1 and k_2. (a) $\{k_1, k_2\} = \{0.0104, 0.0104\}$. (b) $\{k_1, k_2\} = \{0.0156, 0.0156\}$. (c) $\{k_1, k_2\} = \{0.00693, 0.00693\}$.

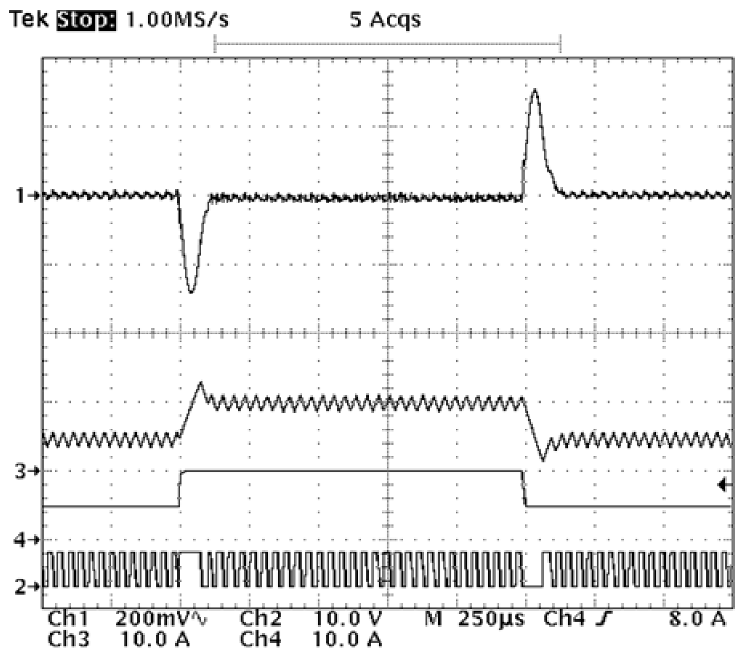

(a)

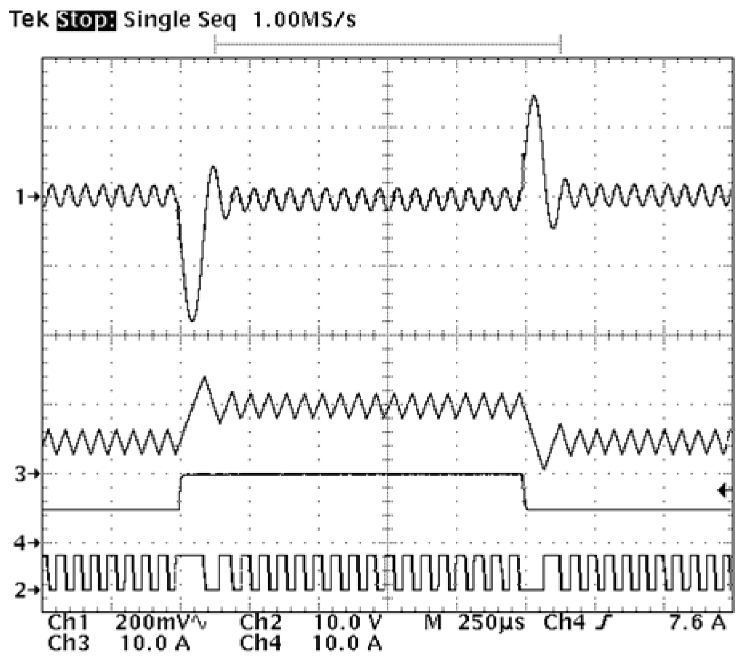

(b)

Fig. 3.15 Transient response of buck converter when load change from 5 A to 10 A and vice versa for different value of k_1 and k_2. [Ch1: v_o (200 mV/div), Ch2: v_g (10 V/div), Ch3: i_L (10 A/div), Ch4: i_o (10 A/div)] (Timebase: 250µs/div) (a) $\{k_1, k_2\} = \{0.0156, 0.0156\}$. (b) $\{k_1, k_2\} = \{0.00693, 0.00693\}$.

3.8 Chapter Summary

A comparative study on the performance characteristics of the buck converters with boundary control using a first-order switching surface and a recently proposed second-order switching surface has been given. Detailed discussions have been devoted to the steady-state and transient response. Generally, converters with the second-order surface are found to give better dynamic responses than the ones with the first-order surface. While the ripple voltage is kept at a low level, the switching frequency with σ^2 is higher than that of the one with σ^1.

CHAPTER 4

A COMPARATIVE STUDY: DISCONTINUOUS CONDUCTION MODE

4.1 Introduction

This chapter extends the scope of *Chapter 3* on comparing the performance characteristics of buck converters with the first- (σ^1) and second-order (σ^2) switching surfaces. Major emphasis is given to converters operating in discontinuous conduction mode (DCM). Similar to *Chapter 3*, performance attributes under investigation in this chapter includes the average output voltage, output ripple voltage, switching frequency, parametric sensitivities to the component values, and large-signal characteristics. Due to the presence of the output hysteresis band, an additional switching boundary formed by the zero-inductor-current trajectory is created. This phenomenon causes a shift of the operating point in converters with σ^1. Conversely, the operating point remains unchanged in converters with σ^2. As well as in continuous conduction mode (CCM), σ^2 can make the converter revert to the steady state in two switching cycles in DCM and gives better static and dynamic responses than σ^1 in both CCM and DCM. Most importantly, its control law and settings are the same in both modes. Experimental results of a prototype are found to be in good agreement with theoretical predictions.

4.2 Discontinuous Conduction Mode

As expressed in (3.31) and (3.46), the critical resistances of the buck converters with σ^1 and σ^2 theoretically tend to infinity with zero hysteresis band and thus DCM does not occur for a large-signal stable switching surface. However, as shown in eqs. (3.51) and (3.53), the switching frequency will also tend to infinitive. Thus, a hysteresis band will usually be introduced to limit the switching frequency. With nonzero hysteresis band, an additional switching boundary formed by zero-inductor-current trajectory is created and possibly makes the converter enter into DCM. Fig. 4.1(a) depicts the state trajectories and Fig. 4.1(b) shows the time-domain output voltage and inductor current waveforms of converters in DCM with σ^1. The output capacitor discharges to the load and the trajectory will move along the x-axis, when the main switch and the diode are off from t_2 to t_3. This results in a shift of the average output voltage. Fig. 4.2(a) illustrates the output voltage shift when the output load is changed from R_1 to R_2, where $R_2 > R_{crit}^{<1>} > R_1$ and $R_{crit}^{<1>}$ is the critical resistance. The operating point is shifted from 'O$_1$' (when the load is R_1) to a new operating point 'O$_2$' (when the load is R_2). When the load is R_1, the converter operates in CCM. The average output voltage is close to the reference voltage v_{ref}, as expressed in (3.29). However, when the load is R_2, the average output will move away from 'O$_1$'.

For converters with σ^2, the operating point remains unchanged. Fig. 3.2(b) shows the state trajectories when the load is changed from R_1 to R_2. In this respect, σ^2 exhibits a better static behavior than σ^1.

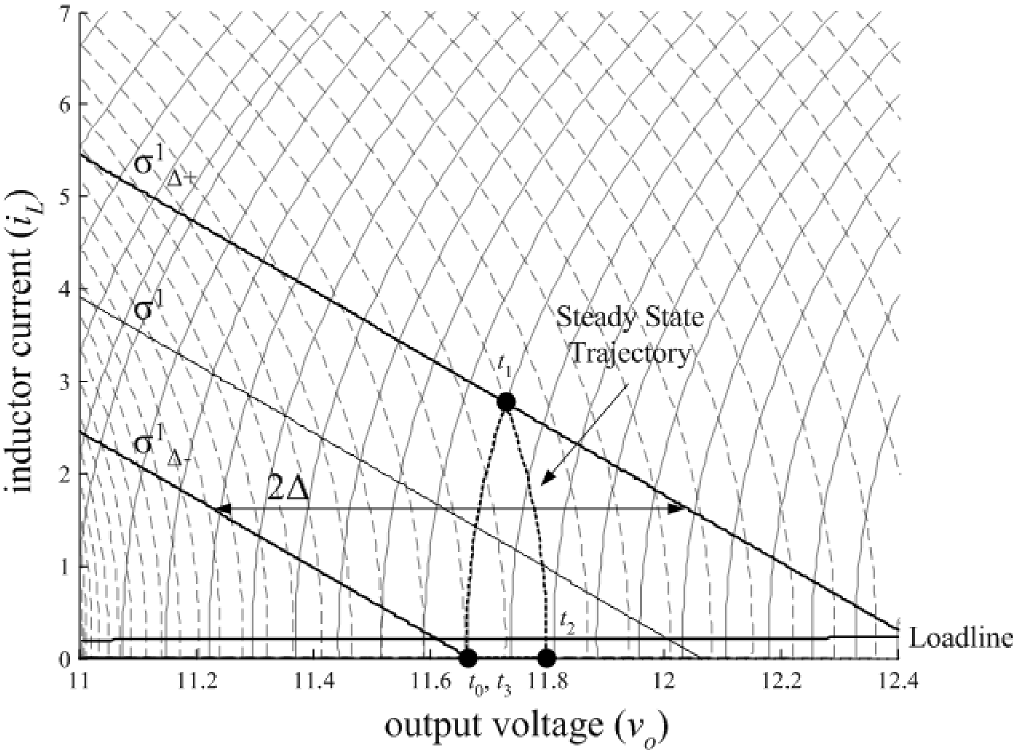

(a)

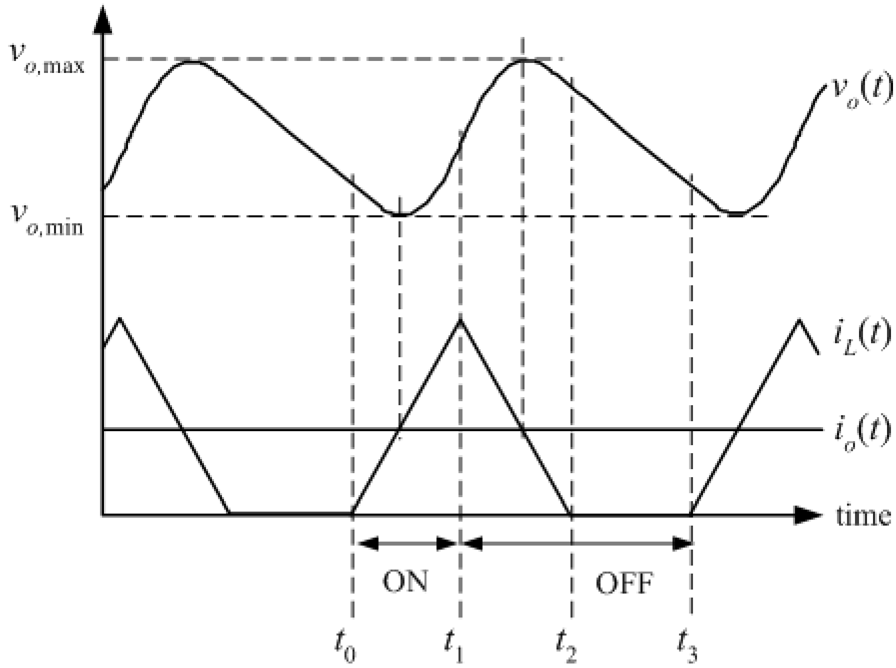

(b)

Fig. 4.1 Phase-plane and waveforms of the buck converter in DCM. (a) State trajectories with nonzero hysteresis band. (b) Time-domain output voltage and inductor current waveforms.

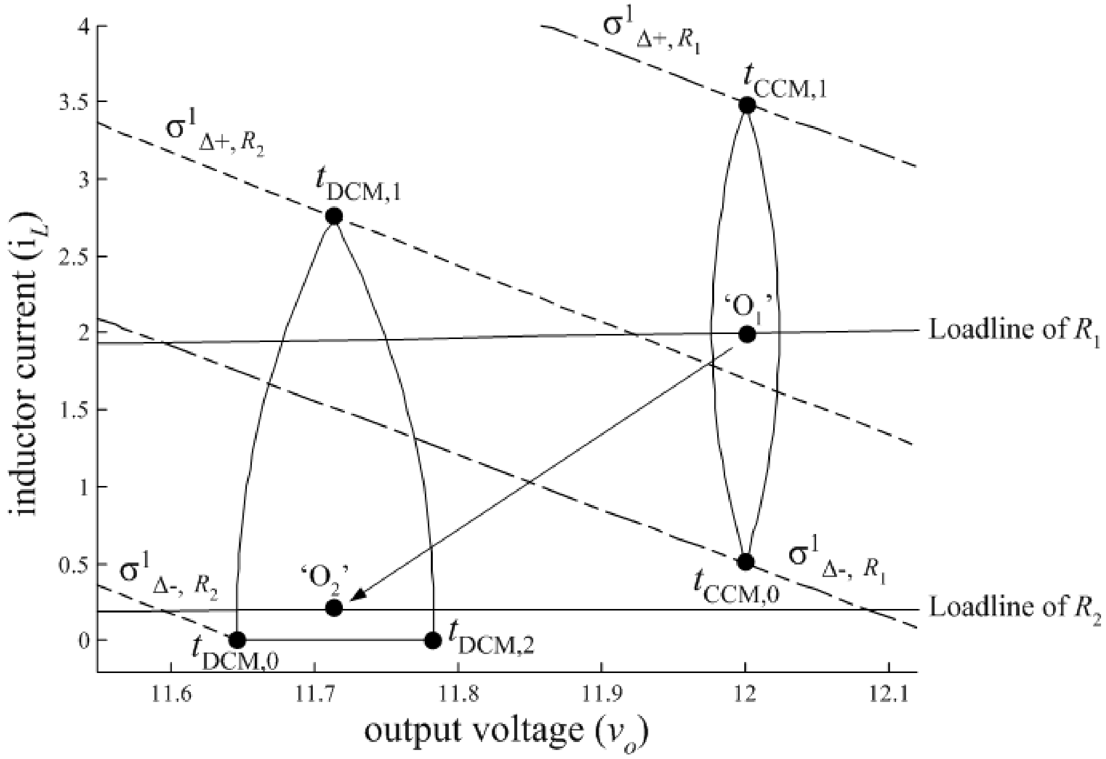

(a)

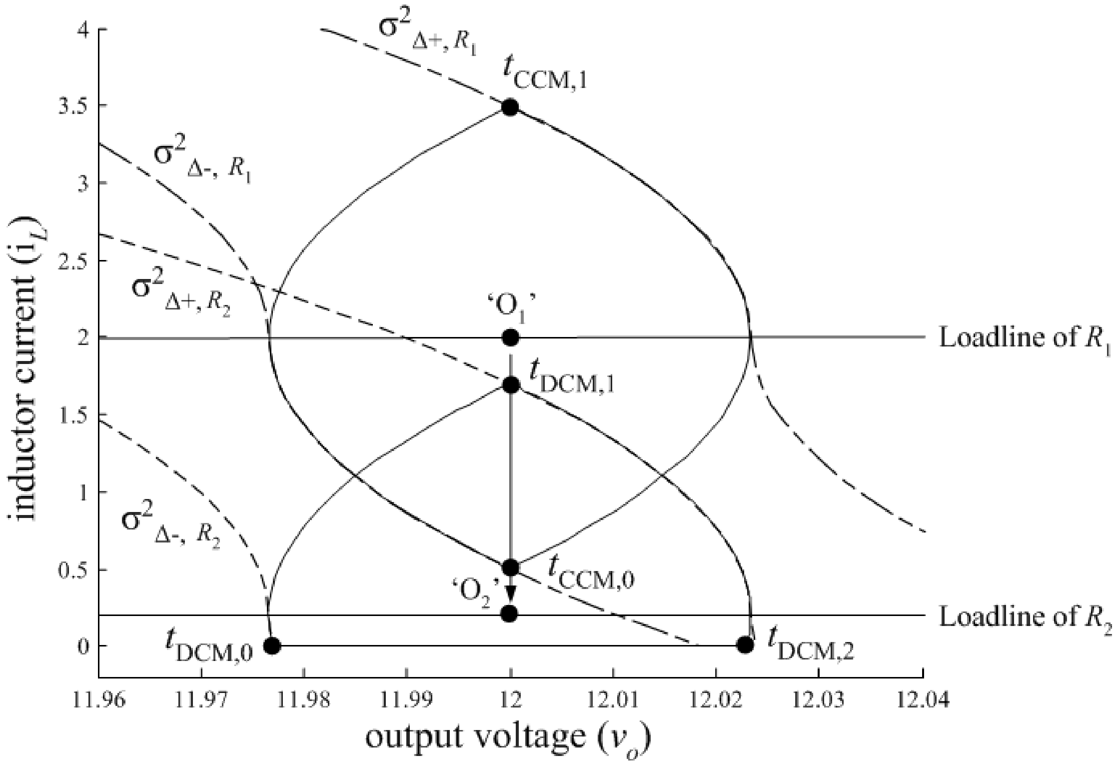

(b)

Fig. 4.2 Shift of operating point of the converter in DCM with different loads. (a) σ^1. (b) σ^2.

4.3 Definitions and Formulas

The basic definitions and formulas in *Chapter 3* are used in the following analysis. The converter can be described by the state-space equation of

$$\begin{aligned} \dot{x} &= A_0\, x + B_0\, u + (A_1\, x + B_1\, u)\, q_1 + (A_2\, x + B_2\, u)\, q_2 \\ y &= C\, x \end{aligned} \tag{4.1}$$

where $x = [i_L \quad v_C]$, $y = v_o$, A_i, B_i, and C are constant matrices, and q_i represents the state of the switch S_i. If S_i is on, q_i = 1, and vice versa. S_1 represents the main switch and S_2 represents the diode. Matrices A_0, B_0, A_1, B_1, A_2, and B_2 are defined as

$$A_0 = \begin{bmatrix} 0 & 0 \\ 0 & -\dfrac{1}{C(R+r_C)} \end{bmatrix},\ B_0 = \begin{bmatrix} 0 \\ 0 \end{bmatrix},\ A_1 = A_2 = \begin{bmatrix} -\dfrac{R\, r_C}{L(R+r_C)} & -\dfrac{R}{L(R+r_C)} \\ \dfrac{R}{C(R+r_C)} & 0 \end{bmatrix},\ B_1 = \begin{bmatrix} \dfrac{1}{L} \\ 0 \end{bmatrix},$$

$$B_2 = \begin{bmatrix} 0 \\ 0 \end{bmatrix} \text{ and } C = \begin{bmatrix} \dfrac{R\, r_C}{R+r_C} & \dfrac{R}{R+r_C} \end{bmatrix}.$$

4.3.1 On- and Off-State Trajectories

When S_1 is on and S_2 is off, the on-state trajectory $\{v_{o,on}, i_{L,on}\}$ is

$$\begin{aligned} v_{o,on} &= \frac{L}{2C\,(v_i - v_{ref})}\left(\left(i_{L,on} - \frac{v_{o,on}}{R}\right)^2 - \left(i_{L,0} - \frac{v_{o,0}}{R}\right)^2\right) + v_{o,0} \\ &\quad + r_C\left(\left(i_{L,on} - \frac{v_{o,on}}{R}\right) - \left(i_{L,0} - \frac{v_{o,0}}{R}\right)\right) \end{aligned} \tag{4.2}$$

where $i_{L,0}$ and $v_{o,0}$ are the initial values of i_L and v_o, respectively, in this stage.

When S_1 is off and S_2 is on, the off-state trajectory $\{v_{o,off}, i_{L,off}\}$ is

$$\begin{aligned} v_{o,off} &= -\frac{L}{2C\,v_{ref}}\left(\left(i_{L,off} - \frac{v_{o,off}}{R}\right)^2 - \left(i_{L,1} - \frac{v_{o,1}}{R}\right)^2\right) + v_{o,1} \\ &\quad + r_C\left(\left(i_{L,off} - \frac{v_{o,off}}{R}\right) - \left(i_{L,1} - \frac{v_{o,1}}{R}\right)\right) \end{aligned} \tag{4.3}$$

where $i_{L,1}$ and $v_{o,1}$ are the initial values of i_L and v_o, respectively, in this stage.

When both S_1 and S_2 are off, the trajectory moves along the x-axis and $i_L = 0$.

4.3.2 Modeling of σ¹ *and* σ²

The general form of σ^1 can be written as

$$\sigma^1{}_{\Delta+} = c_1\left(i_L - \frac{v_o}{R}\right) + \left(v_o - \left(v_{ref} + \Delta_1\right)\right) = 0 \tag{4.4}$$

$$\sigma^1{}_{\Delta-} = c_1\left(i_L - \frac{v_o}{R}\right) + \left(v_o - \left(v_{ref} - \Delta_1\right)\right) = 0 \tag{4.5}$$

where c_1 is a constant and v_{ref} is the reference output. i_L and v_o are in a linear relationship.

The general form of σ^2 is defined as

$$\sigma^2{}_{\Delta+} = k_1\left(i_L - \frac{v_o}{R}\right)^2 + \left(v_o - \left(v_{ref} + \Delta_2\right)\right), \quad \left(i_L - \frac{v_o}{R}\right) > 0 \tag{4.6}$$

$$\sigma^2{}_{\Delta-} = -k_2\left(i_L - \frac{v_o}{R}\right)^2 + \left(v_o - \left(v_{ref} - \Delta_2\right)\right), \quad \left(i_L - \frac{v_o}{R}\right) < 0 \tag{4.7}$$

where k_1 and k_2 are constants.

If $r_C = 0$, the ideal values of k_1 and k_2 are

$$\{k_1, k_2\} = \left\{\frac{L}{2\,C\,v_{ref}}, \frac{L}{2\,C\,(v_i - v_{ref})}\right\} \tag{4.8}$$

4.3.3 Average Output Voltage and Output Ripple Voltage

The average output voltage v_{avg} is defined as the mean of the minimum output voltage $v_{o,\min}$ and the maximum output voltage $v_{o,\max}$. That is,

$$v_{avg} = \frac{v_{o,\min} + v_{o,\max}}{2} \tag{4.9}$$

The output ripple voltage v_{ripple} is defined as

$$v_{ripple} = v_{o,\max} - v_{o,\min} \tag{4.10}$$

4.4 Steady-State Characteristics

Fig. 4.3(a) and (b) show the trajectory with σ^1 and σ^2 in DCM, respectively, with $r_C = 0$,

$$v_{o,0} = v_{o,3} \tag{4.11}$$

and

$$i_{L,0} = i_{L,3} \tag{4.12}$$

where $v_o(t_0) = v_{o,0}$, $v_o(t_3) = v_{o,3}$, $i_L(t_0) = i_{L,0}$ and $i_L(t_3) = i_{L,3}$.

In DCM, both S_1 and S_2 are off from t_2 to t_3, therefore,

$$i_{L,0} = i_{L,2} = i_{L,3} = 0 \tag{4.13}$$

where $i_L(t_2) = i_{L,2}$.

By putting (4.11)-(4.13) into (4.2),

$$v_{o,1} = \frac{L}{2C(v_i - v_{ref})}\left(\left(i_{L,1} - \frac{v_{o,1}}{R}\right)^2 - \left(\frac{v_{o,0}}{R}\right)^2\right) + v_{o,0} \tag{4.14}$$

where $v_o(t_1) = v_{o,1}$, $i_L(t_1) = i_{L,1}$.

Similarly, by putting (4.11)-(4.13) into (4.3),

$$v_{o,2} = -\frac{L}{2C v_{ref}}\left(\left(\frac{v_{o,2}}{R}\right)^2 - \left(i_{L,1} - \frac{v_{o,1}}{R}\right)^2\right) + v_{o,1} \tag{4.15}$$

where $v_o(t_2) = v_{o,2}$.

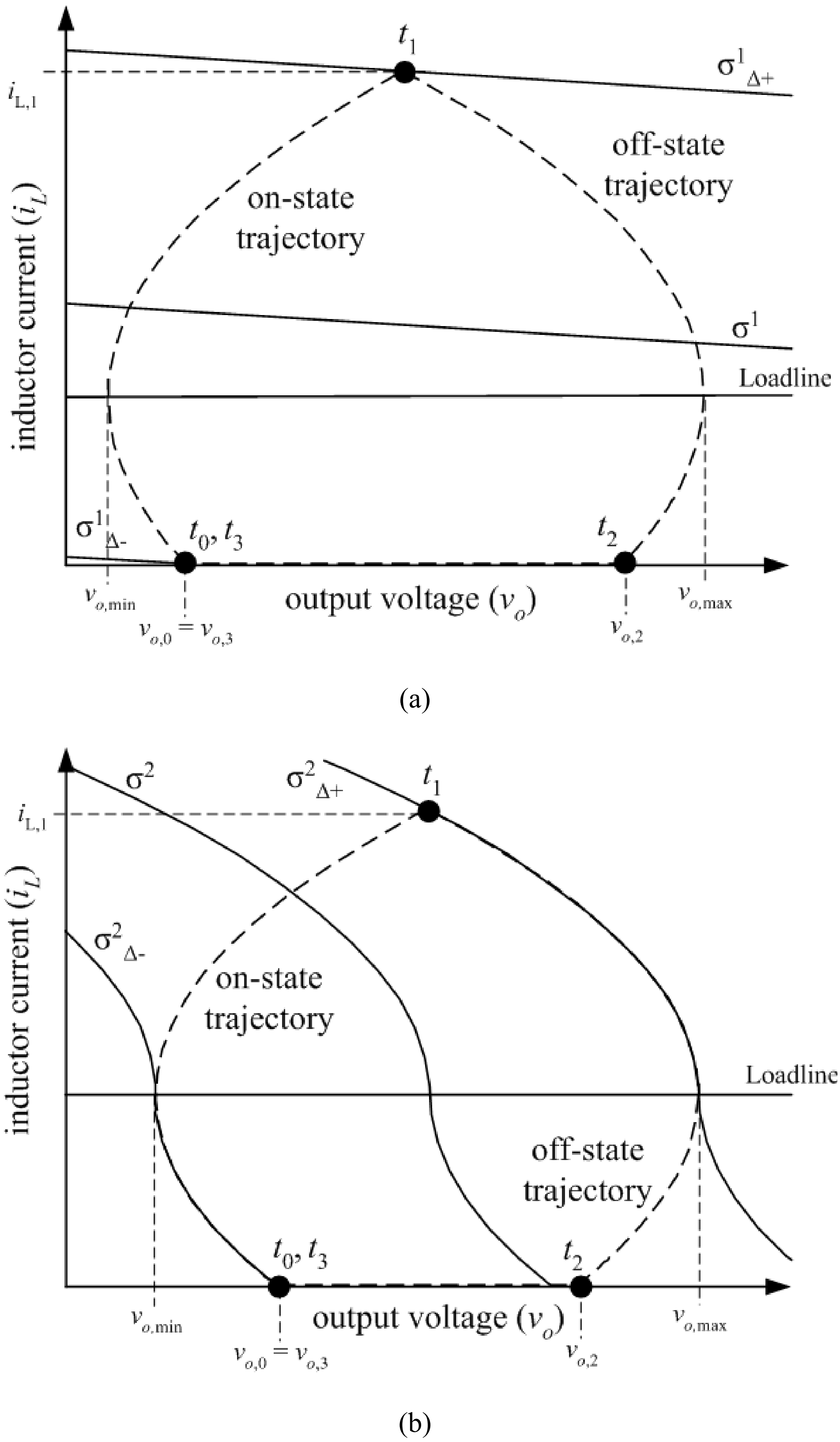

Fig. 4.3 Steady-state trajectories in DCM. (a) σ^1. (b) σ^2.

4.4.1 Average Output Voltage and Output Ripple Voltage

4.4.1.1 With σ^1

As derived in (3.31), the converter is in critical mode, when

$$R = R_{crit}^{<1>} = \frac{v_{ref}\ c_1}{\Delta_1} \tag{4.16}$$

where $R_{crit}^{<1>}$ is the critical load resistance for $r_C = 0$.

By putting (4.13) into (4.4) and (4.5), they give

$$\sigma^1{}_{\Delta+} = c_1 \left(i_{L,1} - \frac{v_{o,1}}{R} \right) + \left(v_{o,1} - \left(v_{ref} + \Delta_1 \right) \right) = 0 \tag{4.17}$$

$$\sigma^1{}_{\Delta-} = c_1 \left(- \frac{v_{o,0}}{R} \right) + \left(v_{o,0} - \left(v_{ref} - \Delta_1 \right) \right) = 0 \tag{4.18}$$

By rearranging (4.18),

$$v_{o,0} = \frac{R}{R - c_1} \left(v_{ref} - \Delta_1 \right) \tag{4.19}$$

By using (4.17) and (4.19) to solve (4.14),

$$v_{o,1} = v_{ref} + \Delta_1 - \Psi_1 \tag{4.20}$$

where $\Psi_1 = \dfrac{\sqrt{1 + 8\,\alpha\,\Delta_1 - 4\,\Phi_1\,\alpha} - 1}{2\,\alpha}$, $\Phi_1 = \dfrac{c_1}{R - c_1}\left(v_{ref} - \Delta_1 \right)\left(1 - \dfrac{c_1\,\alpha\left(v_{ref} - \Delta_1 \right)}{R - c_1} \right)$,

$\alpha = \dfrac{L}{2\,C\,c_1{}^2 \left(v_i - v_{ref} \right)}$.

By substituting (4.20) into (4.17), it can be shown that

$$i_{L,1} = \frac{v_{ref} + \Delta_1 - \Psi_1}{R} + \frac{\Psi_1}{c_1} \tag{4.21}$$

By substituting (4.20) and (4.21) into (4.15), it can be shown that

$$v_{o,2} = \frac{C\,R^2\,v_{ref}}{L} \left(-1 + \sqrt{1 + \frac{2L}{C\,R^2\,v_{ref}} \left(v_{ref} + \Delta_1 - \Psi_1 + \frac{L}{2\,C\,c_1{}^2\,v_{ref}} \Psi_1{}^2 \right)} \right) \tag{4.22}$$

As shown in (3.25) and (3.27), $v_{o,\max}$ and $v_{o,\min}$ can be derived as

$$v_{o,\max} = v_{o,1} + \frac{L}{2\,C\,v_{ref}} \left(i_{L,1} - \frac{v_{o,1}}{R} \right)^2 \tag{4.23}$$

$$v_{o,\min} = v_{o,0} - \frac{L}{2\,C\left(v_i - v_{ref}\right)} \left(i_{L,0} - \frac{v_{o,0}}{R} \right)^2 \tag{4.24}$$

By using (4.20) and (4.21), equation (4.23) can be expressed as,

$$v_{o,\max} = v_{ref} - \Delta_1 + \Phi_1 + \frac{v_i\,\alpha}{v_{ref}}\,\Psi_1^{\,2} \tag{4.25}$$

By using (4.13) and (4.19), equation (4.24) can be expressed as,

$$v_{o,\min} = v_{ref} - \Delta_1 + \Phi_1 \tag{4.26}$$

Thus, by putting (4.25) and (4.26) into (4.9),

$$v_{avg} = v_{ref} - \Delta_1 + \Phi_1 + \frac{v_i\,\alpha}{2\,v_{ref}}\,\Psi_1^{\,2} \tag{4.27}$$

Thus, the value of v_{avg} with σ^1 is dependent on Δ_1.

By putting (4.25) and (4.26) into (4.10), it can be shown that

$$v_{ripple} = \frac{v_i\,\alpha}{v_{ref}}\,\Psi_1^{\,2} \tag{4.28}$$

When $R \to \infty$ and $\Phi_1 \to 0$,

$$v_{avg} = v_{ref} - \Delta_1 + \frac{v_i}{8\,v_{ref}\,\alpha}\left(\sqrt{1 + 8\,\alpha\,\Delta_1} - 1\right)^2 \tag{4.29}$$

$$v_{ripple} = \frac{v_i}{4\,v_{ref}\,\alpha}\left(\sqrt{1 + 8\,\alpha\,\Delta_1} - 1\right)^2 \tag{4.30}$$

4.4.1.2 With σ^2

As derived in (3.46), the converter is in critical mode, when

$$R = R_{crit}^{<2>} = \frac{v_{ref} - \dfrac{k_1 - k_2}{k_1 + k_2}\Delta_2}{\sqrt{\dfrac{2\Delta_2}{k_1 + k_2}}} \tag{4.31}$$

where $R_{crit}^{<2>}$ is the critical load resistance for $r_C = 0$.

By putting (4.13) into (4.6) and (4.7),

$$\sigma^2{}_{\Delta+} = k_1 \left(i_{L,1} - \frac{v_{o,1}}{R} \right)^2 + \left(v_{o,1} - \left(v_{ref} + \Delta_2 \right) \right) = 0 \tag{4.32}$$

$$\sigma^2{}_{\Delta-} = -k_2 \left(\frac{v_{o,0}}{R} \right)^2 + \left(v_{o,0} - \left(v_{ref} - \Delta_2 \right) \right) = 0 \tag{4.33}$$

By solving (4.33) for $v_{o,0}$, it gives

$$v_{o,0} = \frac{R^2}{2k_2} \left(1 - \sqrt{1 - \frac{4k_2}{R^2} \left(v_{ref} - \Delta_2 \right)} \right) \tag{34}$$

By solving (4.14) with (4.32) and (4.34), it gives

$$v_{o,1} = v_{ref} + \Delta_2 - \Psi_2 \tag{4.35}$$

where $\Psi_2 = \dfrac{2\Delta_2 - \Phi_2}{1+\beta}$, $\Phi_2 = \left(k_2 - \beta k_1 \right) \left(\dfrac{R}{2k_2} \left(1 - \sqrt{1 - \dfrac{4k_2}{R^2} \left(v_{ref} - \Delta_2 \right)} \right) \right)^2$,

$\beta = \dfrac{L}{2 C k_1 \left(v_i - v_{ref} \right)}$.

By substituting (4.35) into (4.32), it can shown that

$$i_{L,1} = \frac{v_{ref} + \Delta_2 - \Psi_2}{R} + \sqrt{\frac{\Psi_2}{k_1}} \tag{4.36}$$

By substituting (4.35) and (4.36) into (4.15), it can shown that

$$v_{o,2} = \frac{C R^2 v_{ref}}{L} \left(-1 + \sqrt{1 + \frac{2L}{C R^2 v_{ref}} \left(v_{ref} + \Delta_2 - \Psi_2 + \frac{L}{2 C v_{ref} k_1} \Psi_2 \right)} \right) \tag{4.37}$$

By using (4.35) and (4.36), equation (4.23) can be expressed as,

$$v_{o,\max} = v_{ref} - \Delta_2 + \Phi_2 + \frac{v_i \beta}{v_{ref}} \Psi_2 \tag{4.38}$$

By using (4.13) and (4.34), equation (4.24) can be expressed as,

$$v_{o,\min} = v_{ref} - \Delta_2 + \Phi_2 \tag{4.39}$$

By substituting (4.38) and (4.39) into (4.9), it can shown that

$$v_{avg} = v_{ref} - \Delta_2 + \Phi_2 + \frac{v_i \beta}{2 v_{ref}} \Psi_2 \tag{4.40}$$

By putting (4.38) and (4.39) into (4.10),

$$v_{ripple} = \frac{v_i \beta}{v_{ref}} \Psi_2 \tag{4.41}$$

When $R \to \infty$ and $\Phi_2 \to 0$,

$$v_{avg} = v_{ref} - \Delta_2 + \frac{\beta}{1+\beta} \frac{v_{in}}{v_{ref}} \Delta_2 \tag{4.42}$$

$$v_{ripple} = \frac{2\beta}{1+\beta} \frac{v_i}{v_{ref}} \Delta_2 \tag{4.43}$$

With the ideal values of k_1 and k_2 in (4.8),

$$v_{avg} = v_{ref} \tag{4.44}$$

$$v_{ripple} = 2\Delta_2 \tag{4.45}$$

for $R > R_{crit}^{<2>}$. It can be noted that v_{avg} is independent on Δ_2.

4.4.2 Switching Frequency

In DCM, $i_{L,0} = i_{L,2} = i_{L,3} = 0$ and $v_{o,0} = v_{o,3}$. For $r_C = 0$, the average output current I_o can be expressed as,

$$I_o = \bar{i}_L = \frac{1}{T_S} \int_{t_0}^{t_3} i_L \, dt = \frac{1}{T_S} \left(\int_{t_0}^{t_1} i_L \, dt + \int_{t_1}^{t_2} i_L \, dt + \int_{t_2}^{t_3} i_L \, dt \right) \tag{4.46}$$

$$I_o = \frac{1}{T_S} \left(\int_{i_{L,0}}^{i_{L,1}} \frac{L i_L}{v_i - v_{ref}} di_L + \int_{i_{L,1}}^{i_{L,2}} \frac{-L i_L}{v_{ref}} di_L + \int_{i_{L,2}}^{i_{L,3}} 0 \, di_L \right) = \frac{1}{T_S} \frac{L v_i \, i_{L,1}{}^2}{2 v_{ref} \left(v_i - v_{ref} \right)} \tag{4.47}$$

Therefore, the switching frequency f_S can be expressed as

$$f_S = \frac{1}{T_S} = \frac{2 v_{ref} \left(v_i - v_{ref} \right)}{L v_i \, i_{L,1}{}^2} I_o \tag{4.48}$$

4.4.2.1 With σ¹

Thus, the switching frequency for σ^1 can be obtained by substituting (4.21) into (4.48),

$$f_S = \frac{1}{T_S} = \frac{2 v_{ref}\left(v_i - v_{ref}\right)}{L v_i \left(\frac{v_{ref} + \Delta_1 - \Psi_1}{R} + \frac{\Psi_1}{c_1}\right)^2} I_o \tag{4.49}$$

4.4.2.2 With σ²

The switching frequency with σ^2 can be calculated by substituting (4.36) into (4.48),

$$f_S = \frac{1}{T_S} = \frac{2 v_{ref}\left(v_i - v_{ref}\right)}{L v_i \left(\frac{v_{ref} + \Delta_2 - \Psi_2}{R} + \sqrt{\frac{\Psi_2}{k_1}}\right)^2} I_o \tag{4.50}$$

4.4.3 Simplified Expressions of v_{avg}, v_{ripple}, and f_S

Eqs. (4.29), (4.30), and (4.49) give the expressions of v_{avg}, v_{ripple}, and f_S for converters with σ^1, while Eqs. (4.40), (4.41), and (4.50) give the expressions for converters with σ^2. In order to study their relationships with the load current, some simplifications have been adopted and discussed in the following.

4.4.3.1 With σ¹

By substituting $[i_{L,0}, v_{o,0}] = [0, v_{o,\min}]$ into (4.5) and assuming $v_{o,\min} \approx v_{avg}$,

$$v_{avg} = c_1 I_o + v_{ref} - \Delta_1 \tag{4.51}$$

where $I_o = \frac{v_{avg}}{R}$.

By substituting $v_{o,1}$ with v_{avg} in (4.20) and comparing the result with (4.51), it gives

$$\Psi_1 = 2\,\Delta_1 - c_1\,I_o \tag{4.52}$$

Then, by putting (4.52) into (4.28), it gives

$$v_{ripple} = \frac{v_i\,\alpha}{v_{ref}}\left(c_1\,I_o - 2\,\Delta_1\right)^2 \tag{4.53}$$

By putting (4.20) and (4.52) into (4.21), it can be shown that

$$i_{L,1} = \frac{2\,\Delta_1}{c_1} \tag{4.54}$$

Thus, by substituting (4.54) into (4.48), the switching frequency can be expressed as,

$$f_S = \frac{1}{T_S} = \frac{2\,v_{ref}\left(v_i - v_{ref}\right)}{L\,v_i\left(\dfrac{2\,\Delta_1}{c_1}\right)^2}\,I_o \tag{4.55}$$

Fig. 4.4 shows the steady-state characteristics against the load current I_o. $I_{o,crit}$ is the value of I_o when $R = R_{crit}^{<1>}$.

4.4.3.2 With σ^2

For the ideal values of k_1 and k_2 in (4.8), $k_2 - \beta\,k_1 = 0 \Rightarrow \Phi_2 = 0$. Thus,

$$\Psi_2 = \frac{2\,\Delta_2}{1+\beta} \tag{4.56}$$

By substituting $v_{o,1}$ with v_{avg}, and (4.35) into (4.36), (4.40), and (4.41), it can be shown that

$$i_{L,1} = I_o + \sqrt{\frac{2\,\Delta_2}{k_1\left(1+\beta\right)}} = I_o + \sqrt{\frac{2\,\Delta_2}{k_1 + k_2}} \tag{4.57}$$

and

$$v_{avg} = v_{ref} + \left(\frac{v_i}{v_{ref}} \frac{\beta}{1+\beta} - 1 \right) \Delta_2 \tag{4.58}$$

and

$$v_{ripple} = \frac{2\, v_i}{v_{ref}} \frac{\beta}{1+\beta} \Delta_2 \tag{4.59}$$

Thus, by putting (4.57) into (4.48), the switching frequency can be expressed as

$$f_S = \frac{1}{T_S} = \frac{2\, v_{ref} \left(v_i - v_{ref} \right)}{L\, v_i \left(I_o + \sqrt{\dfrac{2\,\Delta_2}{k_1 + k_2}} \right)^2} I_o \tag{4.60}$$

Fig. 4.5 shows the steady-state characteristics against the load current I_o.

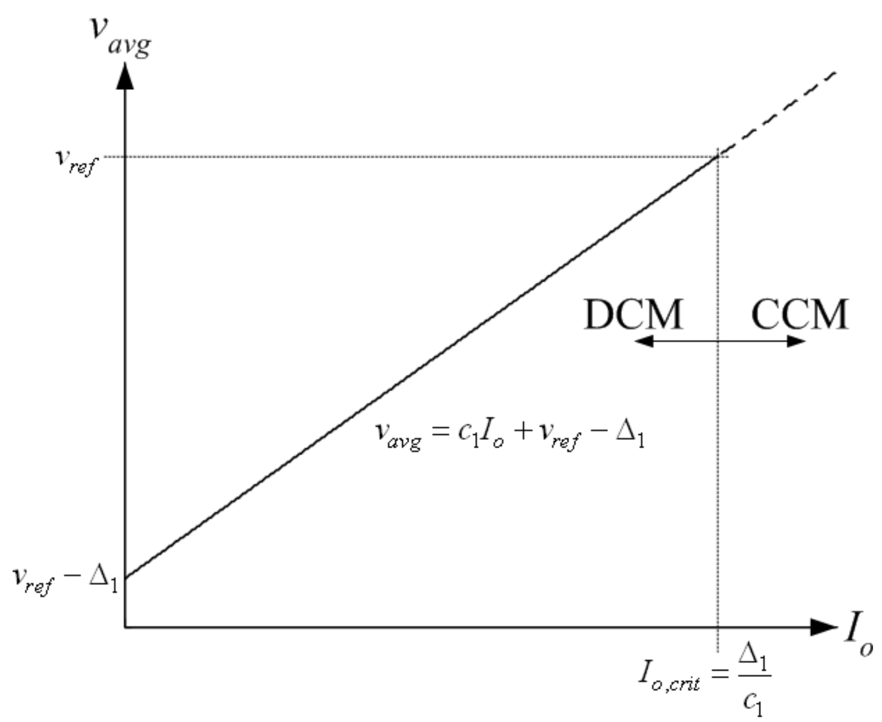

(a)

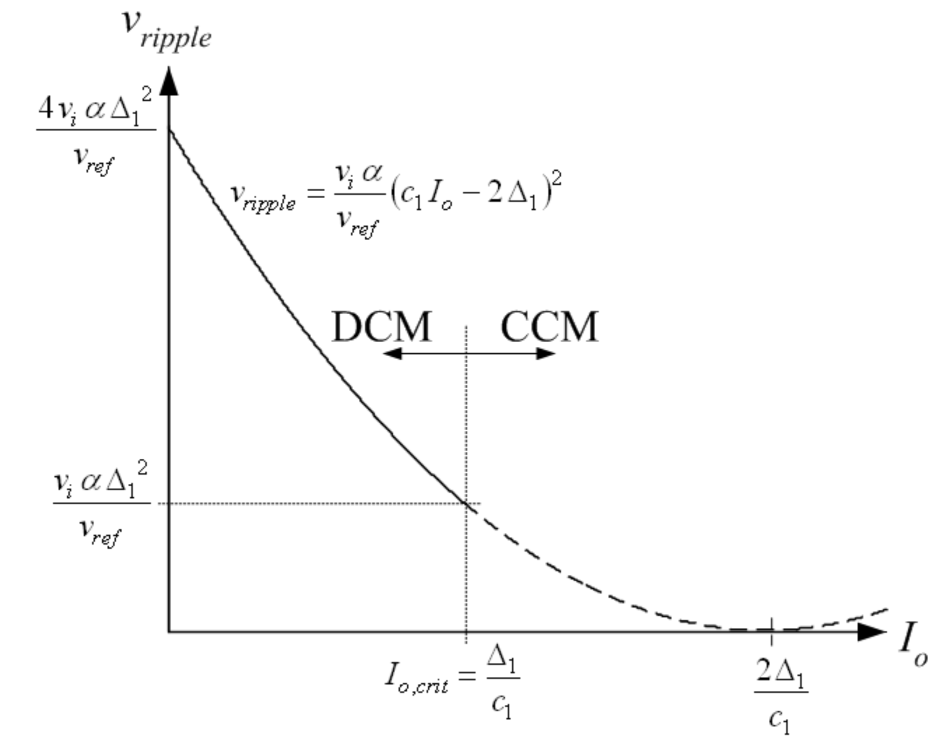

(b)

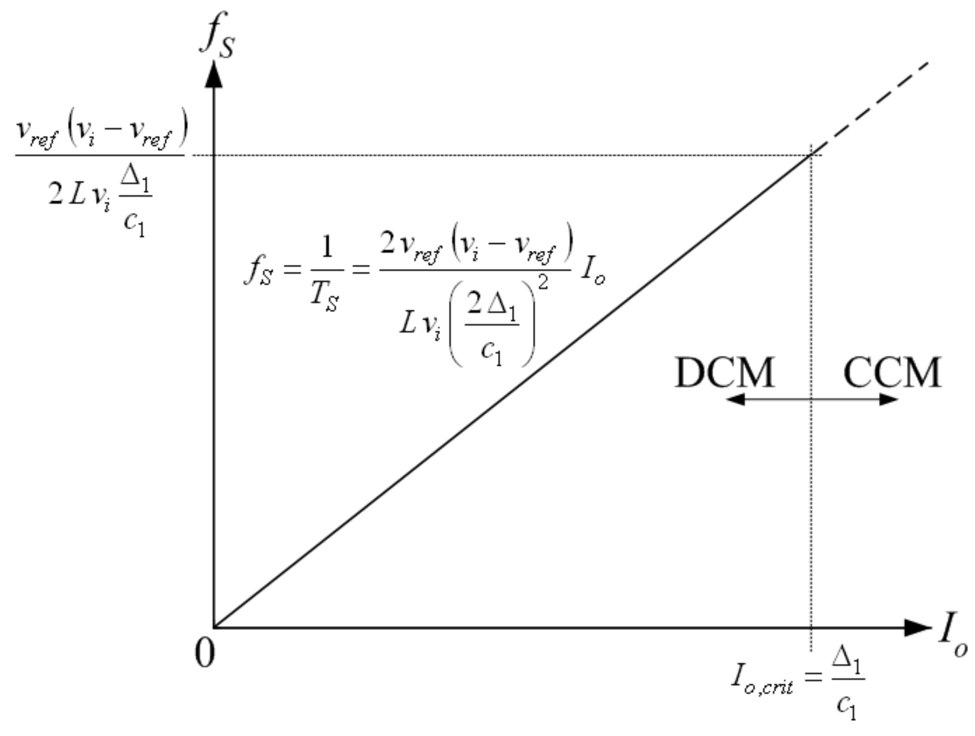

(c)

Fig. 4.4 Steady-state characteristics of converters with σ^1. (a) v_{avg}. (b) v_{ripple}. (c) f_S.

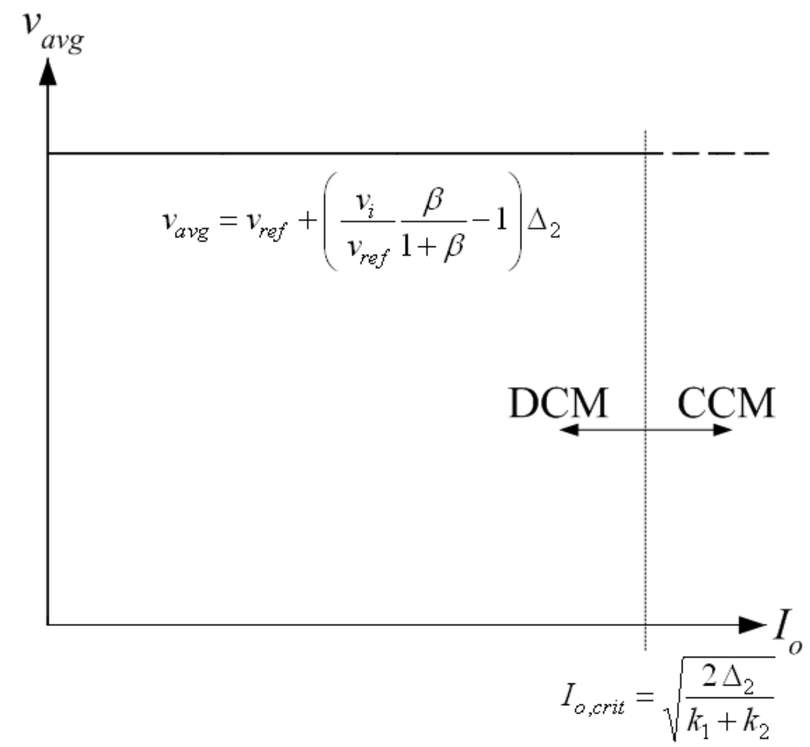

v_{avg}
$v_{avg} = v_{ref} + \left(\frac{v_i}{v_{ref}} \frac{\beta}{1+\beta} - 1 \right) \Delta_2$
DCM
CCM
I_o
$I_{o,crit} = \sqrt{\frac{2\Delta_2}{k_1 + k_2}}$

(a)

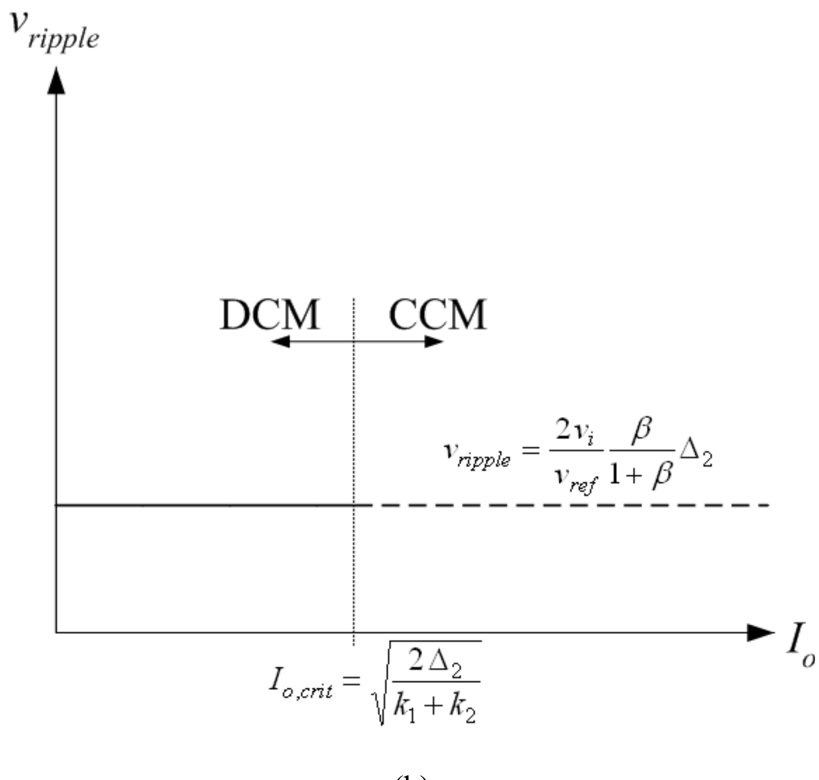

v_{ripple}
DCM
CCM
$v_{ripple} = \frac{2v_i}{v_{ref}} \frac{\beta}{1+\beta} \Delta_2$
I_o
$I_{o,crit} = \sqrt{\frac{2\Delta_2}{k_1 + k_2}}$

(b)

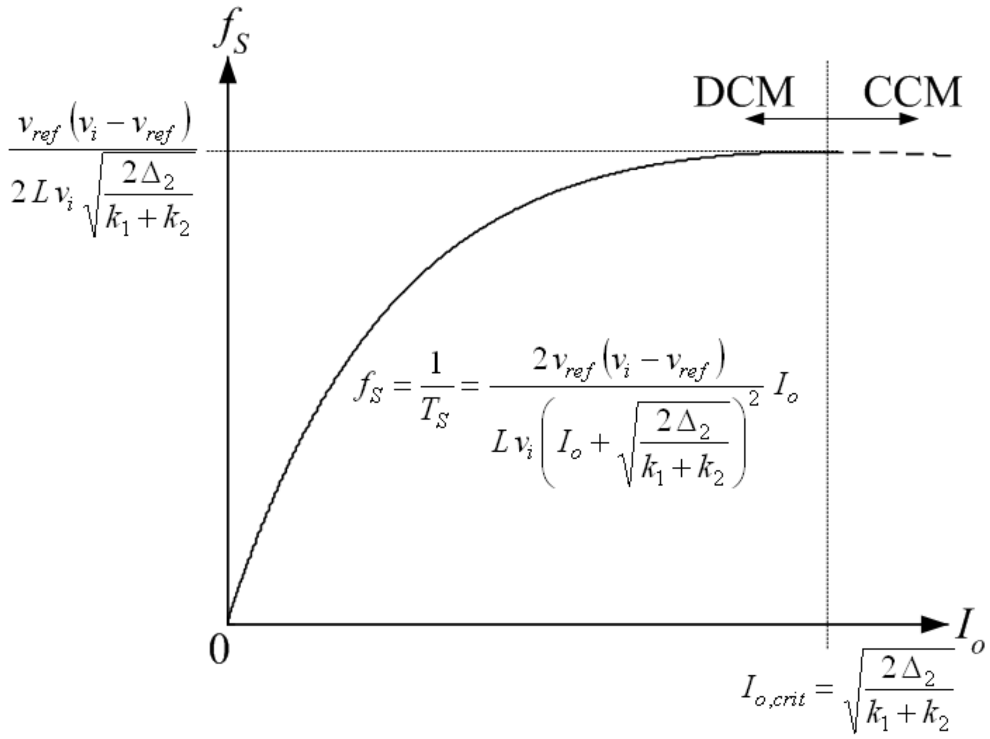

(c)

Fig. 4.5 Steady-state characteristics of converters with σ^2. (a) v_{avg}. (b) v_{ripple}. (c) f_S.

4.4.4. Effects of r_C on the Operating Mode

As illustrated in Fig. 4.6(a), the on- and off-state trajectories vary with r_C. Figs. 4.6(b) and (c) show the shifts of the steady-state trajectories with different values of r_C for the converter with σ^1 and σ^2, respectively. The analyses are based on the component values tabulated in Table 4.1. The converter changes from DCM to CCM, as r_C increases. Moreover, the steady-state on and off trajectories will move along the same path and become a straight line. Similar to the method described in *Chapter 3*, a straight line of slope *m* connecting the two switching instants t_0 and t_1 can be expressed as

$$m = \frac{i_{L,1} - i_{L,0}}{v_{o,1} - v_{o,0}} = \frac{R + r_C}{R\,r_C} \tag{4.61}$$

By putting $i_{L,0}$ = 0 and assuming that the line passes through the point $\{ v_{ref}$, $\frac{v_{ref}}{R} \}$ in CCM, (4.61) can be expressed as

$$r_C = \left(\frac{v_{ref}}{v_{o,0}} - 1 \right) R \tag{4.62}$$

Thus, the critical value of r_C, $r_{C,crit}$, that the converter starts operating in CCM can be calculated by substituting (4.19) into (4.62) for σ^1, and (4.34) into (4.62) for σ^2. For σ^1,

$$r_{C,crit}^{<1>} = R\left(\frac{\Delta_1}{v_{ref} - \Delta_1} \right) - c_1 \left(\frac{v_{ref}}{v_{ref} - \Delta_1} \right) \tag{4.63}$$

For σ^2,

$$r_{C,crit}^{<2>} = \left(\frac{2k_2 v_{ref}}{R^2 \left(1 - \sqrt{1 - \frac{4k_2}{R^2}\left(v_{ref} - \Delta_2 \right)} \right)} - 1 \right) R \tag{4.64}$$

Table 4.1 Component values of the prototype

Parameter	Value
v_i	24 V
v_{ref}	12 V
L	100 μH
C	400 μF
R	60 Ω
c_1	0.2702
$\{k_1 , k_2\}$	{0.0104, 0.0104}
f_S	20 kHz
Δ_1	405.3 mV
Δ_2	23.4 mV

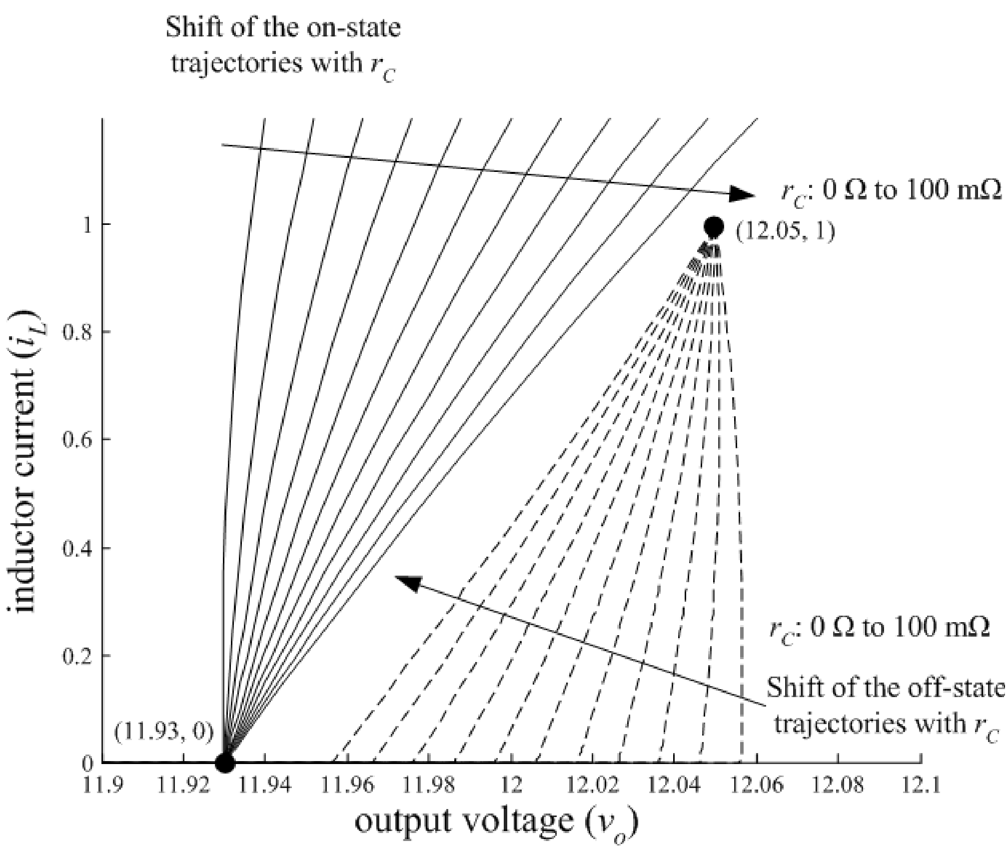

Shift of the on-state trajectories with r_C
r_C: 0 Ω to 100 mΩ
(12.05, 1)
inductor current (i_L)
r_C: 0 Ω to 100 mΩ
Shift of the off-state trajectories with r_C
(11.93, 0)
output voltage (v_o)

(a)

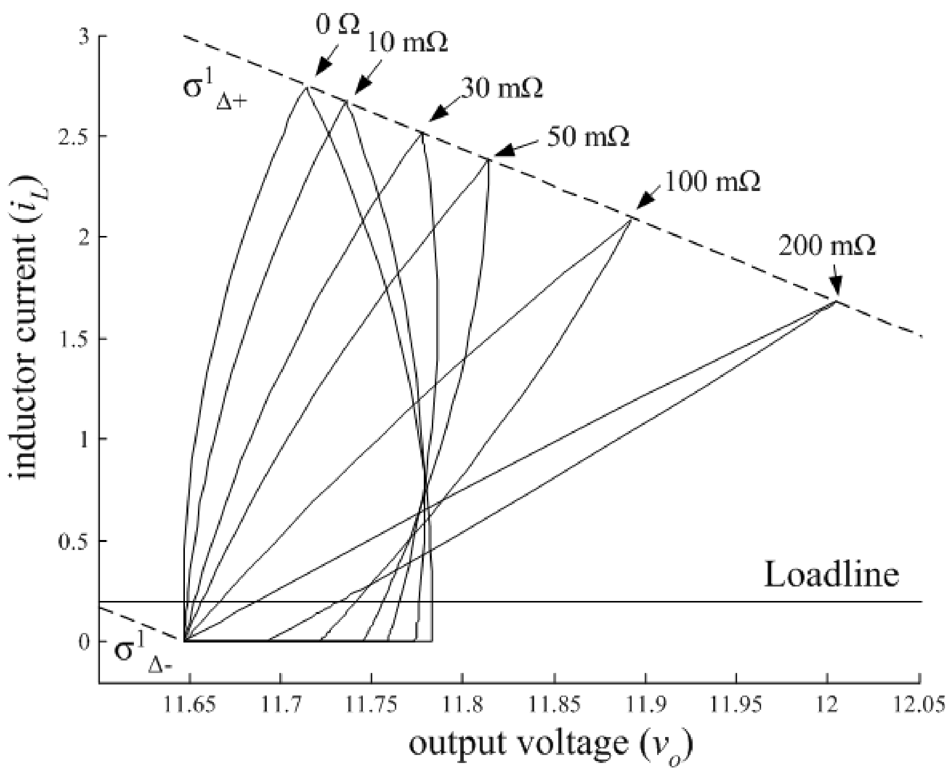

0 Ω
10 mΩ
30 mΩ
50 mΩ
100 mΩ
200 mΩ
$\sigma^1_{\Delta+}$
inductor current (i_L)
Loadline
$\sigma^1_{\Delta-}$
output voltage (v_o)

(b)

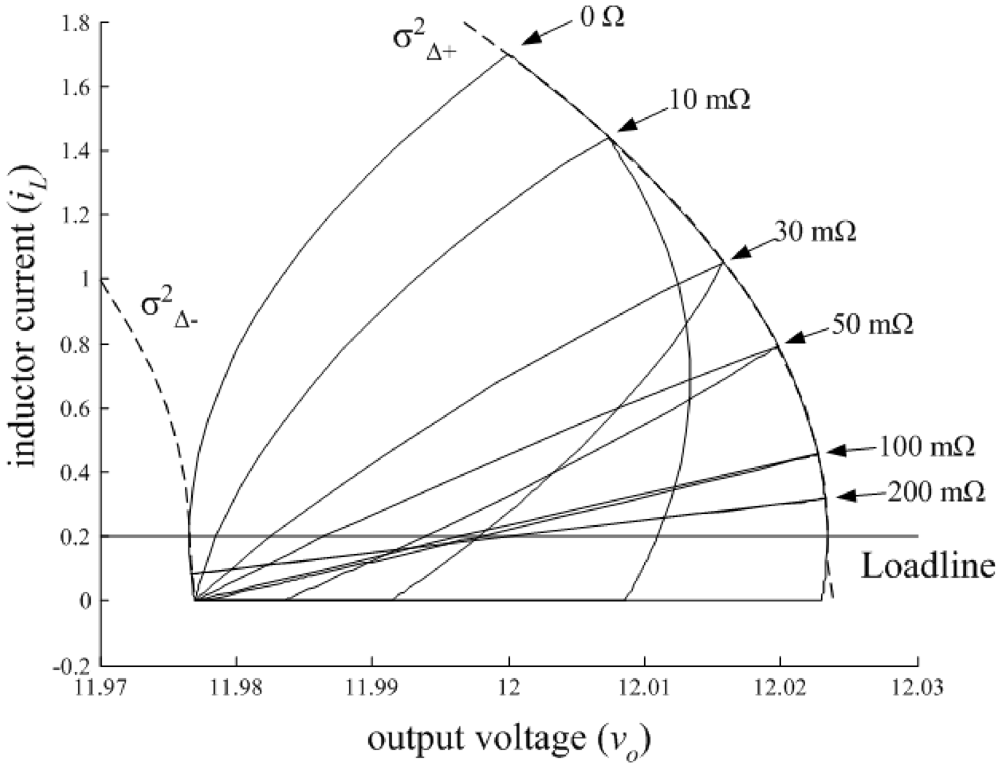

(c)

Fig. 4.6 Shift of steady-state trajectories against r_C. (a) on-state and off-state trajectories. (b) Converter trajectories with σ^1. (c) Converter trajectories with σ^2.

4.5 Parametric Variations on Converter Characteristics

The components L and C, and v_i are subject to variation

$$v_i = v_{i,N}\left(1+\delta_1\right) \tag{4.65}$$

$$L = L_N\left(1+\delta_2\right) \tag{4.66}$$

$$C = C_N\left(1+\delta_3\right) \tag{4.67}$$

where $v_{i,N}$, L_N, and C_N are the nominal values of v_i, L and C, respectively, δ_1, δ_2 and δ_3 are the fractional variations of v_i, L and C, respectively. Sensitivities of v_{avg}, v_{ripple}, and f_S to δ_1, δ_2 and δ_3 are based on eqs. (4.51), (4.53), (4.55) for σ^1 and eqs. (4.58)-(4.60) for σ^2.

4.5.1 With σ^1

By substituting (4.65)-(4.67) into (4.51), (4.53) and (4.55), the % change of v_{avg}, v_{ripple}, and f_S from its nominal value are

$$\%\Delta v_{avg} = \frac{v_{avg}\left(v_i, L, C\right) - v_{avg}\left(v_{i,N}, L_N, C_N\right)}{v_{avg}\left(v_{i,N}, L_N, C_N\right)} = 0 \tag{4.68}$$

$$\%\Delta v_{ripple} = \frac{v_{ripple}(v_i, L, C) - v_{ripple}(v_{i,N}, L_N, C_N)}{v_{ripple}(v_{i,N}, L_N, C_N)} = \xi_1(\delta_1, \delta_2, \delta_3) \tag{4.69}$$

$$\%\Delta f_S = \frac{f_S(v_i, L, C) - f_S(v_{i,N}, L_N, C_N)}{f_S(v_{i,N}, L_N, C_N)} = \xi_2(\delta_1, \delta_2, \delta_3) \tag{4.70}$$

where $D_N = \frac{v_{ref}}{v_{i,N}}$ is nominal duty cycle, $\xi_1(\delta_1, \delta_2, \delta_3) = \frac{\left(1+\delta_1\right)\left(1+\delta_2\right)\left(1-D_N\right)}{\left(1+\delta_3\right)\left(1+\delta_1-D_N\right)} - 1$, and $\xi_2(\delta_1, \delta_2, \delta_3) = \frac{\left(1+\delta_1\right) - D_N}{\left(1+\delta_1\right)\left(1+\delta_2\right)\left(1-D_N\right)} - 1$.

4.5.2 With σ^2

By substituting (4.65)-(4.67) into (4.58), (4.59) and (4.60), the % change of v_{avg}, v_{ripple}, and f_S from its nominal value are

$$\%\Delta v_{avg} = \xi_3(\delta_1, \delta_2, \delta_3)\ \frac{\Delta_2}{v_{ref}} \tag{4.71}$$

$$\%\Delta v_{ripple} = \xi_3(\delta_1, \delta_2, \delta_3) \tag{4.72}$$

$$\%\Delta f_S = \xi_2(\delta_1, \delta_2, \delta_3) \tag{4.73}$$

where $\xi_3(\delta_1, \delta_2, \delta_3) = \frac{\left(1+\delta_1\right)\left(1+\delta_2\right)}{\left(1+\delta_1\right)\left(1+\delta_3\right) + D_N\left(\delta_2 - \delta_3\right)} - 1$.

By using the function of "fmincon" on MATLAB, Fig. 4.7 shows the maximum value of ξ_1, ξ_2, and ξ_3 at different duty cycle D_N from 0.1 to 0.7, where v_i is subject to a maximum variation of ±20% (i.e., $\delta_1 \in [-0.2, +0.2]$) , and *L* and *C* are subject to a maximum variation of ±10% (i.e., $\delta_2, \delta_3 \in [-0.1, +0.1]$).

v_{avg} in σ^2 [eq. (4.71)] is sensitive to the component variation, as compared with σ^1 [eq. (4.68)]. It is mainly because σ^2 is dependent on the component values, while σ^1 is explicitly determined. However, as shown in (4.71), $\Delta_2 << v_{ref}$, the variation of v_{avg} with respect to parametric variation is very small.

Compared (4.69) with (4.72), the variation of v_{ripple} in σ^2 is much less than that of σ^1. The former one only varies between -15% and +20%, while the latter one can be up to 200%.

Compared (4.70) with (4.73), the frequency variations in the two switching surfaces are the same.

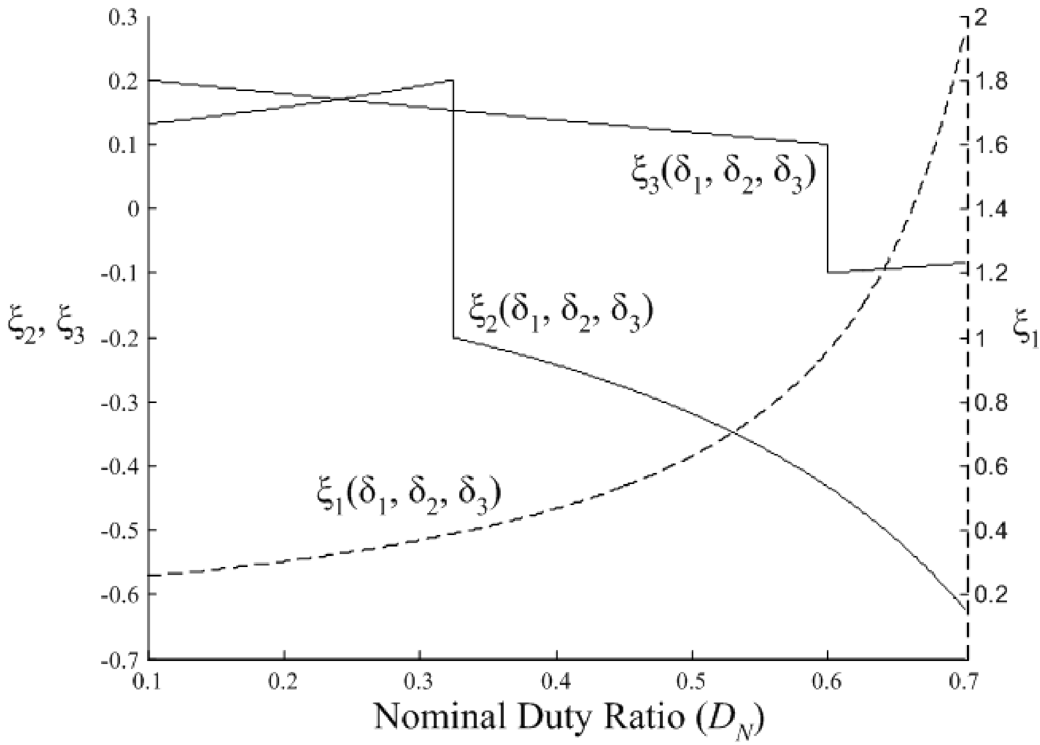

Fig. 4.7 Maximum values of ξ_1, ξ_2, and ξ_3 at different duty cycle D_N .

4.6 Large-Signal Characteristics

The large-signal analysis method shown in *Chapter 3* is based on assuming that the hysteresis band is zero. As DCM is introduced by nonzero hysteresis band, the large-signal characteristics are studied by considering the transition boundaries of the upper and lower bounds. The transition boundaries with σ^1 and σ^2 are shown in Fig. 4.8. As illustrated in Fig. 4.8(a), the transition boundaries for $\sigma^1_{\Delta-}$ and $\sigma^1_{\Delta+}$ are all in the reflective regions (as shown in Fig. 3.5(a)) and thus the converter is in the sliding mode. The transition boundaries for $\sigma^2_{\Delta-}$ and $\sigma^2_{\Delta+}$ are similar to the ones in CCM and are always on the boundaries of reflective and refractive regions [Fig. 4.8(b)]. It exhibits the advantages of providing near-optimum transient response to large-signal disturbances. Detailed discussions can be found in *Chapter 3*.

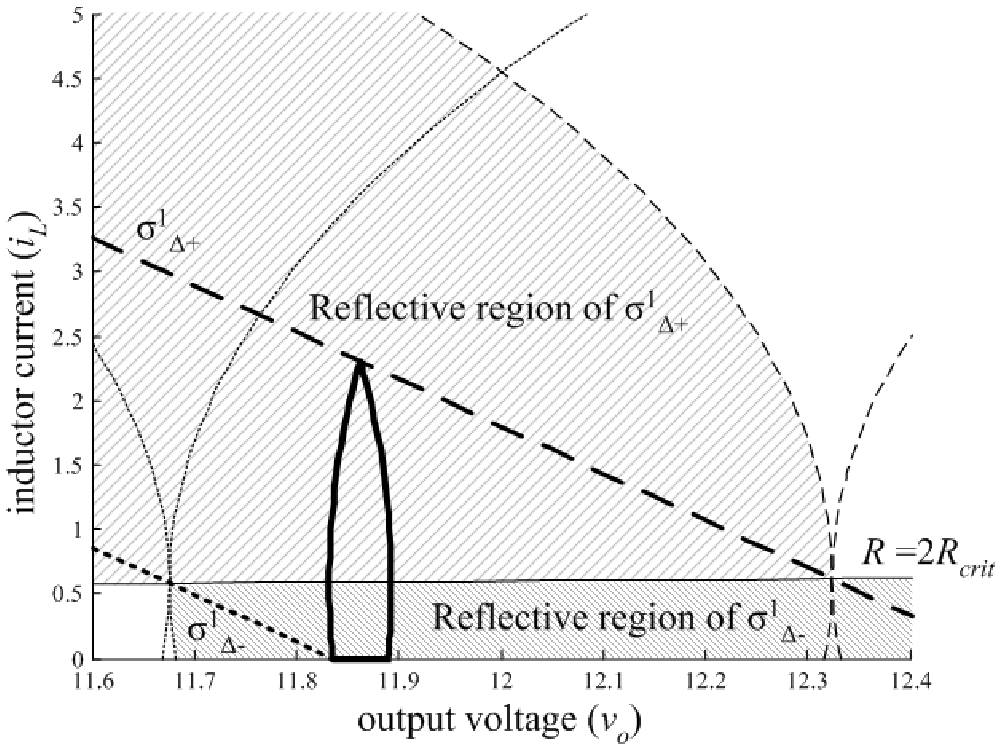

(a)

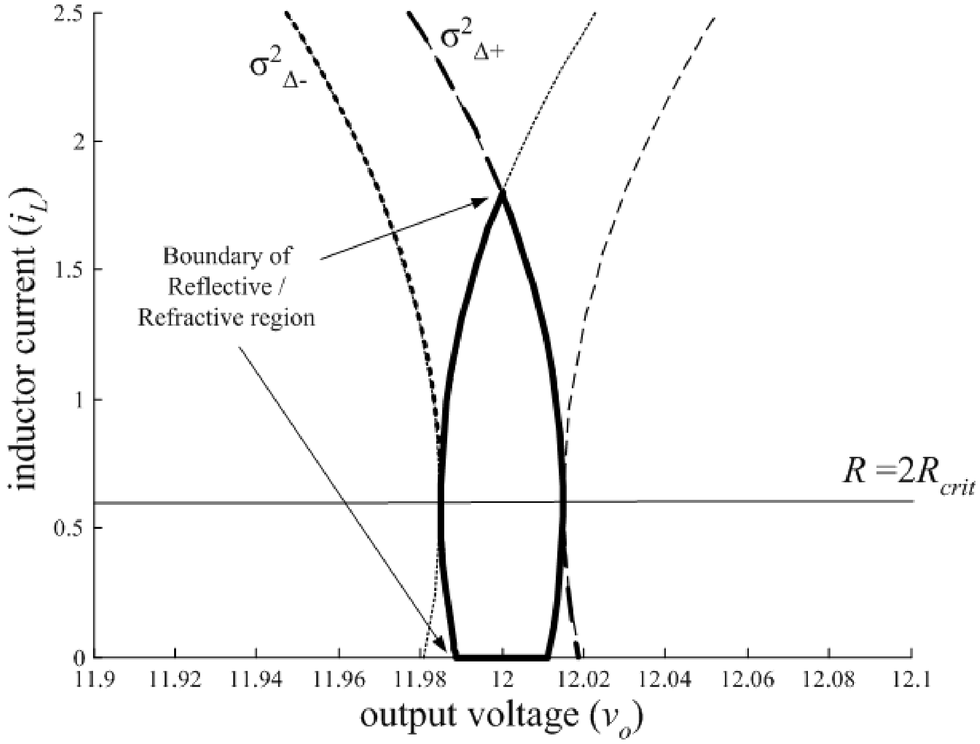

(b)

Fig. 4.8 Transition boundaries of the upper and lower bounds. (a) σ^1. (b) σ^2.

4.7 Experimental Verifications

A buck converter with the component values tabulated in Table 4.1 is studied. The parameter c_1 in σ^1 is obtained by optimizing the startup transient as in *Chapter 3*. Fig. 4.9 shows the transient responses with σ^1 and σ^2, respectively, when the output load is changed from 0.2 A (2.4 W) to 0.8 A (9.6 W), and vice versa. It can be seen that the output has a voltage drift in σ^1 and does not appear in σ^2. σ^1 takes about 200μs to settle, while σ^2 seems to have no transient period. Fig. 4.10 shows the converter response when it is subject to a large-signal change that the load is changed from 0.5 A (6 W) to 3 A (36 W), and vice versa. The operating mode of the converter is switched between DCM and CCM. The converter with σ^1 takes more than 500μs to settle from 0.5 A to 3 A and takes 200μs from 3 A to 0.5 A. The one with σ^2 takes about 50μs to settle from 0.5 A to 3 A and takes 150μs from 3 A to 0.5 A. Thus, σ^2 exhibits better dynamic response than σ^1. With the same control law, the converter with σ^2 can regulate the output in both modes and there is no voltage drift. The dynamic response with σ^2 is much better than that of σ^1. Fig. 4.11(a)-(d) shows the converter output with r_C equal to 30 mΩ, 50 mΩ, 100 mΩ and 200 mΩ, respectively. The output current is changed from 2 A to 0.2 A. The equivalent value of R when I_o = 0.2 A is 60 Ω. Based on (4.64), $r_{C,crit}^{<2>}$ = 115 mΩ. When r_C = 100 mΩ, the converter at I_o = 0.2 A is close to the critical mode [Fig. 4.11(c)]. When r_C = 200 mΩ, the converter at I_o = 0.2 A is in CCM [Fig. 4.11(d)]. This confirms the discussion in Sec. 4.4. Fig 4.12 shows the measurement results of v_{avg}, v_{ripple}, and f_S with σ^1 and σ^2, as compared with eqs. (4.29), (4.30), and (4.49) for σ^1 and eqs. (4.40), (4.41) and (4.50) for σ^2. Theoretical predictions are in good agreement with experimental results.

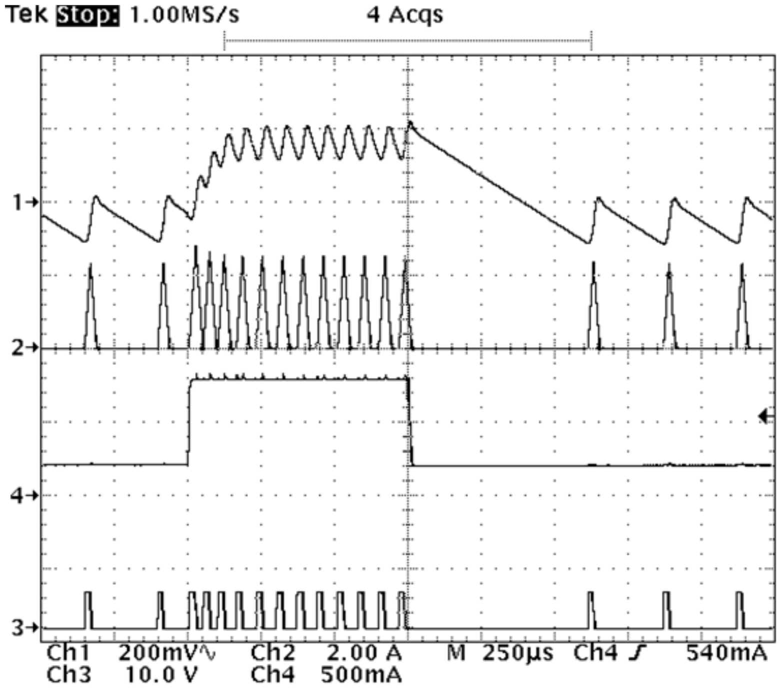

(a)

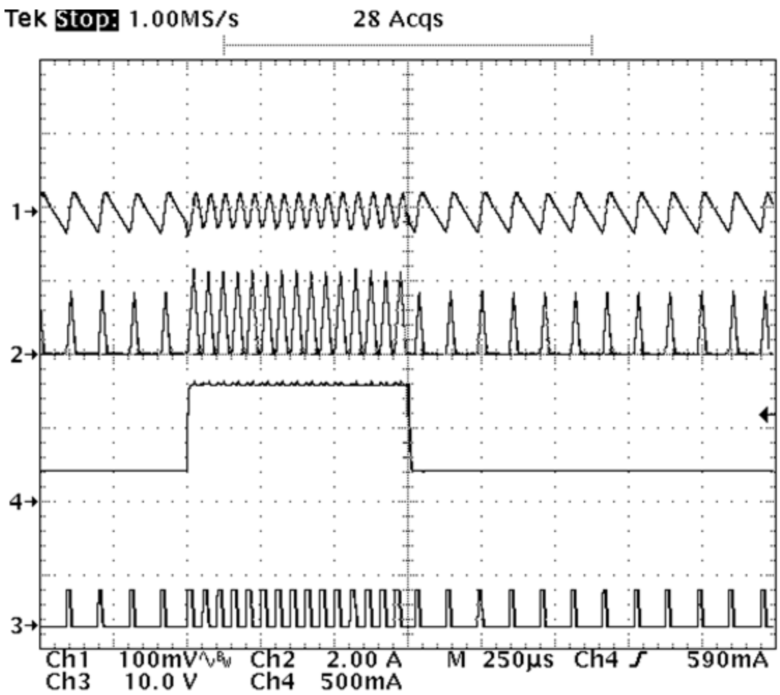

(b)

Fig. 4.9 Transient response of buck converter when load change from 0.2 A (2.4 W) to 0.8 A (9.6 W), and vice versa. [Ch2: i_L (2 A/div), Ch3: v_g (10 V/div), Ch4: i_o (500 mA/div)] (Timebase: 250μs/div) (a) σ^1 [Ch1: v_o (200 mV/div)]. (b) σ^2 [Ch1: v_o (100 mV/div)].

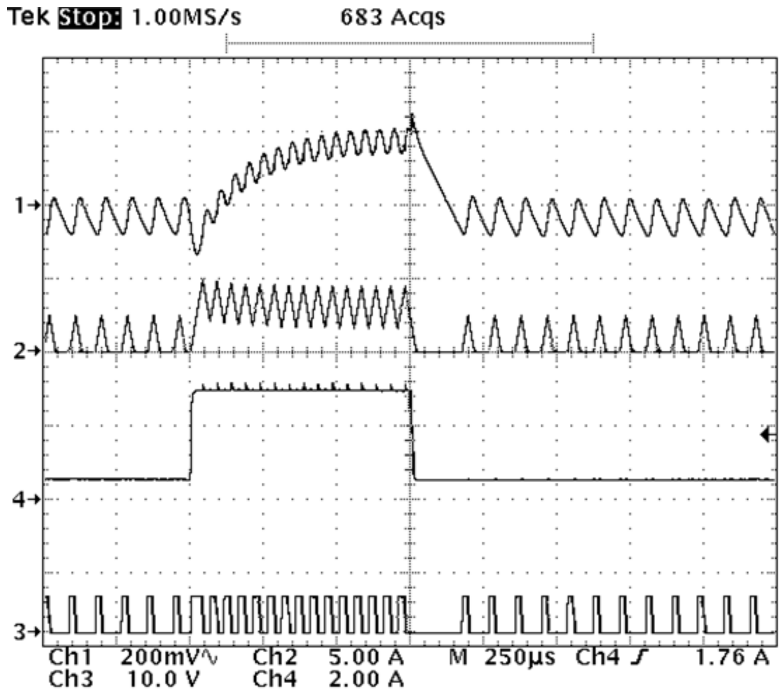

(a)

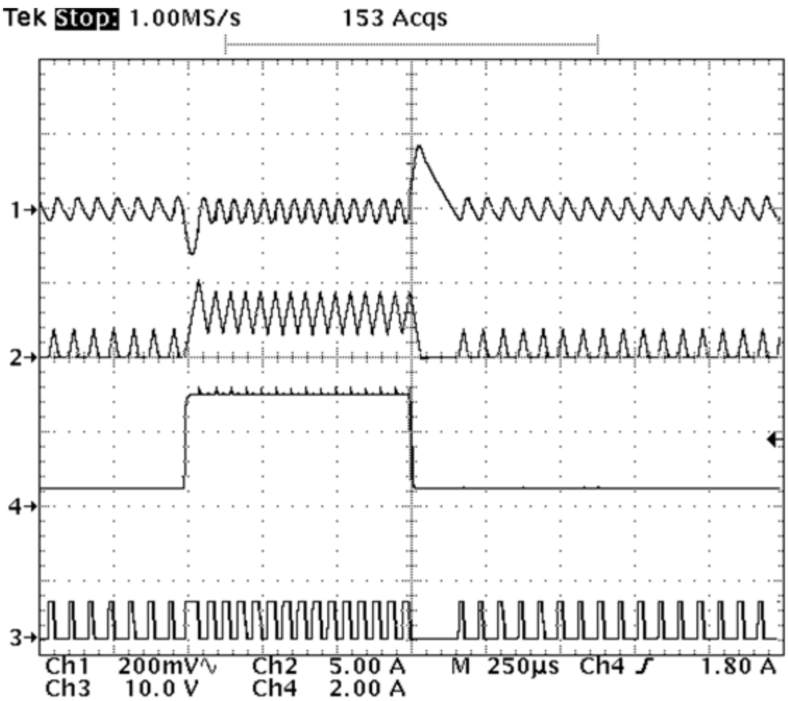

(b)

Fig. 4.10 Transient response of buck converter when load change from 0.5 A (6 W) to 3 A (36 W), and vice versa. [Ch1: v_o (200 mV/div), Ch2: i_L (5 A/div), Ch3: v_g (10 V/div), Ch4: i_o (2 A/div)] (Timebase: 250μs/div) (a) σ^1. (b) σ^2.

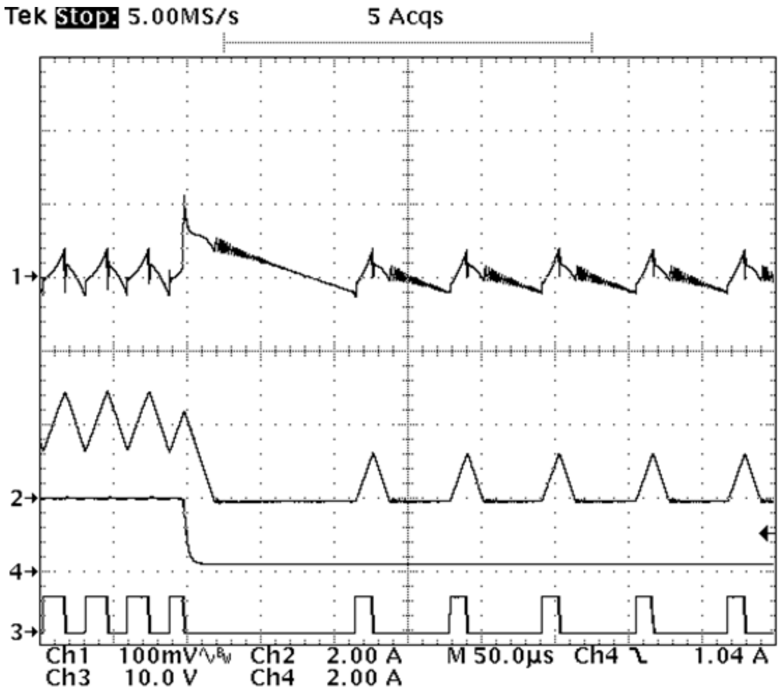
Tek Stop: 5.00MS/s
5 Acqs
1→
2→
4→
3→
Ch1 100mV Ch2 2.00 A M 50.0µs Ch4 1.04 A
Ch3 10.0 V Ch4 2.00 A

(a)

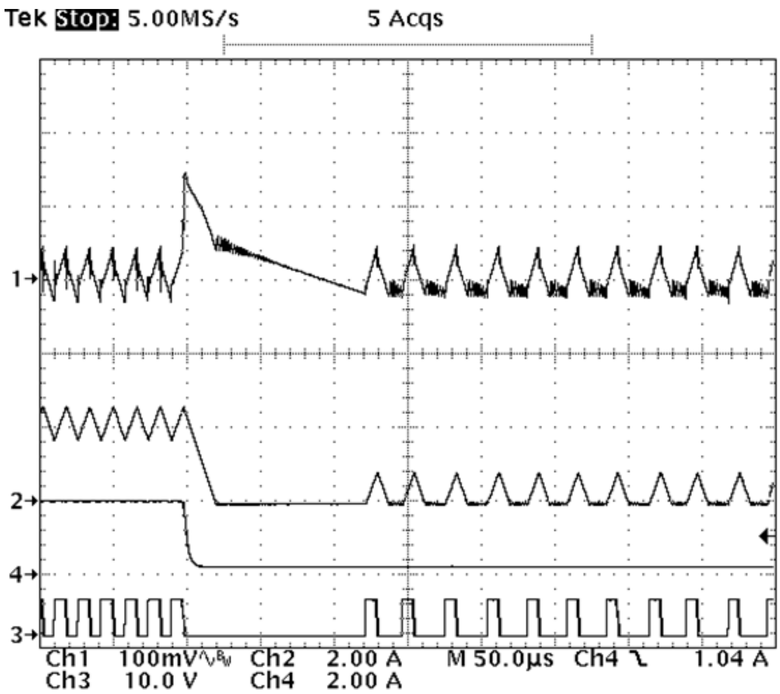
Tek Stop: 5.00MS/s
5 Acqs
1→
2→
4→
3→
Ch1 100mV Ch2 2.00 A M 50.0µs Ch4 1.04 A
Ch3 10.0 V Ch4 2.00 A

(b)

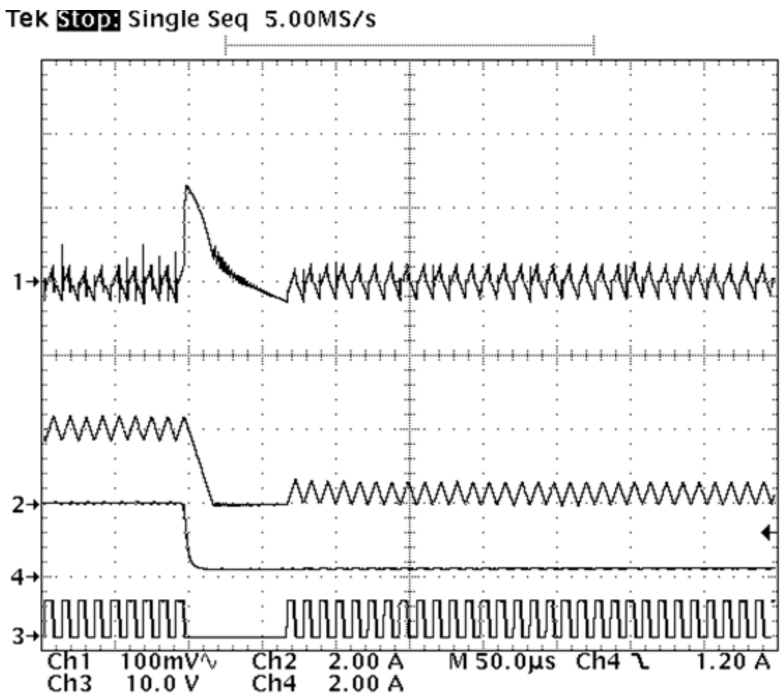

(c)

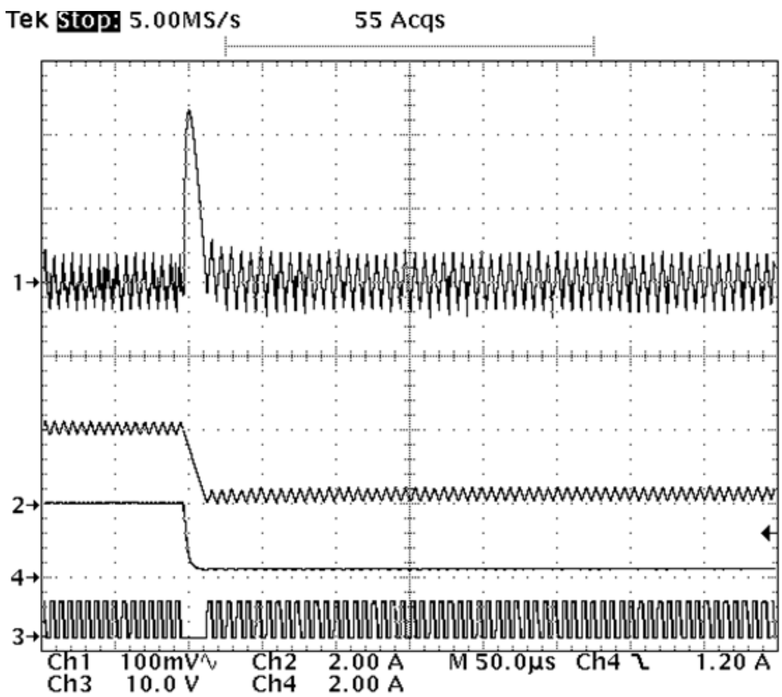

(d)

Fig. 4.11 Transient response of buck converter when I_o is changed from 2 A (24 W) to 0.2 A (2.4 W). [Ch1: v_o (100 mV/div), Ch2: i_L (2 A/div), Ch3: v_g (10 V/div), Ch4: i_o (2 A/div)] (Timebase: 50μs/div). (a) r_C = 30 mΩ. (b) r_C = 50 mΩ. (c) r_C = 100 mΩ. (d) r_C = 200 mΩ.

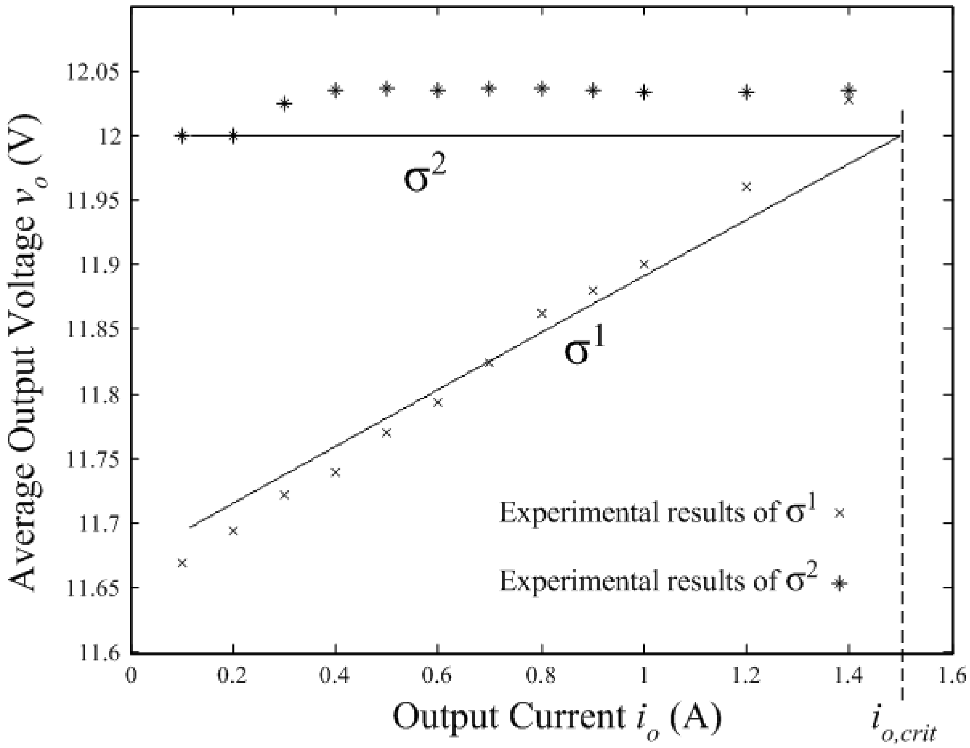

Average Output Voltage v_o (V)
12.05
12
11.95
11.9
11.85
11.8
11.75
11.7
11.65
11.6
0
0.2
0.4
0.6
0.8
1
1.2
1.4
1.6
σ^2
σ^1
Experimental results of σ^1
Experimental results of σ^2
Output Current i_o (A)
$i_{o,crit}$

(a)

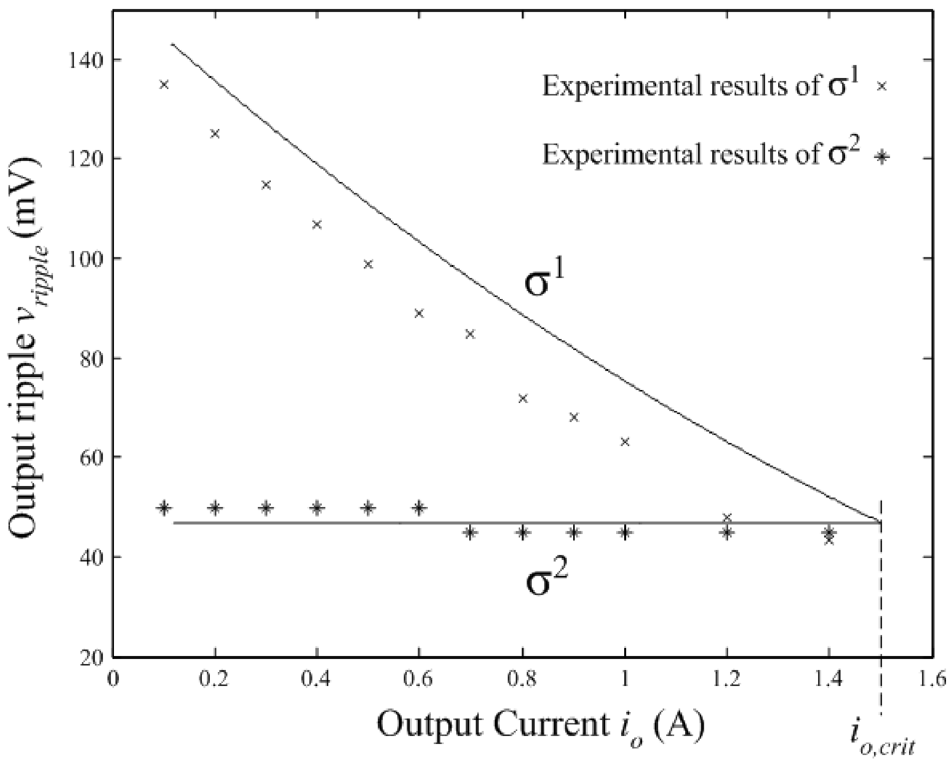

Output ripple v_{ripple} (mV)
140
120
100
80
60
40
20
0
0.2
0.4
0.6
0.8
1
1.2
1.4
1.6
Experimental results of σ^1
Experimental results of σ^2
σ^1
σ^2
Output Current i_o (A)
$i_{o,crit}$

(b)

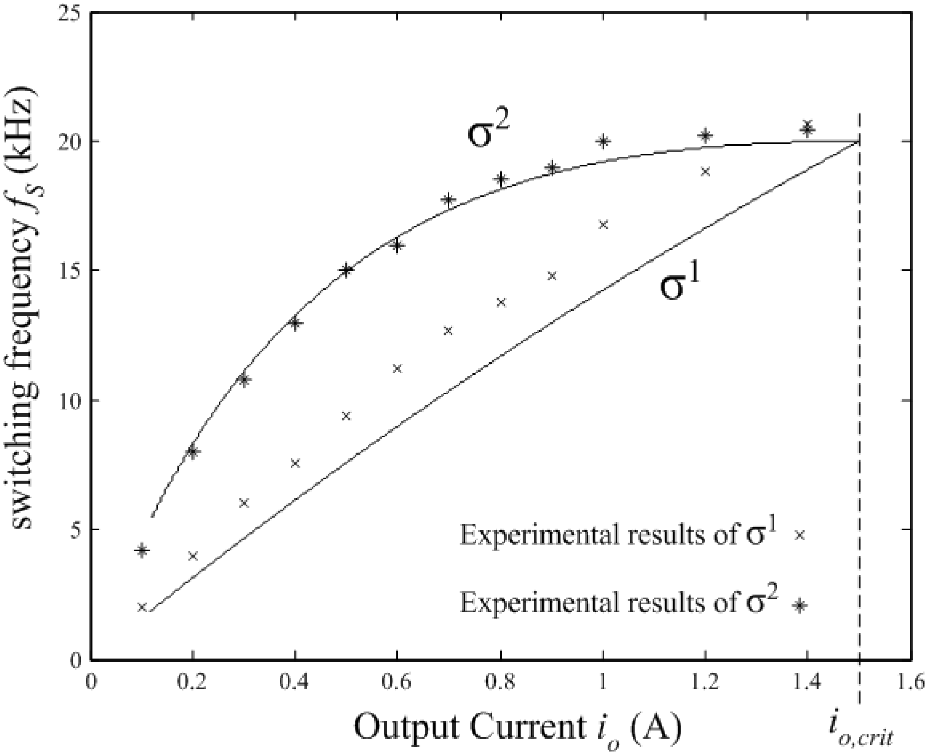

(c)

Fig. 4.12 Experimental measurement of the steady-state characteristics of converters with σ^1 and σ^2. (a) v_{avg}. (b) v_{ripple}. (c) f_S.

4.8 Chapter Summary

A comparative study of the static and dynamic behaviors of buck converters operating in DCM with the first-order and second-order switching boundaries have been examined. Detailed mathematical analyses have been given and have been supported by experimental measurements. Generally, converters with the second-order surface are found to give better dynamic responses and than the ones with the first-order surface.

CHAPTER 5

USE OF SECOND-ORDER SWITCHING SURFACE IN BOUNDARY CONTROL OF INVERTERS

5.1 Introduction

Concept of using a second-order switching surface in the boundary control of inverters is derived in this chapter. The switching surface is formulated by estimating the state trajectory movement after a switching action. It results in a high state trajectory velocity along the switching surface. This phenomenon accelerates the trajectory moving towards the target operating point. Time-domain responses of the inverter with the proposed boundary control method under large-signal variations have been analyzed. The proposed control scheme has been successfully applied to a 100 W full-bridge inverter. Practical implementation of the system will be provided. Dynamic responses of the inverter supplying to different kinds of loads, including resistive load, inductive load, and diode-capacitor rectifying circuit, have been studied. Experimental results show that the inverter output voltage can attain a low total harmonic distortion at different load conditions and fast response when it is subject to a large-signal load disturbance and an output reference voltage change.

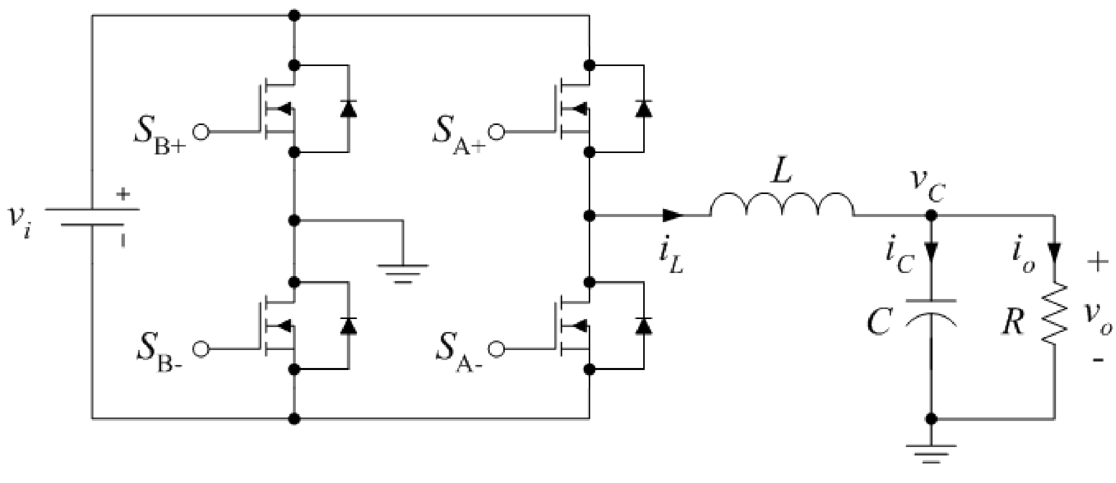

Fig. 5.1 Circuit schematic of typical full-bridge dc-ac inverter.

5.2 Principle of Operation

Fig. 5.1 shows a single-phase full-bridge dc-ac inverter. The inverter is supplied from a dc source v_i through a low-pass *LC* filter. The load is represented by a resistor *R*. Switches (S_{A+}, S_{B-}) are switched in anti-phase with (S_{A-}, S_{B+}). The system can be represented by the following state-space equations,

$$\dot{x} = A_0 x + B_0 u + (A_1 x + B_1 u)q_1 + (A_2 x + B_2 u)q_2 \tag{5.1}$$

where $x = \begin{bmatrix} i_L & v_C \end{bmatrix}$, $u = v_i$, A_n and B_n are constant matrix and q_i represents the state of the switches. (S_{A+}, S_{B-}) are on if $\{q_1, q_2\} = \{1, 0\}$, and (S_{A-}, S_{B+}) are on if $\{q_1, q_2\} = \{0, 1\}$. Matrices A_0, B_0, A_1, B_1, A_2, and B_2 are defined as $A_0 = \begin{bmatrix} 0 & -1/L \\ 1/C & -1/RC \end{bmatrix}$,

$B_0 = \begin{bmatrix} 0 \\ 0 \end{bmatrix}$, $A_1 = \begin{bmatrix} 0 & 0 \\ 0 & 0 \end{bmatrix}$, $B_1 = \begin{bmatrix} 1/L \\ 0 \end{bmatrix}$, $A_2 = \begin{bmatrix} 0 & 0 \\ 0 & 0 \end{bmatrix}$, $B_2 = \begin{bmatrix} -1/L \\ 0 \end{bmatrix}$.

A family of the state-space trajectories and the load line are shown in Fig. 5.2. Fig. 5.2(a) shows the characteristics when R = 5 Ω. Fig. 5.2(b) shows the characteristics when R = 1 Ω. The component values used in the analysis are tabulated in Table 5.1. The trajectories consist of two main types - the positive-state trajectories and the negative-state trajectories. They are obtained by solving (5.1) with different initial conditions. The positive-state trajectory is obtained by setting $\{q_1, q_2\} = \{1, 0\}$, while the negative-state trajectory is obtained by setting $\{q_1, q_2\} = \{0, 1\}$. As discussed in [Munzert and Krein 1996], the tangential component of the state-trajectory velocity on the switching surface determines the rate at which successor points approach or recede from the target operating point. An ideal switching surface σ^i that gives optimum dynamics should be on the only trajectory passing through the target operating point. σ^i for target operating point at +12 V is shown in Fig. 5.2. For dc-ac application, the output voltage v_o is time varying and follow the reference signal. Therefore, the target operating point of σ^i is also time-dependent. Although σ^i can achieve steady-state operation for a step change in the output current or reference voltage in one on/off control, it is load-dependent and requires sophisticated computation for solving the only positive- and negative-state trajectory that passes each of the target operating points in a time varying system.

A second-order surface σ^2, which is close to the ideal surface around the operating point, is derived in the following. The concept is based on estimating the state trajectory after a hypothesized switching action. As the switching frequency of the switches is much higher than the signal frequency, the output current i_o is relatively constant over a switching cycle. The gate signals to the switches are determined by the following criteria.

5.2.1 *Criteria for Switching on* (S_{A-}, S_{B+})

Fig. 5.3 shows the typical waveforms of v_o, i_L, i_o and i_C. (S_{A-}, S_{B+}) are originally off and are switched on at the hypothesized time instant t_1, so that v_o equals $v_{o,\max}$ at t_2 (at which $i_C = 0$). Thus,

$$i_C = C\frac{dv_C}{dt} = C\frac{dv_o}{dt} \tag{5.2}$$

$$-\left(v_i + v_o\right) = L\frac{di_L}{dt} \tag{5.3}$$

By using $i_L = i_C + i_o$ and assuming i_o to be constant,

$$\frac{di_C}{dt} = \frac{di_L}{dt} = -\frac{v_i + v_o}{L} \Rightarrow dt = -\frac{L}{v_i + v_o}di_C \tag{5.4}$$

Based on (5.2),

$$\Delta v_{o,1} = v_o(t_2) - v_o(t_1) = v_{o,\max} - v_o(t_1) = \frac{1}{C}\int_{t_1}^{t_2} i_C dt \tag{5.5}$$

By substituting (5.4) and $i_C(t_2) = 0$ into $\frac{1}{C}\int_{t_1}^{t_2} i_C dt$, eq. (5.5) can be expressed to ensure that v_o will not go above $v_{o,\max}$, (S_{A-}, S_{B+}) should be switched on when

$$v_o(t_1) \geq v_{o,\max} - \frac{L}{2C(v_i + v_o)} i_C^{\ 2}(t_1) = v_{o,\max} - k_1(v_i, v_o) i_C^{\ 2}(t_1) \tag{5.6}$$

and

$$i_C(t_1) > 0 \tag{5.7}$$

5.2.2 Criteria for Switching on (S_{A+}, S_{B-})

As shown in Fig. 5.3, (S_{A+}, S_{B-}) are originally off and are switched on at the hypothesized time instant t_3, so that v_o equals $v_{o,\min}$ at t_4 (at which $i_C = 0$). Thus,

$$i_C = C\frac{dv_C}{dt} = C\frac{dv_o}{dt} \tag{5.8}$$

$$v_i - v_o = L\frac{di_L}{dt} \tag{5.9}$$

By using $i_L = i_C + i_o$ and assuming i_o to be constant,

$$dt = \frac{L}{v_i - v_o} di_C \tag{5.10}$$

Based on (5.8),

$$\Delta v_{o,2} = v_o(t_4) - v_o(t_3) = v_{o,\min} - v_o(t_3) = \frac{1}{C}\int_{t_3}^{t_4} i_C dt \tag{5.11}$$

By substituting (5.10) and $i_C(t_4) = 0$ into $\frac{1}{C}\int_{t_3}^{t_4} i_C dt$, eq. (5.11) can be expressed to ensure that v_o will not go below $v_{o,\min}$, (S_{A+}, S_{B-}) should be switched on when

$$v_o(t_3) \leq v_{o,\min} + \frac{L}{2C(v_i - v_o)} i_C^{\ 2}(t_3) = v_{o,\min} + k_2(v_i, v_o) i_C^{\ 2}(t_3) \tag{5.12}$$

and

$$i_C(t_3) < 0 \tag{5.13}$$

Based on (6), (7), (12), (13) and $v_{o,\min} = v_{o,\max} = v_{ref}$, the following σ^2 can be concluded,

$$\sigma^2(i_L, v_o) = \begin{cases} k_1\, i_C^{\ 2} + (v_o - v_{ref}), & i_C > 0 \\ -k_2\, i_C^{\ 2} + (v_o - v_{ref}), & i_C < 0 \end{cases} \tag{5.14}$$

The equation can further be written into a single expression of

$$\sigma^2(i_L, v_o) = c_2\, i_C^{\;2} + \left(v_o - v_{ref}\right) \tag{5.15}$$

where $c_2 = \frac{k_1}{2}\left(1 + \operatorname{sgn}\left(i_C\right)\right) - \frac{k_2}{2}\left(1 - \operatorname{sgn}\left(i_C\right)\right)$.

σ^2 consists of a second-order term and is close to σ^i near the operating point. However, discrepancies occur, when the state is far from the operating point because of the approximations in (5.4) and (5.10). Fig. 5.2 shows that the discrepancy increases between σ^i and σ^2 when R decreases. However, near the target operating point ("Region A"), both σ^i and σ^2 are still approximately equal. A phenomenon can be observed from Fig. 5.2(b), for any initial states below σ^2. The positive-state trajectory finally enters "Region A", where σ^2 maintains the ideal switching surface property. Practically, the discrepancy does not affect the inverter performance.

The control circuit can be implemented by using simple analog devices. Multipliers are required to compute the function of k_1, k_2, and i_C^2, the remaining parts can be handled by using a simple logic circuitry. Fig. 5.4(a) shows the block diagram of the controller and Fig. 5.4(b) shows the corresponding practical implementation.

Table 5.1 Component Values of the Full Bridge Inverter

Parameter	Value
v_i	24 V
L	500 μH
C	100 μF
R	1 Ω

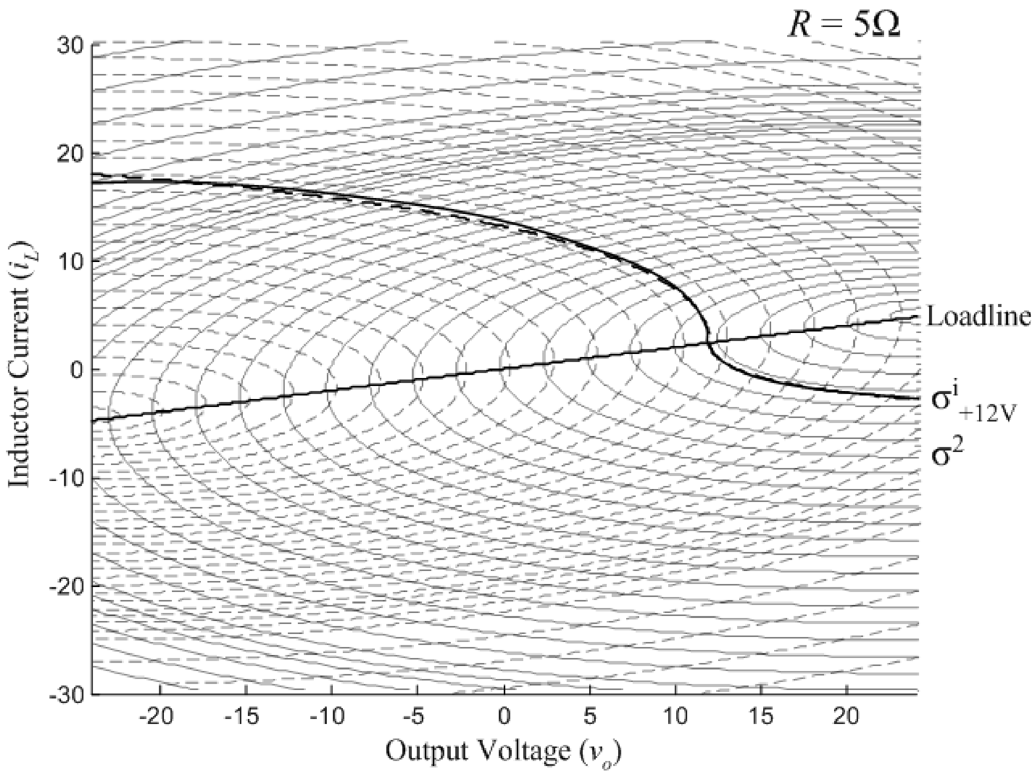

(a)

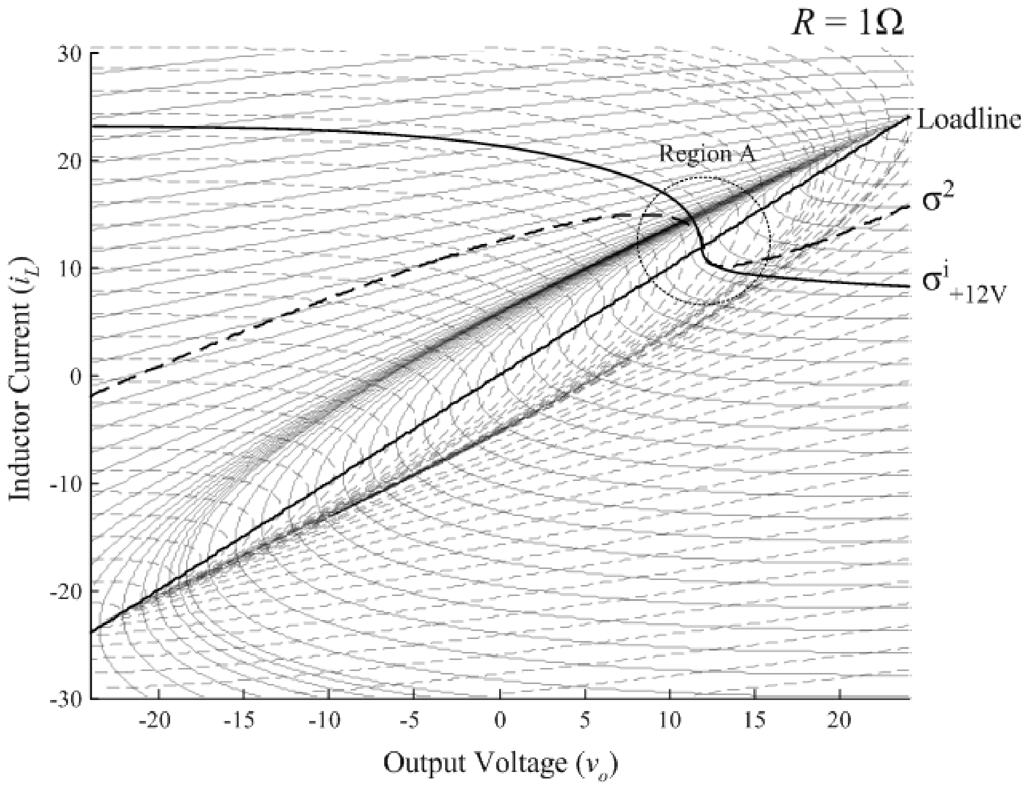

(b)

Fig. 5.2 Positive- and negative-state trajectories, loadline, σ^i and σ^2 of the inverter. (a) R = 5 Ω. (b) R = 1 Ω.

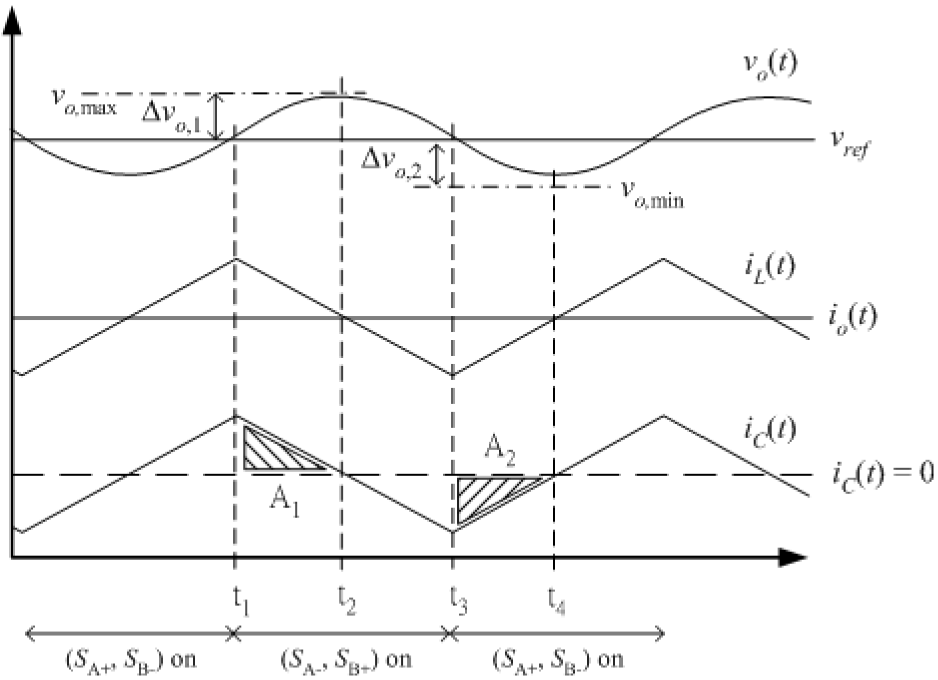

Fig. 5.3 Typical waveforms of v_o, i_L, i_o and i_C.

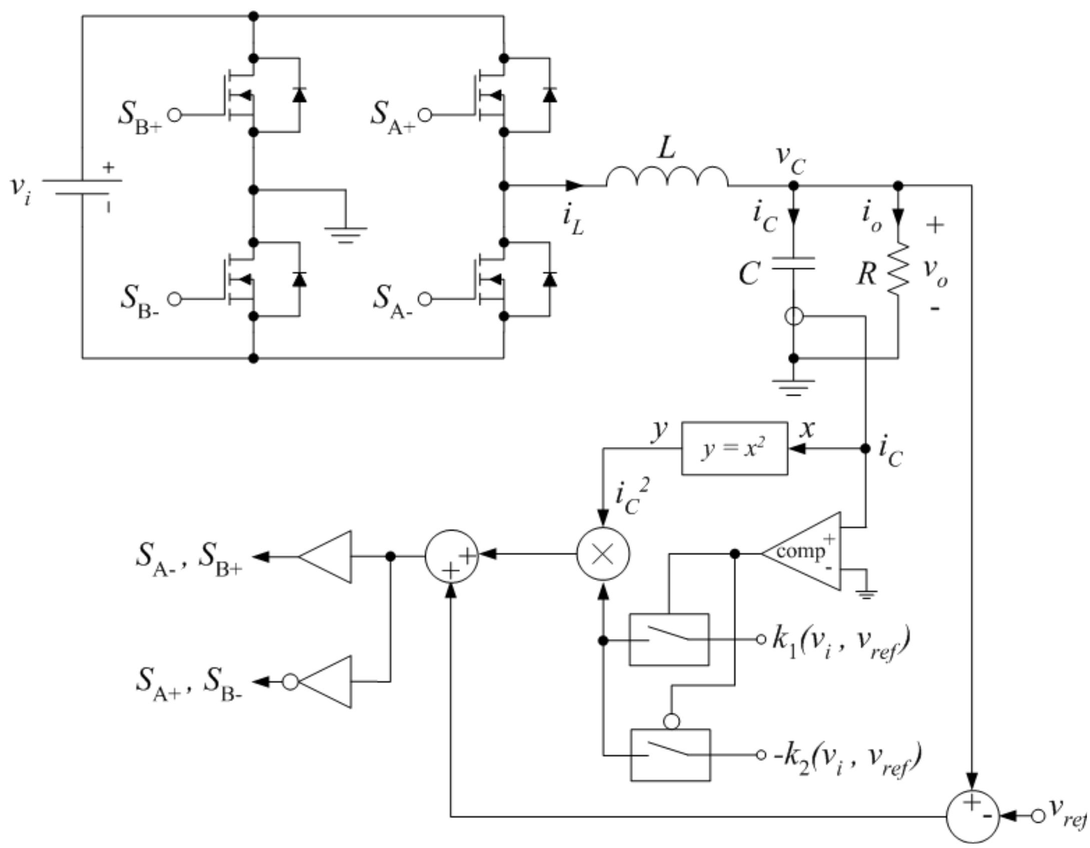

(a)

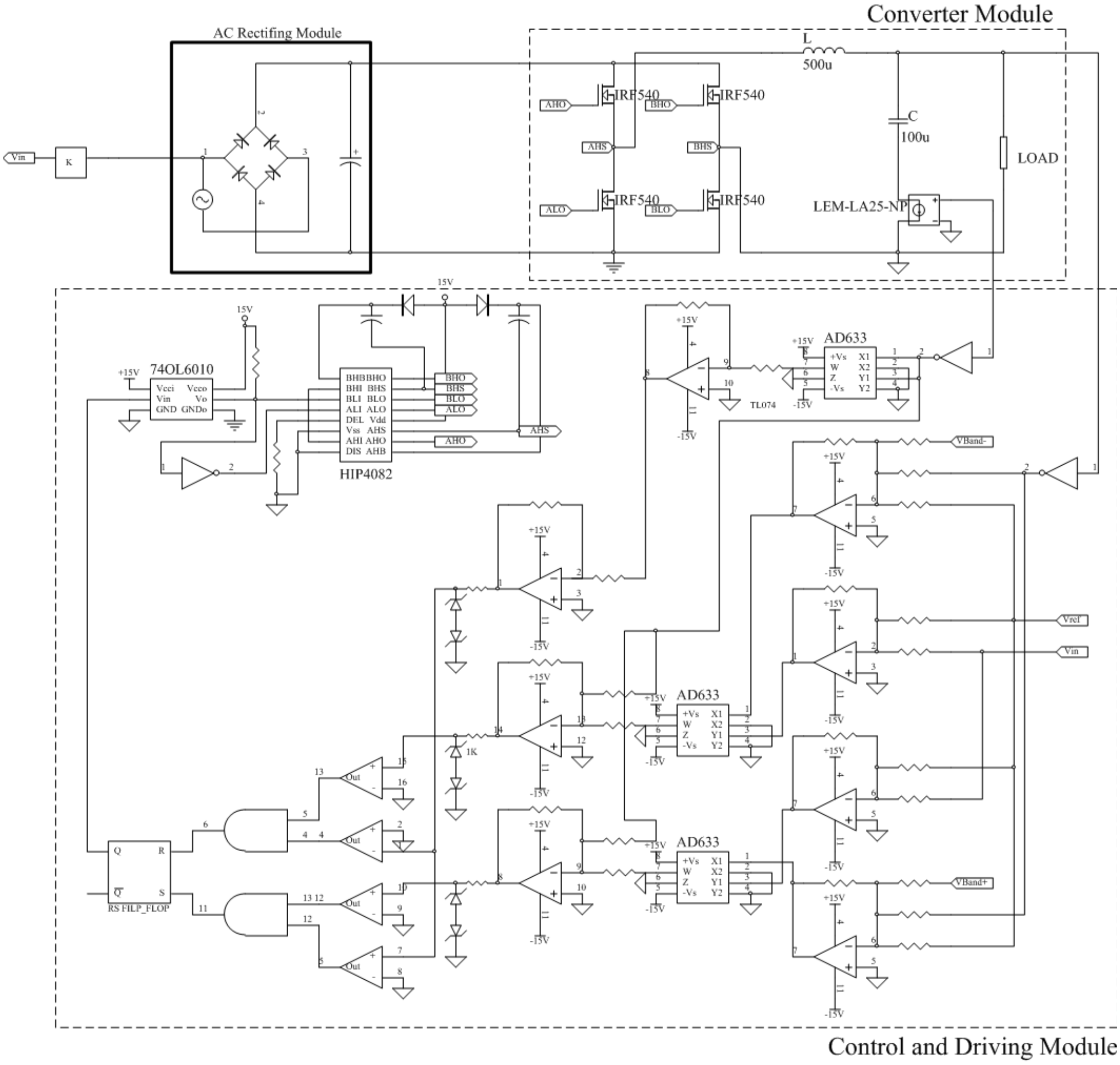

Fig. 5.4 Implementation of the controller. (a) Block diagram. (b) Practical implementation.

5.3 Large-Signal Stability

Points along $\sigma = 0$ can be classified into refractive, reflective, and rejective modes. The dynamics of the system will be exhibited differently in these regions. For σ^2, the transition boundary is obtained by differentiating (5.15) so that

$$\left.\frac{di_L}{dv_o}\right|_{on,off} = \frac{1}{R} + \frac{1}{2}\frac{i_L - \frac{v_o}{R}}{v_o - v_{ref}} \tag{5.16}$$

The expression at the left-hand side can be derived by using the state equations in (5.1). Based on (5.16), the transition boundary with (S_{A+}, S_{B-}) on is

$$\frac{C}{L}\left(\frac{v_i - v_o}{i_L - \frac{v_o}{R}}\right) = \frac{1}{R} + \frac{1}{2}\,\frac{i_L - \frac{v_o}{R}}{v_o - v_{ref}} \tag{5.17}$$

And the transition boundary with (S_{A-}, S_{B+}) on is

$$-\frac{C}{L}\left(\frac{v_i + v_o}{i_L - \frac{v_C}{R}}\right) = \frac{1}{R} + \frac{1}{2}\,\frac{i_L - \frac{v_o}{R}}{v_o - v_{ref}} \tag{5.18}$$

5.4 Simulation Verifications

An inverter with the component values tabulated in Table 5.1 is studied. Fig. 5.5 shows the steady-state performance of the inverter operated at R = 1 Ω and $v_{o,\mathrm{rms}}$ = 10 V_{rms}. Fig. 5.6 shows the dynamic responses (the time-domain waveforms in Fig. 5.6(a) and the phase plane in Fig. 5.6(b)) of the inverter under a load change from 5 Ω to 1 Ω and vice versa. σ^2 determines the switching actions of the switches when the converter is subject to a large signal disturbance. In fig. 5.6(b), just before the load change from 5 Ω to 1 Ω, the output voltage is approximately equal to 14 V (i_o = 2.8 A). When the load change to 1 Ω, $[i_L \quad v_o]$ below σ^2 and the movement of $[i_L \quad v_o]$ will follow the positive-state trajectory until it touch the switching surface. σ^2 is nearly the same as the ideal switching surface when the final states of $[i_L \quad v_o]$ is near the target operating point. Therefore, the output can revert back to the ac profile in two switching action. Fig. 5.7 shows the simulated time-domain waveforms and state trajectories of the converter when v_{ref} is suddenly changed.

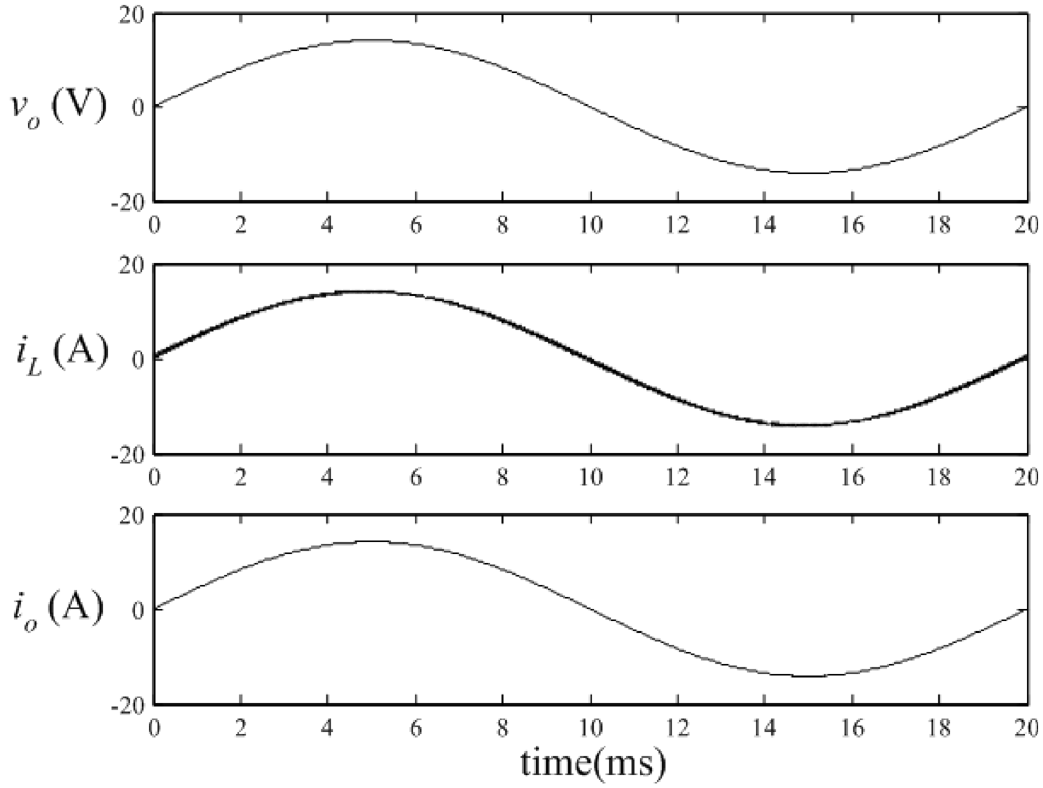

(a)

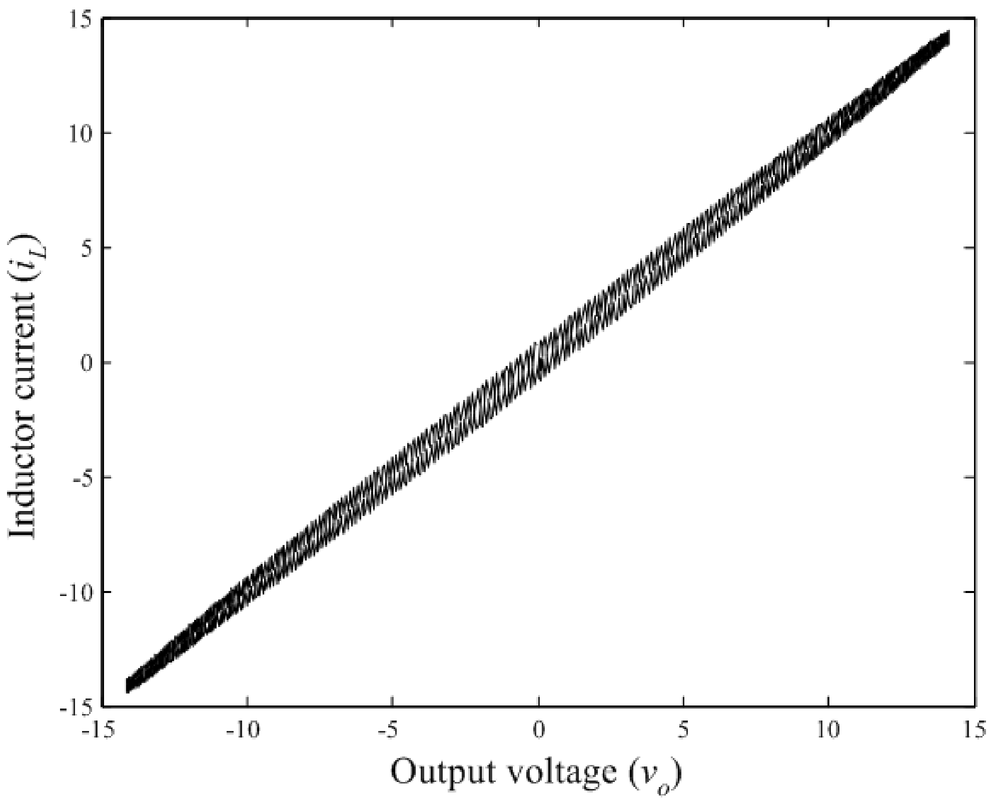

(b)

Fig. 5.5 Steady-state performance of the inverter when R = 1 Ω. (a) Time-domain. (b) State-plane.

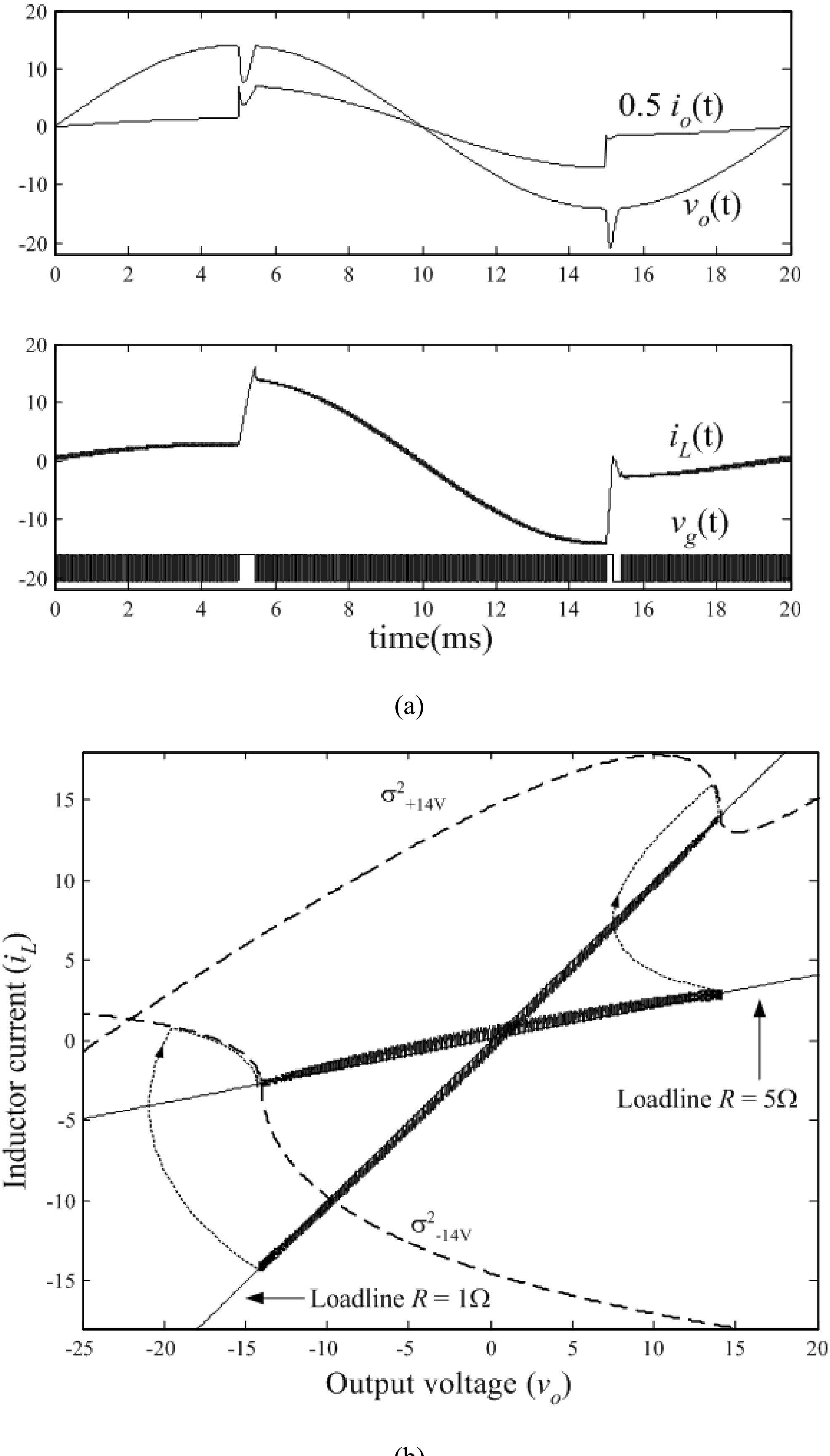

(b)

Fig. 5.6 dynamics performance of the inverter under load change from 5 Ω to 1 Ω and vice versa. (a) Time-domain. (b) State-plane.

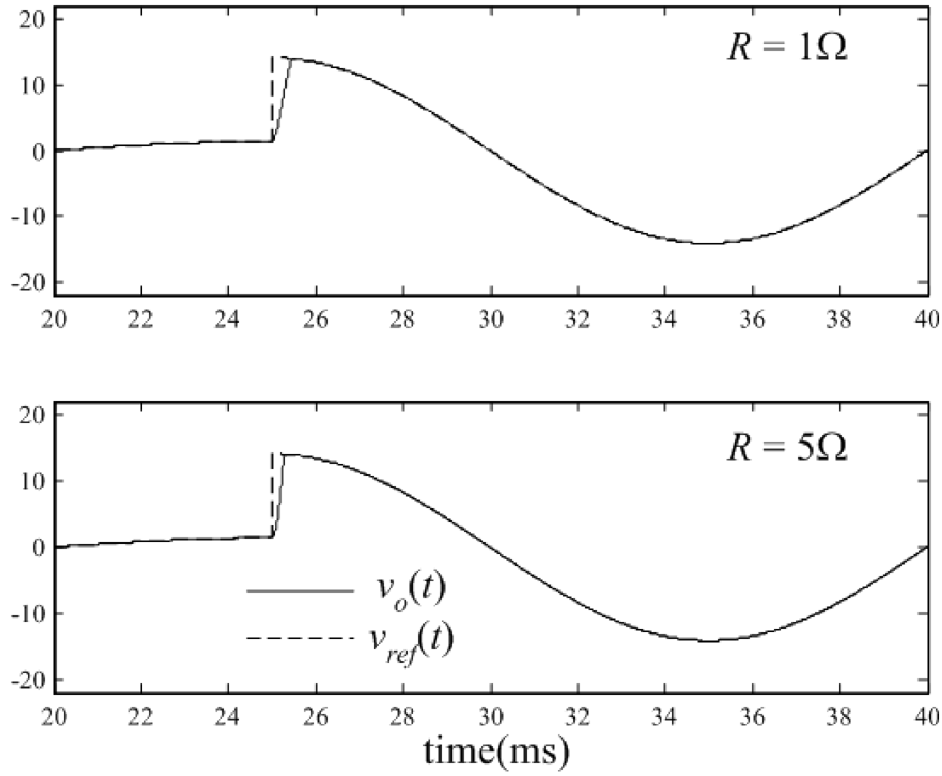

(a)

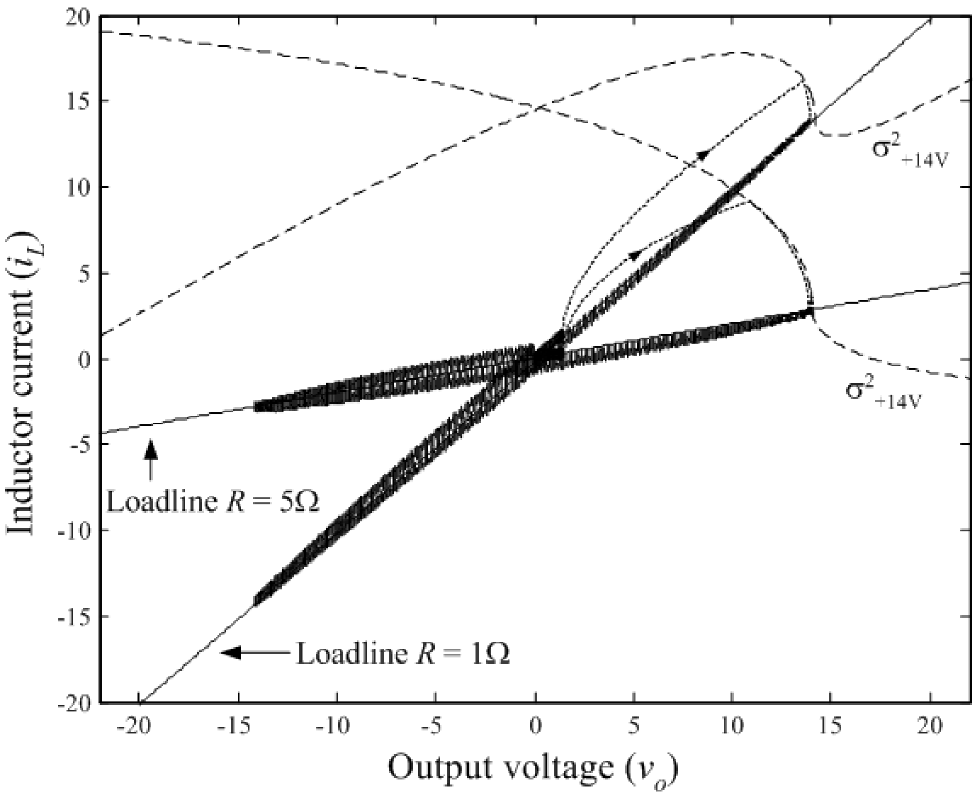

(b)

Fig. 5.7 Output voltage tracking with σ^2 for R = 1 Ω and 5 Ω. (a) Time-domain. (b) State-plane.

5.5 Experimental Verifications

A 100 W full bridge inverter has been built to verify the theoretical prediction and simulation results. The component values of the experimental prototype are tabulated in Table 5.1. Fig. 5.8 shows the steady state operation when R = 1 Ω (full load) and R = 5 Ω. The output voltage is regulated at 10 V_{rms}. Fig. 5.9 shows the transient response when R is changed from 5 Ω to 1 Ω. The output voltage can revert to the ac reference within two switching actions. Fig. 5.10 shows the output voltage tracking performance when R = 1 Ω, a 50 Hz ac reference, dynamic change from 10 V_{rms} to 1 V_{rms} is used to demonstrate the voltage tracking ability of the controller. Again, the output voltage can obtain near optimal response for increasing or decreasing of voltage reference.

In practical application, a full-wave rectifier may be connected to the output of the full-bridge inverter for providing a rectified dc. Fig. 5.11 shows the steady-state output for a full-wave rectifier load with $i_{o,\text{rms}}$ = 2.76 A and $v_{o,\text{rectified}}$ = 9.3 V. Performance of the inverter supplying to an inductive load has been studied. Fig. 5.12 shows the output voltage with an inductive load, which is formed by connecting a 1 mH inductor in series with a 1 Ω resistor. A phase shift of 17.4^{o} (0.97ms) between v_o and i_o is observed.

Then, the DC input voltage source is replaced by a diode-capacitor rectifying circuit with input capacitance equal to 2000 μF in order to show the inverter performance with input voltage variation. Fig. 5.13 shows the response of the inverter operating at 36 W. A variation of 33% (8.4 $V_{p\text{-}p}$) change in input voltage does not affect the output waveform. Fig. 5.14 shows the harmonic spectra of the output voltage v_o for different loading condition. Table 5.2 shows the total harmonic distortions (THDs) of the output voltage with four loads in Fig. 5.14. They are all below 0.3%.

Finally, in order to study the dynamic response at the output, the sinusoidal reference is replaced by a square-wave one. Fig. 5.15 and 5.16 shows the macroscopic and microscopic view of output voltage for 4 V, 12 V, 28 V and 40 V peak-to-peak square-wave reference. It can be observed that when a transient occurs, v_o can follow v_{ref} without overshoots. For a larger signal swing, it is necessary to have one more switching action, in order to make v_o reaching the desired value.

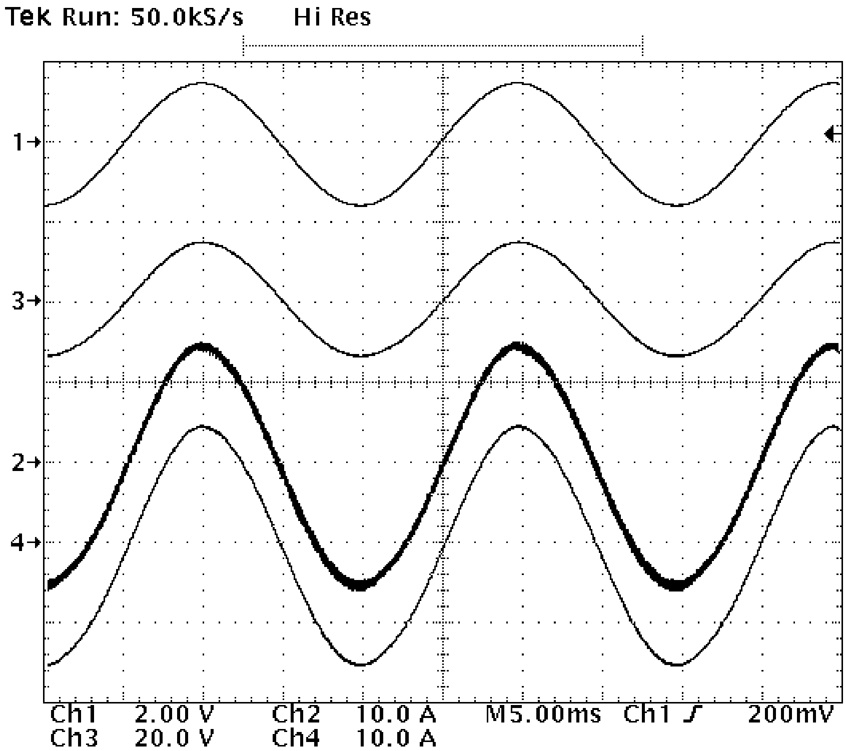

(a)

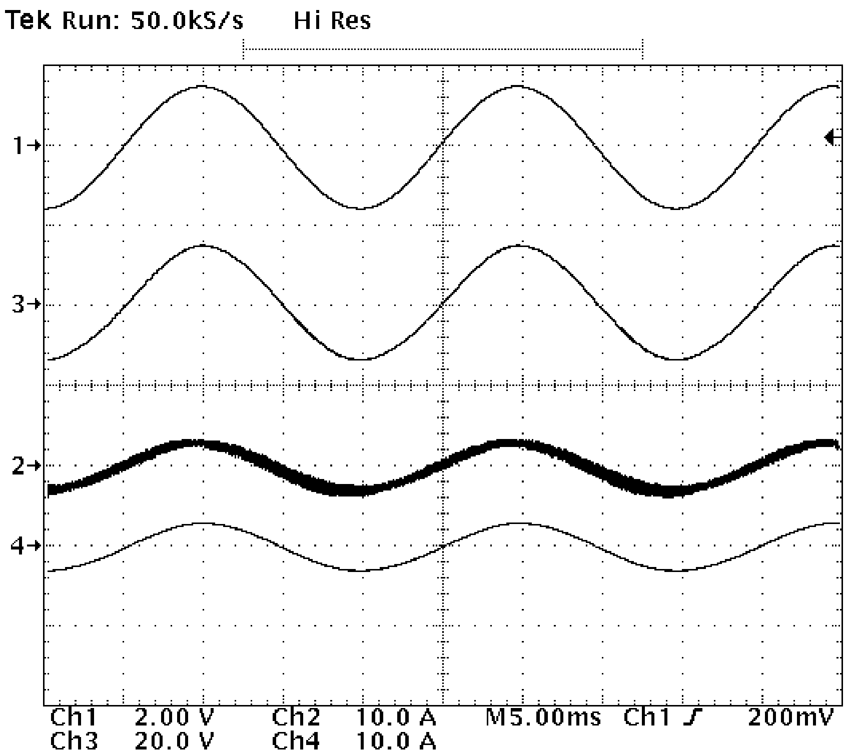

(b)

Fig. 5.8 Steady-state operation. [Ch1: v_{ref} (2 V/div), Ch2: i_L(10 A/div), Ch3: v_o(20 V/div), Ch4: i_o(10 A/div)]. (a) $R = 1\ \Omega$ (full load). (b) $R = 5\ \Omega$.

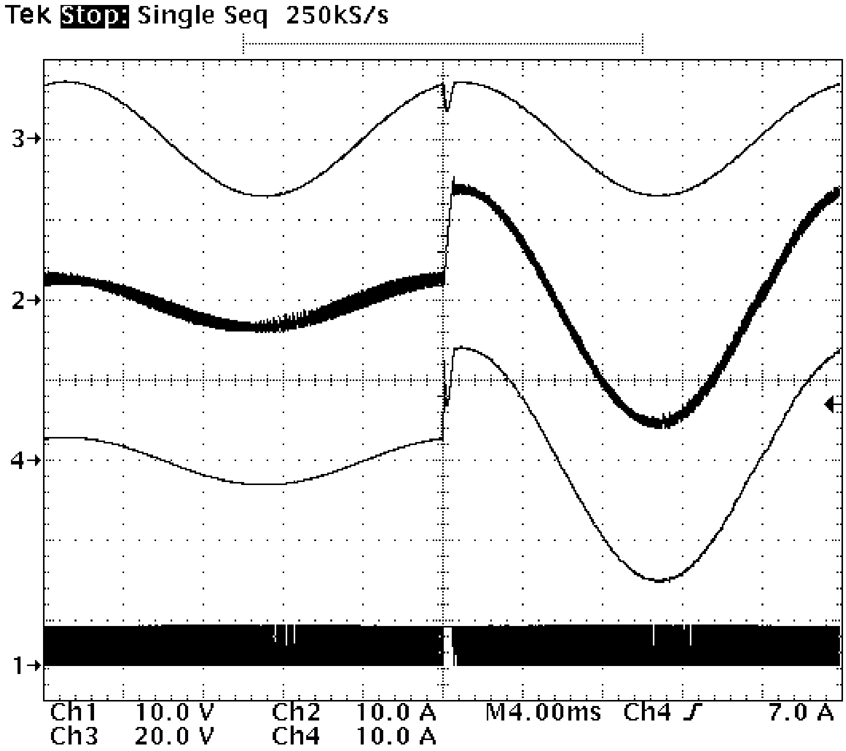

(a)

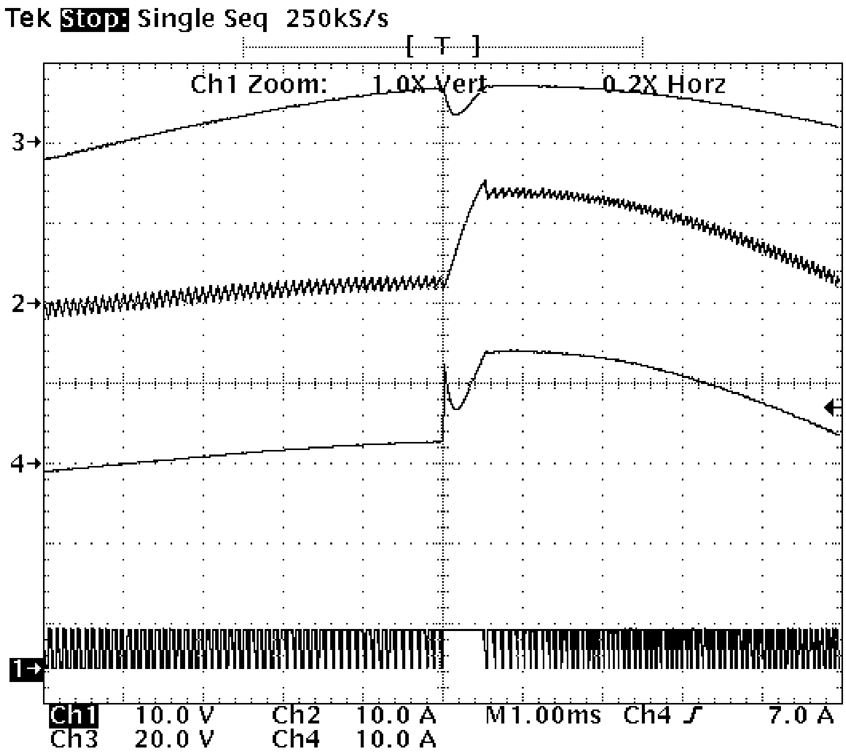

(b)

Fig. 5.9 Transient response of the full-bridge inverter when R change from 5Ω to 1Ω. [Ch1: v_g (10 V/div), Ch2: i_L (10 A/div), Ch3: v_o (20 V/div), Ch4: i_o (10 A/div)]. (a) Timebase = 4ms. (b) Timebase = 1ms.

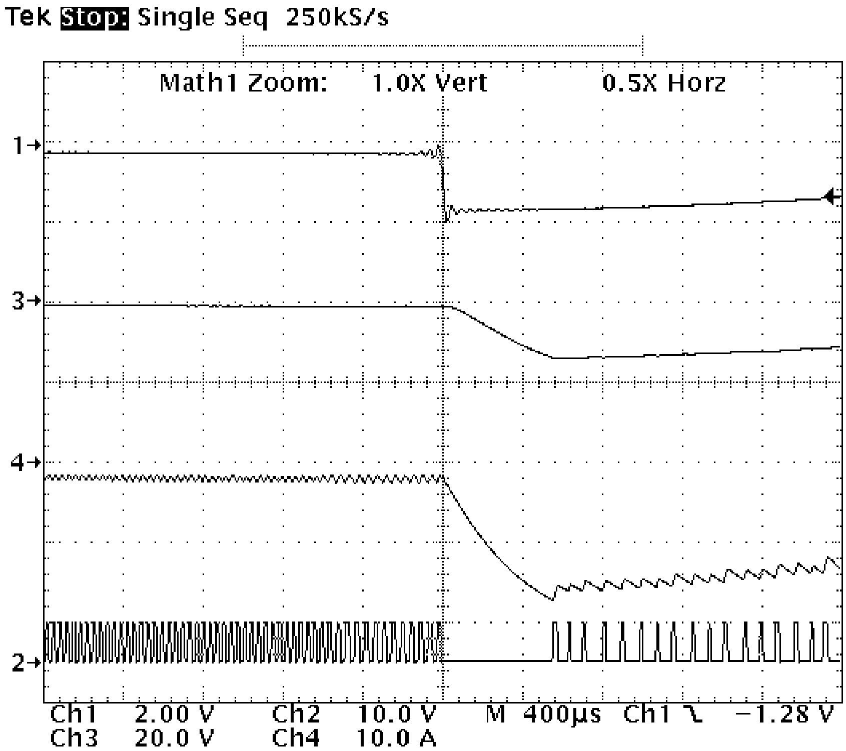

(a)

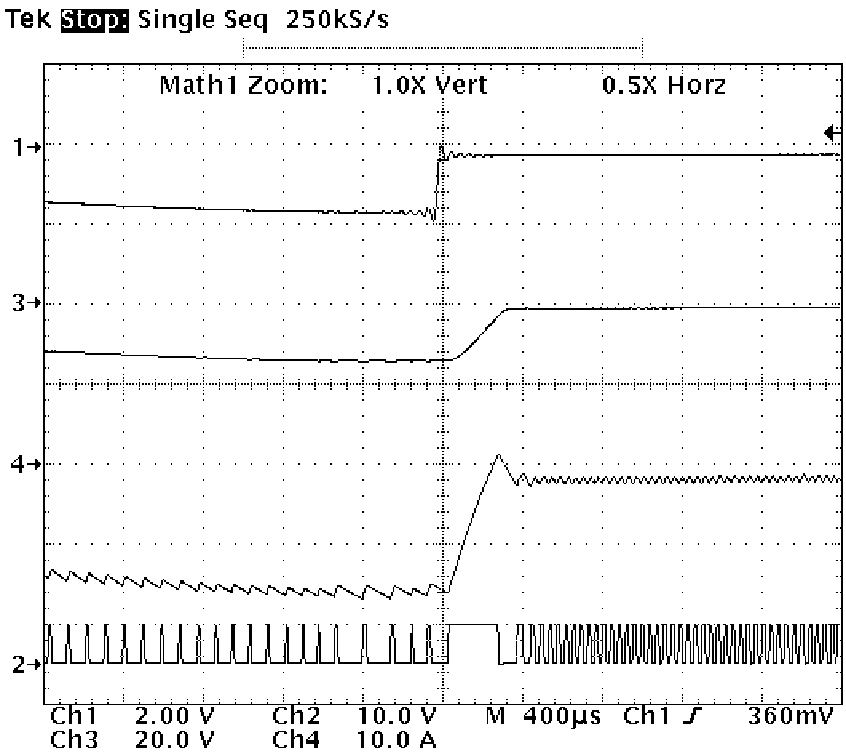

(b)

Fig. 5.10 Output voltage tracking when $R = 1\Omega$. [Ch1: v_{ref} (2 V/div), Ch2: v_g (10 V/div), Ch3: v_o (20 V/div), Ch4: i_L (10 A/div)]. (a) v_{ref} increases from 1 V_{rms} to 10 V_{rms}. (b) v_{ref} decreases from 10 V_{rms} to 1 V_{rms}.

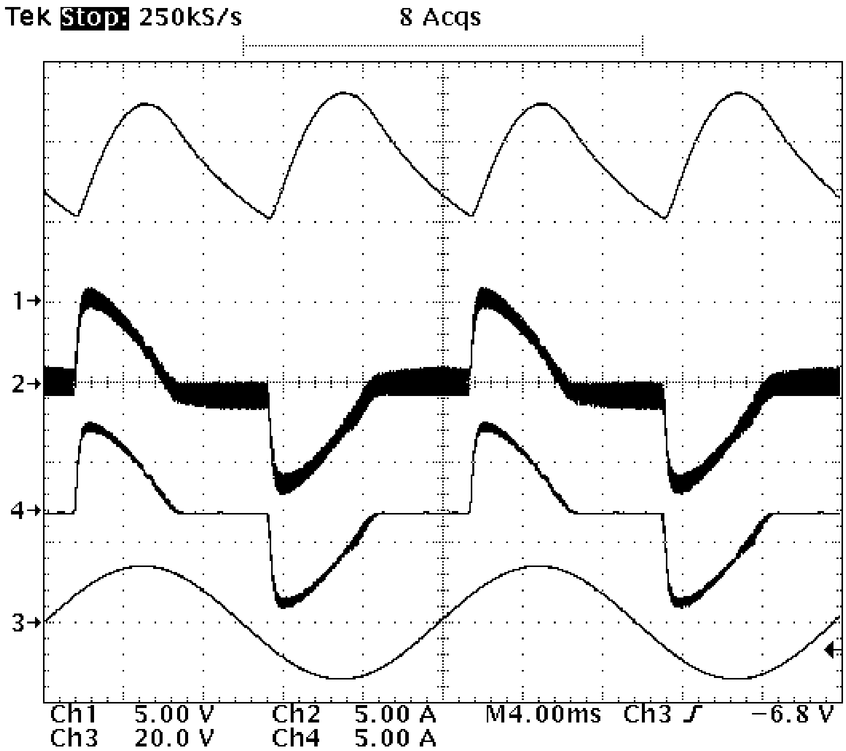

Fig. 5.11 Steady-state output for a full-wave rectifier load. [Ch1: $v_{o,\mathrm{rectified}}$ (5 V/div), Ch2: i_L (5 A/div), Ch3: v_o (20 V/div), Ch4: i_o (5 A/div)].

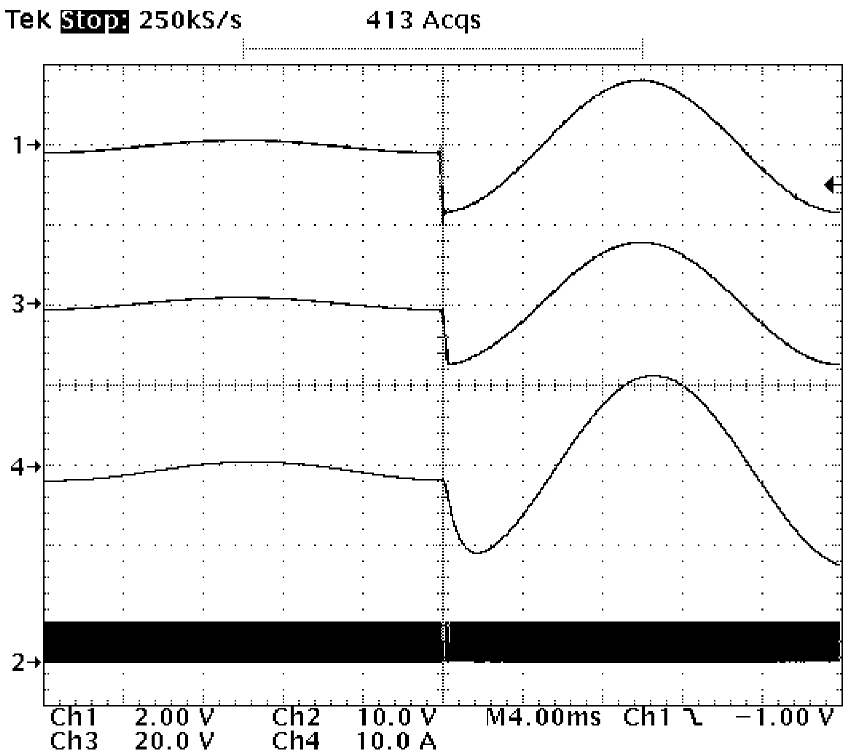

(a)

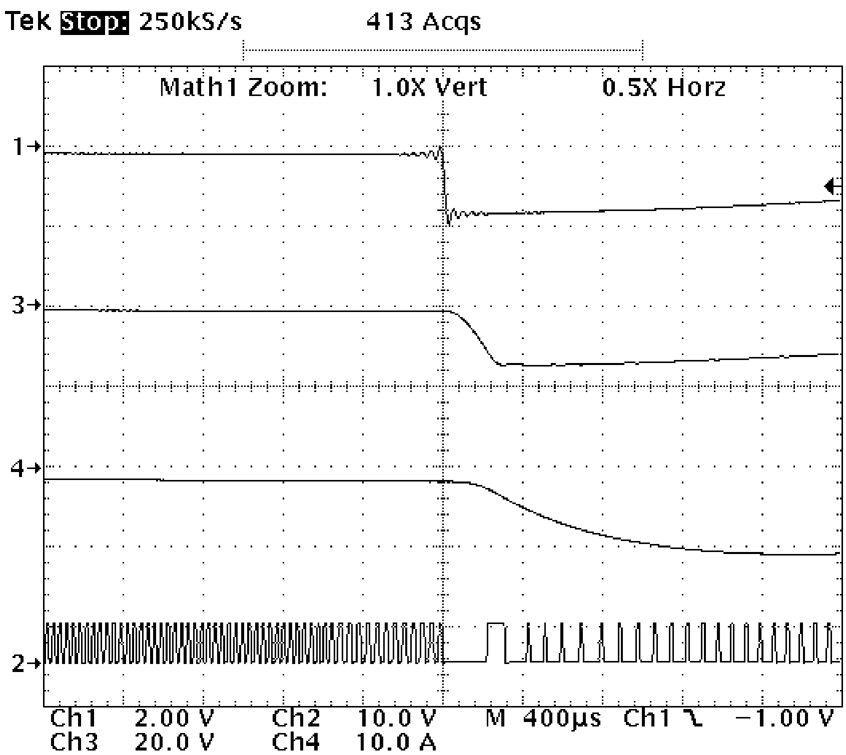

(b)

Fig. 5.12 Output voltage tracking with inductive load. [Ch1: v_{ref} (2 V/div), Ch2: v_g (10 V/div), Ch3: v_o (20 V/div), Ch4: i_o (10 A/div)]. (a) Timebase = 4ms. (b) Timebase = 400us.

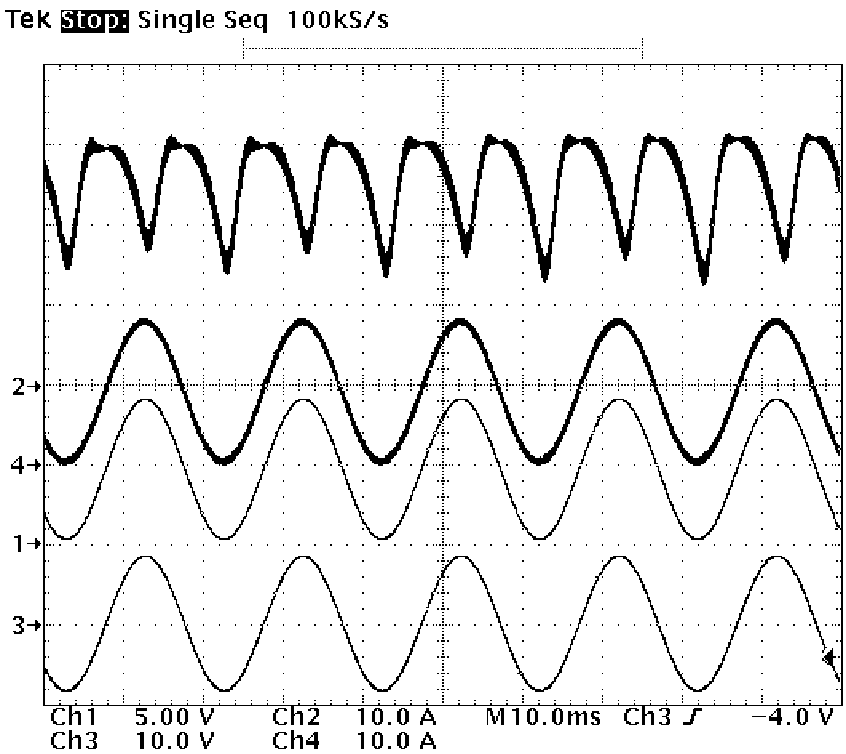

Fig. 5.13 Steady-state output with 33% of input voltage variation. [Ch1: v_i (5 V/div), Ch2: i_L (10 V/div), Ch3: v_o (10 V/div), Ch4: i_o (10 A/div)].

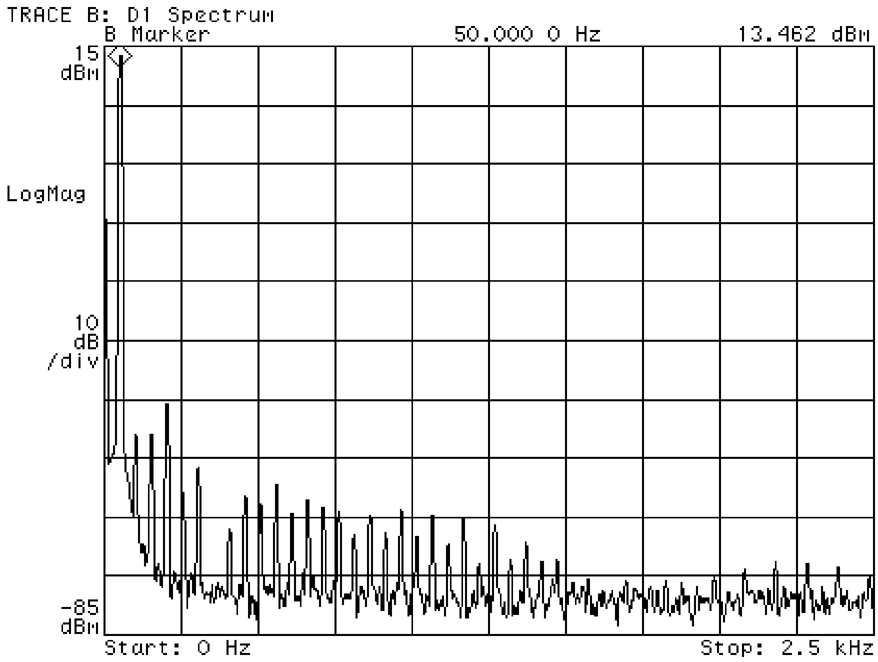

TRACE B: D1 Spectrum
B Marker
50.000 0 Hz
13.462 dBm
15
dBm
LogMag
10
dB
/div
-85
dBm
Start: 0 Hz
Stop: 2.5 kHz

(a)

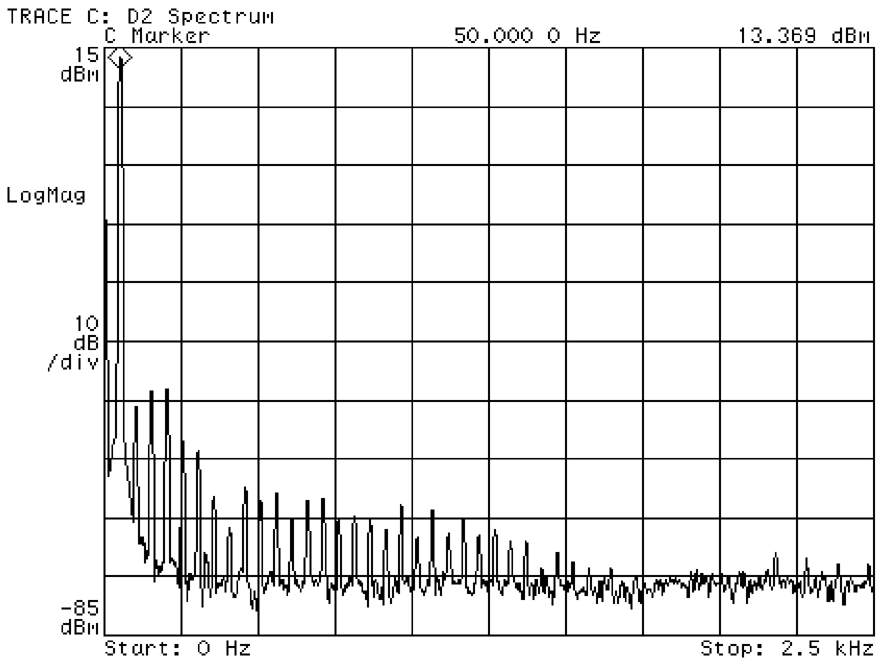

TRACE C: D2 Spectrum
C Marker
50.000 0 Hz
13.369 dBm
15
dBm
LogMag
10
dB
/div
-85
dBm
Start: 0 Hz
Stop: 2.5 kHz

(b)

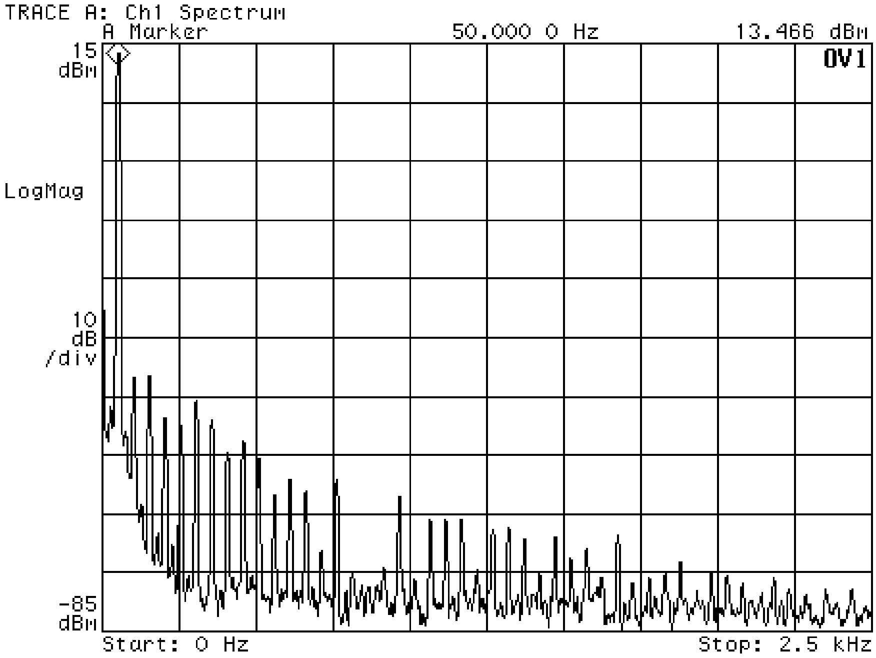

(c)

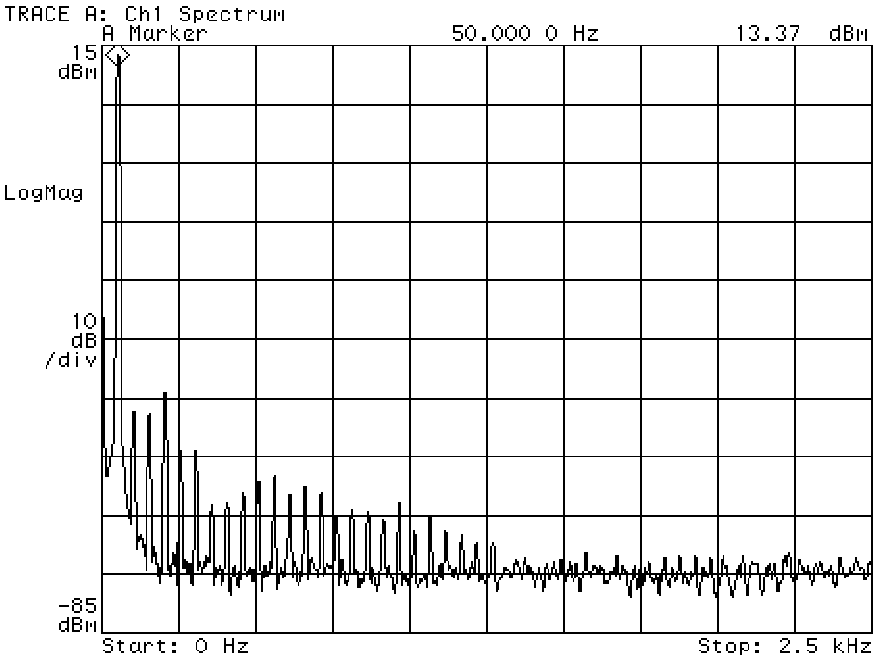

(d)

Fig. 5.14 Harmonic spectra of the output voltage v_o for different loading condition. (a) Resistive load for R = 5 Ω. (b) Resistive load for R = 1 Ω. (c) Full wave rectified load for P_o = 36 W. (d) Inductive load for L = 1 mH, R = 1 Ω.

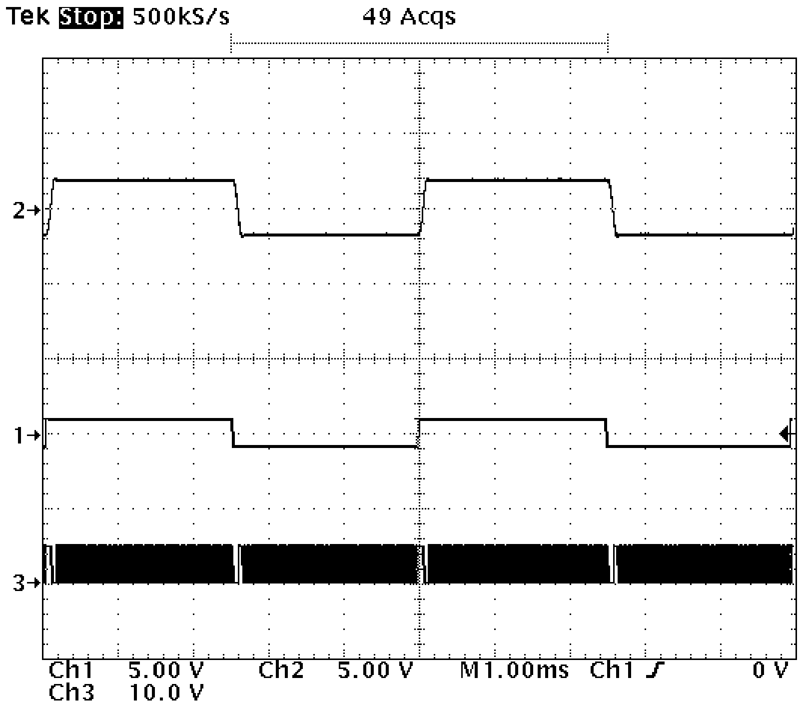
Tek Stop: 500kS/s
49 Acqs
2
1
3
Ch1 5.00 V Ch2 5.00 V M1.00ms Ch1 ∫ 0 V
Ch3 10.0 V

(a)

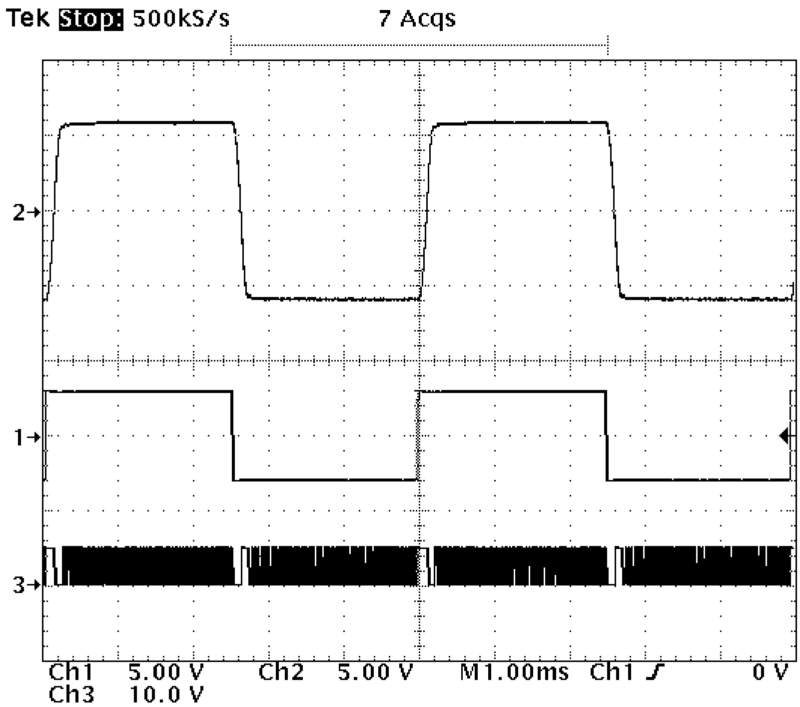
Tek Stop: 500kS/s
7 Acqs
2
1
3
Ch1 5.00 V Ch2 5.00 V M1.00ms Ch1 ∫ 0 V
Ch3 10.0 V

(b)

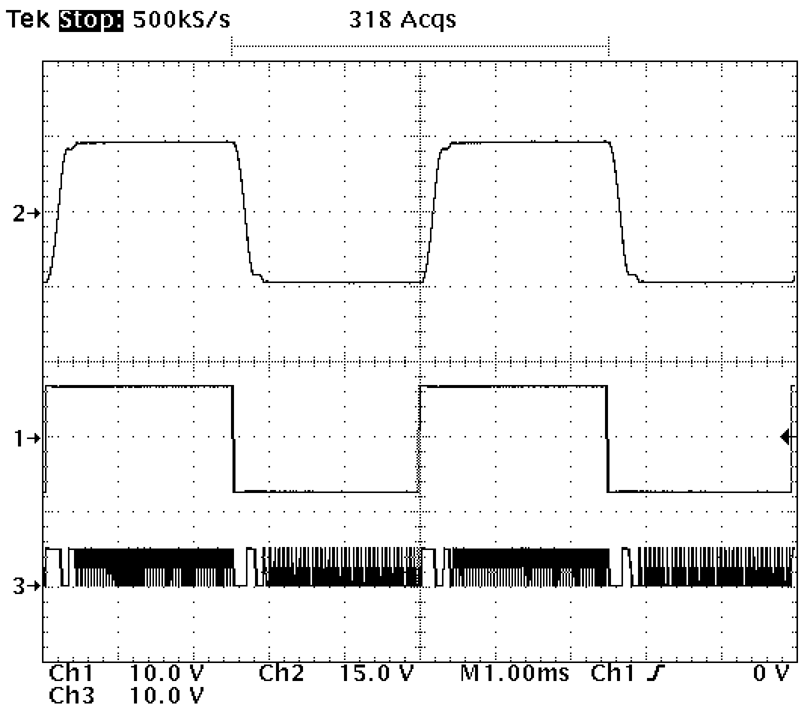

(c)

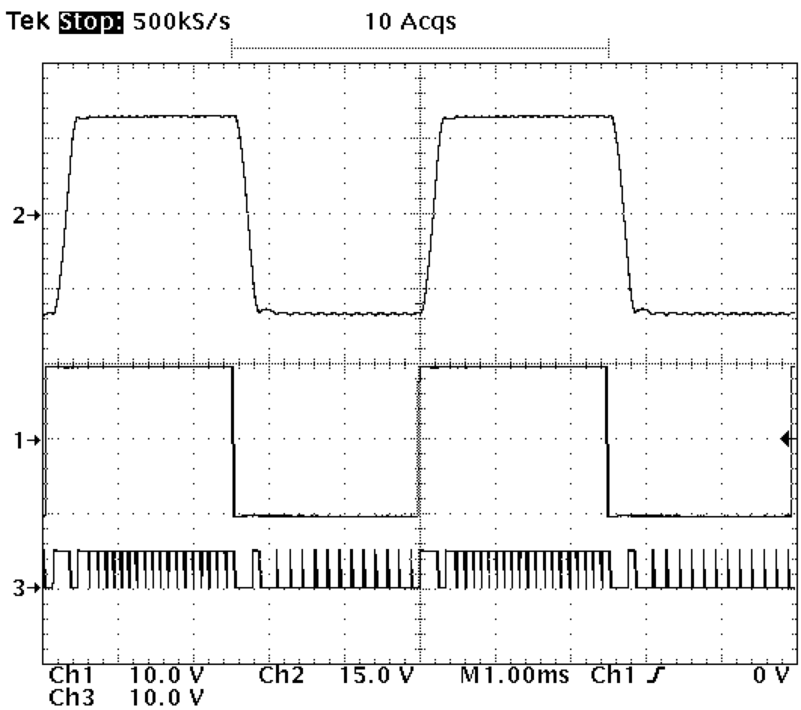

(d)

Fig. 5.15 Experimental results of dynamic behaviors for different values of the desired pulsating reference voltages in macroscopic view. [Ch3: v_{gate} (10 V/div)] (a) 4 Vp-p. [Ch1: v_{ref} (5 V/div), Ch2: v_o (5 V/div)] (b) 12 Vp-p. (c) 28 Vp-p. [Ch1: v_{ref} (10 V/div), Ch2: v_o (15 V/div)] (d) 40 Vp-p

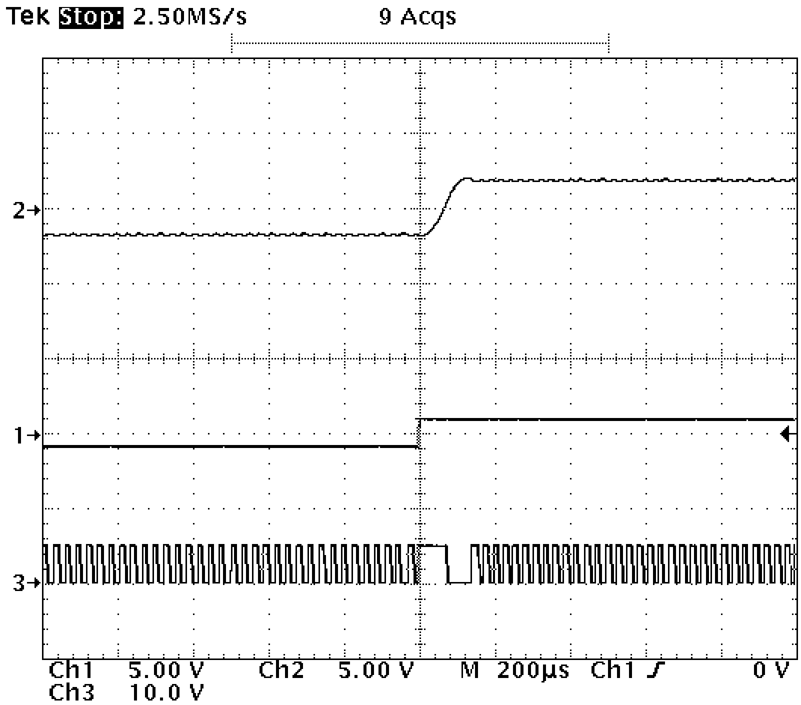
Tek Stop: 2.50MS/s
9 Acqs
2→
1→
3→
Ch1 5.00 V
Ch2 5.00 V
M 200µs Ch1 ƒ 0 V
Ch3 10.0 V

(a)

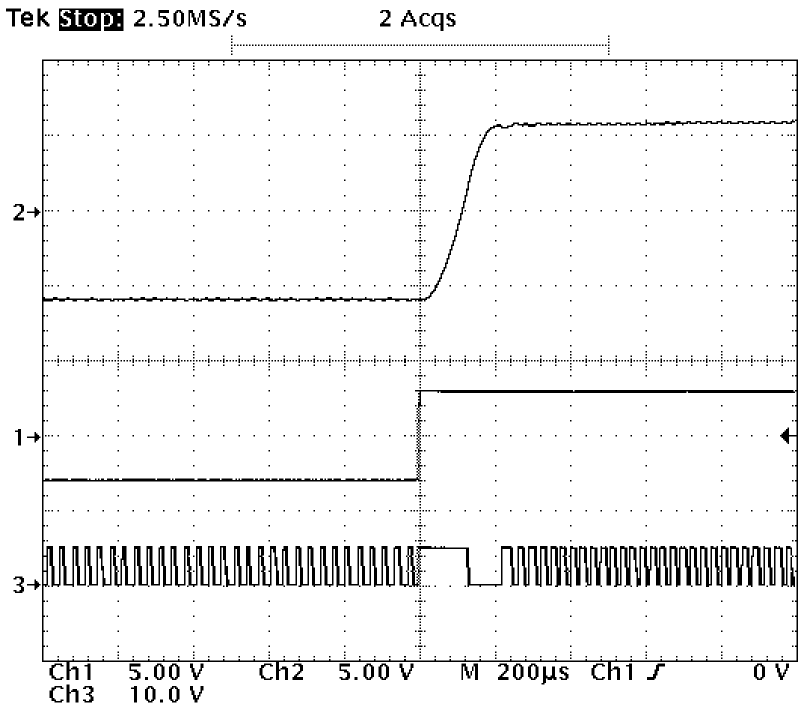
Tek Stop: 2.50MS/s
2 Acqs
2→
1→
3→
Ch1 5.00 V
Ch2 5.00 V
M 200µs Ch1 ƒ 0 V
Ch3 10.0 V

(b)

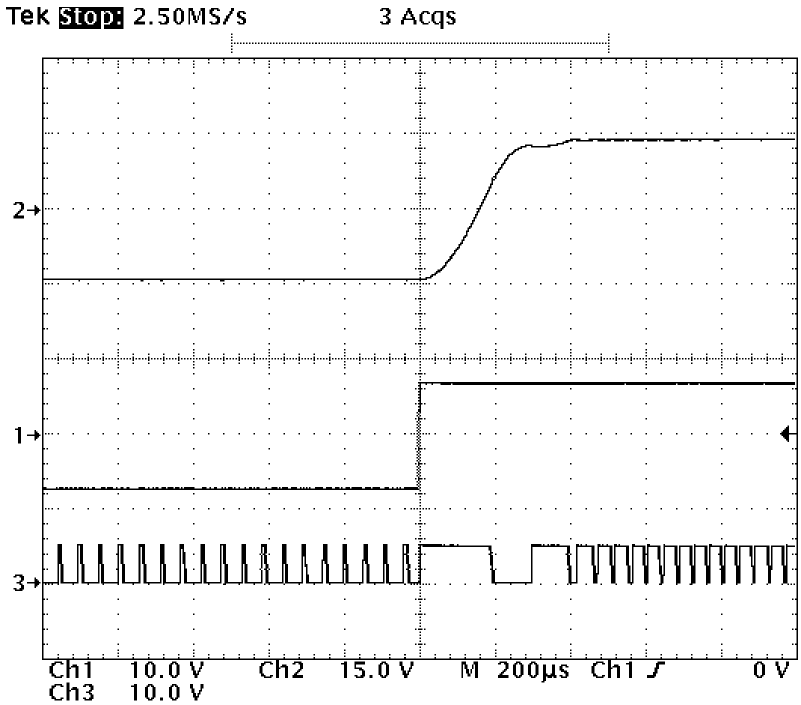

(c)

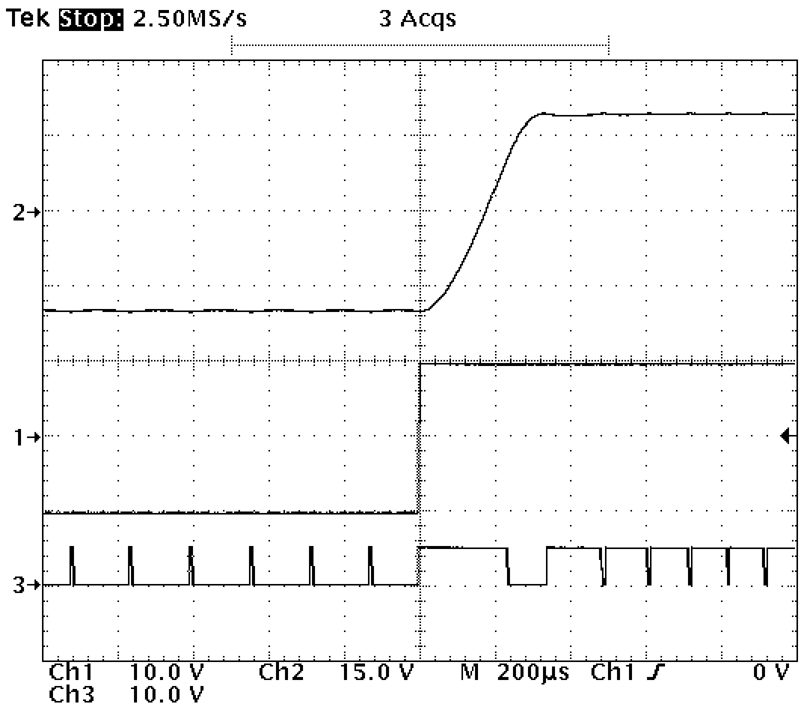

(d)

Fig. 5.16 Experimental results of dynamic behaviors for different values of the desired pulsating reference voltages in microscopic view. [Ch3: v_{gate} (10 V/div)] (a) 4 Vp-p. [Ch1: v_{ref} (5 V/div), Ch2: v_o (5 V/div)] (b) 12 Vp-p. (c) 28 Vp-p. [Ch1: v_{ref} (10 V/div), Ch2: v_o (15 V/div)] (d) 40 Vp-p

Table 5.2 Total harmonic distortions (THDs) of the output voltage

v_o = 10 V_{rms} Noise Level = -80 dB Signal Freq = 50 Hz THD calculation Freq Band: 0 Hz to 2.5 kHz (>43 orders)	
Loading Condition	**THD + N%**
Resistive load for R = 5 Ω.	0.178046905
Resistive load for R = 1 Ω.	0.275200479
Full wave rectified load for P_o = 36 W.	0.306318266
Inductive load for L = 1 mH, R = 1 Ω.	0.206875159

5.6 Chapter Summary

A second-order switching surface for boundary control of DC-AC inverter is proposed in this chapter. The control method is simple and does not require any complicated calculation of the system transfer function or control loop compensation. The output voltage can obtain near-optimal response, when it is subject to large-signal disturbances or input voltage variation. The control methods have been studied experimentally with a 100 W inverter prototype and provide good agreement with theoretical prediction.

CHAPTER 6

CONCLUSIONS AND SUGGESTIONS FOR FURTHER RESEARCH

6.1 Conclusions

This thesis has proposed the use of second-order switching surface to control the power electronics converters. The concept of modifying hysteresis band with state-trajectory prediction to achieve near-optimum transient response for buck converter has been proposed. As studied from the simulation and experimental results of the converter behaviors, it is found that the output voltage can be revert to the steady state in two switching actions after a large-signal disturbance with the state-trajectory prediction method. For the sake of simplicity, the four switching criteria for modifying the hysteresis band are combined into a single control rule. By comparing the control rule with the first-order switching surface in boundary control, it was found that the newly proposed switching surface consists of a second-order term which is formed by squaring one of the state variables. Therefore, the surface is named as *second-order switching surface* (σ^2).

A comparative study has been carried out for studying the first- and second-order switching surface in continuous conduction mode (CCM) and discontinuous conduction mode (DCM) in a buck converter. The second-order switching surface not only exhibits better transient behaviors than the one with first-order switching surface, but it is also applicable for both CCM and DCM with the same set of control parameters. A detailed investigation into the steady-state and large-signal characteristics has been given. The mathematical predictions of the effect on equivalent series resistance (ESR) and parameter variation have been verified with simulation and experimental results.

The proposed control scheme is then applied to the control of inverters. A 100 W full-bridge inverter has been built. Dynamic responses of the inverter supplying to different kinds of loads, including resistive load, inductive load, and diode-capacitor rectifying circuit, have been studied. Experimental results show that the inverter output voltage can attain a low total harmonic distortion at different loading conditions, fast response to a large-signal load disturbance, and reference change.

Major contributions and results of this thesis are summarized as follows. Suggestions for further research are described in the next section.

6.2 Major Contributions

The major contributions to the second-order switching surface in boundary control can be summarized to the following aspects.

(i) Developed the concept of state trajectory prediction (STP) technique to achieve near-optimum transient response of power converters.

(ii) Simplified the switching criteria into a second-order switching surface to enable the use of boundary control theory in analyzing the system performance.

(iii) Studied the steady-state and large-signal characteristics of the buck converter operating in CCM and DCM with first- and second-order switching surface.

(iv) Studied the effect of equivalent series resistance of output capacitor and parameter variation, including simplification technique in DCM analysis.

(v) Extended the use of second-order switching surface into the control of inverters.

6.3 Suggestions for Further Research

6.3.1 Controlling Boost and Flyback Converters

Boost and flyback converter exhibit different on- and off-state system topologies as compared with buck converter. For the buck converter, similar set of state equations can be derived in the on- and off-state topologies. However, the boost and flyback converters consist of two separated circuit equation during the on and off states. This leads to distinct characteristics at the on and off states, respectively. Therefore, the second-order switching surface cannot be directly applied to the control of boost and flyback converters. A piecewise second-order switching surface is required. In addition, capacitor current no longer provides enough information for predicting the trajectory motion. Thus, the inductor and output current is sensed to estimate the required capacitor current in order to preserve the predictive characteristic of the switching surface.

A cycle-by-cycle control with piecewise switching surface combining the first- and second-order functions is used to test the idea. A near-optimum transient response can be obtained. However, boundary control theory hasn't been applied into the investigation of the proposed switching surface. Further investigation will focus on this subject.

6.3.2 Transient Boost Technique to Further Enhance Transient Responses

Control technique without modifying the converter topology cannot reduce the peak transient voltage drop but only the response time [Nabeshima and Harada 1981, O'Connor 1996, Yao *et al* 2004]. A possible solution of reducing the transient voltage drop is to boost up the input voltage during transient period [Chiu *et al* 2004]. However, this will vary the controller from its desired operating condition and degrades its transient performance.

In contrast, by considering the state-plane geometry, change of input voltage does not change the shape of the off-state-trajectory family. Therefore, second-order switching surface can still provide near-optimal control in dictating the turn-off action under input voltage variation. In order to enhance the converter output performance, charge-pump technique can be employed to double the input voltage when transient occurs. After the transient response, input voltage will return to its normal value and therefore, doesn't affect the controller operation but reduces undershoot of output voltage. Practical prototype has been built to test the possibility of the proposed idea. Fig. 6.1 shows transient output waveform with and without using the transient boost technique. Furthermore, this technique will be useful in inverter application because the output capacitance value will always be limited.

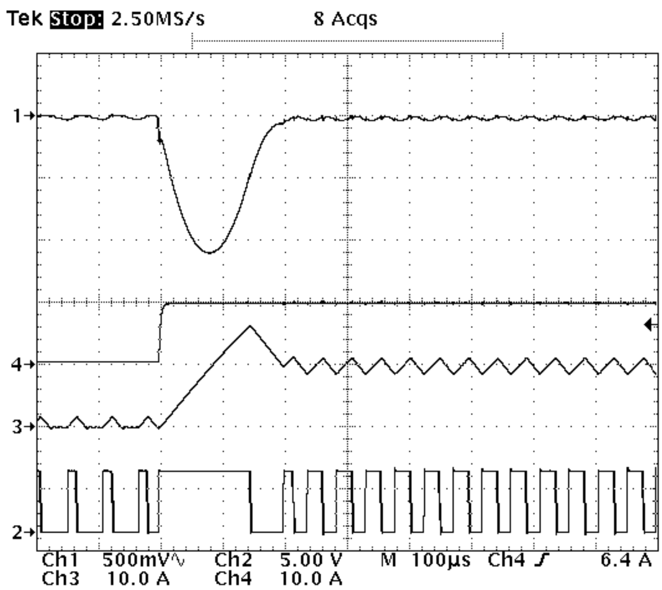

(a)

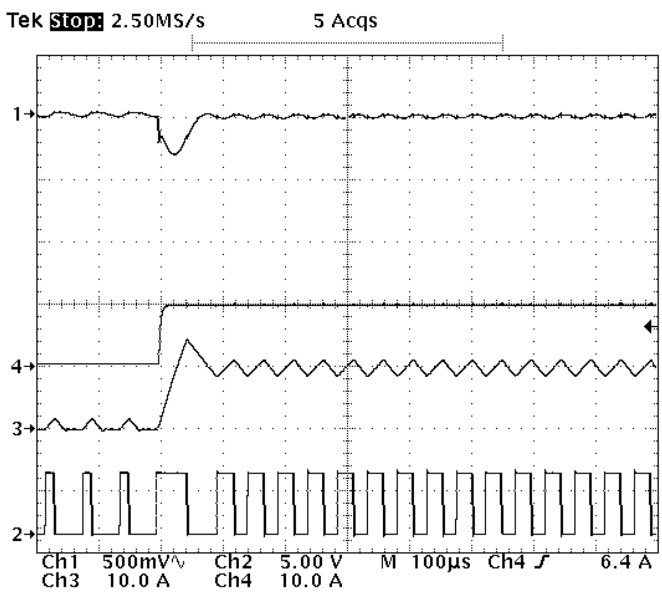

(b)

Fig. 6.1 Transient response when output current change from 0.5 A (6 W) to 10 A (100 W). [Ch1: v_o (500 mV/div), Ch2: v_{gate} (5 V/div), Ch3: i_L (10 A/div), Ch4: i_o (10 A/div)]. (a) Without transient boost. (b) With transient boost

6.3.3 Load Current Profile Predicting Characteristic in Inverter Applications

Derivation of the second-order switching surface is based on assuming constant output current during transient. This approximation is valid around the target operating points in inverter application. However, for tracking the reference voltage at extreme load variation, large-signal swing in the output occurs and thus degrades the transient performance. As the discrepancy is due to the assumption of constant output current, adding the load current profile prediction factor in the second-order switching surface might tackle the problem. Further research is suggested to research into this area.

APPENDIX A

PRACTICAL IMPLEMENTATION OF FIRST- AND SECOND-ORDER SWITCHING SURFACE

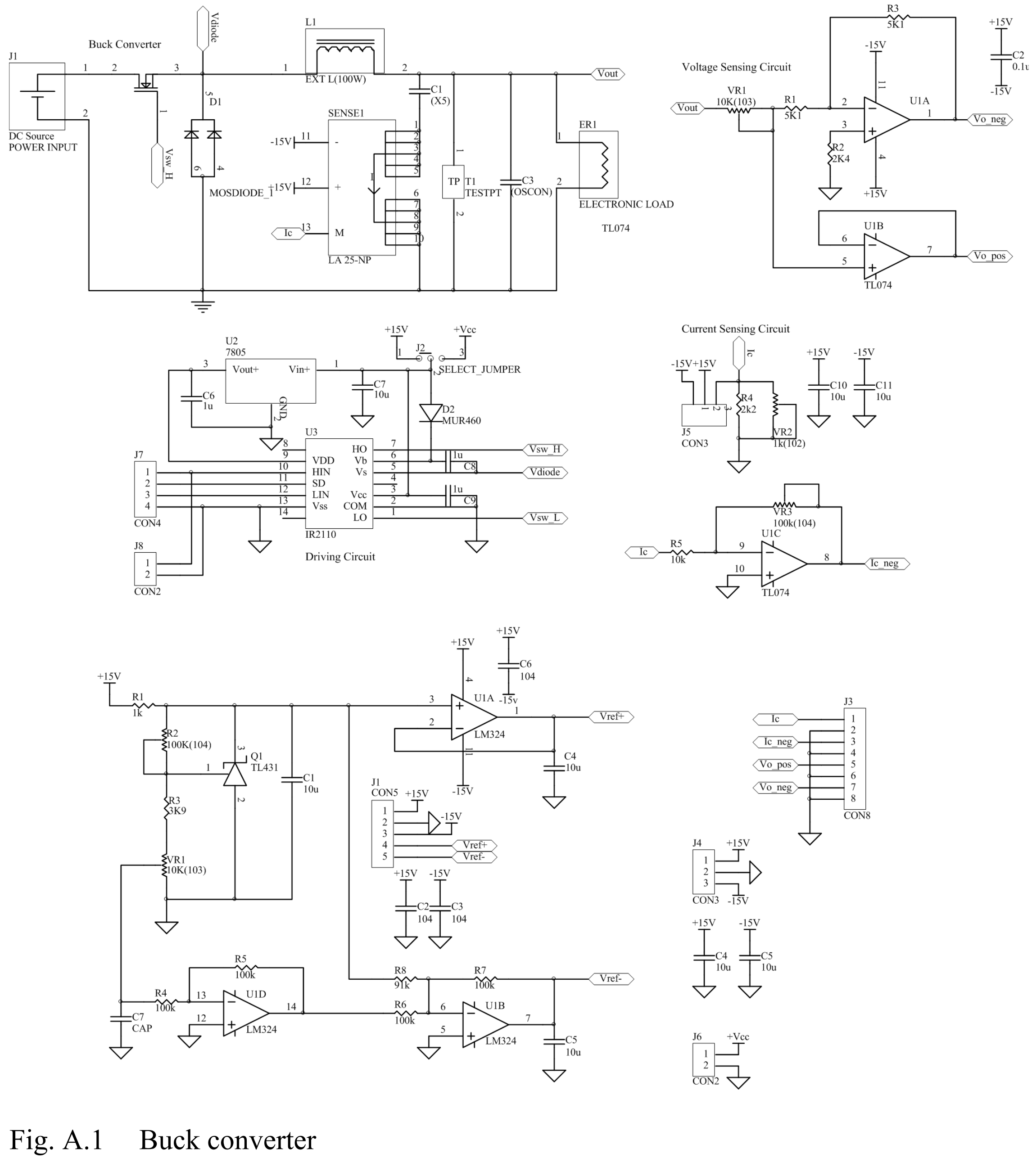

Fig. A.1 Buck converter

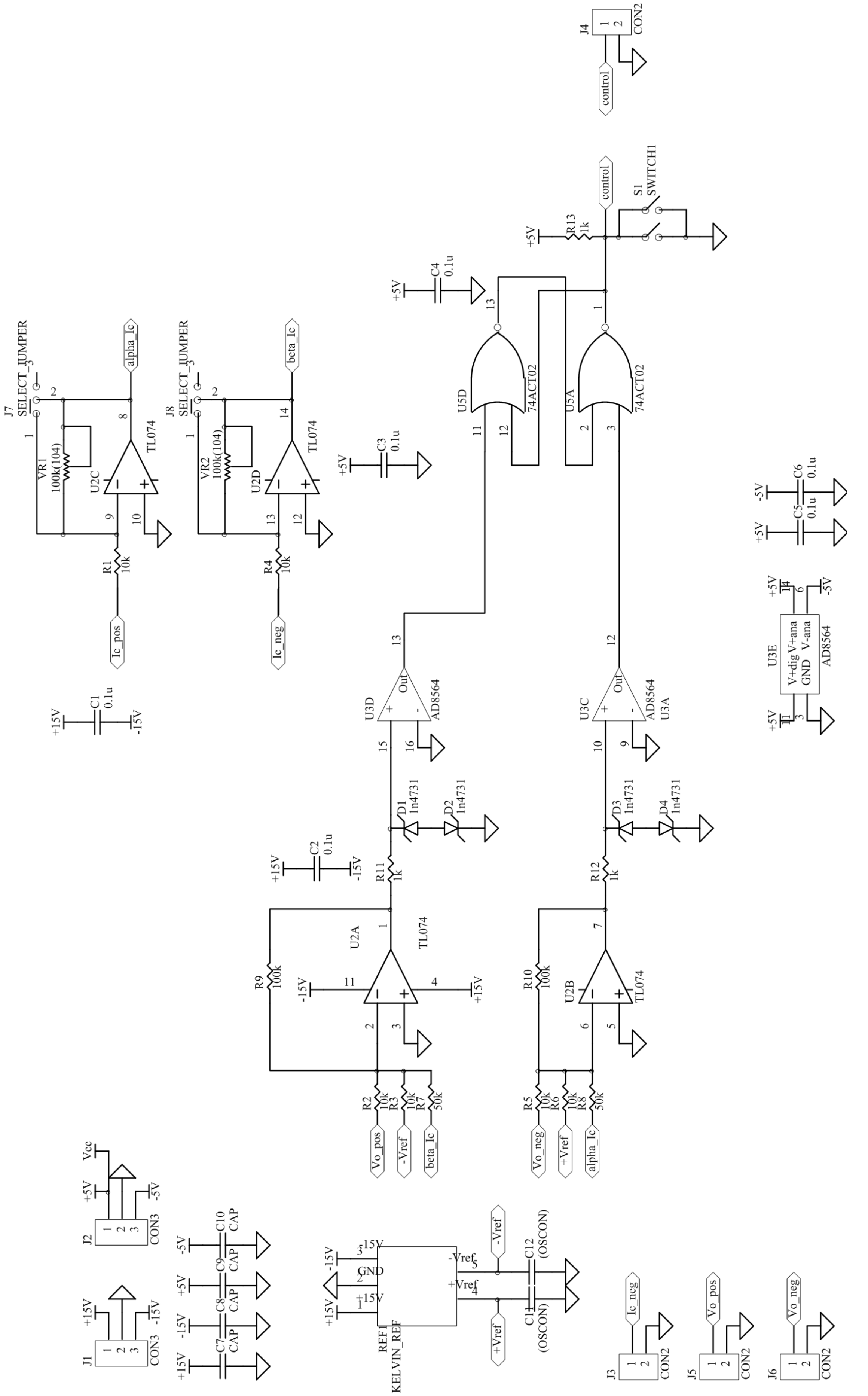

Fig. A.2 First-order switching surface controller

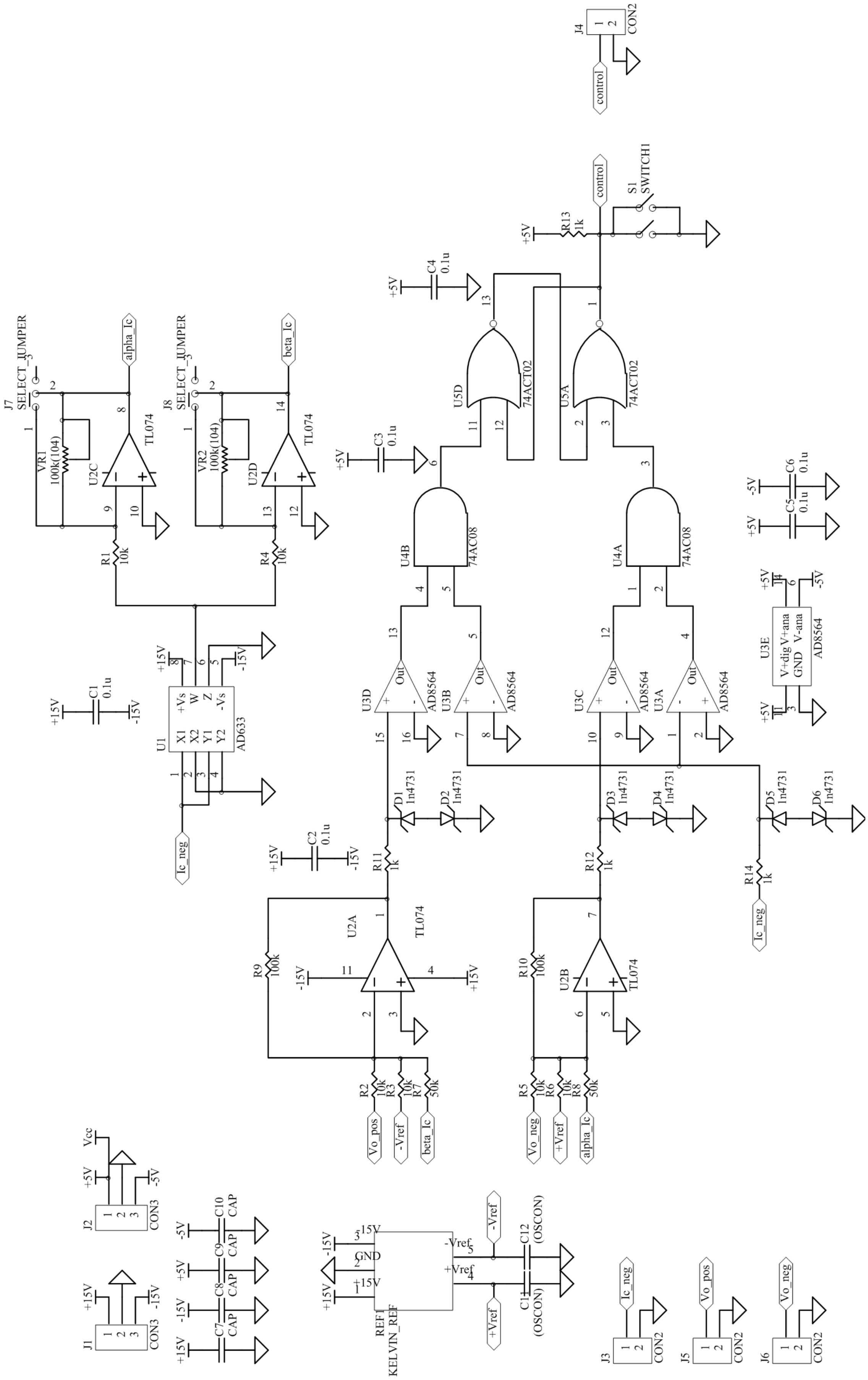

Fig. A.3 Second-order switching surface controller

APPENDIX B

DERIVATION THE EQUATIONS IN *CHAPTER 2*

B.1 Proofs of (2.4) and (2.5)

During the off-state, by assuming that $V_o = v_{ref}$ in steady-state,

$$i_C = C\frac{dv_C}{dt} = C\frac{dv_o}{dt} \tag{B.1}$$

$$-V_o = -v_{ref} = L\frac{di_L}{dt} \tag{B.2}$$

By using $i_L = i_C + i_o$ and assuming i_o be constant,

$$\frac{di_C}{dt} = \frac{di_L}{dt} \cong -\frac{v_{ref}}{L}$$

$$dt = -\frac{L}{v_{ref}} di_C \tag{B.3}$$

Based on (B.1),

$$\int_{t_1}^{t_2} dv_o = \frac{1}{C}\int_{t_1}^{t_2} i_C dt \tag{B.4}$$

Thus, eq. (2.4) can be derived from (B.4) that

$$\Delta v_{o,1} = v_o(t_2) - v_o(t_1) = v_{o,\max} - v_o(t_1) = \frac{1}{C}\int_{t_1}^{t_2} i_C dt \tag{B.5}$$

By substituting (B.3) and $i_C(t_2) = 0$ into $\frac{1}{C}\int_{t_1}^{t_2} i_C dt$, eq. (2.5) can be expressed

as

$$\int_{t_1}^{t_2} i_C dt = \int_{i_C(t_1)}^{i_C(t_2)} i_C \cdot \left(-\frac{L}{v_{ref}}\right) di_C$$

$$\int_{t_1}^{t_2} i_C dt = -\frac{L}{v_{ref}}\int_{i_C(t_1)}^{0} i_C di_C = \frac{1}{2}\frac{L\, i_C{}^2(t_1)}{v_{ref}} \tag{B.6}$$

B.2 Proofs of (2.8) and (2.9)

During the on-state,

$$i_C = C\frac{dv_C}{dt} = C\frac{dv_o}{dt} \tag{B.7}$$

$$v_i - V_o = v_i - v_{ref} = L\frac{di_L}{dt} \tag{B.8}$$

By using $i_L = i_C + i_o$ and assuming i_o be constant,

$$\frac{di_C}{dt} = \frac{di_L}{dt} \cong \frac{v_i - v_{ref}}{L}$$

$$dt = \frac{L}{v_i - v_{ref}} di_C \tag{B.9}$$

Based on (B.7),

$$\int_{t_3}^{t_4} dv_o = \frac{1}{C}\int_{t_3}^{t_4} i_C dt \tag{B.10}$$

Thus, eq. (2.8) can be derived from (B.10)

$$\Delta v_{o,2} = v_o(t_4) - v_o(t_3) = v_{o,\min} - v_o(t_3) = \frac{1}{C}\int_{t_3}^{t_4} i_C dt \tag{B.11}$$

By substituting (B.9) and $i_C(t_4) = 0$ into $\frac{1}{C}\int_{t_3}^{t_4} i_C dt$, eq. (2.9) can be expressed as

$$\int_{t_3}^{t_4} i_C dt = \int_{i_C(t_3)}^{i_C(t_4)} i_C \cdot \left(\frac{L}{v_i - v_{ref}}\right) di_C$$

$$\int_{t_3}^{t_4} i_C dt = \frac{L}{v_i - v_{ref}} \int_{i_C(t_3)}^{0} i_C di_C = -\frac{1}{2}\frac{L\, i_C^{\ 2}(t_3)}{v_i - v_{ref}} \tag{B.12}$$

APPENDIX C

DERIVATION THE EQUATIONS IN *CHAPTER 3*

C.1 Proofs of (3.2) and (3.3)

Assume that $V_o = v_{ref}$. When S_1 is on and S_2 is off,

$$i_C = C\frac{dv_C}{dt} \tag{C.1}$$

$$v_i - V_o = v_i - v_{ref} = L\frac{di_L}{dt} \tag{C.2}$$

By using $i_L = i_C + i_o$ and assuming i_o to be constant

$$\frac{di_C}{dt} = \frac{di_L}{dt} = \frac{v_i - v_{ref}}{L} \tag{C.3}$$

By substituting $v_C = v_o - r_C\, i_C$ into (C.1),

$$\int_{t_0}^{t_{on}} dv_o = \frac{1}{C}\int_{t_0}^{t_{on}} i_C\, dt + r_C \int_{t_0}^{t_{on}} di_C \tag{C.4}$$

By substituting (C.3) into (C.4), Eq. (3.2) can be derived.

When S_1 is off and S_2 is on,

$$i_C = C\frac{dv_C}{dt} \tag{C.5}$$

$$-V_o = -v_{ref} = L\frac{di_L}{dt} \tag{C.6}$$

By using $i_L = i_C + i_o$ and assuming i_o to be constant

$$\frac{di_C}{dt} = \frac{di_L}{dt} = -\frac{v_{ref}}{L} \tag{C.7}$$

By substituting $v_C = v_o - r_C\, i_C$ into (C.6),

$$\int_{t_1}^{t_{off}} dv_o = \frac{1}{C}\int_{t_1}^{t_{off}} i_C\, dt + r_C \int_{t_1}^{t_{off}} di_C \tag{C.8}$$

By substituting (C.7) into (C.8), Eq. (3.3) can be derived

C.2 Proof of (3.62)

Substitute $\Delta_1 = 0$ into (3.4) and differentiate both sides,

$$c_1 \frac{d\,(i_L - \frac{v_o}{R})}{d\,t} + \frac{d\,(v_o - v_{ref})}{d\,t} = 0 \qquad \text{(C.9)}$$

$$\frac{d\,i_L}{d\,v_o} = \frac{1}{R} - \frac{1}{c_1}$$

By equating $\sigma^1 = 0$ using (3.4),

$$\frac{1}{c_1} = -\frac{i_L - \frac{v_o}{R}}{v_o - v_{ref}} \qquad \text{(C.10)}$$

By substitute (C.10) into (C.9), eq. (3.62) can be derived.

C.3 Proofs of (3.63) and (3.64)

Assume $R >> r_C$ and substitute $R + r_C \to R$ into (1),

$$\begin{bmatrix} \dot{i}_L \\ \dot{v}_C \end{bmatrix} = \begin{bmatrix} -\frac{r_C}{L} & -\frac{1}{L} \\ \frac{1}{C} & -\frac{1}{CR} \end{bmatrix} \begin{bmatrix} i_L \\ v_C \end{bmatrix} + \begin{bmatrix} \frac{1}{L} \\ 0 \end{bmatrix} v_{in}\, q_1 \qquad \text{(C.11)}$$

$$v_o = \begin{bmatrix} r_C & 1 \end{bmatrix} \begin{bmatrix} i_L \\ v_C \end{bmatrix}$$

Based on (C.11),

$$\left.\frac{di_L}{dv_o}\right|_{off} = \frac{C}{L} \frac{-r_C i_L - v_o}{\frac{r_C C}{L}\left(-r_C i_L - v_o\right) + i_L - \frac{v_o}{R}} \qquad \text{(C.12)}$$

$$\left.\frac{di_L}{dv_o}\right|_{on} = \frac{C}{L} \frac{-r_C i_L - v_o + v_i}{\frac{r_C C}{L}\left(-r_C i_L - v_o + v_i\right) + i_L - \frac{v_o}{R}} \qquad \text{(C.13)}$$

By equating (C.12) with (3.62), eq. (3.63) can be derived. Similarly, by equating (C.13) with (3.62), eq. (3.64) can be derived.

C.4 Proof of (3.67)

The solution is real if they satisfy the conditions of

$$v_{o,off} \geq 0 \tag{C.14}$$

and

$$i_{L,off} - \frac{v_{o,off}}{R} > 0 \tag{C.15}$$

Thus, by considering (3.66) and (C.14),

$$R > c_1 \tag{C.16}$$

By substituting (3.66) into (C.15),

$$c_1 > 0 \tag{C.17}$$

Based on (C.16) and (C.17), (3.67) can be obtained.

C.5 Proof of (3.70)

The solution is real if they satisfy the conditions of

$$v_{o,on} < v_i \tag{C.18}$$

and

$$i_{L,on} - \frac{v_{o,on}}{R} < 0 \tag{C.19}$$

Thus, by considering (3.69) and (C.18),

$$R > c_1 \tag{C.20}$$

By substituting (3.69) into (C.19),

$$c_1 > 0 \tag{C.21}$$

Based on (C.20) and (C.21), (3.70) can be obtained. The above calculation for c_1 is valid for $i_{L,on}^2 > 0$.

C.6 Proof of (3.71)

For the switching boundary (3.6) and (3.7), it can further be written into a single expression of,

$$\sigma^2 = c_2\left(i_L - \frac{v_o}{R}\right)^2 + \left(v_o - v_{ref}\right) \tag{C.22}$$

where $c_2 = \frac{k_1}{2}\left(1+\mathrm{sgn}\left(i_L - \frac{v_o}{R}\right)\right) - \frac{k_2}{2}\left(1-\mathrm{sgn}\left(i_L - \frac{v_o}{R}\right)\right)$.

By differentiating both sides of (C.22),

$$\begin{aligned}
c_2\,\frac{d\,(i_L - \frac{v_o}{R})^2}{d\,t} + \frac{d\,(v_o - v_{ref})}{d\,t} &= 0 \\
2\,c_2\,(i_L - \frac{v_o}{R})\,(\frac{d\,i_L}{d\,t} - \frac{1}{R}\frac{d\,v_o}{d\,t}) + \frac{d\,v_o}{d\,t} &= 0 \\
\frac{\frac{d\,i_L}{d\,t}}{\frac{d\,v_o}{d\,t}} &= \frac{2\,c_2\,(i_L - \frac{v_o}{R})\,\frac{1}{R} - 1}{2\,c_2\,(i_L - \frac{v_o}{R})} \\
\frac{d\,i_L}{d\,v_o} &= \frac{1}{R} - \frac{1}{2\,c_2\,(i_L - \frac{v_o}{R})}
\end{aligned} \tag{C.23}$$

By equating $\sigma^2 = 0$ using (C.22),

$$\frac{1}{c_2} = -\frac{(i_L - \frac{v_o}{R})^2}{v_o - v_{ref}} \tag{C.24}$$

Substitute (C.24) into (C.23), it can be shown that

$$\frac{d\,i_L}{d\,v_o} = \frac{1}{R} + \frac{i_L - \frac{v_o}{R}}{2\,(v_o - v_{ref})} \tag{C.25}$$

C.7 Proofs of (3.77)-(3.80)

The solutions $[i_{L,on}^2, v_{o,on}^2]$ and $[i_{L,on}^3, v_{o,on}^3]$ are real if

$$\xi_1 \geq 0 \quad \Rightarrow \quad k_1 \geq \frac{2CLR^2 - L^2}{4C^2R^2 v_{ref}} \tag{C.26}$$

They must also satisfy the conditions of

$$v_{o,off} \geq 0 \tag{C.27}$$

and

$$i_{L,off} - \frac{v_{o,off}}{R} > 0 \tag{C.28}$$

Thus, by considering (3.75)-(3.76), and (C.27),

$$\alpha_1 \geq 0 \quad \Rightarrow \quad \Phi_1 + 4\sqrt{\xi_1} \geq 0 \tag{C.29}$$

and

$$\beta_1 \geq 0 \quad \Rightarrow \quad \Phi_1 - 4\sqrt{\xi_1} \geq 0 \tag{C.30}$$

Based on (C.29), it can be shown that

$$k_1 \geq \frac{2CLR^2 - L^2}{4C^2R^2 v_{ref}} \quad \text{if } L - CR^2 < 0 \tag{C.31}$$

and

$$k_1 \geq \frac{R^2}{4v_{ref}} \quad \text{if } L - CR^2 \geq 0 \tag{C.32}$$

will give real solutions.

Based on (C.30), it can be shown that

$$k_1 \leq \frac{R^2}{4\, v_{ref}} \quad \text{if } L - CR^2 < 0 \tag{C.33}$$

will have a real solution. There is no real solution for $L - CR^2 \geq 0$.

By substituting the solution set of (3.75) into (C.28), it can be shown that

$$k_1 < \frac{L}{2C v_{ref}} \tag{C.34}$$

will have a real solution.

Similarly, by substituting the solution set of (3.76) into (C.28),

$$k_1 > \frac{2CLR^2 - L^2}{4C^2R^2v_{ref}} \tag{C.35}$$

will have a real solution.

Thus, based on (C.26), (C.31), (C.32) and (C.34), (3.77) and (3.78) can be obtained. Based on (C.26), (C.33) and (C.35), (3.79) and (3.80) can be obtained.

C.8 Proof of (3.84)-(3.87)

The solutions $[i_{L,on}^2, v_{o,on}^2]$ and $[i_{L,on}^3, v_{o,on}^3]$ are real if

$$\xi_2 \geq 0 \quad \Rightarrow \quad k_2 \geq \frac{2CLR^2 - L^2}{4C^2R^2(v_i - v_{ref})} \tag{C.36}$$

They must also satisfy the conditions of

$$v_{o,on} \leq v_i \tag{C.37}$$

and

$$i_{L,on} - \frac{v_{o,on}}{R} < 0 \tag{C.38}$$

Thus, based on (3.82)-(3.83), and (C.37),

$$\alpha_2 L - 8C^2R^2v_ik_2 \leq 0 \tag{C.39}$$

and

$$\beta_2 L - 8C^2R^2v_ik_2 \leq 0 \tag{C.40}$$

By using (C.39), it can be shown that

$$k_2 \geq \frac{2CLR^2 - L^2}{4C^2R^2(v_i - v_{ref})}, \quad \text{if } L - CR^2 < 0 \tag{C.41}$$

and

$$k_2 \geq \frac{R^2}{4(v_i - v_{ref})}, \quad \text{if } L - CR^2 \geq 0 \tag{C.42}$$

will give real solutions.

Based on (C.40), it can be shown that

$$k_2 \le \frac{R^2}{4\left(v_i - v_{ref}\right)}, \quad \text{if } L - CR^2 < 0 \tag{C.43}$$

will have a real solution. There is no real solution for $L - CR^2 \ge 0$.

By substituting the solution set of (3.82) into (C.38), it can be shown that

$$k_2 < \frac{L}{2C\left(v_i - v_{ref}\right)} \tag{C.44}$$

will give a real solution.

By substituting the solution set of (3.83) into (C.38), it can be shown that

$$k_2 > \frac{2CLR^2 - L^2}{4C^2R^2\left(v_i - v_{ref}\right)} \tag{C.45}$$

will give a real solution.

Thus, based on (C.36), (C.41), (C.42) and (C.44), (3.77) and (3.78) can be obtained. Based on (C.36), (C.43) and (C.45), (3.79) and (3.80) can be obtained. The above calculation for k_2 is valid for $i_{L,on}^2 > 0$ and $i_{L,on}^3 > 0$.

C.9 Proofs of (3.93) and (3.94)

The start-up on-state trajectory (i.e., 'X_1' to 'A' in Fig. 3.10) can be written as

$$\dot{x} = (A_0 + A_1)x + (B_0 + B_1)u, \quad x_0 = x_{X_1} \tag{C.46}$$

The off-state trajectory (i.e., 'A' to 'B' in Fig. 3.10) can be replaced with the equivalent time reversed system, which is given as

$$\dot{x} = -(A_0 + A_2)x - (B_0 + B_2)u, \quad x_0 = x_B \tag{C.47}$$

where multiplying the system's A and B matrices by -1 reverses the state velocity vector and therefore gives the output $x(-t)$.

The intersection point 'A' of vector $x_A = [\, i_{L,A} \quad v_{o,A} \,]$ can be obtained by solving (C.46) and (C.47) numerically. By substituting $v_{o,A}$ and $i_{L,A}$ into (3.4) with $\Delta_1 = 0$, it can be shown that

$$c_1 = -\frac{v_{o,A} - v_{ref}}{i_{L,A} - \frac{v_{o,A}}{R}} \tag{C.48}$$

By substituting $v_{C,A}$ and $i_{L,A}$ into (3.6) with $\Delta_2 = 0$, it can be shown that

$$k_1 = -\frac{v_{o,A} - v_{ref}}{(i_{L,A} - \frac{v_{o,A}}{R})^2} \tag{C.49}$$

C.10 Proof of (3.95)

The off-state trajectory (i.e., ‘X_2’ to ‘C’ in Fig. 3.10) can be written as

$$\dot{x} = (A_0 + A_2)x + (B_0 + B_2)u\,,\quad x_0 = x_{X_2} \tag{C.57}$$

The on-state trajectory (i.e., from point ‘C’ to point ‘B’ in Fig. 3.10) can be replaced with the equivalent time reversed system given by

$$\dot{x} = -(A_0 + A_1)x - (B_0 + B_1)u\,,\quad x_0 = x_{\mathrm{B}} \tag{C.58}$$

The intersection point ‘C’ of vector $x_C = [\,i_{L,C} \quad v_{o,C}\,]$ can be obtained by solving (C.57) and (C.58) numerically.

By substituting $v_{o,\mathrm{C}}$ and $i_{L,C}$ into (3.6) with $\Delta_2 = 0$, it can be shown that

$$k_2 = \frac{v_{o,C} - v_{ref}}{(i_{L,C} - \frac{v_{o,C}}{R})^2} \tag{C.59}$$

PUBLICATIONS FROM THIS THESIS

Journal / Transaction Papers

[1] Kelvin K. S. Leung and Henry S. H. Chung, "Derivation of a Second-Order Switching Surface in the Boundary Control of Buck Converters", *IEEE Power Electronics Letters*, vol. 2, no. 2, pp. 63-67, June 2004.

[2] Kelvin K. S. Leung and Henry S. H. Chung, "Dynamic Hysteresis Band Control of the Buck Converter with Fast Transient Response", *IEEE Transactions on Circuits and Systems II: Express Briefs*, vol. 52, no. 7, pp. 398-402, July 2005.

[3] Kelvin K. S. Leung and Henry S. H. Chung, "A Comparative Study of the Boundary Control of Buck Converters Using First- and Second-Order Switching Surfaces –Part I: Continuous Conduction Mode", *IEEE Transactions on Power Electronics*. (Submitted)

[4] Kelvin K. S. Leung and Henry S. H. Chung, "A Comparative Study of the Boundary Control of Buck Converters Using First- and Second-Order Switching Surfaces –Part II: Discontinuous Conduction Mode", *IEEE Transactions on Power Electronics*. (Submitted)

Conference Papers

[5] Kelvin K. S. Leung, Henry S. H. Chung, and S. Y. R. Hui, "Use of State Trajectory Prediction in Hysteresis Control for Achieving Fast Transient Response of the Buck Converter", *in Proc. IEEE International Symposium on Circuits and Systems* (ISCAS), May 2003, pp. 439-442.

[6] Kelvin K. S. Leung and Henry S. H. Chung, "State Trajectory Prediction Control for Boost Converters", *in Proc. IEEE International Symposium on Circuits and Systems* (ISCAS), May 2004, pp. 556-559.

[7] Kelvin K. S. Leung and Henry S. H. Chung, "Use of Second-Order Switching Surface in the Boundary Control of Buck Converter", *in Proc. 35th IEEE Power Electronics Specialists Conference* (PESC), June 2004, pp. 1587-1593.

[8] Kelvin K. S. Leung and Henry S. H. Chung, "Near-optimal Dynamic Regulation DC-DC Converters Using Non-linear Switching", *in Proc. 6th IEEE Hong Kong Workshop on SMPS*, Nov. 2004, pp. 57-63.

[9] Kelvin K. S. Leung, Julian Y. C. Chiu and Henry S. H. Chung, "Boundary Control of a Bipolar Square-Wave Generator Using Second-Order Switching Surface", *in Proc IEEE International Symposium on Circuits and Systems* (ISCAS), May 2005, pp. 3079-3082.

[10] Kelvin K. S. Leung and Henry S. H. Chung, "A Comparative Study of the Boundary Control of Buck Converters Using First- and Second-Order Switching Surfaces –Part I: Continuous Conduction Mode", *in Proc. IEEE 36th Power Electronics Specialists Conference* (PESC), June 2005, pp. 2133-2139.

[11] Kelvin K. S. Leung and Henry S. H. Chung, "A Comparative Study of the Boundary Control of Buck Converters Using First- and Second-Order Switching Surfaces –Part II: Discontinuous Conduction Mode", *in Proc. IEEE 36th Power Electronics Specialists Conference* (PESC), June 2005, pp. 2126-2132.

[12] Kelvin K. S. Leung, Julian Y. C. Chiu and Henry S. H. Chung, "Boundary Control of Inverter Using Second-Order Switching Surface", *in Proc. IEEE 36th Power Electronics Specialists Conference* (PESC), June 2005, pp. 936-942.

REFERENCES

1. Abu-Qahouq J. A., Pongratananukul N., Batarseh I., and Kasparis T., 2002, "Novel transient cancellation control method for future generation of microprocessors," *in Proc. IEEE Applied Power Electronics Conf. and Expo.*, March, pp. 216-222.
2. Ahmed M., Kuisma M., Tolsa K., and Silventoinen P., 2003, "Implementing sliding mode control for buck converter," *in Proc. IEEE Power Electronics Specialist Conf.*, June, pp. 634-637.
3. Ahmed M., Kuisma M., Silventoinen P., and Pyrhonen O., 2003, "Effect of implementing sliding mode control on the dynamic behaviour and robustness of switch mode power supply (buck converter)," *in Proc. IEEE Power Electronics and Drive Systems*, Nov., pp. 1364-1368.
4. Barrado A., Vazquez R., Lazaro A., Pleite J. and Olias E., 2002, "Fast transient response dc/dc converter for low output voltage," *IEEE Electronics Letters*, Sept., pp. 1127-1128.
5. Bass R. M., and Krein P. K., 1989, "Switching boundary geometry and the control of single-phase inverters," *in Proc. IEEE Industry Application Society Annual Meeting*, Oct., pp. 1052-1056.
6. Bass R. M., and Krein P. K., 1990, "Limit cycle geometry and control in power electronic systems," *in Proc. Midwest Symposium on Circuits and Systems*, Aug., pp. 785-787.
7. Bass R. M., and Krein P. K., 1990, "State-plane animation of power electronic systems: a tool for understanding feedback control and stability," *in Proc. Applied Power Electronics Conf. and Expo.*, March, pp. 641-648.
8. Bass R. M., and Krein P. K., 1991, "Large-signal design alternatives for switching power converter control," *in Proc. IEEE Power Electronics Specialists Conf.*, June, pp. 882-887.

9. Batarseh I., 2004, “dc-ac inverters,” *Power Electronic Circuits*, John Wiley & Sons, Ch. 9.

10. Bibian S., and Jin H., 2002, “High performance predictive dead-beat digital controller for dc power supplies,” *IEEE Trans. Power Electronics*, vol. 17, no. 3, May, pp. 420-427.

11. Biel D., Martinez L., Tenor J., and Jammes B., 1996, “Optimum dynamic performance of a buck converter,” *in Proc. IEEE International Symposium on Circuits and Systems*, May, pp. 589-592.

12. Biel D., Martinez-Salamero L., Lopez J., Perez Y., Jammes B., and Marpinard J. C., “Minimum-time control of a buck converter for bipolar square-wave generation,” *in Proc. European Space Power Conference*, Sept., pp. 345-350.

13. Biel D., Fossas E., Guinjoan F. Alarcon E., and Poveda A., 2001, “Application of sliding-mode control to the design of a buck-based sinusoidal generator,” *IEEE Trans. Industrial Electronics*, vol. 48, no. 3, June, pp. 563-571.

14. Biel D., Guinjoan F., Fossas E., and Chavarria J., 2004, “Sliding-mode control design of a boost-buck switching converter for ac signal generation,” *IEEE Trans. Circuits and Systems-I: Regular paper*, vol. 51, no. 8, Aug., pp. 1539-1551.

15. Burns W. W., and Wilson T. G., 1976, “State trajectories used to observe and control dc-to-dc converters,” *IEEE Trans. Aerospace and Electronic Systems*, vol. 12, no. 6, Nov., pp. 706-717.

16. Burns W. W., and Wilson T. G., 1977, “Analysis derivation and evaluation of a state-trajectory control law for dc-to-dc converters,” *in Proc. Power Electronics Specialist Conf.*, pp. 70-85.

17. Cardoso B. J., Moreira A. F., Menezes B. R., and Cortizo P. C., 1992, "Analysis of switching frequency reduction methods applied to sliding mode controlled dc-dc converters," *in Proc. IEEE Applied Power Electronics Conf. and Expo.*, Feb., pp. 403-410.

18. Carpita M., and Marchesoni M., 1996, "Experimental study of a power conditioning system using sliding mode control," *IEEE Trans. Power Electronics*, vol. 11, no. 5, pp. 731-742.

19. Chetty P. R. K., 1982, "Modeling and design of switching regulators," *IEEE Trans. Aerospace and Electric Systems*, vol. 18, no. 3, May, pp. 333-344.

20. Chiu Y. C., Zhou B., Chung H. S. H., and Lau W. H., 2004, "The implementation of transient dc-link boost based digital amplifier for eliminating pulse-dropping distortion," *in Proc. IEEE International Symposium on Circuits and Systems*, May, pp. 864-867.

21. DeCarlo R., Zak S. H., and Matthews G. P., 1988, "Variable structure control of nonlinear multivariable systems: A tutorial," *Proceeding of the IEEE*, vol. 76, no. 3, March, pp. 212-232.

22. Edwards C., and Spurgeon S. K., 1998, *Sliding Mode Control: Theory and Applications*, Taylor & Francis Ltd.

23. Erickson R. W., and Maksimovic D., 2000, "AC equivalent circuit modeling," *Fundamentals of Power Electronics*, Ch. 7.

24. Erisman B., and Redl R., 1999, "Modify your switching-supply architecture for improved transient response," Available: http://www.edn.com/article/CA46325.html.

25. Fairchild Semiconductor, 1998, "Applcation bulletin AB-20: Optimum current sensing techniques in CPU converters," Available: http://www.fairchildsemi.com.

26. Filho W. M. P., and Perin A. J., 1997, "An approach of the variable structure analysis for power electronics applications," *IEEE Industry Applications Society Annual Meeting*, Oct., pp. 844-851.

27. Forghani-Zadeh H. P., and Rincon-Mora G. A., 2002, "Current-sensing technique for dc-dc converters," *in Proc. Midwest Symposium on Circuits and Systems*, Aug., pp. 577-580.

28. Garcera G., Carbonell P. J., and Abellan A., 1999, "Sensibility study of the control loops of voltage and current mode controlled dc-dc converters by means of robust parametric control theory," *in Proc. ISIE*, pp. 613-617.

29. Goder D., and Pelletier W. R., 1996, "V^2 architecture provides ultra-fast transient response in switch mode power supplies," *in Proc. HFPC*.

30. Gow J. A., and Manning C. D., 2001, "Novel fast-acting predictive current mode controller for power electronic converters," *IEE Electronics Power Applications*, vol. 148, no. 2, March, pp. 133-139.

31. Greuel M., Muyshondt R., and Krein P. T., 1997, "Design approaches to boundary controllers," *in Proc. IEEE Power Electronics Specialists Conf.*, June, pp. 672-678.

32. Habetler T. G., and Harley R. G., 2001, "Power electronic converter and system control," *Proceedings of the IEEE*, vol. 89, no. 6, June, pp. 913-925.

33. Holtz J., and Beyer B., 1993, "Optimal synchronous pulsewidth modulation with a trajectory-tracking scheme for high-dynamic performance," *IEE Trans. Industry Applications*, vol. 29, no. 6, Nov.-Dec., pp. 1098-1105.

34. Holtz J., 1994, "Pulsewidth modulation for electronic power conversion," *Processing of the IEEE*, vol. 82, Aug., pp. 1194-1214.

35. Huang W., 2000, "A new control for multi-phase buck converter with fast transient response," *in Proc. IEEE Applied Power Electronics Conf. and Expo.*, pp. 273-279.

36. Huffman S. D., Burns W. W., Wilson T. G., and Owen H. A., 1977, "Fast-response free-running dc-to-dc converter employing a state-trajectory control law," *in Proc. Power Electronics Specialist Conf.*, pp. 180-189.

37. Hung J. Y., Gao W., and Hung J. C., 1993, "Variable structure control: a survey," *IEEE Trans. Industrial Electronics*, vol. 40, no. 1, Feb., pp. 2-22.

38. Hur N., Jung J., and Nam K., 2001, "A fast dynamic dc-link power-balancing scheme for a PWM converter-inverter system," *IEEE Trans. Industrial Electronics*, vol. 48, no. 4, Aug., pp. 794-803.

39. Jung S. H., Kim N. I., and Cho G. H., 2002, "Class D audio power amplifier with fine hysteresis control," *IEEE Electronics Letters*, vol. 38, no. 22, Oct., pp. 1302-1303.

40. Kang B. J. and Liaw C. M., 2001, "Robust hysteresis current-controlled PWM scheme with fixed switching frequency," *IEE Electronics Power Application*, vol. 148, no. 6, Nov., pp. 503-512.

41. Kato T. and Miyao K., 1988, "Modified hysteresis control with minor loops for single-phase full-bridge inverters," *in Proc. IEEE Industry Application Society Annual Meeting*, Oct., pp. 689-693.

42. Kazmierkowski M. P., Krishnan R., and Blaabjerg F., 2002, *Control in Power Electronics: Selected Problems*, Academic Press.

43. Kelley A. W., and Titus J. E., 1991, "DC current sensor for PWM converters," *in Proc. Power Electronics Specialists Conf.*, June, pp. 641-650.

44. Kolar J. W., Ertl H., and Zach F. C., 1991, "Influence of the modulation method on the conduction and switching losses of a PWM converter systems," *IEEE Trans. Industry Applications*, vol. 27, no. 6, Nov.-Dec., pp. 1063-1075.

45. Krein P. T., 1998, "Geometric control for power converters," *Elements of Power Electronics*, 1998, Ch. 17.

46. Krein P. T., 1999, "Ripple correlation control, with some application," *in Proc. IEEE International Symposium on Circuits and Systems*, May, pp. 283-286.

47. Krein P. T., 2001, "Sliding mode and switching surface control," *Nonlinear Phenomena in Power Electronics*, pp. 357-370, IEEE Press.

48. Kundur P., 1994, "Eigenproperties of the state matrix," *Power System Stability and Control*, Ch. 12.2.

49. Lahyani A., Venet P., Grellet G., and Viverge P. J., 1998, "Failure prediction of electrolytic capacitors during operation of a switchmode power supply," *IEEE Trans. Power Electronics*, vol. 13, no. 6, Nov., pp. 1199-1207.

50. Liao J. C., and Yeh S. N., 2000, "A novel instantaneous power control strategy and analytic model for integrated rectifier / inverter systems," *IEEE Trans. Power Electronics*, vol. 15, no. 6, Nov., pp. 996-1006.

51. Luo J., Batarseh I., and Wu G. T., 2002, "Transient current compensation for low-voltage high-current voltage regulator modules," *in Proc. Applied Power Electronics Conf. and Expo.*, March, pp. 223-228.

52. Malesani L., Rossetto L., Spiazzi G., and Tenti P., 1995, "Performance optimization of Cuk converters by sliding-mode control," *IEEE Trans. Power Electronics*, vol. 10, no. 3, May, pp. 302-309.

53. Malesani L., Rossetto L., Spiazzi G., and Zuccato A., 1996, "An ac power supply with sliding-mode control," *IEEE Industry Applications Magazine*, Sept. / Oct., pp. 32-38.

54. Malesani L., Mattavelli P., and Tomasin P., "Improved constant-frequency hysteresis current control of VSI inverters with simple feedforward bandwidth prediction," *IEEE Trans. Industry Applications*, vol. 33, no. 5, Sept., pp. 1194-1202.

55. Mattavelli P., Rossetto L., Spiazzi G., and Tenti P., 1993, “General-purpose sliding-mode controller for dc/dc converter applications,” *in Proc. IEEE Power Electronics Specialists Conf.*, June, pp. 609-615.

56. Middlebrook R. D., 1989, “Modeling current-programmed buck and boost regulators,” *IEEE Trans. Power Electronics*, vol. 4, no. 1, Jan., pp. 36-52.

57. Midya P., and Krein P. T., 1992, “Optimal control approaches to switching power converters,” *in Proc. IEEE Power Electronics Specialists Conf.*, July, pp. 741-748.

58. Miftakhutdinov R., 2001, “Optimal design of interleaved synchronous buck converter at high slew-rate load current transients,” *in Proc. IEEE Power Electronics Specialists Conf.*, June, pp. 1714-1718.

59. Mohan N., Undeland T. M., and Robbins W. P., 1995, “Control of switch-mode dc power supplies,” *Power Electronics: Converters, Applications, and Design*, Ch. 10-5.

60. Morel C., Guignard J. C., and Guillet M., 2002, “Sliding mode control of dc-to-dc power converters,” *in Proc. IEEE International Conference on Circuits and Systems*, Sept., pp. 971-974.

61. Munzert R., and Krein P. T., 1996, “Issues in boundary control,” *in Proc. IEEE Power Electronics Specialists Conf.*, pp. 810-816.

62. Nabeshima T., and Harada K., 1981, “Large-signal transient responses of a switching regulator,” *IEEE Trans. Aerospace and Electronic Systems*, vol. AES-18, no. 5, Sept., pp. 545-550.

63. Nguyen V. M., and Lee C. Q., 1995, “Tracking control of buck converter using sliding-mode with adaptive hysteresis,” *in Proc. Power Electronics Specialists Conf.*, June, pp. 1086-1093.

64. Nguyen V. M., and Lee C. Q., 1996, "Indirect implementations of sliding-mode control law in buck-type converters," *in Proc. IEEE Applied Power Electronics Conf. and Expo.*, March, pp. 111-115.

65. Nicolas B., Fadel M., and Cheron Y., 1996, "Fixed-frequency sliding mode control of a single-phase voltage source inverter with input filter," *in Proc. IEEE International Symposium on Industrial Electronics*, June, pp. 470-475.

66. O'Connor J. A., 1996, "Converter optimization for powering low voltage, high performance microprocessors," *in Proc. IEEE Applied Power Electronics Conf. and Expo.*, pp. 984-989.

67. Olm J. M., Fossas E., and Biel D., 1996, "A sliding approach to tracking problems in dc-dc power converters," *in Proc. Conf. on Decision and Control*, Dec., pp. 4008-4009.

68. On Semiconductor, 1999, "Handling EMI in switch mode power supply design," Available: http://onsemi.com.

69. On Semiconductor, 2001, "CS5150: CPU 4-bit synchronous buck controller," Available: http://onsemi.com.

70. Oppenheimer M., Husain I., Elbuluk M., and Abreu-Garcia J. A. D., 1996, "Sliding mode control of the Cuk converter," *in Proc. Power Electronics Specialists Conf.*, June, pp. 1519-1526.

71. Poon N. K., Liu C. P., and Pong M. H., 2001, "A low cost dc-dc stepping inductance voltage regulator with fast transient loading response," *in Proc. IEEE Applied Power Electronics Conf. and Expo.*, pp. 268-272.

72. Perry A. G., Feng G., Liu Y. F., and Sen P. C., 2004, "A new sliding mode like control method for buck converter," *in Proc. IEEE Power Electronics Specialists Conf.*, June, pp. 3688-3693.

73. Qu S., 2001, "Modeling and design considerations of V^2 controlled buck regulator," *in Proc. Applied Power Electronics Conf. and Expo.*, March, pp. 507-513.

74. Redl R., and Sokal N. O., 1986, "Near-optimum dynamic regulation of dc-dc converters using feedforward of output current and input voltage with current-mode control," *IEEE Trans. Power Electronics*, vol. 1, no. 3, June, pp. 181-192.

75. Ramos R. R., Biel D., Fossas E., and Guinjoan F., 2003, "A fixed-frequency quasi-sliding control algorithm: application to power inverters design by means of FPGA implementation," *IEEE Trans. Power Electronics*, vol. 18, no. 1, Jan., pp. 344-355.

76. Silva J. F., 1992, "Sliding mode voltage control in current mode PWM inverters," *IEEE Power Electronics Specialists Conf.*, June, pp. 762-769.

77. Silva J. F., 2001, "Power converter control using state-space averaged models," *Power Electronics Handbook*, Ch. 19.2.

78. Sira-Ramirez H. J., and Ilic M., 1988, "A geometric approach to the feedback control of switch mode dc-to-dc power supplies," *IEEE Trans. Circuits and Systems*, vol. 35, no. 10, Oct., pp. 1291-1298.

79. Slotine J. J. E., and Li W., 1991, "Sliding mode," *Applied Nonlinear Control*, Ch. 7.

80. Sobolev L. B., 1993, "Optimal control of transients in dc/dc converters," *in Proc. IEEE Power Conversion Conf.*, April, pp. 194-199.

81. Soto A., Alou P. Cobos J. A., and Uceda J., 2004, "High input voltage (48V) multiphase VRM with feed-forward of the load current for fast dynamics," *in Proc. IEEE Power Electronics Specialists Conf.*, June, pp. 747-752.

82. Spiazzi G., Mattavelli P., and Rossetto L., 1997, "Sliding mode control of dc-dc converters," *in Proc. Congresso Brasileiro de Elettronica de Potencia*, Dec., pp. 59-68.

83. Sprock D., and Hsu P., "Predictive discrete time control of switch-mode applications," *in Proc. IEEE Power Electronics Specialists Conf.*, June, pp. 175-181.

84. Szepesi T., 1987, "Stabilizing the frequency of hysteretic current-mode dc-dc converters," *IEEE Trans. Power Electronics*, vol. 2, no. 4, Oct., pp. 302-312.

85. Tan S. C., Lai Y. M., Tse C. K., and Cheung M. K. H., 2004, "An adaptive sliding mode controller for buck converter in continuous conduction mode," *in Proc. IEEE Applied Power Electronics Conf. and Expo.*, Feb., pp. 1395-1400.

86. Tan S. C., Lai Y. M., Cheung M. K. H., and Tse C. K., 2005, "On the practical design of a sliding mode voltage controlled buck converter," *IEEE Trans. Power Electronics*, vol. 20, no. 2, March, pp. 425-437.

87. Taniguchi K., Ogino Y., and Irie H., 1988, "PWM technique for power MOSFET inverter," *IEEE Trans. Power Electronics*, vol. 3, no. 3, pp. 328-334.

88. Tso C. H., and Wu J. C., 2003, "A ripple control buck regulator with fixed output frequency," *IEEE Power Electronics Letters*, vol. 1, no. 3, Sept., pp. 61-63.

89. Umez-Eronini E., 1999, "Stability of dynamic systems," *System Dynamics and Control*, Ch. 10.

90. Venkataramanan R., Sabanoivc A., and Cuk S., 1985, "Sliding mode control of dc-to-dc converters," *in Proc. IEEE Conf. Industrial Electronics, Control Instrumentations*, pp. 251-258.

91. Vicor Corporation, 2002, "Power supply design considerations for high di/dt loads," Available: http://vicr.com.

92. Vorperian V., 1990, "Simplified analysis of PWM switch part I: continuous conduction mode," *IEEE Trans. Aerospace and Electronic Systems*, vol. 26, no. 3, May, pp. 490-496.
93. Vorperian V., 1990, "Simplified analysis of PWM switch part II: discontinuous conduction mode," *IEEE Trans. Aerospace and Electronic Systems*, vol. 26, no. 3, May, pp. 497-505.
94. Wang M., 1999, "Power supply design with fast transient response using V^2 control scheme," *in Proc. Record International IC Conf.*, pp. 189-193.
95. Wong P., Wu Q., Xu P., Yang B., and Lee F. C., 2000, "Investigating coupling inductors in the interleaving QSW VRM," *in Proc. IEEE Applied Power Electronics Conf. and Expo.*, pp. 268-272.
96. Wu K. C., 1997, *Pulse Width Modulated DC-DC Converters*, Chapman & Hall.
97. Yao K., Ren Y., and Lee F. C., 2004, "Critical bandwidth for the load transient response of voltage regulator modules," *IEEE Trans. Power Electronics*, vol. 19, no. 6, Nov., pp. 1454-1461.
98. Zhou X., Wong P., Xu P., Lee F. C., and Huang A. Q., 2000, "Investigation of candidate VRM topologies for future microprocessors," *IEEE Trans. Power Electronics*, vol. 15, no. 6, Nov., pp. 1172-1182.